

DISSERTATION

RAINFALL ESTIMATION FROM SPACEBORNE AND GROUND BASED
RADARS USING NEURAL NETWORKS

Submitted by

Amin Alqudah

Department of Electrical and Computer Engineering

In partial fulfillment of the requirements

For the Degree of Doctor of Philosophy

Colorado State University

Fort Collins, Colorado

Summer, 2009

UMI Number: 3385187

All rights reserved

INFORMATION TO ALL USERS

The quality of this reproduction is dependent upon the quality of the copy submitted.

In the unlikely event that the author did not send a complete manuscript and there are missing pages, these will be noted. Also, if material had to be removed, a note will indicate the deletion.



UMI 3385187

Copyright 2009 by ProQuest LLC.

All rights reserved. This edition of the work is protected against unauthorized copying under Title 17, United States Code.



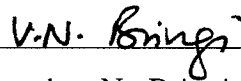
ProQuest LLC
789 East Eisenhower Parkway
P.O. Box 1346
Ann Arbor, MI 48106-1346

COLORADO STATE UNIVERSITY

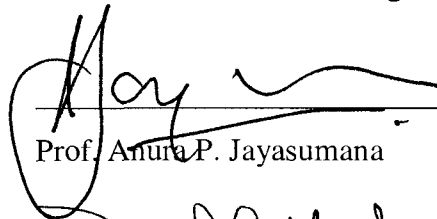
June 24, 2009

WE HEREBY RECOMMEND THAT THE DISSERTATION PREPARED UNDER OUR SUPERVISION BY AMIN ALQUDAH ENTITLED RAINFALL ESTIMATION FROM SPACEBORNE AND GROUND BASED RADARS USING NEURAL NETWORKS BE ACCEPTED AS FULFILLING IN PART REQUIREMENTS FOR THE DEGREE OF DOCTOR OF PHILOSOPHY.

Committee on Graduate Work



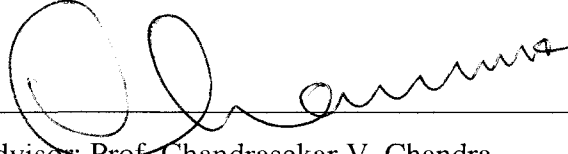
Prof. Viswanathan N. Bringi



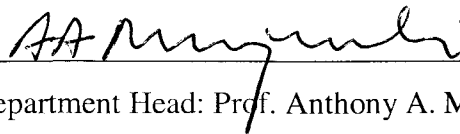
Prof. Anura P. Jayasumana



Prof. Darrell G. Fontane



Advisor: Prof. Chandrasekar V. Chandra



Department Head: Prof. Anthony A. Maciejewski

ABSTRACT OF DISSERTATION

RAINFALL ESTIMATION FROM SPACEBORNE AND GROUND BASED RADARS USING NEURAL NETWORKS

Rainfall observed on the ground is dependent on the four dimensional radar observations. However it is difficult to express this in a simple form. The key challenge in radar rainfall estimation is the space-time variability in precipitation microphysics, such as DSD and drop shapes. A simple Z-R relation is not sufficient and has large uncertainty and it needs to be adaptively adjusted. Prior research has shown that neural networks can be used to estimate ground rainfall from radar measurements. Neural network is a nonparametric method to represent the relationship between radar measurements and rainfall rate. The usefulness of the neural network is subject to many factors such as the representativeness and sufficiency of the training data set, the generalization capability of the network, seasonal changes, and regional changes. Tropical Rainfall Measuring Mission (TRMM) Precipitation Radar (PR) is the first space borne observation platform for mapping precipitation over the tropics. TRMM measured rainfall is important in order to study the precipitation distribution all over the globe in the tropics. TRMM ground validation is a critical important component to ensure the measurement accuracy. However, this ground validation has quite different characteristics from TRMM in terms of resolution, scale, viewing aspect, and

uncertainties. This makes the use of ground radar rainfall information to correct TRMM rainfall estimates a very challenging task. In this dissertation, rainfall estimation using neural networks is investigated in order to improve rainfall estimation based on measurements taken by ground radars and TRMM PR. Ground Radar measurements will be used to estimate rainfall using adaptive neural network techniques. Improvements are also suggested and performed including the use of Principal Components Analysis, ensemble average neural network technique, and the use of Bayesian Neural Networks. For TRMM-PR purposes a single neural network is not efficient to extract the relation between TRMM-PR measurements and the rain gauges; this is because of the resolution differences between TRMM-PR profile and the rain gauges and the low number of TRMM overpasses over these gauges which will make the training data set to have less number of profiles and not be able to generalize. Therefore, a novel hybrid Neural Network model is presented to train ground radars for rainfall estimate using rain gauge data and subsequently the trained ground radar rain estimates to train TRMM PR based Neural Networks for rainfall estimation. This hybrid neural network model will derive the relation between rain gauges and ground radar measurements, and transfer this relation to adaptive rainfall estimation for TRMM PR in order to estimate rainfall and generate global rainfall maps.

Amin Alqudah
Department of Electrical and Computer Engineering
Colorado State University
Fort Collins, Colorado 80523
Summer 2009

ACKNOWLEDGEMENTS

First of all, I would like to thank God for everything. I also would like to thank all the people who helped me during this work. I am especially thankful to my advisor, Dr. V. Chandrasekar, for his kindness, support, guidance and encouragement during my graduate study. Also, I would like to thank Dr. V. Bringi, Dr. Anura P. Jayasumana and Dr. D. G. Fontane for agreeing to be on my dissertation committee and reviewing my dissertation.

I would like also to extend my gratitude to the crew at the Radar and Communication Lab at Colorado State University for the help given to me during the various stages of my dissertation.

I would like also to thank my parents, brothers and sisters for their love and support while I was far away from home. Finally, I would like to thank my wife, Ayat Alsmadi and my daughter Afnan for all their love, support and encouragement over the years and while doing my dissertation.

DEDICATION

To...

*My beloved parents, wife, sons, daughters, brothers and
sisters.*

TABLE OF CONTENTS

Abstract of Dissertation	iii
Acknowledgements	v
Dedication	vi
CHAPTER 1.....	1
INTRODUCTION.....	1
1.1 Introduction.....	1
1.2 Literature Review.....	3
1.2.1 Rainfall Estimation Based On Ground Radar Measurements.....	3
1.2.2 Rainfall Estimation Based On Space Borne Radar Measurements.....	5
1.3 Problem Statement.....	6
1.3.1 Research Question.....	8
1.4 Objectives of the Research.....	8
CHAPTER 2.....	11
BACKGROUND.....	11
2.1 Rain Rate Estimation.....	11
2.2 Radar Reflectivity Factor and Rain Rate Estimate.....	12
2.3 Weather Surveillance Radar: WSR-88D.....	13
2.3.1 Introduction.....	13
2.3.2 Weather Radars.....	14
2.3.3 WSR-88D System Overview.....	14
2.3.4 Scanning Strategies.....	16
2.3.5 NEXRAD Rainfall Rate Estimate	17
2.4 Rain Gauge Data Source.....	18
2.5 Evaluation of the Z-R Relation against the Rain Gauge Measurement around KMLB and KHGX Sites	19

CHAPTER 3.....	33
TROPICAL RAINFALL MEASURING MISSION (TRMM)	33
3.1 Introduction.....	33
3.2 TRMM Instruments.....	33
3.3 TRMM Measurement Levels.....	35
3.3.1 Level-1.....	36
3.3.2 Level-2.....	38
3.3.3 Level-3.....	39
3.4 TRMM-PR Description.....	39
3.4.1 TRMM –PR Overview.....	39
3.4.2 TRMM-PR Rain Rate Estimation.....	41
3.5 TRMM Validation.....	45
3.5.1 TRMM-PR Measured Reflectivity/Estimated Rain Rate Validation.....	46
 CHAPTER 4.....	 54
RAIN RATE ESTIMATION USING NEXRAD GROUND RADAR MEASUREMENTS BASED ON NEURAL NETWORK.....	 54
4.1 Introduction.....	54
4.2 Radial Basis Function Neural Network.....	55
4.2.1 RBF Neural Network Architecture.....	56
4.2.2 Input/Target of the RBF Neural Network.....	57
4.2.3 Training the RBF Neural Network.....	58
4.2.3.1 Finding the Optimal Centers and their Sizes.....	58
4.2.3.2 Finding the Optimal Weights.....	59
4.2.3.3 Adaptively Training the RBFNN.....	61
4.2.3.4 Pruning the RBFNN.....	62
4.3 Performance Evaluation of the Adaptive Radial Basis Function Neural Network.....	 64
4.3.1 Training the Network.....	64
4.3.2 Testing and Validating the Network.....	65

4.3.3 Performance Evaluation.....	65
4.3.4 Testing the Designed Network with Alternative Radar/Gauge Data.....	77
4.3.5 Effect of Radar Measurement Heights on Rain Rate estimation Using Neural Networks.....	77
4.4 Using Principal Component Analysis to Improve the Performance of the RBF NN	82
4.4.1 Principal Component Analysis.....	82
4.4.2 Performance Evaluation of RBF NN Using PCA	84
4.5 Using Bayesian Neural Network to Improve Rainfall Estimation.....	88
4.5.1 Introduction.....	88
4.5.2 Multilayer Perceptrons Neural Network Architecture.....	89
4.5.3 Bayesian Neural Network Development.....	90
4.5.4 Performance of the Bayesian Neural Network.....	92
4.6 Using Ensemble Average Neural Network Technique to Improve Rainfall Estimation.....	96
4.6.1 Introduction.....	96
4.6.2 Ensemble Method.....	97
4.6.3 Performance of the Ensemble Average Neural Networks.....	98
4.7 Validation Against TRMM Ground Validation at KWAJ site.....	101
4.7.1 TRMM Ground Validation.....	101
4.7.2 Validation against KWAJ Radar Rainfall Estimate.....	102
CHAPTER 5.....	105
RAIN RATE ESTIMATION USING TRMM-PR MEASUREMENTS BASED ON NEURAL NETWORK.....	105
5.1 Introduction.....	105
5.2 Two-Stage Neural Network for TRMM-PR Rainfall Estimation.....	106
5.3 Development of the Hybrid Neural Network Technique for TRMM-PR Rainfall Estimation.....	107
5.3.1 Ground Validation Neural Network Design.....	107

5.3.2 TRMM-PR and Ground Radar Data Alignment.....	108
5.3.3 Designing TRMM-PR Neural Network.....	110
5.3.4 Product Validation.....	111
5.3.5 Results and Evaluation.....	112
5.3.6 Testing Each Network with Alternative Radar/Gauge Data.....	122
5.3.7 Rainfall Maps Generation.....	125
5.3.8 Rainfall Maps Generation Using Alternative Site's Neural Network.....	131
5.3.9 Rainfall Maps Generation Using Data from Other NEXRAD Sites.....	138
5.4 Global Rainfall Maps Generation	145
 CHAPTER 6.....	 175
SUMMARY AND FUTURE WORK.....	175
6.1 Summary.....	175
6.2 Future Work.....	180
BIBLIOGRAPHY.....	182

CHAPTER 1

INTRODUCTION

1.1 INTRODUCTION

Rainfall observed on the ground is dependent on the four dimensional radar observations. However it is difficult to express it in a simple form. The key challenge in radar rainfall estimation is the space-time variability in precipitation microphysics, such as Drop Size Distribution (DSD) and drop shapes. The empirical Z - R relation is not sufficient to capture the variability and has large uncertainty and it needs to be adaptively adjusted based on validation. Prior research has shown that neural networks can be used to estimate ground rainfall from radar measurements (Xiao and Chandrasekar, 1997, Liu et al., 2001, Stefano and Isabella, 2000). Neural network is a nonparametric method to represent the relationship between radar measurements and rainfall rate. The relationship is derived directly from a dataset consisting of radar measurements and rain gauge measurements. The usefulness of the rainfall estimation using neural networks is subject to many factors such as the representativeness and sufficiency of the training dataset, the generalization capability of the network to new data, seasonal changes, regional changes, and so on.

Tropical Rainfall Measuring Mission (TRMM) Precipitation Radar (PR) is known to be the first observation platform for mapping precipitation over the tropics. TRMM is a joint mission between the National Aeronautic and Space Administration (NASA) of

the United States and the Japanese Aerospace Exploration Agency (JAXA) of Japan. TRMM measured rainfall is important in order to study the precipitation distribution all over the tropics globally. TRMM ground validation is a critically important component in TRMM system to ensure the measurement accuracy and its successful application using certain ground based weather radars and rain gauge networks of stable and sufficient quality. However, this ground validation has quite different characterizations from TRMM in terms of resolution, scale, viewing aspect, and uncertainties in the sensing environments. This makes the use of ground radar rainfall information in order to get TRMM point of view a very challenging task.

In this dissertation, rainfall estimation is investigated using neural network techniques based on measurements taken by ground radars and TRMM PR radar. Ground Radar measurements will be used to estimate rainfall using adaptive neural networks techniques. Investigations are also performed including: the use of Principal Components Analysis, the use of Bayesian Neural Networks, and the use of Ensemble Average Neural Networks Technique. For TRMM-PR purposes, a single neural network is not efficient to extract the relation between TRMM-PR measurements and the rain gauges; this is because of the resolution differences between TRMM-PR profiles and the rain gauges and the low number of TRMM overpasses over these gauges which will make the training data set to have less number of profiles and not be able to generalize. Therefore, a novel hybrid Neural Network model is presented to train ground radars for rainfall estimate using rain gauge data and subsequently the trained ground radar rain estimates as target to train TRMM PR based Neural Networks for rainfall estimation. This hybrid

neural network model will derive the relation between rain gauges and ground radar measurements, and transfer this relation to adaptive rainfall estimation for TRMM precipitation radar. The main product of this technique is to produce local and instant rainfall rate maps as well as global rainfall accumulation maps.

1.2 LITERATURE REVIEW

Rainfall estimation based on radar measurements has been an important topic in radar meteorology for decades. This research problem has been addressed using a parametric approach where a simple Z-R relation is used to estimate rainfall from radar reflectivity factor. This approach is also used in TRMM-PR algorithm to estimate rain rate where different Z-R relations are used based on the rain type and height. Neural Networks technique was introduced to address this problem by taking into account the three-dimensional (3-D) structure of the radar observations. Many approaches were tried to improve rainfall estimation using either ground radar measurements or TRMM measurements. These approaches are presented in this section.

1.2.1 RAINFALL ESTIMATION BASED ON GROUND RADAR MEASUREMENTS

Neural network technique to estimate rainfall on the ground from radar observations was introduced by (Xiao and Chandrasekar, 1997). That neural network technique was tested using data set gathered during a few storm events. The neural network developed in that time was a multilayer perceptron network MLP which was not best suited for long term applications such as over months and years because of the long time it takes to train the network. Another attempt came later where an adaptive Radial

Basis Function (RBF) neural network was developed for radar rainfall estimation based on horizontal reflectivity profiles (Liu et al, 2001). Although the network was adaptively trained and tested on large data sets with reasonable computations, that adaptive RBF technique used a 9-point input vector sampled on a horizontal plane; which increases the complexity of a neural network, and ignores other weather data within the rain region. This issue (network complexity) was investigated later by (Li, et al., 2003) and it was shown that reducing the size of the input vector will reduce the complexity of the designed network without having significant effect on the estimation. Another attempt to improve the adaptive technique mentioned above was done by (Li and Chandrasekar, 2002). The improvement was done through a classification network, where a limit on the rainfall estimate was performed in order not to overestimate the rain rate.

Rainfall estimation using Neural Networks has also been done by (Orlandini and Morlini, 2000); different neural network architectures were tried in order to get good rainfall estimate. They explored the capabilities of three artificial neural networks in order to identify and reproduce the functional relationship between Z and R . The three networks that were used were multilayer perceptron (MLP), Bayesian network, and radial basis function network. Results using these three networks were good compared to Z - R relation. A weakness in their work was that all networks were not adaptive; the networks need to be retrained from the beginning each time new data became available, making it a time consuming process especially if data sets of a year or more need to be processed. This was already solved in the previous group (Liu et al, 2001) where adaptively training the neural network was started.

Another investigation to enhance rainfall estimation using neural network technique was also done by (Teschl et al., 2007). This group added the height of precipitation as another input to the neural network, and they used MLP network to do the estimation. This addition (the height of precipitation) was studied by (Li et al., 2003), and it was shown that radar measurements up to 4 km in height is enough to give good rainfall estimation based on neural networks.

1.2.2 RAINFALL ESTIMATION BASED ON SPACE BORNE RADAR MEASUREMENTS

In contrast to estimating rainfall based on ground radar measurements using neural network; there is not much research done to do so based on TRMM-PR measurements. In the year TRMM was launched, (Tsintikidis et al., 1997) used an MLP neural network to do rainfall estimation where the input was the brightness temperature (BT) obtained from the Special Sensor Microwave/Imager (SSM/I) instrument (Hollinger et al., 1990) onboard the F10 and F11 satellites launched in 1987 as part of the Defense Meteorological Satellite Program (DMSP). The input vector of the network was the (BT) which has low resolution especially at the low frequency measurements (25 x 25 km at the low frequencies and 12.5 x 12.5 at the high frequencies) which makes it difficult and potentially inaccurate to validate against rain gauges. Using this technique would be again inaccurate and inconvenient to use with the Microwave Imager on top of TRMM (TMI) for the same resolution issue (7 x 5 km at the high frequencies and 37 km x 63 km at the low frequencies (Viltard et al., 2006)).

The same technique used in (Tsintikidis et al., 1997) was also used by (Gairola et al., 2001) and (Tapiador, et al., 2004) and was applied on TRMM data to estimate rain rate from brightness temperature. In these two latter works, neither one used the rain gauge to validate against. In (Gairola et al., 2001) the validation was against PR rain rate product (2A25 TRMM product), while in (Tapiador, et al., 2004) the validation was against rain rate estimated using a Bayesian approach (2A12 TRMM product) for previously calculated profiles using the Goddard Profiling (GPROF) algorithm (Kummerow et al. 1996). This makes the estimation and validation not complete enough because the validation in both techniques was based on calculated estimates (2A25 and 2A12 TRMM products).

1.3 PROBLEM STATEMENT

There is a recognized need to accurately estimate rainfall on a variety of temporal and spatial scales. There are many real life aspects and applications that would depend on rainfall estimation: including climate monitoring, severe weather and flood warnings, river monitoring and control as well as numerical weather prediction models initialization and verification (Ebert and Le, 1995). In addition, other areas like agriculture would depend on the weather conditions in general and on rainfall in particular (Barrett and Martin, 1981).

Rainfall on the ground is dependent on the four dimensional radar observations. The relation between the rain rate on the ground and the four-dimensional radar observations is difficult to express in a simple form. The key challenge in radar rainfall

estimation is the space-time variability in precipitation microphysics, such as DSD and drop shapes. Empirical Z - R relation is not sufficient to capture the variability and has a large uncertainty and needs to be adaptively adjusted based on validation.

Prior research has shown that neural networks can be used to estimate ground rainfall from radar measurements. The usefulness of the rainfall estimation using neural networks is subject to many factors such as the representativeness and sufficiency of the training dataset, the generalization capability of the network to new data, seasonal changes, and regional changes. Therefore, improving the performance of a neural network technique to use in rainfall estimation based on ground radar measurements and rain gauges is a very important topic for decades.

TRMM Precipitation Radar (PR) is a unique instrument, capable of providing high resolution vertical profile of precipitation. However, fundamental challenges exist in performing TRMM ground validation. The horizontal resolution of TRMM PR is about 5km; much coarser when compared to rain gauges in the spatial scale. Another challenge is that during a single weather event, available data pairs for comparison (TRMM vertical profile of reflectivity versus rain gauge measurement) are scarce because of TRMM's limited overpasses. It is impractical to deploy a dense gauge network for TRMM PR validation.

1.3.1 RESEARCH QUESTION

The main goal of this research is to use and to improve the use of neural networks techniques in ground rainfall estimation using ground radar /satellite radar measurements.

This study attempts to address the following question:

“How much can we improve ground rainfall estimation compared to rain gauge measurements using ground and/or satellite radar measurements, rain gauge measurements and neural networks, taking into considerations the time/complexity issues of the designed network?”

1.4 OBJECTIVES OF THE RESEARCH

The following points summarize the objectives of the research in this dissertation.

- **Estimate Rainfall from ground radar measurements using neural networks:**
 - Examine the effect of the radar vertical profile height on rainfall estimation using neural networks.
 - Improve rainfall estimation using neural networks and compare it against rain gauge measurements and against other empirical and statistical estimators like Z-R relation and the best fit method.
 - Validate the performance of the proposed method using different datasets from different years and different locations.

- Improve the performance of the proposed neural network method by input conditioning using methods such as “Principal Component Analysis” (PCA) concept.
- Improve the rainfall estimation by applying other Neural Network architecture such as “Bayesian Neural Networks”.
- Improve the rainfall estimation by applying “Ensemble Average Neural Networks” technique.
- **Estimate Rainfall from satellite radar measurements (TRMM-PR) using neural networks:**
 - Estimate rainfall from TRMM-PR measurements using a novel hybrid neural network technique.
 - Improve rainfall estimation using neural networks and compare it against rain gauge measurements and against TRMM rain rate estimate products.
 - Validate the performance of the proposed technique using different datasets from a variety of years and different locations.
- **Generate Rainfall maps based on radar/satellite measurements using neural network estimators.**
 - Generate local and instantaneous rainfall maps by ground radar measurements.
 - Generate local and instantaneous rainfall maps by using TRMM-PR radar measurements.

- Compare the maps generated by both neural network estimators against maps generated by TRMM product.
- Generate global rainfall accumulation maps by using TRMM-PR radar measurements using the hybrid neural network.

CHAPTER 2

BACKGROUND

2.1 RAIN RATE ESTIMATION

Relationships of radar reflectivity factor Z with rain rate R are established through measurements of rain drop size distributions (DSD). Rain rates are either measured by rain gauge or estimated from the observed drop size distributions. A widely used DSD is the Marshall-Palmer DSD (Marshall, and Palmer, 1948) which has a one-parameter exponential expression as the following,

$$N(D) = N_0 \exp(-\Lambda D) \quad (2.1)$$

where $N(D)$ ($m^{-3}mm^{-1}$) is the number of raindrops per unit volume per unit size in diameter interval D (mm) and $D + \Delta D(mm)$, $N_0 = 8000 m^{-3}mm^{-1}$, and Λ is related to D_0 by

$$\Lambda = \frac{3.67}{D_0} \quad (2.2)$$

where D_0 (mm) is the median volume diameter and defined such that all drops up to size D_0 contribute to half of the rainwater content.

Rain rate which can be defined as the measure of the intensity of rainfall by calculating the amount of rain that would fall over a given interval of time if the rainfall intensity were constant over that time period. The rate is typically expressed in terms of length (depth) per unit time, for example, millimeters per hour, or inches per hour. Rain rate can be computed as the third moment of $N(D)$ as follows,

$$R = \frac{\pi}{6} \int_0^{\infty} D^3 N(D) v(D) dD \quad (2.3)$$

where $v(D) = 17.67D^{0.67}$ is the raindrop terminal velocity (D in centimeter) (Atlas, and Ulbrich, 1977). Marshall and Palmer in (Marshall, and Palmer, 1948) found that $\Lambda = 4.1 R^{-0.21} mm^{-1}$ to be good over a wide range of rain rates, but other values also have been reported in (Louis, 1973).

2.2 RADAR REFLECTIVITY FACTOR AND RAINRATE ESTIMATE

In Rayleigh scattering, where the drop diameter is much less than the wavelength, the radar reflectivity factor Z can be defined as the sixth moment of $N(D)$ (Atlas and Ulbrich, 1977) as follows:

$$Z = \int_0^{\infty} D^6 N(D) dD \quad (2.4)$$

Using the Marshall and Palmer DSD, Z can be written as follows:

$$Z = \int_0^{\infty} N_0 \exp(-\Lambda D) D^6 dD = 6! N_0 \Lambda^{-7} (mm^6 m^{-3}) \quad (2.5)$$

and by applying $\Lambda = 4.1 R^{-0.21} mm^{-1}$ (2.5) can be reduced to a power law Z-R relation:

$$Z = aR^b \quad (2.6)$$

where the coefficients a and b are determined by least squares fit to large samples of observations of Z and R . For various data and models, a ranges from 127 to 505, while b ranges from 1.41 to 2.39. A very common pair of the coefficients a and b is $a=200$ and, $b=1.6$ (Marshall, and Palmer, 1948).

2.3 WEATHER SURVEILLANCE RADAR: WSR-88D

2.3.1 INTRODUCTION

Across the United States, various groups use the Doppler radar to gather information vital to our everyday life. From weather forecasting to emergency management, **Next generation weather Radar** or NEXRAD ensures public safety. A world wide network of 167 NEXRAD radars provides weather coverage for the entire United States and selected international locations as shown in Figure 2.1.

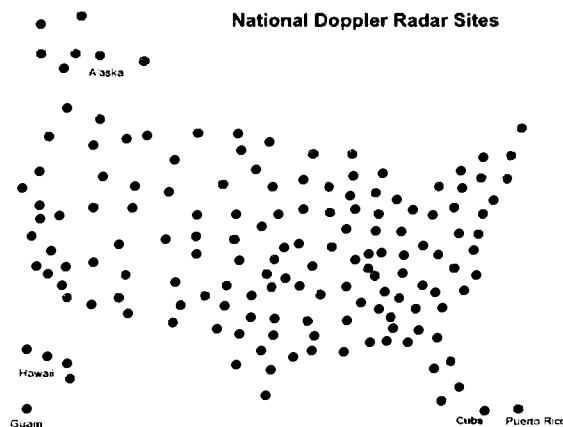


Figure 2.1: Locations of NEXRAD radars in the United States (<http://www.roc.noaa.gov>).

The formal name of NEXRAD radars is WSR-88D which stands for **W**eather **S**urveillance **R**adar established in 1988 and *D* stands for **D**oppler. The radar network is operated by the National Weather Service which is an agency of the National Oceanic and Atmospheric Administration (NOAA) and it is directly supported by a Radar Operation Center ROC in Oklahoma. The mission there is to keep the radars running smoothly and improve radar technology and capabilities to maintain peak performance from all radars.

2.3.2 WEATHER RADARS

The radar collects data by sending a radio signal out to a target. The signal bounces off the target (raindrops in this case) and returns to the radar. The returned signal conveys three important properties of the target. The first is the time it takes the signal to bounce off the target and return determines the distance from the target to the radar and the location of the storm. Second is the strength of the returned signal also known as reflectivity, is proportional to the size and number of raindrops (DSD) in the storm. Third is the frequency shift of the returned signal reveals whether the winds are moving toward or away from the radar, as well as their speeds. The data is converted into visual images and used by the National Weather Service forecasters.

2.3.3 WSR-88D SYSTEM OVERVIEW

The WSR-88D system generates three basic meteorological radar quantities mainly: radar reflectivity, mean radial velocity and spectrum width. Using these basic quantities, WSR-88D system generates numerous analysis of meteorological products.

There are three major functional components of the WSR-88D system, The RDA (Radar Data Acquisition), the RPG (Radar Products Generator) and the PUP (Principal User Processor). Detailed description of these components can be found in (<http://www.roc.noaa.gov/eng/nexradtech.asp>).

The RDA considered as the information gathering component of the system, and it is composed of four primary components which are the antenna, the transmitter, the receiver and the signal processor. The RDA component transfer the measured information about the base data (radar reflectivity, mean radial velocity and spectrum width) to the next component (RPG) where this information is temporarily stored to be used by the algorithms that reside at the RPG.

The RPG takes the base data and generates user requested meteorological and hydrological products. The RPG calls analysis programs (algorithms) that convert the base data from RDA into different meteorological and hydrological products. These products are stored so that they can be used by the users. The RPG also passes these products to the PUP component where they will be displayed and analyzed to be shown to the meteorologist. Table 2.1 shows some of the technical characteristics of WSR-88D or NEXRAD system.

Table 2.1: NEXRAD Radar Characteristics (http://trmm-fc.gsfc.nasa.gov/trmm_gv).

Type	S-band
Antenna size	8.53 m
Beam width	0.88-0.96 deg
Gain at 2850 MHz	45.5 dB
Wave length	10.0 - 11.1 cm
Peak power	750 kW (peak) 1.5 kw (Avg.)
Pulse width	1.5 - 4.5 ms
Polarization	Single, Horizontal
Range	460 km
Frequency	2.7-3.0 GHz
Sensitivity	10 dBZ
Normal Scan	+0.5 to +19.5 Degree
Range increment	250 m
Azimuth increment	1 deg

2.3.4 SCANNING STRATEGIES

The antenna of the WSR-88D radar continuously scans the atmosphere in a sequence of 360° in the azimuth at various elevation angles. The antenna has two different patterns of scans and they are done alternatively based on the status of the atmosphere (Precipitation/No precipitation). In the “No precipitation” case or the “Clear air” mode, the antenna completes 360 in the azimuth in ten minutes at five elevation angles (0.5° to 4.5°). In the “Precipitation mode”, the antenna completes 360° in the azimuth in five minutes at 14 elevation angles (0.5° to 19.5°). Figure 2.2 shows the beam width and the height above the earth surface as a function of range for the five and fourteen elevation angles (both Precipitation/No precipitation modes).

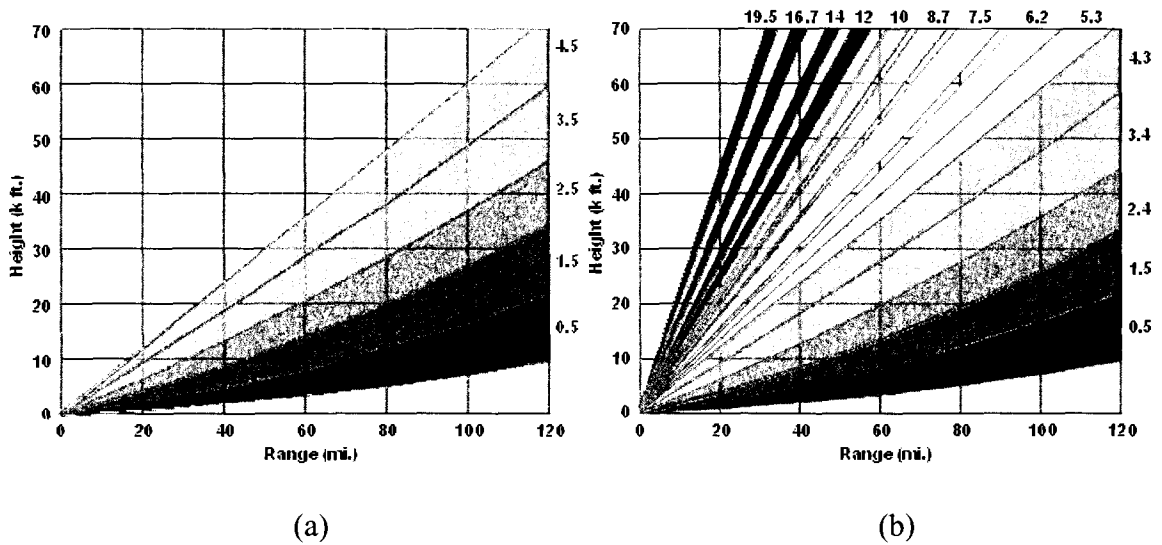


Figure 2.2: Beam width and height above the earth surface as a function of range for the (a) five elevation angles (No precipitation modes) and (b) for the fourteen elevation angles (Precipitation).
 (Adopted from: <http://www.desktopdoppler.com/help/nws-nexrad.htm>).

2.3.5 NEXRAD RAINFALL RATE ESTIMATE

The NEXRAD PUP system mentioned before automatically determines the rainfall rate, and produces an estimated rainfall map of its scan area (<http://www.roc.noaa.gov/eng/nexradtech.asp>). The calculations are based on a simple Z-R relation. This method of calculating the rainfall estimates is often in error. Error sources can be measurements of radar reflectivity factor, evaporation, variations in the DSD, and gauge- radar sampling differences. Equation (2.7) shows the Z-R relation used in NEXRAD.

$$Z = 300R^{1.4} \quad (2.7)$$

2.4 RAIN GAUGE DATA SOURCE

NEXRAD system uses a wide rain gauge network to help to do the radar calibration and Z-R relation adjustments. A rain gauge is a type of instrument used to gather and measure the amount of rain liquid over a set period of time. “Millimeter” is a common unit of measure, and when we are talking about rain rate this unit becomes Millimeter per hour. Tipping bucket gauges are commonly used in NEXRAD rain gauge networks. Rain gauges are not free of errors and limitations. Attempting to collect rain data during a very strong storm can be nearly impossible and unreliable due to wind extremes. Also, rain gauge measurements are limited to the local areas they are representing.

Five rain gauge networks were considered in this study. Three over Melbourne- FL NEXRAD site (KMLB: 28.113°N, 80.654°W), one over Houston-TX (KHGX: 29.472°N, 95.079°W), and one over Kwajalein-Marshall Islands (KWAJ: 8.7189°N, 167.7319°E). The three networks over KMLB were: South FLorida Water Management District (SFL), St. Johns Water Management District (STJ), and Kennedy Space Center (KSC). Within a 100 km radius around KMLB site, these networks have 46, 99, and 33 rain gauges, respectively. KHGX has only one rain gauge network around it, it is called: Houston-Area Raingauge (HAR) which has 160 rain gauges within a 100 km radius. KWAJ network has only 20 rain gauges and all of them are within a 100 km radius a way from the radar. Figure 2.3 shows these sites with their corresponding gauge networks.

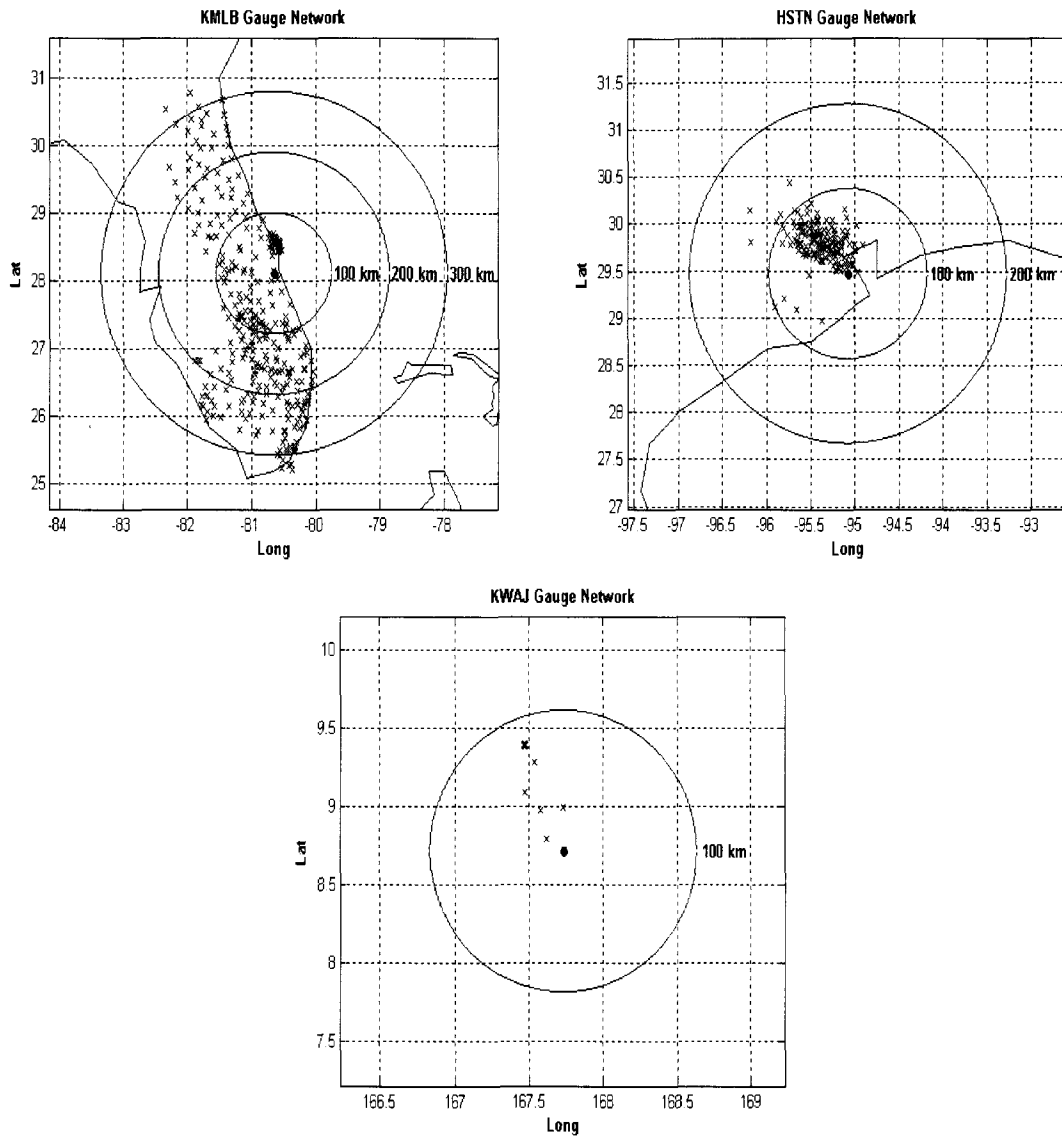


Figure 2.3: KMLB, KHGX and KWAJ gauge networks.

2.5 EVALUATION OF THE Z-R RELATION AGAINST THE RAIN GAUGE MEASUREMENT AROUND KMLB, KWAJ AND KHGX SITES

To show the importance and the need of using neural networks to estimate rain rate from ground radar measurements, the rain rate was calculated using the Z-R relation

shown in (2.7). Rain rate was also estimated using a best fit. Radar data and rain gauge observations were used during different years (2005, 2006, 2007 and 2008) over Melbourne-Florida, Houston-Texas sites, and Kwajalein-Marshall Islands. Radar data were collected by the three radars Constant Altitude Plan Position Indicator (CAPPI) scans .The lowest height of the CAPPI scans is 1 km and it was used in this regard. The horizontal resolution of the resampled desired output (radar reflectivity factor Z_h) was set to be 1x1 km. The gauge data were maintained by NASA TRMM program. As mentioned before, data within 100km radius around the site was only considered. The radar parameter of interest in this evaluation was only radar reflectivity factor Z_h at 1km height. The performance of the Z-R relation was evaluated using the following metrics:

$$FracBias = \frac{1}{Ng} \frac{\sum_{i=1}^{Ng} (RFn (i) - RFg (i))}{\overline{RFg}} \quad (2.8)$$

$$Corr = \frac{\frac{1}{Ng} \sum_{i=1}^{Ng} (RFg (i) - \overline{RFg})(RFn (i) - \overline{RFn})}{\sigma (RFg).\sigma (RFn)}} \quad (2.9)$$

$$NSE = \frac{\frac{1}{Ng} \sum_{i=1}^{Ng} |RFg (i) - RFn (i)|}{\overline{RFg}} \quad (2.10)$$

$$FRMSE = \frac{\left(\frac{1}{Ng} \sum_{i=1}^{Ng} (RFg (i) - RFn (i))^2 \right)^{1/2}}{\overline{RFg}} \quad (2.11)$$

where FracBias , Corr , NSE , and FRMSE are fractional bias, correlation, normalized standard error, and fractional root mean square error, respectively. RFn and RFg represent the estimated rainfall and the actual rain gauge, respectively, and Ng is the size of the data.

Hourly rainfall accumulation comparisons are shown in the scatter plots in Figures 2.5, 2.6, 2.7, 2.10, 2.12, 2.13, 2.14, 2.16 and 2.17, in the standard deviation plots in Figures 2.11, 2.15 and 2.18, and in Tables 2.2, 2.3, 2.4, 2.6, 2.7, 2.8, 2.9, 2.10 and 2.11. As it can be seen in the simple Z-R relation shows a poor performance compared with the best fit technique used when they were both compared with the gauge. The best fit was done adaptively “after the fact” in order to find the best fit parameters of the Z-R relation “a” and “b”. The simple Z-R relation shows a poor performance in terms of all the evaluation parameters used. The best fit estimation showed better estimate, and our goal later is to have a neural network technique to seek or improve upon the best fit performance. The results show how the bias of the simple Z-R relation was significant; the correlation was not good enough, which would make the other evaluation parameters (NSE and the FRMSE) large. The same conclusion was seen for the instantaneous rain rate comparisons in Figures 2.4, 2.8 and 2.9 and Table 2.5; it is easy to see that a simple Z-R relation is not able and not enough to capture the variations in the rain gauge. It is worth mentioning that the simple Z-R relation was underestimating the rain rate in comparison with the corresponding rain gauge most of the times.

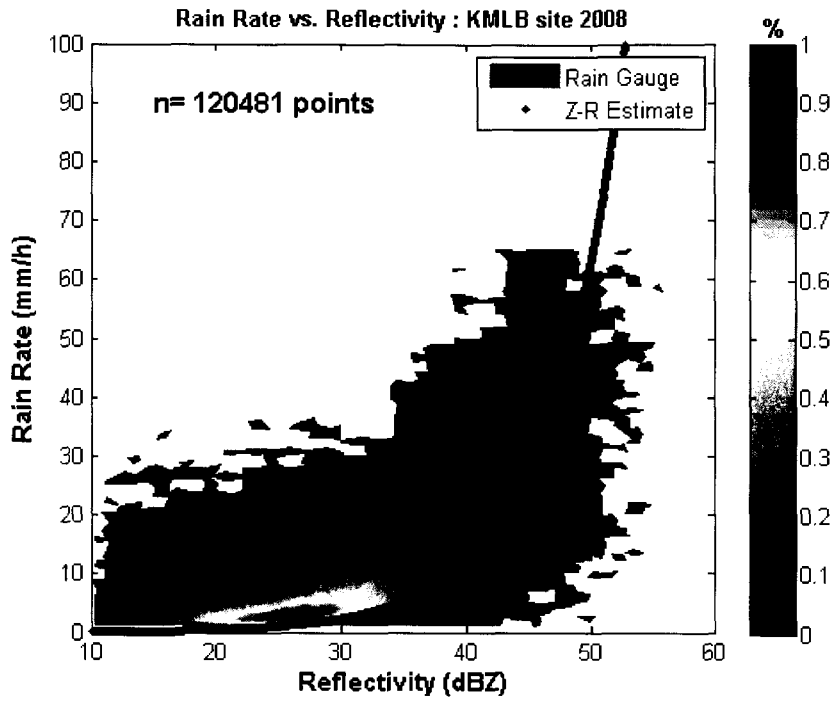
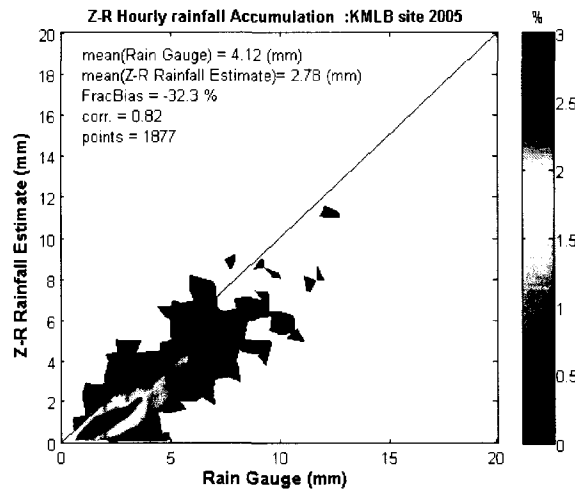


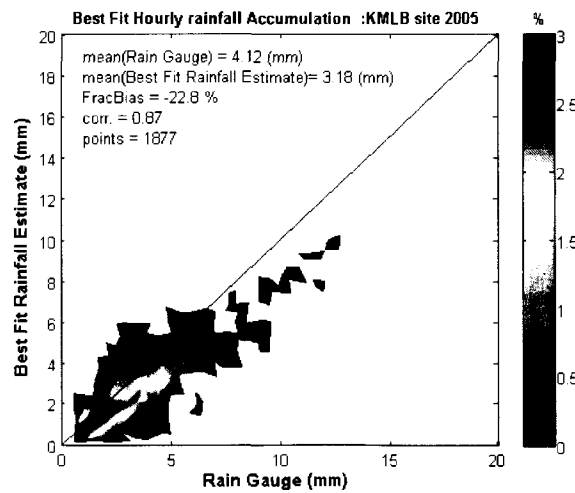
Figure 2.4: Z-R rain rate estimate and Rain gauge vs. Reflectivity. Data from year 2008 over KMLB. (Instantaneous Rainfall).

Table 2.2: Performance evaluation of the Z-R relation and the Best-Fit method used in estimating rain rate. Data from year 2005 over KMLB. (Hourly Rainfall Accumulation).

KMLB 2005	FracBias (%)	Corr.	NSE	FRMSE (%)
Z-R Est. vs. Rain Gauge	-32.3	0.82	0.40	54.3
Best Fit Est. vs. Rain Gauge	-22.8	0.87	0.30	44.0



(a)

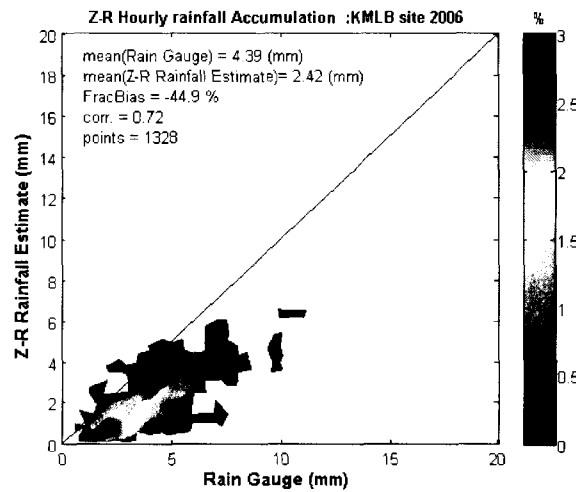


(b)

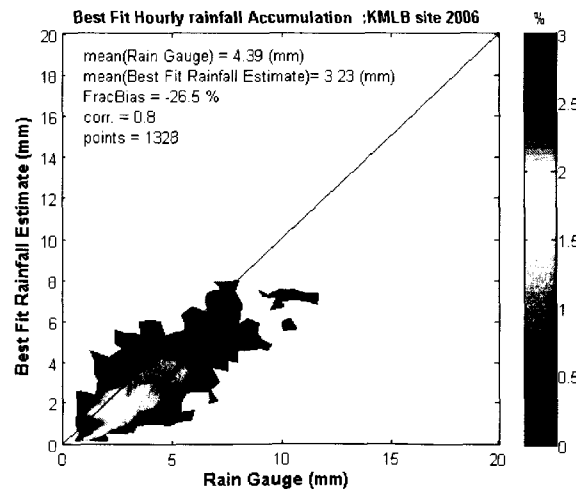
Figure 2.5: Actual rain gauge vs. a) Z-R estimate b) Best Fit estimate. Data from year 2005 over KMLB. (Hourly Rainfall Accumulation).

Table 2.3: Performance evaluation of the Z-R relation and the Best-Fit method used in estimating rain rate. Data from year 2006 over KMLB. (Hourly Rainfall Accumulation).

KMLB 2006	FracBias (%)	Corr.	NSE	FRMSE (%)
Z-R Est. vs. Rain Gauge	-44.9	0.72	0.50	68.8
Best Fit Est. vs. Rain Gauge	-26.5	0.80	0.36	51.5



(a)

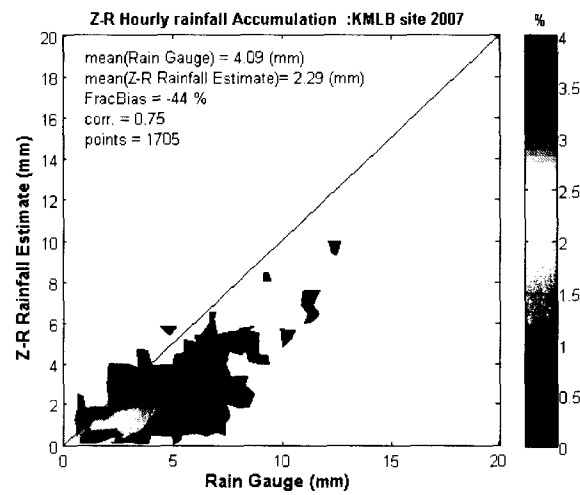


(b)

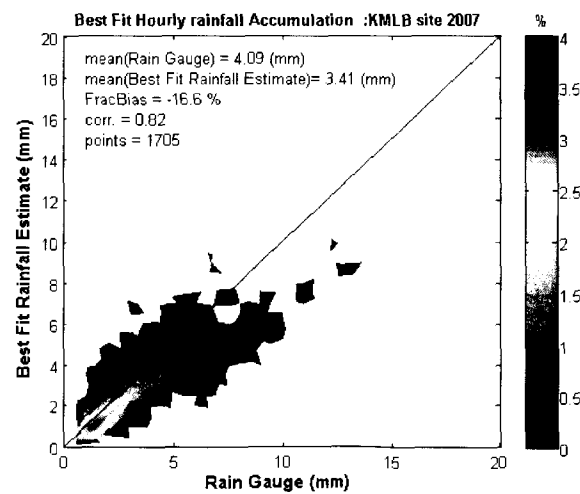
Figure 2.6: Actual rain gauge vs. a) Z-R estimate b) Best Fit estimate. Data from year 2006 over KMLB. (Hourly Rainfall Accumulation).

Table 2.4 Performance evaluation of the Z-R relation and the Best-Fit method used in estimating rain rate.
Data from year 2007 over KMLB. (Hourly Rainfall Accumulation).

KMLB 2007	FracBias (%)	Corr.	NSE	FRMSE (%)
Z-R Est. vs. Rain Gauge	-44.0	0.75	0.51	68.4
Best Fit Est. vs. Rain Gauge	-16.6	0.82	0.32	46.8



(a)



(b)

Figure 2.7: Actual rain gauge vs. a) Z-R estimate b) Best Fit estimate. Data from year 2007 over KMLB. (Hourly Rainfall Accumulation).

Table 2.5: Performance evaluation of the Z-R relation and the Best-Fit method used in estimating rain rate. Data from year 2008 over KMLB. (Instantaneous Rainfall).

KMLB 2008	FracBias (%)	Corr.	NSE	FRMSE (%)
Z-R Est. vs. Rain Gauge	-44.8	0.62	0.61	104.6
Best Fit Est. vs. Rain Gauge	-11.8	0.74	0.45	70.5

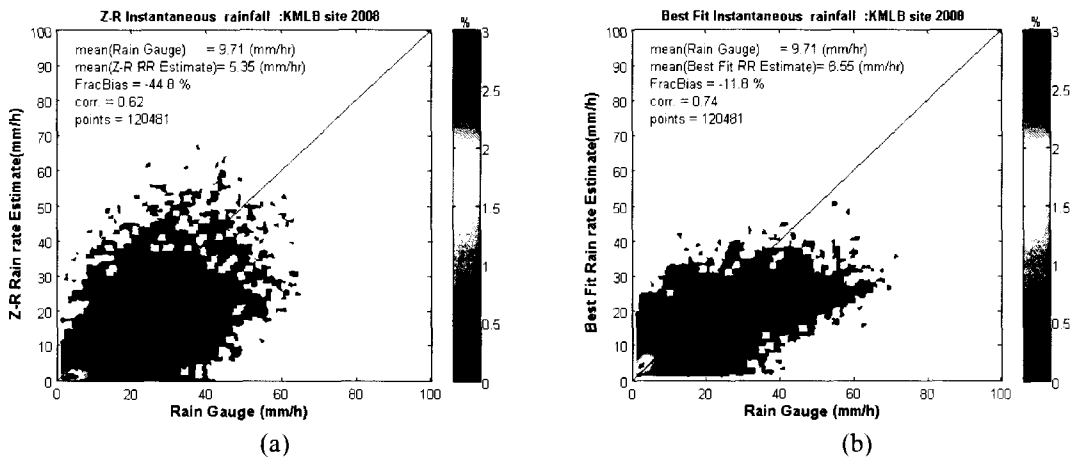


Figure 2.8: Actual rain gauge vs. a) Z-R estimate b) Best Fit estimate. Data from year 2008 over KMLB. (Instantaneous Rainfall).

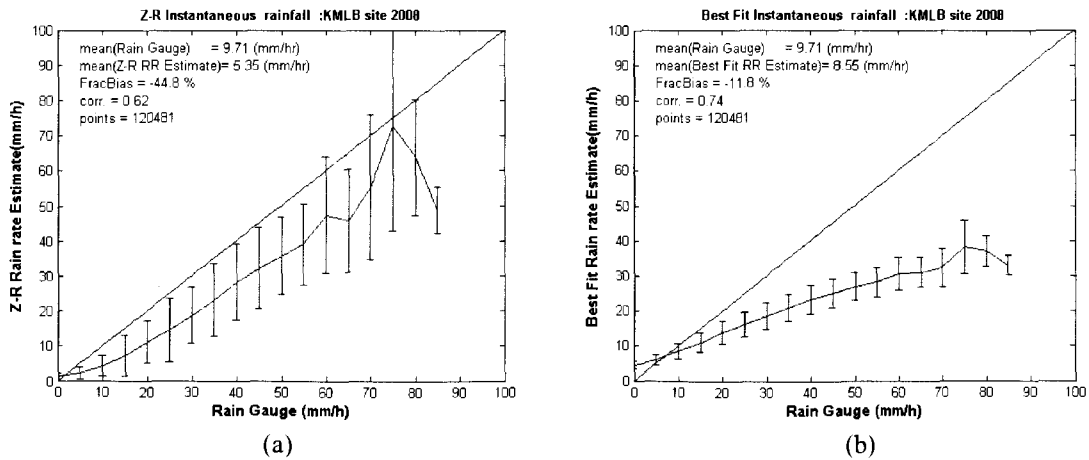


Figure 2.9: Standard deviation plot of actual rain gauge vs. a) Z-R estimate b) Best Fit estimate. Data from year 2008 over KMLB. (Instantaneous Rainfall).

Table 2.6: Performance evaluation of the Z-R relation and the Best-Fit method used in estimating rain rate. Data from year 2008 over KMLB. (Hourly Rainfall Accumulation).

KMLB 2008	FracBias (%)	Corr.	NSE	FRMSE (%)
Z-R Est. vs. Rain Gauge	-44.5	0.65	0.52	74.4
Best Fit Est. vs. Rain Gauge	-19.9	0.83	0.30	45.8

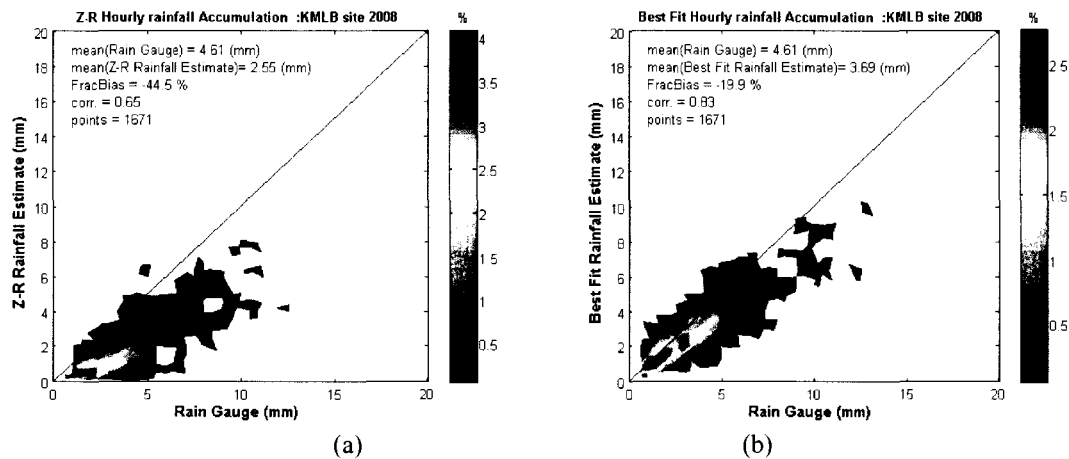


Figure 2.10: Actual rain gauge vs. a) Z-R estimate b) Best Fit estimate. Data from year 2008 over KMLB. (Hourly Rainfall Accumulation).

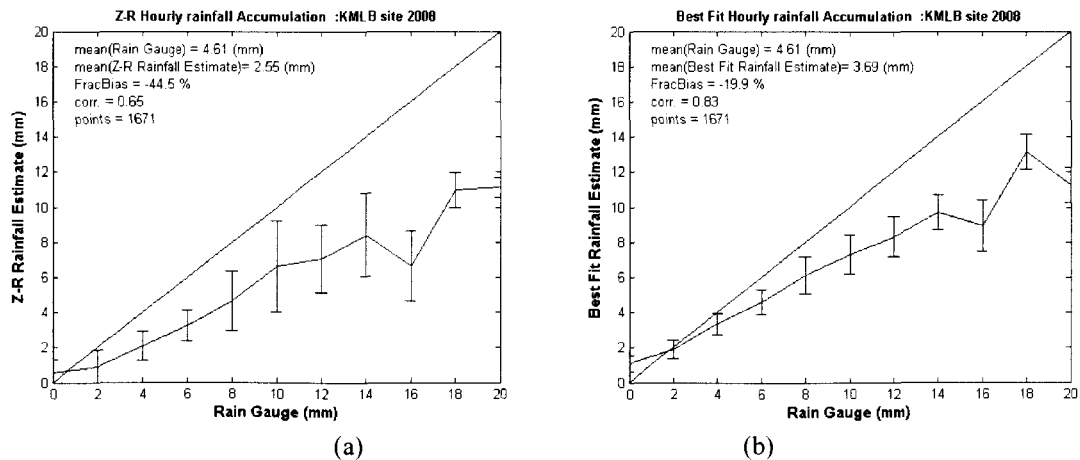
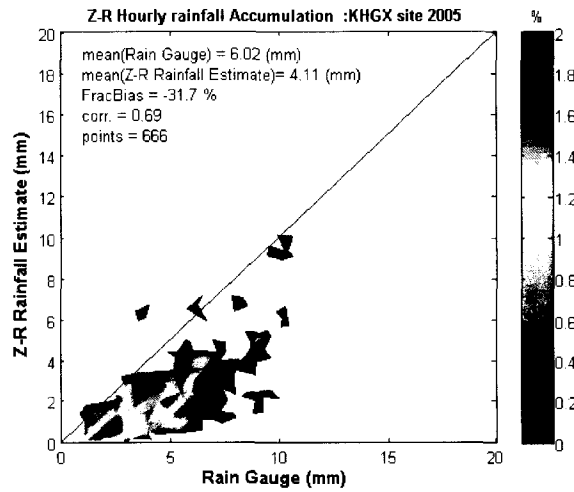


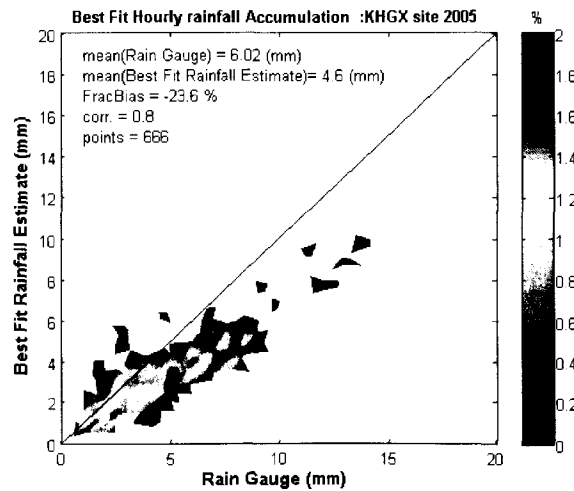
Figure 2.11: Standard deviation plot of actual rain gauge vs. a) Z-R estimate b) Best Fit estimate. Data from year 2008 over KMLB. (Hourly Rainfall Accumulation).

Table 2.7: Performance evaluation of the Z-R relation and the Best-Fit method used in estimating rain rate. Data from year 2005 over KHGX. (Hourly Rainfall Accumulation).

KHGX 2005	FracBias (%)	Corr.	NSE	FRMSE (%)
Z-R Est. vs. Rain Gauge	-31.7	0.69	0.50	69.4
Best Fit Est. vs. Rain Gauge	-23.6	0.80	0.34	44.3



(a)

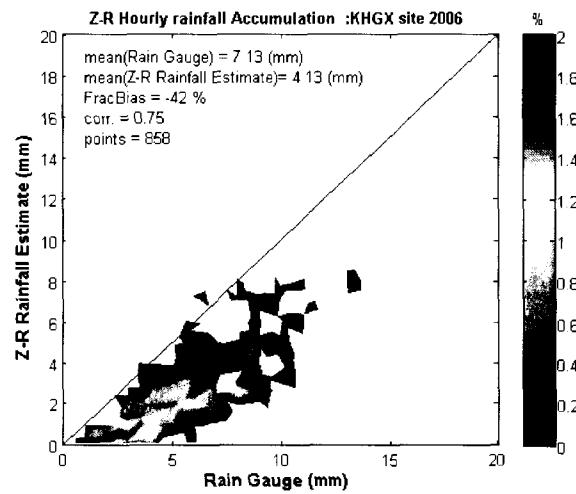


(b)

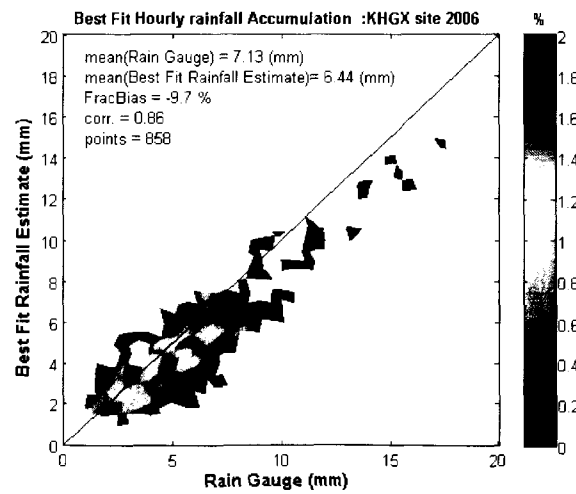
Figure 2.12: Actual rain gauge vs. a) Z-R estimate b) Best Fit estimate. Data from year 2005 over KHGX. (Hourly Rainfall Accumulation).

Table 2.8: Performance evaluation of the Z-R relation and the Best-Fit method used in estimating rain rate.
Data from year 2006 over KHGX. (Hourly Rainfall Accumulation).

KHGX 2006	FracBias (%)	Corr.	NSE	FRMSE (%)
Z-R Est. vs. Rain Gauge	-42.0	0.75	0.48	61.5
Best Fit Est. vs. Rain Gauge	-9.7	0.86	0.24	33.3



(a)



(b)

Figure 2.13: Actual rain gauge vs. a) Z-R estimate b) Best Fit estimate. Data from year 2006 over KHGX. (Hourly Rainfall Accumulation).

Table 2.9: Performance evaluation of the Z-R relation and the Best-Fit method used in estimating rain rate. Data from year 2007 over KHGX. (Hourly Rainfall Accumulation).

KHGX 2007	FracBias (%)	Corr.	NSE	FRMSE (%)
Z-R Est. vs. Rain Gauge	-46.9	0.71	0.53	67.1
Best Fit Est. vs. Rain Gauge	-19.8	0.84	0.29	38.4

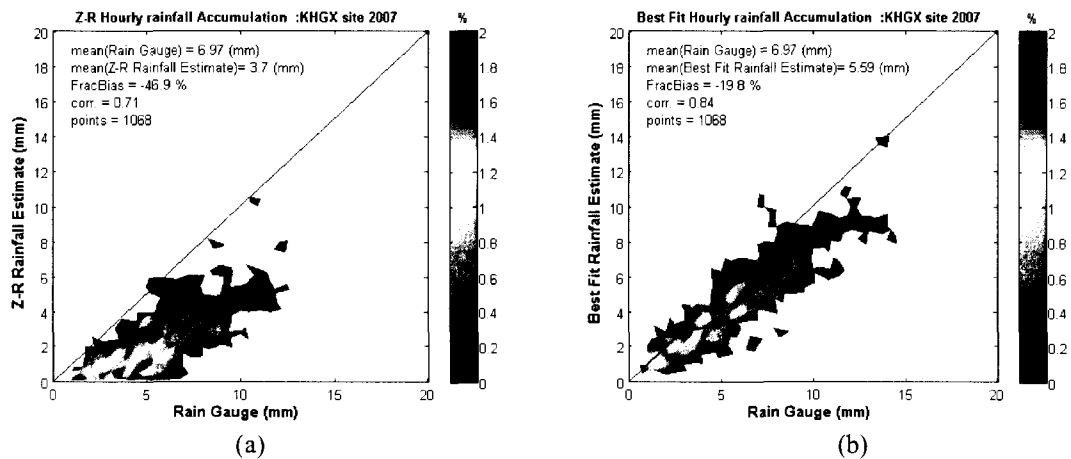


Figure 2.14: Actual rain gauge vs. a) Z-R estimate b) Best Fit estimate. Data from year 2007 over KHGX. (Hourly Rainfall Accumulation).

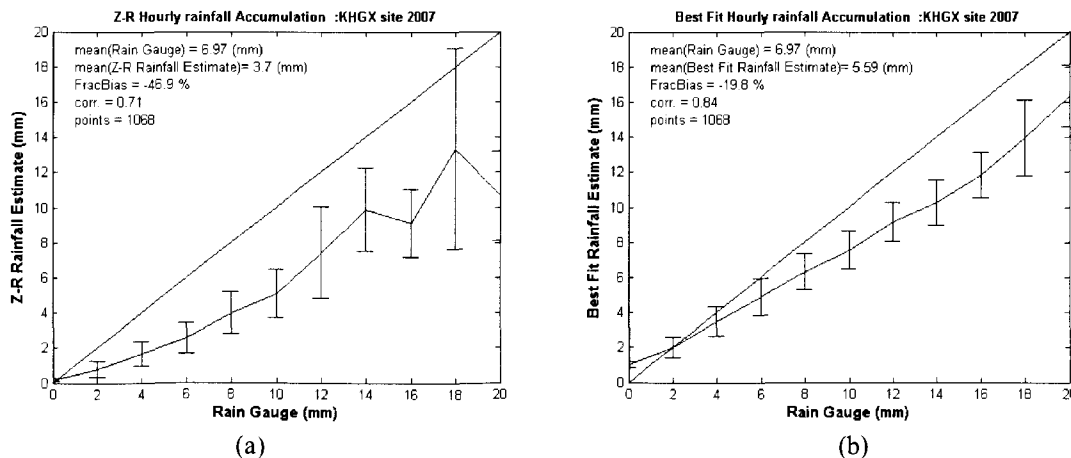
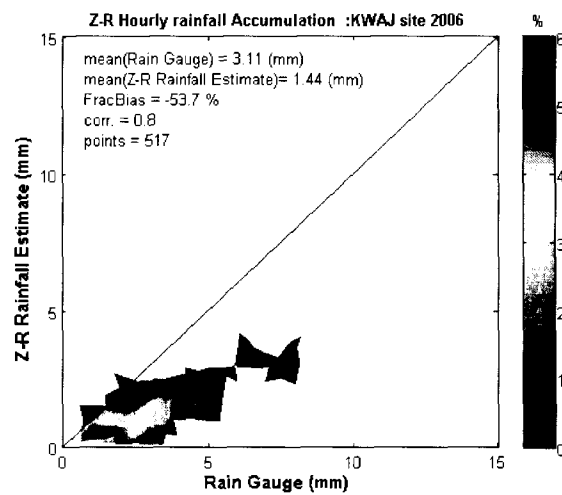


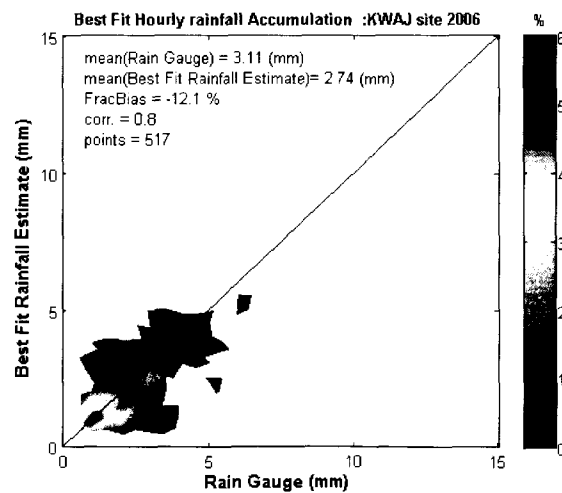
Figure 2.15: Standard deviation plot of actual rain gauge vs. a) Z-R estimate b) Best Fit estimate. Data from year 2007 over KHGX. (Hourly Rainfall Accumulation).

Table 2.10: Performance evaluation of the Z-R relation and the Best-Fit method used in estimating rain rate. Data from year 2006 over KWAJ. (Hourly Rainfall Accumulation).

KWAJ 2006	FracBias (%)	Corr.	NSE	FRMSE (%)
Z-R Est. vs. Rain Gauge	-53.7	0.80	0.57	85.3
Best Fit Est. vs. Rain Gauge	-12.1	0.80	0.37	61.0



(a)



(b)

Figure 2.16: Actual rain gauge vs. a) Z-R estimate b) Best Fit estimate. Data from year 2006 over KWAJ. (Hourly Rainfall Accumulation).

Table 2.11: Performance evaluation of the Z-R relation and the Best-Fit method used in estimating rain rate. Data from year 2007 over KWAJ. (Hourly Rainfall Accumulation).

KWAJ 2007	FracBias (%)	Corr.	NSE	FRMSE (%)
Z-R Est. vs. Rain Gauge	-53.7	0.64	0.60	83.4
Best Fit Est. vs. Rain Gauge	-0.8	0.72	0.40	60.2

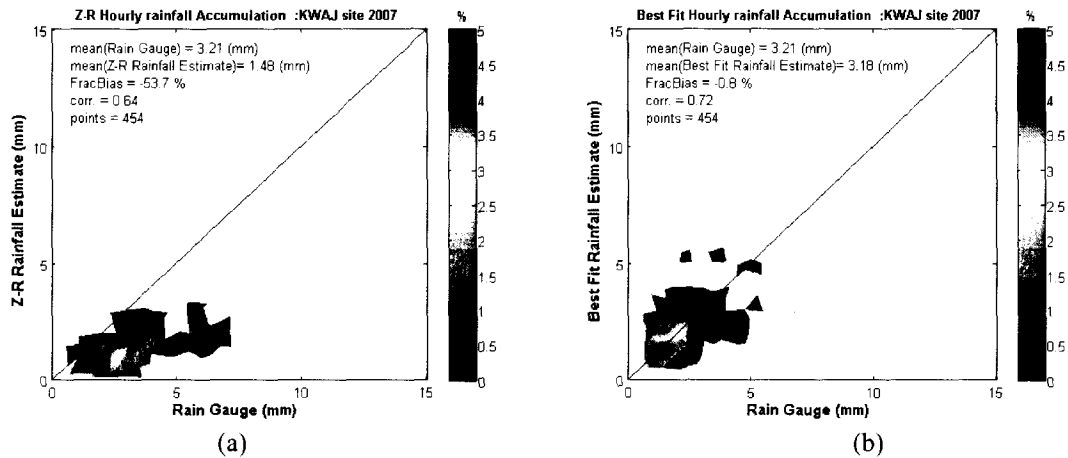


Figure 2.17: Actual rain gauge vs. a) Z-R estimate b) Best Fit estimate. Data from year 2007 over KWAJ. (Hourly Rainfall Accumulation).

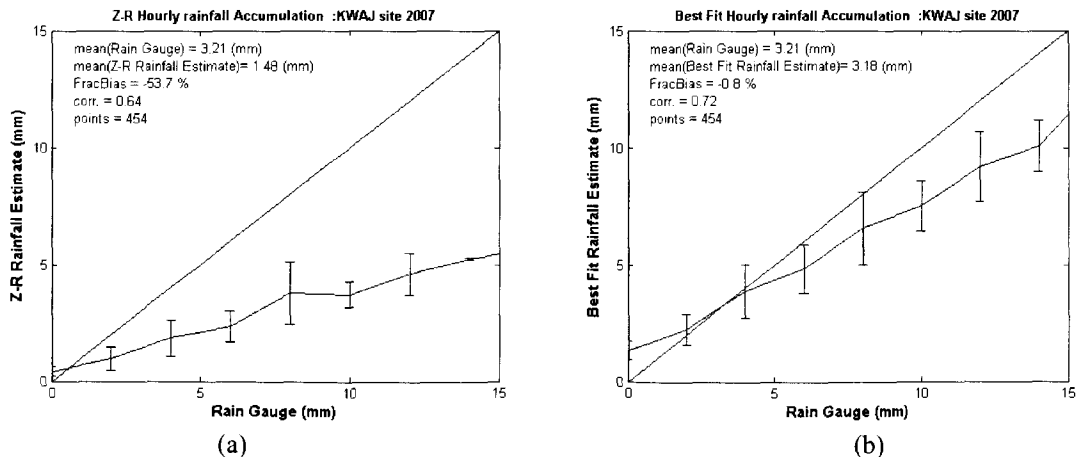


Figure 2.18: Standard deviation plot of actual rain gauge vs. a) Z-R estimate b) Best Fit estimate. Data from year 2007 over KWAJ. (Hourly Rainfall Accumulation).

CHAPTER 3

TROPICAL RAINFALL MEASURING MISSION (TRMM)

3.1 INTRODUCTION

Tropical Rainfall Measuring Mission (TRMM) is a joint mission between the National Aeronautics and Space Administration (NASA) and the Japanese Aerospace Exploration Agency (JAXA). It was launched by the H-II rocket from Tanegashima Space Center on November 28, 1997 (TRMM Manual February 2001). Its main goal is to monitor and study tropical rainfall. TRMM mainly observes rain structure, rain rate and distribution in both tropical and subtropical regions. TRMM measurements are expected to play a very important role in understanding the global climate and monitoring the environmental variation.

3.2 TRMM INSTRUMENTS

As shown in Figure 3.1, TRMM has three primary instruments namely the Precipitation Radar (PR), the TRMM Microwave Imager (TMI), and the Visible and Infrared Scanner (VIRS) (TRMM Manual February 2001), and uses the Clouds and Earth's Radiant Energy System (CERES) and the Lightning Imaging Sensor (LIS). Some of the characteristics of these five instruments are summarized in Table 3.1.

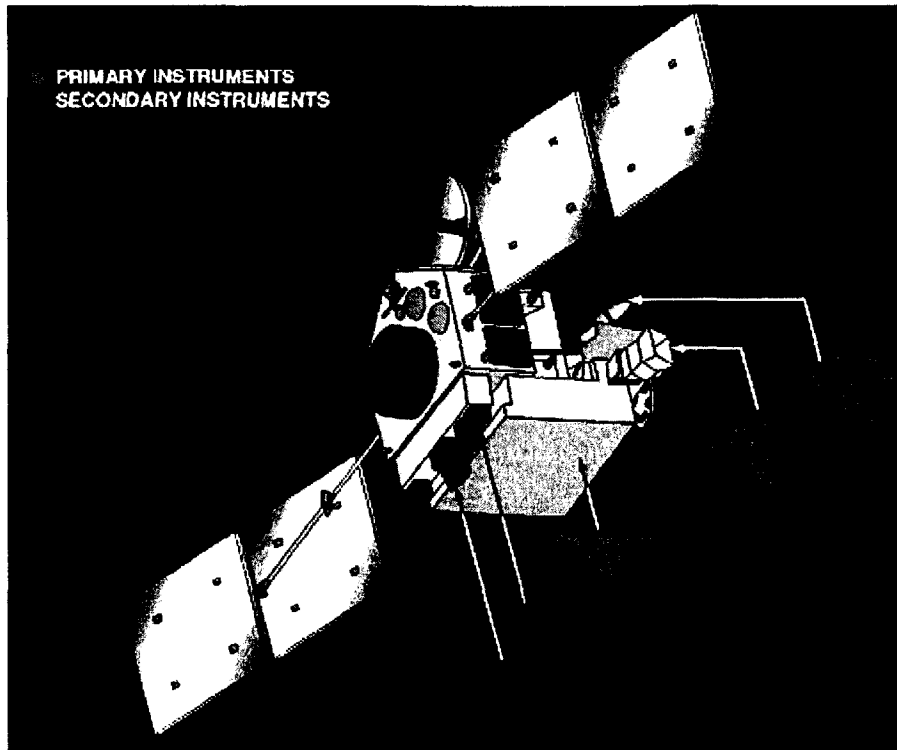


Figure 3.1: TRMM instruments. [http://nasadaacs.eos.nasa.gov/articles/2004/2004_clouds.html].

Table 3.1: TRMM instruments characteristics (TRMM Manual February 2001).

	PR	TMI	VIRS	LIS	CERES
Frequency/ Wavelength	13.8GHz	10.65, 19.35, 21.3, 37.0, 85.5 GHz	0.63, 1.6, 3.75, 10.8, and 12 μm	0.7774 μm	0.3 to 50 μm
Ground Resolution	5.0 km	5.1 km at 85.5 GHz	2.4 km	4km	10km
Swath Width	247 km	878 km	833 km	600km	± 82 deg

The TRMM PR is the first space borne precipitation radar; its operating frequency is 13.8GHz. Its main goal is to provide 3-D maps of storms as well as to estimate rainfall over land and ocean.

The VIRS is a radiometer with five channels of different frequencies or wavelengths (0.63, 1.6, 3.75, 10.8, and 12 μm). The VIRS provides high resolution observations about cloud coverage, cloud type, and cloud top temperatures.

The TMI is a multichannel dual-polarized passive microwave radiometer operating at five different frequencies: 10.65, 19.35, 21.3, 37.0, 85.5 GHz. All these channels operate at dual polarization (Vertical and Horizontal polarization) except the 21.3 GHz channel which operates at single polarization (Vertical polarization). The TMI provides measurements of the brightness temperature, cloud liquid water, cloud ice, rain intensity, and rainfall types (stratiform, convective).

There are two other TRMM instruments: the Lightning Imaging Sensor (LIS) and the Clouds and Earth's Radiant Energy System (CERES). The LIS is an optical sensor operating at 0.7774 μm , and it observes the distribution and the variability of lightning over earth. The LIS data can be used together with data from PR, TMI and VIRS to study the relation between lightning and rainfall. The CERES is a scanning radiometer with operating wavelength ranges from 0.3 to 50 μm . It measures the emitted and the reflected radiative energy from the surface of the earth and from the atmosphere. The goal of CERES is to reduce the uncertainties in predicting long-term changes in the climate.

3.3 TRMM MEASUREMENT LEVELS

The data observed by TRMM's instruments mentioned above are processed by NASA and distributed to the users. The data can be divided into three levels where each level has sublevels in it. In this section we are summarizing the levels that are related to

TRMM-PR instrument. Table 3.2 shows the definition of the TRMM products related to some of those instruments, and Figure 3.2 shows how some of these products are related to each other. For more details about the products of the other instruments, it is recommended to see (TRMM Manual February 2001) and (TRMM-PR Manual, Ver. 6).

Table 3.2: TRMM Products (TRMM Manual February 2001).

Sensor	Processing Level	Product
PR	1B21	Calibrated Received Power
	1C21	Radar Reflectivity
	2A21	Normalized Radar Surface Cross Section
	2A23	PR Qualitative
	2A25	Rain Profile
	3A25	Monthly Statistics of Rain Parameter
	3A26	Monthly Rain Rate using a Statistical Method
TMI	1B11	Brightness Temperature
	2A12	Rain Profile
	3A11	Monthly Oceanic Rainfall
VIRS	1B01	Radiance
COMB	2B31	Rain Profile
	3B31	Monthly Rainfall
	3B42	TRMM & IR Daily Rainfall
	3B43	TRMM & Other Sources Monthly Rainfall

3.3.1 LEVEL-1

The PR Level-1 has two data products; 1B21 and 1C21. They can be shortly described as follows:

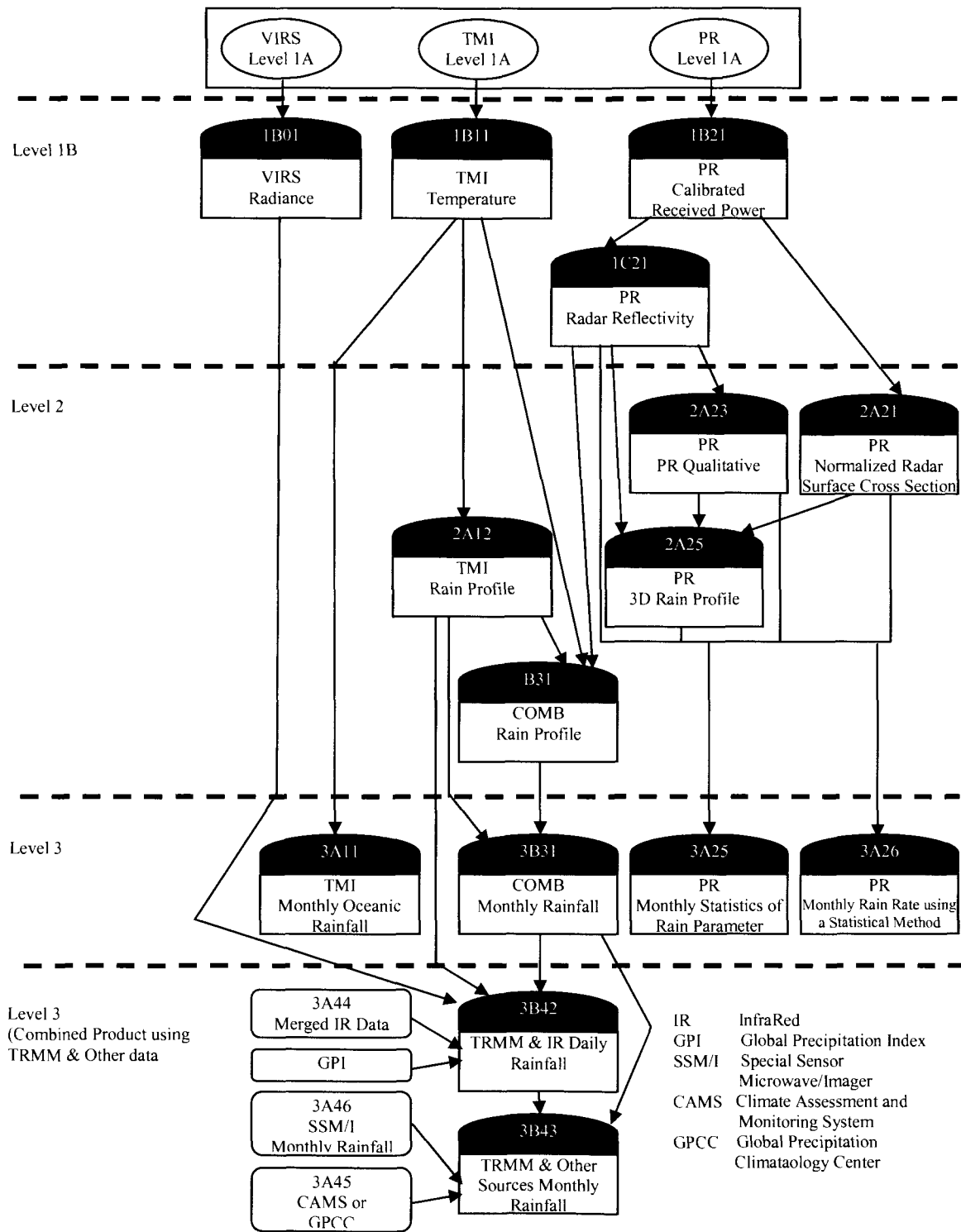


Figure 3.2: TRMM algorithm flow diagram (TRMM Manual February 2001).

- 1B21 is mostly about the calibrated received power. It has other information about the Noise Power, Minimum Echo Flag (Rain/No Rain Flag), Storm Height, etc. The received power is presented in three arrays: normal sample, surface oversample, and rain oversample. Each array is a 3-dimensional array whose dimensions are: scan, ray, and range bin. In the case of normal sample the power has 250 m vertical spacing, otherwise it is 125 m.
- The 1C21 product is known for Radar Reflectivity (Z Factor). It carries information about radar reflectivity without rain attenuation correction. The 1C21 product has the same format as in 1B21. The radar reflectivity factor is calculated from the measured power in 1B21 without rain attenuation correction (TRMM-PR Manual, Version 6).

3.3.2 LEVEL-2

PR Level-2 has three products; 2A21, 2A23, and 2A25.

- 2A21 product is mainly responsible for calculating the Radar Surface Cross Section. In the cases where rain exists, it computes the path integrated attenuation (PIA) with the surface as a target using the Surface Reference Technique (SRT).
- The 2A23 product is referred to as PR Qualitative. It produces the rain flag. In the cases where rain is detected, it will detect the existence of the bright band, and determine its width and height. From there, it can classify the rain profile to be stratiform or convective.
- The 2A25 product is well known as PR Profile. It produces a vertical profile of the rain rate estimate as well as the corrected version of the reflectivity. For ground

validation purposes, the rain rate near the surface and the reflectivity near the surface are also given. In order to correct for attenuation, this algorithm uses a hybrid method of both the surface reference technique (SRT) and Hitschfeld-Bordan method (HB) (Iguchi et al., 2000).

3.3.3 LEVEL-3

The PR Level-3 has two main products; 3A25 and 3A26.

- 3A25 product is the Monthly Statistics of the Rain. It contains monthly statistics of PR Level-1 and Level-2 products (rainfall, reflectivity, Path-Integrated Attenuation, storm height, and bright band height). These statistics are performed using two resolutions; $5^{\circ} \times 5^{\circ}$ and $0.5^{\circ} \times 0.5^{\circ}$ latitude/longitude at 5 layers (2 km, 4km, 6km, 10km and 15km heights). The statistics include probability of occurrence, means and standard deviations, and histograms.
- 3A26: Estimation of space-time rain rate statistics over a $5^{\circ} \times 5^{\circ}$ grid on a monthly basis at 3 layers (2 km, 4 km and 6 km heights). The statistics are the same as in 3A25 above (probability of occurrence, means and standard deviations, histograms and correlation coefficients). This product has monthly global rainfall maps.

3.4 TRMM-PR DESCRIPTION

3.4.1 TRMM –PR OVERVIEW.

The TRMM precipitation radar (PR) is a space borne precipitation radar that has the ability to observe vertical distribution of precipitation all over the tropics. The PR

operates at a frequency of 13.8 GHz, and it provides rainfall estimation over land as well as ocean. Major design and performance parameters of the PR are shown in Table 3.3 (Kozu et al., 2001). Observation geometry of PR is shown in Figure 3.3. The PR antenna beam scans in the cross-track direction over $\pm 17^\circ$ to give 247 km swath. The antenna beam width of the PR is 0.71° and there are 49 angle bins within the scanning angle of $\pm 17^\circ$. The horizontal resolution is around 5 km at nadir. The vertical range resolution of PR is 250 m.

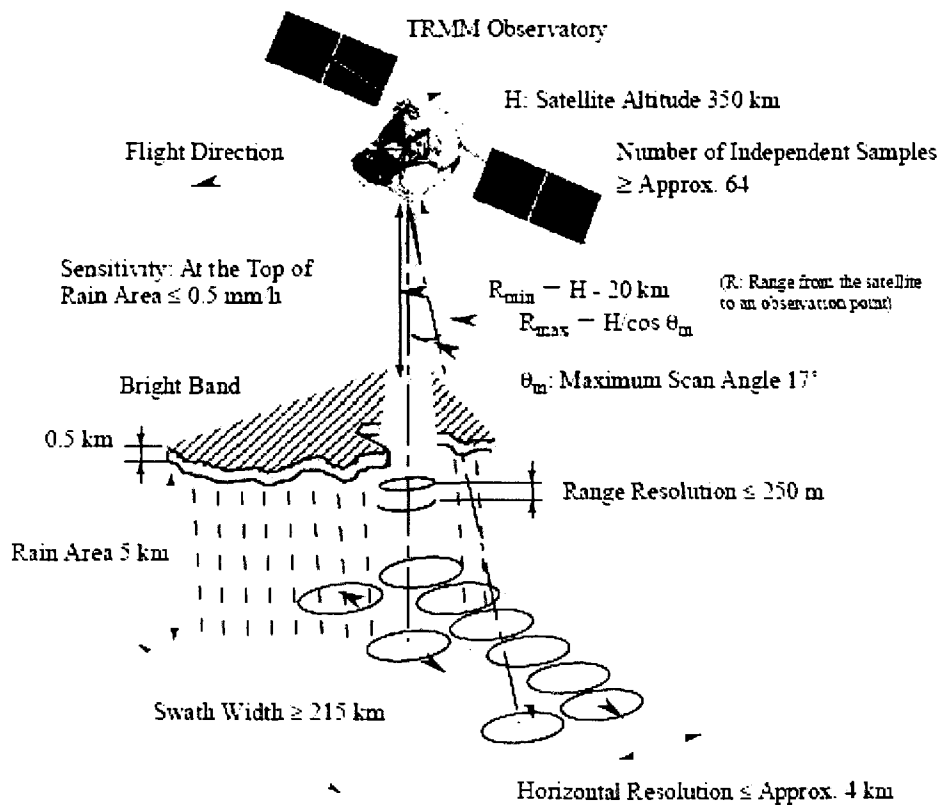


Figure 3.3. The observation concept of the PR (adopted from TRMM Manual 2001).

Table 3.3: Major parameters of TRMM-PR.

Frequency	13.8 GHz
Swath Width	About 247 km
Observable Range	Over 20 km
Range Resolution	250 m
Horizontal Resolution	5 km (nadir)
Weight	465 kg
Power	213 watts
Beam Width	0.71° x 0.71°
Aperture	2.1 m x 2.1 m
Scan Angle	±17°
Gain	About 47.4 dB
Peak Power	Over 700 W

3.4.2 TRMM-PR RAIN RATE ESTIMATION

The TRMM-PR 2A25 product provides a vertical profile of the rain. The rain is simply calculated using the Z-R relation based on global averaged DSD model where Z is the attenuation-corrected version of the measured radar reflectivity factor (Z_m). In this dissertation our concern is to estimate the rain rate near the surface. Therefore, we will deal with the lowest height measurement of the rain vertical profile.

The appropriate selection of the DSD model is very important in estimating the rain rate. Two DSD models were assumed in TRMM-PR product; one for stratiform rain type and the other is for convective rain type. These models were made from a collection of Z-R relations measured near the ocean from widely distributed locations around the world. Typical Z-R relations were found to be (Kozu et al. 1999):

$$\text{Stratiform: } Z = 300R^{1.38} \quad (3.1)$$

$$\text{Convective: } Z = 185R^{1.43} \quad (3.2)$$

For each model, the Z-R relationship is converted into an $N_0 - \Lambda$ relationship, where N_0 and Λ are the parameters in the size distribution:

$$N(D) = N_0 D^\mu e^{-\Lambda D} \quad (3.3)$$

where μ is the shape factor and Λ is related to μ and D_0 as follows:

$$\Lambda = \frac{3.67 + \mu}{D_0} \quad (3.4)$$

Once the DSD model is obtained, the parameters in the k-Z and Z-R relations can be calculated for rain and snow at different temperatures and mixing ratio, where these parameters are functions of the rain type, presence or absence of the bright band, the heights of the 0°C isotherm and storm top.

In the case of stratiform rain with bright band detected, the stratiform DSD model with a vertical profile model defined by (Awaka et al. 1985) is used to calculate the k-Z and Z-R coefficients.

In this model, the coefficients of k-Z and Z-R are computed at 5 levels as shown in Figure 3.4; three levels for snow-water mixture (A,B C), and two levels for water drop (D,E).

Levels A, B and C are defined such that the snow-water mixtures have fractional water contents of 1.1%, 1.7%, and 17%, respectively. Level D was defined where water drops have a temperatures of 0°C, while level E was defined at 20°C. Moreover, Level A

was considered as the storm top, level B was taken to be 500m above the bright band peak while level D was taken to be 500m below that peak.

For other values of the k-Z and Z-R coefficients at intermediate levels, they are calculated by linear interpolation assuming a lapse rate of 5°C/Km.

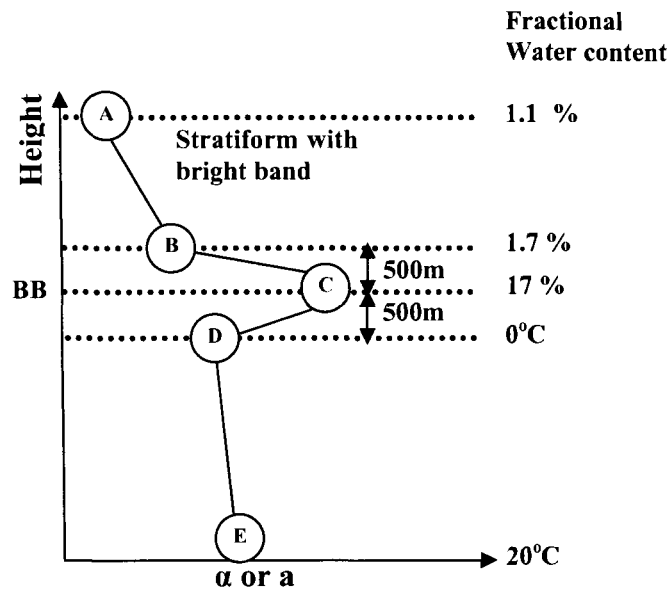


Figure 3.4: Schematic presentation of the profiles for stratiform profile with bright band detected. (Adopted from Iguchi et al., 2000).

In the cases of stratiform rain with no bright band detected or in the cases of convective rain type, the DSD model shown in Figure 3.5 is used to calculate the parameters of the k-Z and Z-R relations. The only difference is that the hydrometeors are assumed to be at 0°C in the 750m on both sides of the 0°C isotherm. Actual values of the k-Z and Z-R parameters used in TRMM-PR 2A25 product are listed in Table 3.4. Other details about TRMM-PR rainfall estimation can be found in (Iguchi et al., 2000).

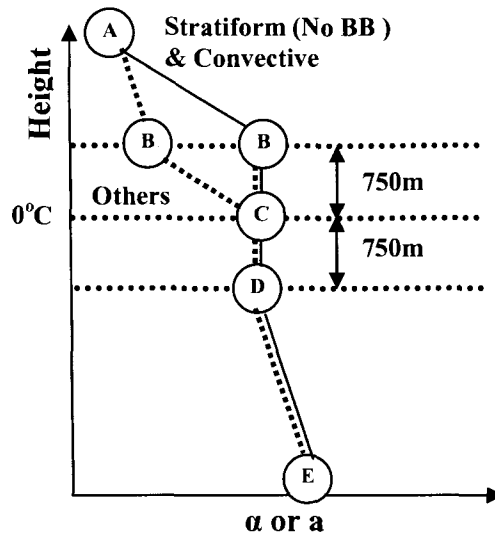


Figure 3.5: Schematic presentation of the profiles for convective profile and for stratiform profile with no bright band detected.(Adopted from Iguchi et al., 2000).

Table 3.4: Initial k - Z and Z - R parameters ($k = \alpha Z^\beta$, $R = aZ^b$, $Z = a''R^{b''}$).

Rain Type	Parameter	A	B	C	C(0°C water)	20°C water
Stratiform	α	0.0000861	0.0001084	0.0004142	0.0002822	0.0002851
	β	0.79230	0.79230	0.79230	0.79230	0.79230
	a	0.01398	0.01263	0.004521	0.02010	0.02282
	b	0.7729	0.7644	0.7288	0.6917	0.6727
	a''	250.8	304.6	1649.3	283.9	275.7
	b''	1.294	1.308	1.372	1.446	1.487
Convective	α	0.0001273	0.0004109	0.0004109	0.0004109	0.0004172
	β	0.7713	0.7713	0.7713	0.7713	0.7713
	a	0.02027	0.03484	0.03484	0.03484	0.04024
	b	0.7556	0.6619	0.6619	0.6619	0.6434
	a''	174.1	159.5	159.5	159.5	147.5
	b''	1.323	1.511	1.511	1.511	1.554
Others	α	0.0001273	0.0001598	0.0004109	0.0004109	0.0004172
	β	0.7713	0.7713	0.7713	0.7713	0.7713
	a	0.02027	0.01871	0.03484	0.03484	0.04024
	b	0.7556	0.7458	0.6619	0.6619	0.6434
	a''	174.1	207.4	159.5	159.5	147.5
	b''	1.323	1.341	1.511	1.511	1.554

3.5 TRMM VALIDATION

TRMM Ground Validation (GV) system is one of the very important systems that are part of TRMM mission. Its function is to support TRMM to improve some of the measuring and estimation techniques (Reflectivity and rain rate). The GV system has 10 ground validation sites around the world as shown in Figure 3.6 in addition to there gauge networks. The main ground validation sites are located at Florida, Texas, Darwin, and Kwajalein.

TRMM measurements require comparisons with well-calibrated ground-based systems (ground radars and rain gauges). The GV system takes TRMM measurements when TRMM overpasses over GV sites and compare there products in order to see how good TRMM measurements are. Results show that the reflectivity factor derived from the PR data after attenuation correction agrees with those obtained from the WSR-88D. Comparisons of rain rates estimated by TRMM-PR with rain gauges showed that TRMM may underestimate rainfall rate (Liao and Meneghini, 2009), (Okamoto et al. 2007).

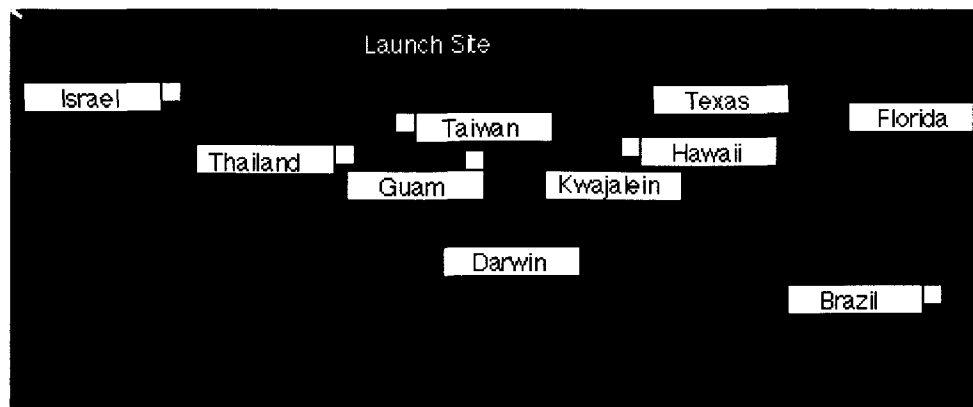


Figure 3.6: TRMM ground validation sites locations around the world.
(http://trmm-fc.gsfc.nasa.gov/trmm_gv/index.html).

3.5.1 TRMM-PR MEASURED REFLECTIVITY/ESTIMATED RAIN RATE VALIDATION

In the years 2005, 2006, 2007 and 2008, TRMM has flown over KMLB, KWAJ and KHGX sites more than 600 times each. However, not all these times have precipitation. Over each site few overpasses were considered as precipitation overpasses. We studied these overpasses in order to evaluate the TRMM-PR measured reflectivity factor. Over KMLB site there were 166 precipitation cases during those four years (32, 15, 41, and 78, respectively). Over KHGX site there were 85 precipitation cases during the years of 2005, 2006 and 2007 (27, 26, and 32, respectively), while over KWAJ site there were 50 precipitation cases during the years of 2006 and 2007 (26, and 24, respectively).

The alignment procedure introduced by (Bolen and Chandrasekar, 2003) is used to align TRMM-PR reflectivity product with the ground radar reflectivity measurements. Resampling the ground-based and spaceborne datasets to a common grid provides a means by which the radar reflectivity factors can be compared at different heights. The results show that radar reflectivity factor derived from the PR data after attenuation correction agrees to within about 2 dB on average and it is within 1 dB for most of the cases.

Figures 3.7, 3.9, 3.10, 3.11, 3.12, 3.14, 3.15, 3.16 and 3.18 represent scatter plots of TRMM-PR reflectivity compared with the ground reflectivity overpassed during the four years mentioned above. Figures 3.8, 3.13 and 3.17 represent standard deviation plots of TRMM-PR reflectivity compared with the ground reflectivity overpassed certain years from the years mentioned above. Results are shown for four heights (1, 2, 3 and 4km).

Results show how close the TRMM-PR reflectivity product to the corresponding ground radar reflectivity product. Goodness is extracted through the good correlation the small bias, and small standard deviation of the bias at each height. The goal of doing the alignment in this dissertation is to use the closeness and the relationship of TRMM-PR reflectivity product and the ground radar reflectivity product and map it to a neural network in order to improve TRMM-PR rain rate estimate as will be shown in Chapter 5.

Comparisons of TRMM PR rain rate product with rain gauge for the same years yield to the indication that TRMM-PR tends to underestimate rain rate compared with the rain gauge as shown in Table 3.5. Rain gauge networks used in this evaluation are those explained in Section 2.5 in the previous chapter. Detailed results of the evaluation in Table 3.5 will be shown in Chapter 5.

Table 3.5: Evaluation of TRMM-PR rain rate estimates vs. rain gauge over KMLB, KHGX and KWAJ. (Instantaneous Rainfall).

Site/Year	FracBias (%)	Corr.	NSE	FRMSE (%)
KMLB 2005	-48.3	0.53	0.58	92.7
KMLB 2006	-27.9	0.46	0.64	105.1
KMLB 2007	-35.2	0.58	0.58	123.3
KMLB 2008	-25.3	0.48	0.64	114.0
KHGX 2005	-54.9	0.20	0.62	113.4
KHGX 2006	-59.9	0.37	0.61	93.0
KHGX 2007	-42.3	0.59	0.48	68.4
KWAJ 2007	-47.5	0.95	0.47	65.8

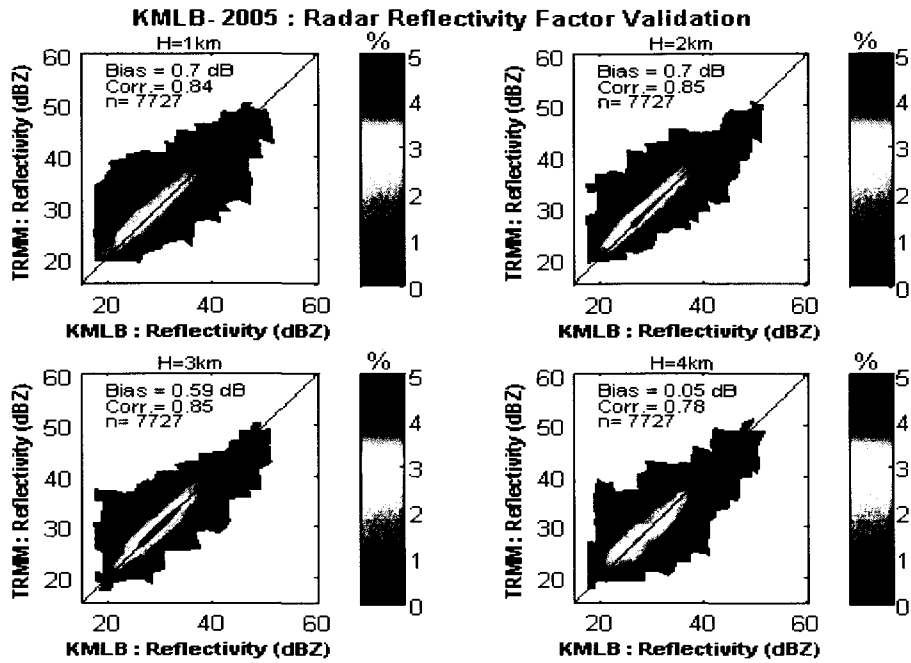


Figure 3.7: TRMM-PR reflectivity vs. KMLB reflectivity. Data from year 2005.

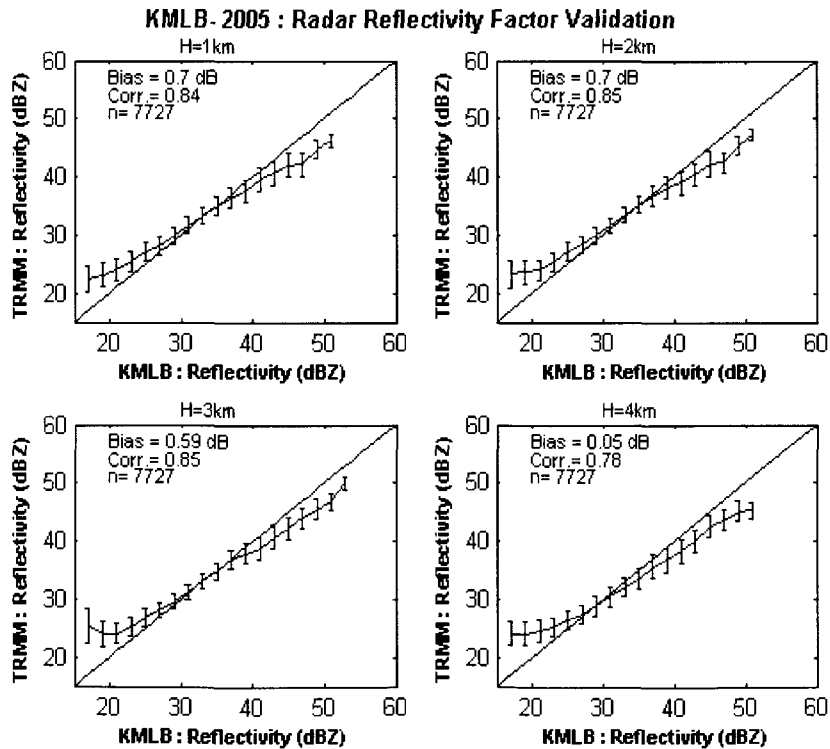


Figure 3.8: Standard deviation plot: TRMM-PR reflectivity vs. KMLB reflectivity. Data from year 2005.

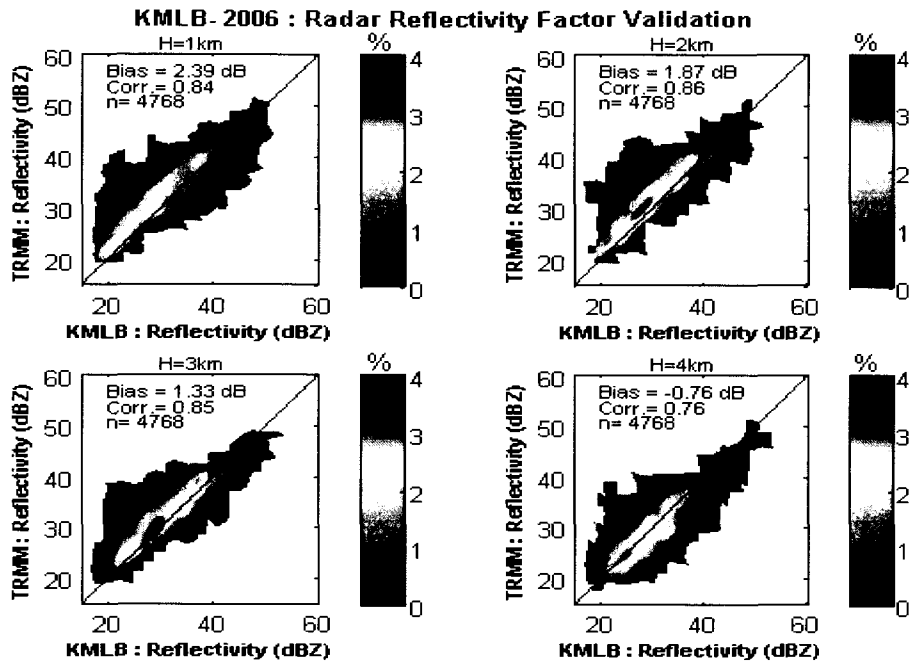


Figure 3.9: TRMM-PR reflectivity vs. KMLB reflectivity. Data from year 2006.

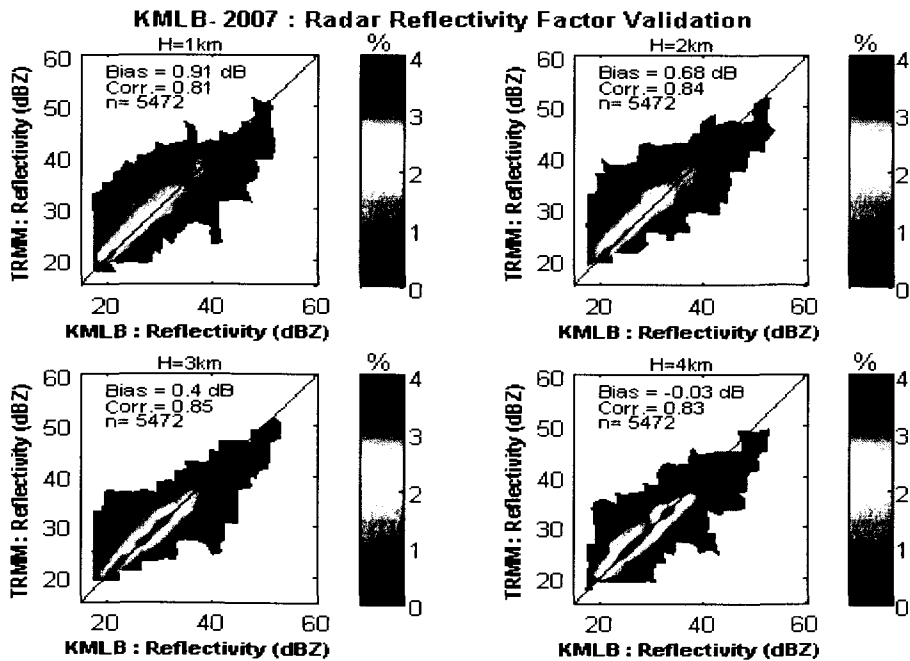


Figure 3.10: TRMM-PR reflectivity vs. KMLB reflectivity. Data from year 2007.

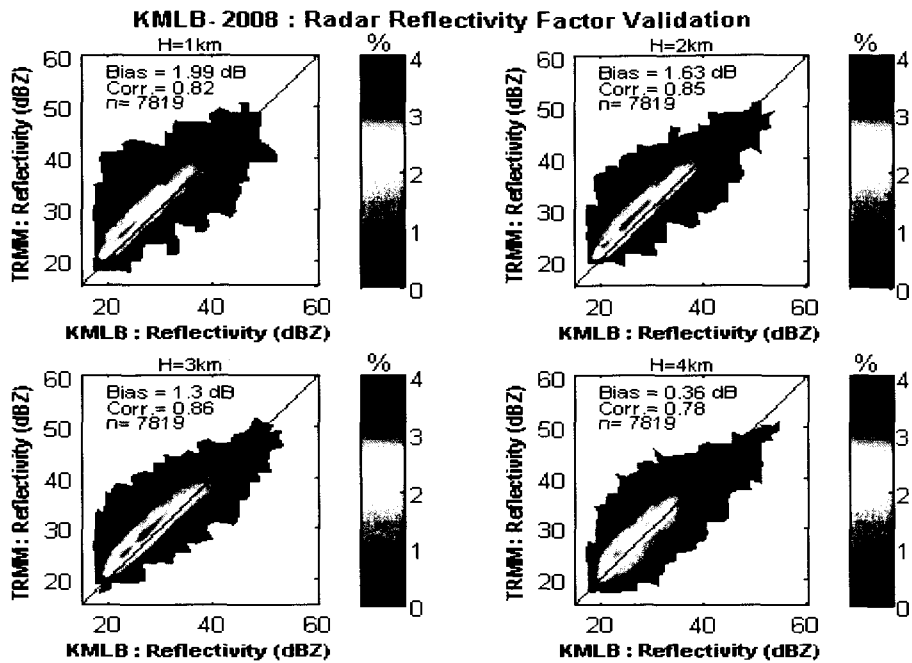


Figure 3.11: TRMM-PR reflectivity vs. KMLB reflectivity. Data from year 2008.

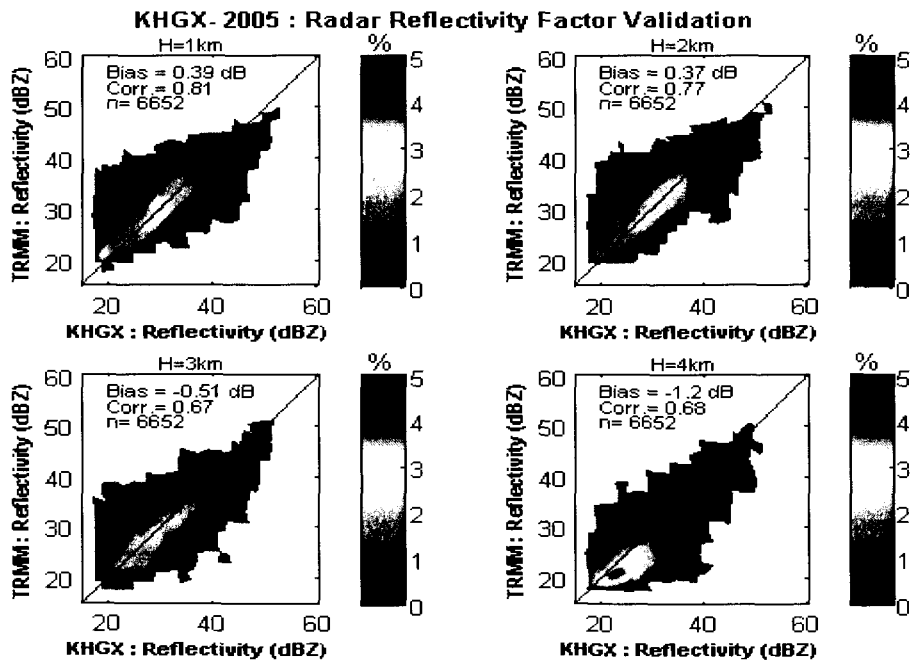


Figure 3.12: TRMM-PR reflectivity vs. KHGX reflectivity. Data from year 2005.

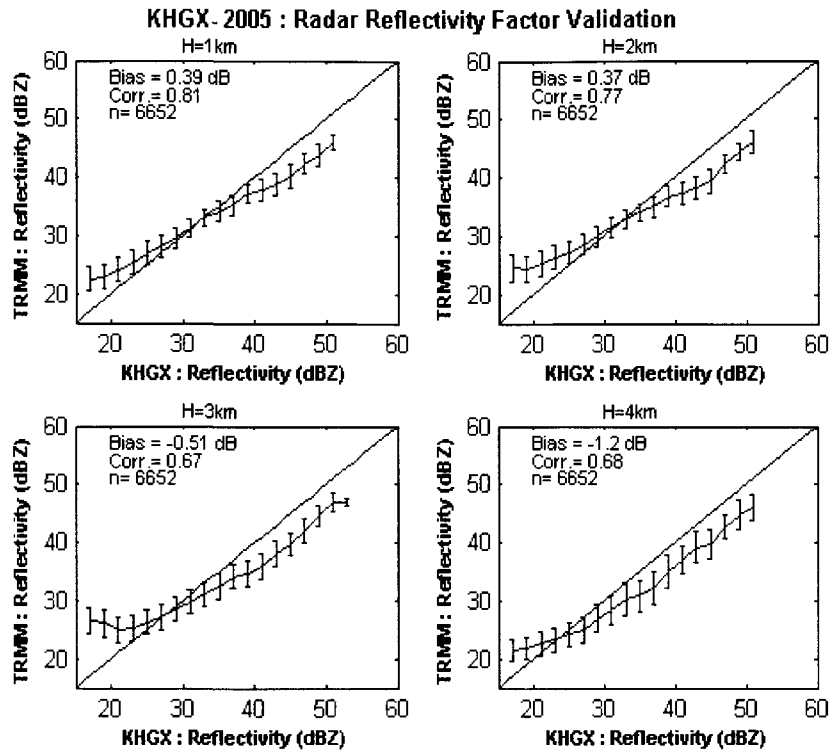


Figure 3.13: Standard deviation plot: TRMM-PR reflectivity vs. KHGX reflectivity. Data from year 2005.

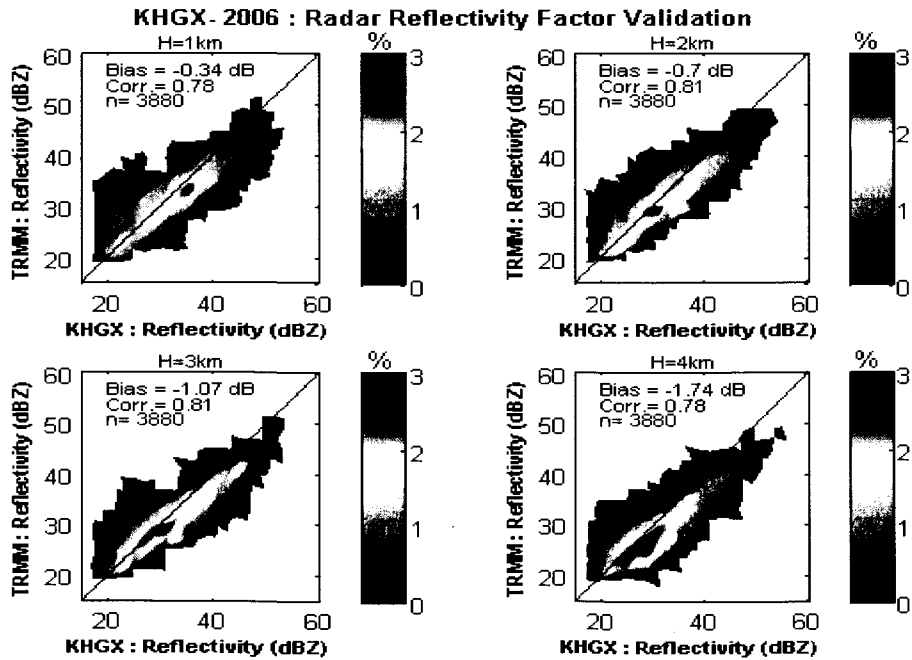


Figure 3.14: TRMM-PR reflectivity vs. KHGX reflectivity. Data from year 2006.

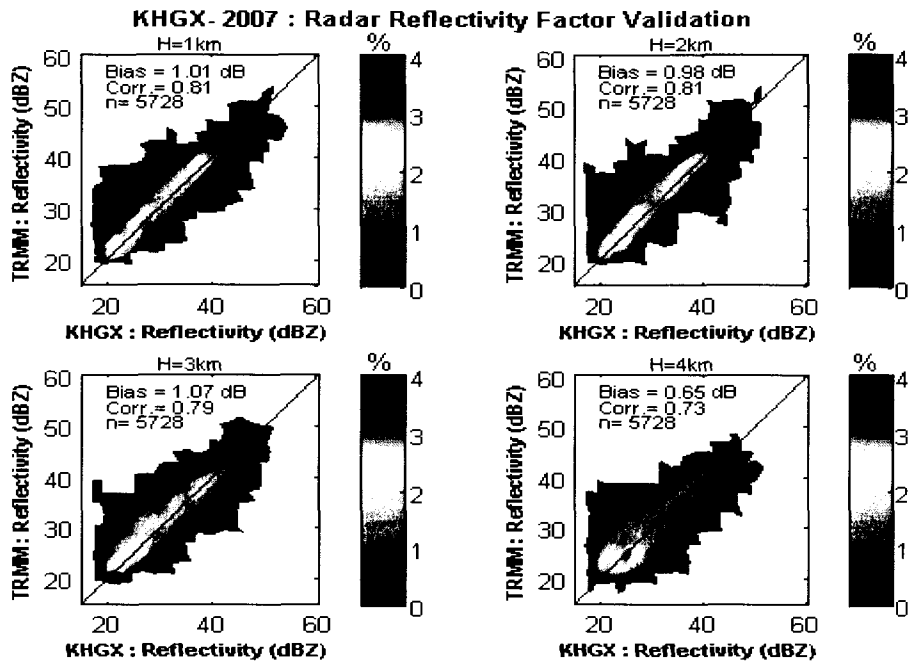


Figure 3.15: TRMM-PR reflectivity vs. KHGX reflectivity. Data from year 2007.

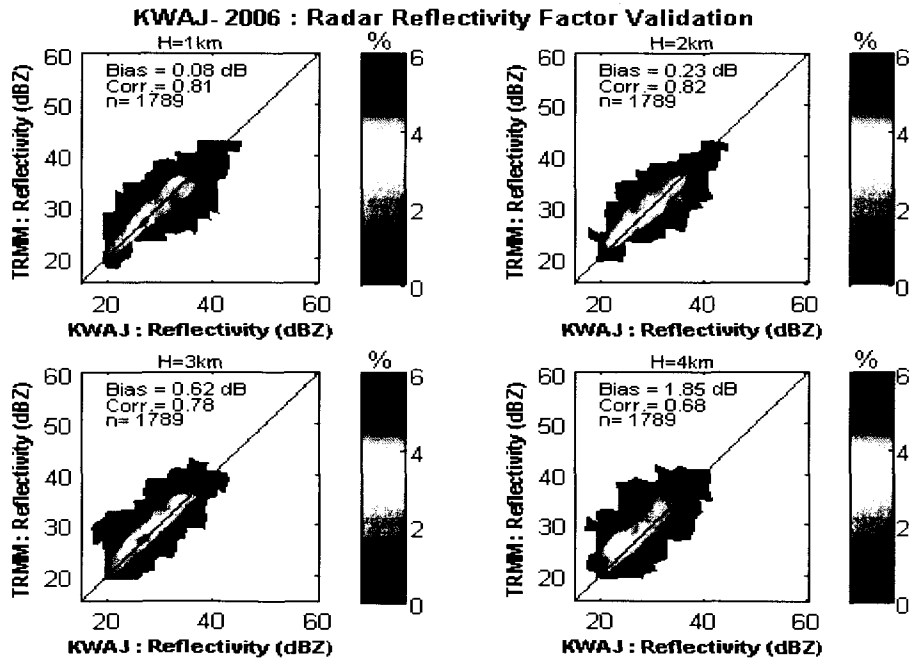


Figure 3.16: TRMM-PR reflectivity vs. KWAJ reflectivity. Data from year 2006.

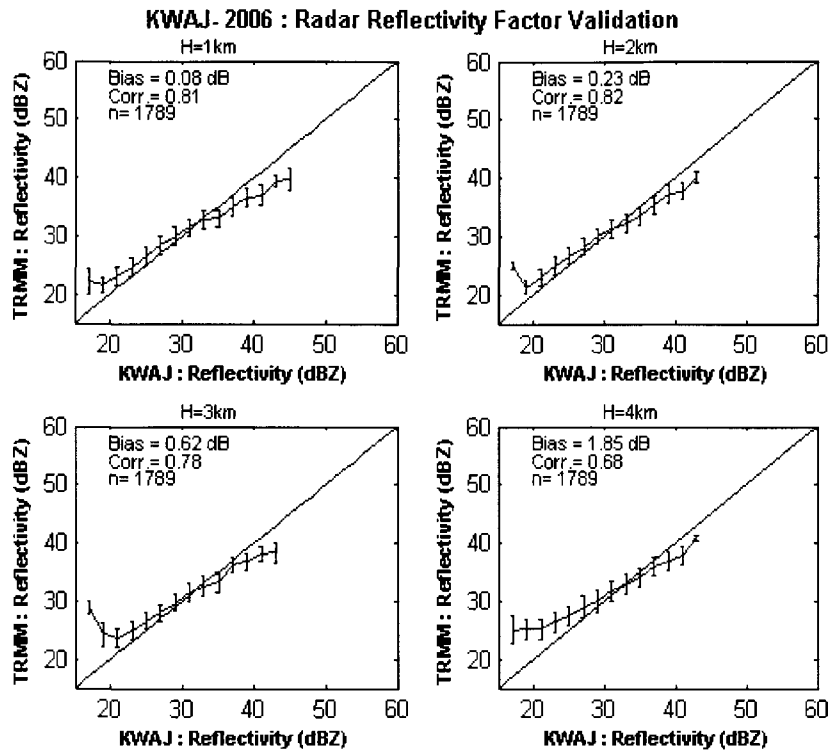


Figure 3.17: Standard deviation plot: TRMM-PR reflectivity vs. KWAJ reflectivity. Data from year 2006.

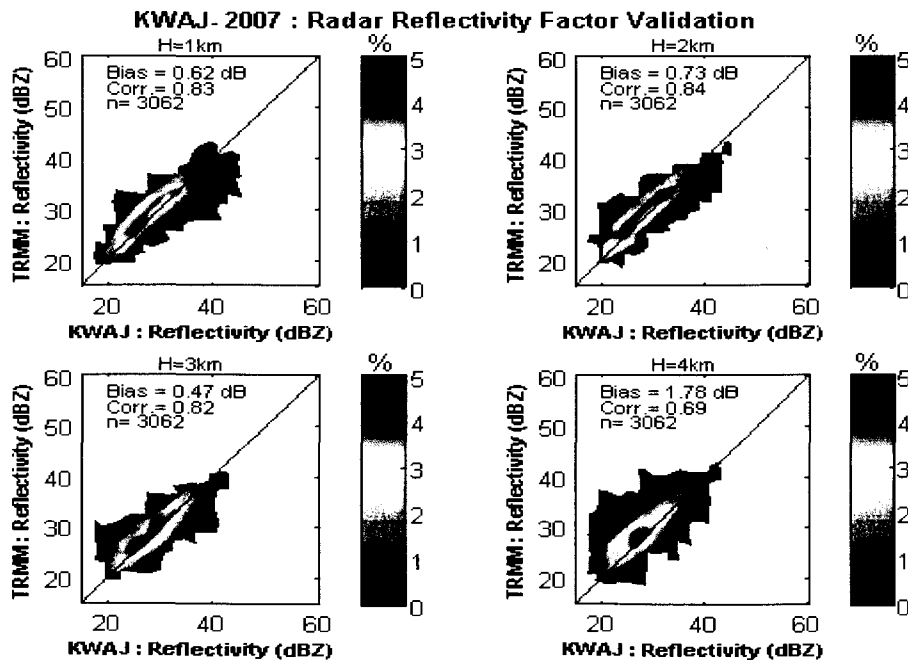


Figure 3.18: TRMM-PR reflectivity vs. KWAJ reflectivity. Data from year 2007.

CHAPTER 4

RAIN RATE ESTIMATION USING NEXRAD GROUND RADAR MEASUREMENTS BASED ON NEURAL NETWORK

4.1 INTRODUCTION

An artificial neural network (ANN), often called a neural network (NN), is a nonparametric method based on biological neural networks. In other words, neural network is a non linear mapping from input space to a target space. It consists of interconnected group of neurons, each characterizing a simple function. The term non parametric does not mean that the network does not have parameters; on the contrast, it means that the number and nature of the parameters are flexible and not fixed in advance. In other words, the method does not rely on any assumptions that the data are drawn from a given parametric model. As a system, the network is adjusted, or trained, so that a particular input leads to a specific target output. A very general representation of a NN is shown in Figure 4.1.

Neural Network techniques are widely used in radar systems. Some major applications can be summarized into snowfall estimation, rain fall estimation, rain detection, and rain type classification. Snowfall estimation was introduced first by (Xiao and Chandrasekar, 1996). Rainfall estimation was introduced by the same authors (Xiao

and Chandrasekar, 1997). A trial to improve rainfall estimation was started in 1998 by (Xiao et al. 1998); improvement was done through the detection of rain existence before going to estimation. As an attempt to do rain type classification, (Zafar and Chandra, 2003) started the idea of using Self Organizing Maps (SOM) in 2003.

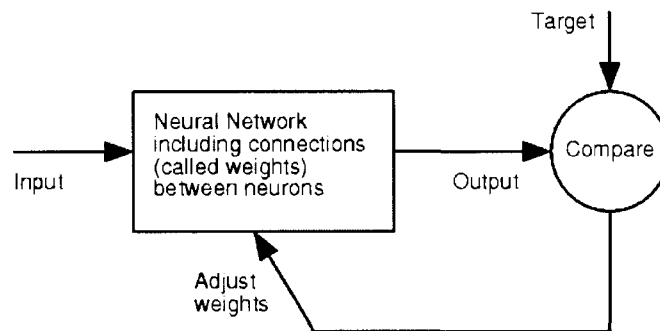


Figure 4.1: Representation of a general Neural Network.

4.2 RADIAL BASIS FUNCTION NEURAL NETWORK

The radial basis function (RBF) network is part of the multilayer feed forward neural network (MFNN) class. It gets its name from the use of the radial basis function as activation function in the hidden layer. Figure 4.2 shows the structure of an RBF network. It contains three layers which are the input layer, the hidden layer and the output layer. The input vectors are fed to the input layer where they pass to the hidden layer. The hidden layer units or neurons have nonlinear radial-basis functions where each has its own center vector and width or size. The output of each neuron is calculated based on the Euclidean distance between the input vector and the center vector of that neuron. The outputs of the hidden layers are weighted and added linearly at the output layer.

4.2.1 RBF NEURAL NETWORK ARCHITECTURE

As mentioned above, the RBF NN has three layers (input, hidden, and output layer). The input layer accepts the input vector $\mathbf{X}=[x_1, x_2, \dots, x_p]^T$. The hidden layer consists of m neurons with $h(\mathbf{x})$ as transfer function. In this work, $h(\mathbf{x})$ was chosen to be the Gaussian RBF given by

$$h_j(\mathbf{x}) = \exp\left[-\sum_{i=1}^p \frac{(x_i - c_{ij})^2}{r_{ij}^2}\right] \quad (4.1)$$

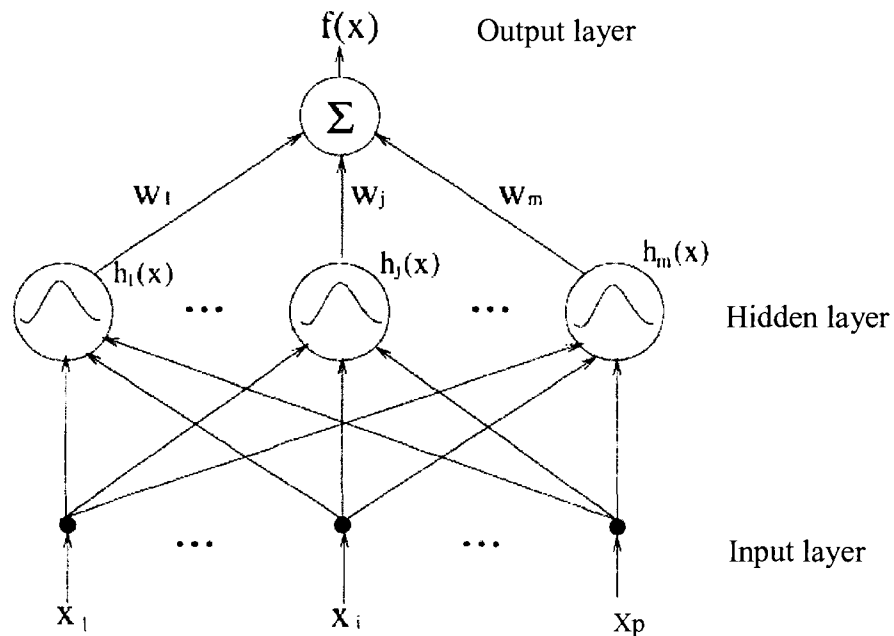


Figure 4.2: The general structure of RBF network.

and the output $f(\mathbf{x})$ can be calculated by a linear combination of the hidden layer outputs as follows:

$$f(\mathbf{x}) = \sum_{j=1}^m w_j h_j(\mathbf{x}) \quad (4.2)$$

where $\mathbf{c}_j = [c_{1j}, c_{2j}, \dots, c_{pj}]^T$ is the center vector of neuron j , $\mathbf{r}_j = [r_{1j}, r_{2j}, \dots, r_{pj}]^T$ is the size or width vector of neuron j , m is the number of neurons in the hidden layer, and w_j is the weight from neuron j to the output layer.

4.2.2 INPUT/TARGET OF THE RBF NEURAL NETWORK

Radar data and rain gauge observations that are used to train and test this RBFNN were during the years 2005, 2006, 2007 and 2008 over Melbourne-Florida, Houston-Texas and Kwajalein-Marshall Islands areas. Radar data (radar reflectivity factor) will be used as an input to the neural network and the rain gauge corresponding to that input will be the target of the neural network. Radar data were collected by the three radars Constant Altitude Plan Position Indicator (CAPPI) scans. The lowest height level of the CAPPI scans is 1 km and the highest level is 4 km. The spacing between the CAPPI levels is chosen to be 1 km. The gauge data were maintained by NASA TRMM program. Around KMLB radar, the gauge networks that were considered are Kennedy Space Center (KSC), South Florida Water Management District (SFL), and St. Johns Water Management District (STJ). Around KHGX radar, Houston-Area Raingauge (HAR) gauge network was the only station available, and around KWAJ radar KWAJ gauge network was the only station there. Data within 100km was only considered. At 100 km from the GR the vertical resolution of the beam is about 1.8 km, and going further than 100km would cause coarse sampling for ground radar measurements. The radar

parameter of interest in this work was only radar reflectivity factor Z_h . CAPPI data containing Z_h values at 1km, 2km, 3km, and 4km heights with 1km horizontal resolution were generated from the radar data as shown in Figure 4.3.

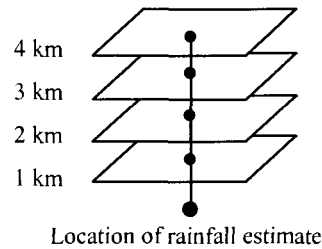


Figure 4.3: Data locations for 4 point input vector.

4.2.3 TRAINING THE RBF NEURAL NETWORK

Training the RBFNN means finding its main parameters, or in other words: finding the center vectors of all neurons, finding the size vectors of all neurons and finding the weights from all the neurons to the output layer. Once these parameters are found, the network is trained and ready to be used.

4.2.3.1 Finding the Optimal Centers and their Sizes

The design or the training of the RBFNN in this work is based on a method called *forward selection*. The network starts with an empty subset. Then we start adding one basis function at a time. The basis function we add is the one that would reduce the sum-squared error most (see equation 4.3), and also keep the convergence condition decrease which is based on the Generalized Cross Validation (GCV) method (Mark, 1996). To speed this up, a faster algorithm was involved where the added basis functions were

based on the *Orthogonal Least Square* (OLS) method (Chen et al., 1991); which means even if the candidate basis function reduces the sum-squared error most and it keeps the convergence condition decrease, it also has to suffice the Orthogonal Least Square condition, which ensures that the new basis function is orthogonal to all previous basis functions.

This method has great advantages:

- 1) There is no need to fix the number of hidden units as used to be in the past.
- 2) The computation requirements are low.

To find the sizes of the centers, we chose a simple way to do that where the size of each center is fixed and is set to be the maximum Euclidean distance between any center and the others, and this can result in a simpler training strategy (Chen et al., 1991).

4.2.3.2 Finding the Optimal Weights

In training a RBFNN, the goal is to map the input data to a target data with the least error. In this concept, the error can be referred as *sum-squared-error* S where S can be defined as

$$S = \sum_{i=1}^p (\hat{y}_i - f(\mathbf{x}_i))^2 \quad (4.3)$$

where \hat{y}_i is the actual output when the input is \mathbf{x}_i . Once the centers and the sizes are found as shown in the previous subsection, all what we need is to find the minimum of S with respect to the weights of the network and this can be done by solving a least square problem and find the set of weights that would minimize S .

To avoid over fitting, and to get better generalization, a penalty should be applied to the weights. A cost function C can be introduced in this regard where C can be defined as

$$C = \sum_{i=1}^p (\hat{y}_i - f(\mathbf{x}_i))^2 + \sum_{j=1}^m \lambda_j w_j^2 \quad (4.4)$$

where λ_j is a regularization or a penalty factor that would be applied to w_j (Mark, 1996). The goal here is to prevent large weights from producing rough output.

The solution of the weight vector \mathbf{w} to minimize the cost function C can be written as

$$\mathbf{w} = \mathbf{A}^{-1} \mathbf{H}^T \mathbf{y} \quad (4.5)$$

where \mathbf{A}^{-1} is the variance matrix and is defined as

$$\mathbf{A}^{-1} = (\mathbf{H}^T \mathbf{H} + \mathbf{\Lambda})^{-1} \quad (4.6)$$

where $\mathbf{\Lambda}$ is a diagonal matrix with λ_j 's on the diagonal, and \mathbf{H} is called the design matrix and can be written as

$$\mathbf{H} = \begin{bmatrix} h_1(x_1) & h_2(x_1) & \cdots & h_m(x_1) \\ h_1(x_2) & h_2(x_2) & \cdots & h_m(x_2) \\ \vdots & \vdots & \ddots & \vdots \\ h_1(x_p) & h_2(x_p) & \cdots & h_m(x_p) \end{bmatrix} \quad (4.7)$$

The regularization parameters λ_j 's can be found using a cross validation technique called Generalized Cross Validation (GCV) as shown in (Mark, 1996).

4.2.3.3 Adaptively Training the RBFNN

The goal in this research is to estimate rainfall in daily base. At the end of any, and if we have new data available, we need to create a new model to test the next day data with. Figure 4.4 shows the idea of daily adapting the neural network.

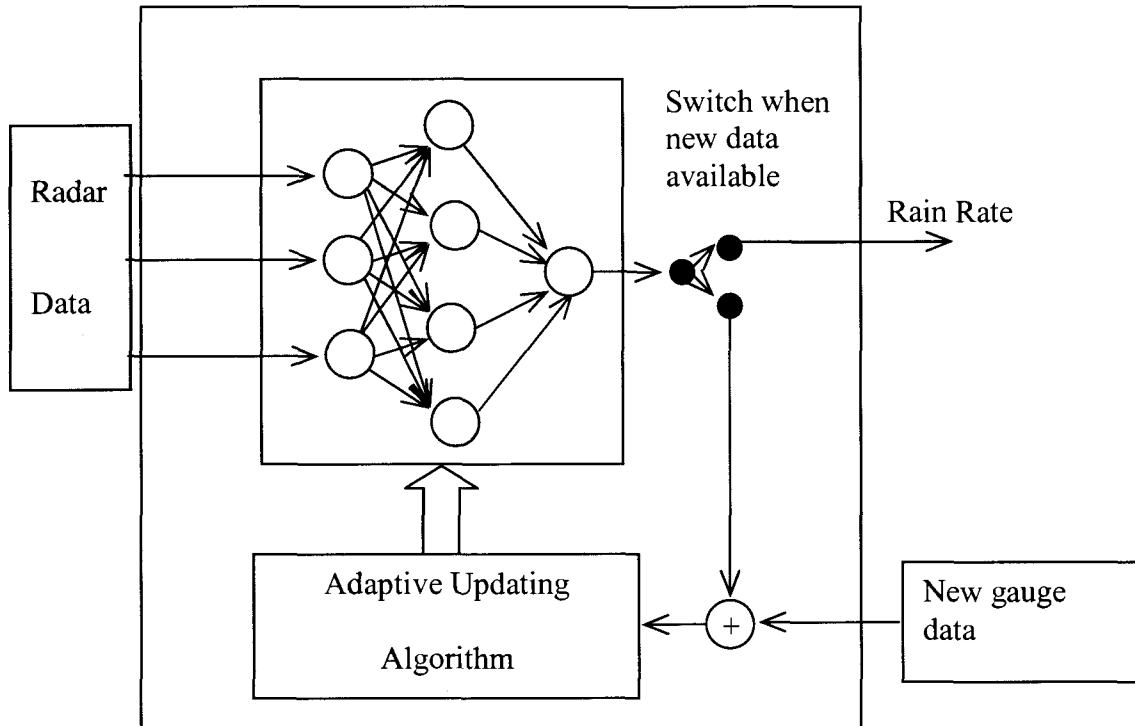


Figure 4.4: Dynamic Neural network.

As we know and especially if our goal is to estimate rainfall over a year, the network might get very large and hard to train from the beginning if we keep adding neurons every time we have new input. Another concern is that the coming data might not carry new information or it might but with slightly different output (gauge). Therefore, the idea of adaptively training the RBFNN on daily base came to the seen (Liu et al., 2001). To include the information from the new data, it is necessary to treat the

network not only by adding some neurons, but also by removing some neurons. If the new data carries similar input data with different output, there is no need to retrain the network again; rather we just need to recalculate the weights from the hidden units to the output unit; and this reduces the complexity of the network, and the redundancy of the data, and by doing this it improves the generalization of the network, and reduces the training time because adjusting the weights is a simple operation and that would make the operation faster.

4.2.3.4 Pruning the RBFNN

The technique of refining the training data mentioned above is not enough; in the cases where we have large data set, the neural network will start to be bigger and bigger even after cleaning up the data. The best way to solve this issue is to refine the network itself; in other words, we need to “prune” those centers that the network has seen before and incorporate those centers that are new (Liu et al., 2001). Figure 4.5 shows the idea of pruning the neural network.

In Figure 4.5, the new network is a combination of a modified version of a pre-existing network and new set of neurons added to it. The procedure of getting a new neural network in this scheme is simple. Using the new input data \mathbf{X} , and using the same method we used to get the centers and widths of the current model, we can get the centers and widths of the new model (see: Finding the Optimal Centers in the previous sections). Assuming the current model has a center vector \mathbf{C}_1 and the new data set has a center vector \mathbf{C}_2 , then a new center vector can be constructed out of these centers as follows:

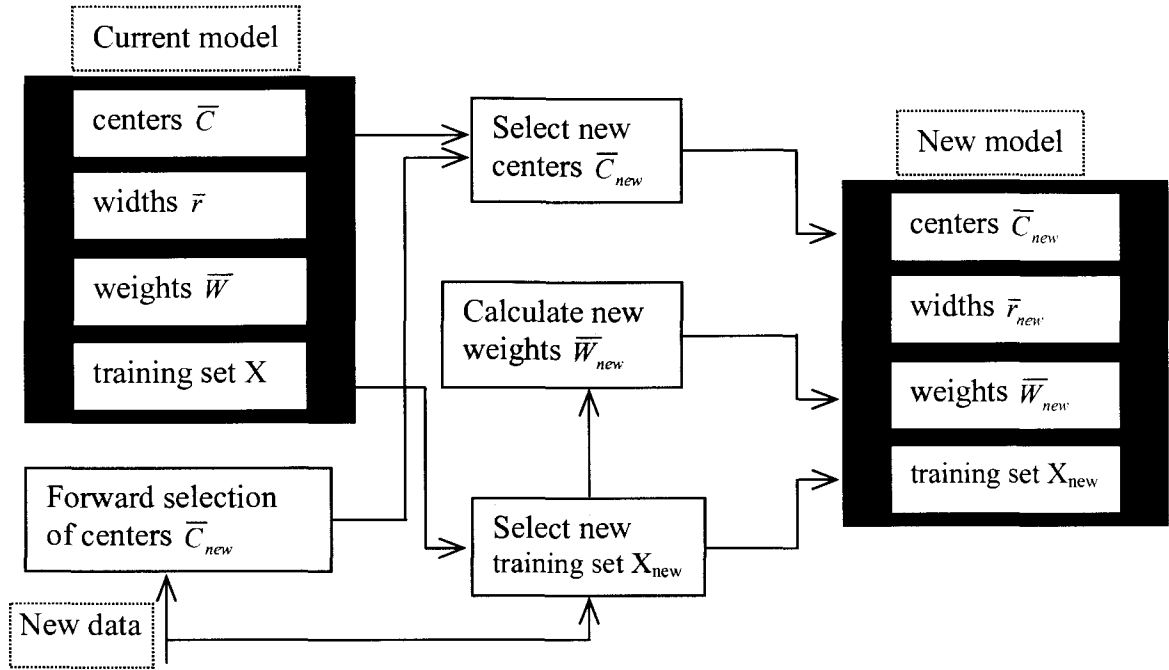


Figure 4.5: Adaptive RBF Neural network technique. (Adopted from Liu et al., 2001).

{ For $C_i \in C_1$ and $C_j \in C_2$,
if $\| C_i - C_j \| \leq T$,
then remove C_i }

where $\| \cdot \|$ is the Euclidean distance, and T is a threshold. For the rest of the centers that were not removed from C_1 or in other words those who have distance with any center in C_2 more than the threshold, we add them to the new centers C_2 and a new set of centers is performed C_{new} . Now, since we have this new model of C_{new} we can calculate a new set of weights to get the target of X (Liu et al., 2001).

This technique gives the priority to the new data and removes redundant data, and this would keep the network growth small, keep the network updated and generalized.

4.3 PERFORMANCE EVALUATION OF THE ADAPTIVE RADIAL BASIS FUNCTION NEURAL NETWORK

4.3.1 TRAINING THE NETWORK

The radar data used in this evaluation were collected by Melbourne-Florida, Houston-Texas and Kwajalein-Marshall Islands sites. The neural network was trained adaptively at the end of every day. The target of the network was the rain gauge measurements that were collected from the tipping bucket rain gauge networks around those three radars. The data were from years 2005, 2006, 2007 and 2008. Data were taken within 100km around the radar. Input training data which was the radar measurements was taken at 1km 2km, 3 km and 4 km heights as shown in Figure 4.3. This would make the size of the input vector to be four ($p=4$). Rain gauge data were averaged over 5 minutes to meet the radar sweep time. Figure 4.6 shows a representation of how the neural network is trained.

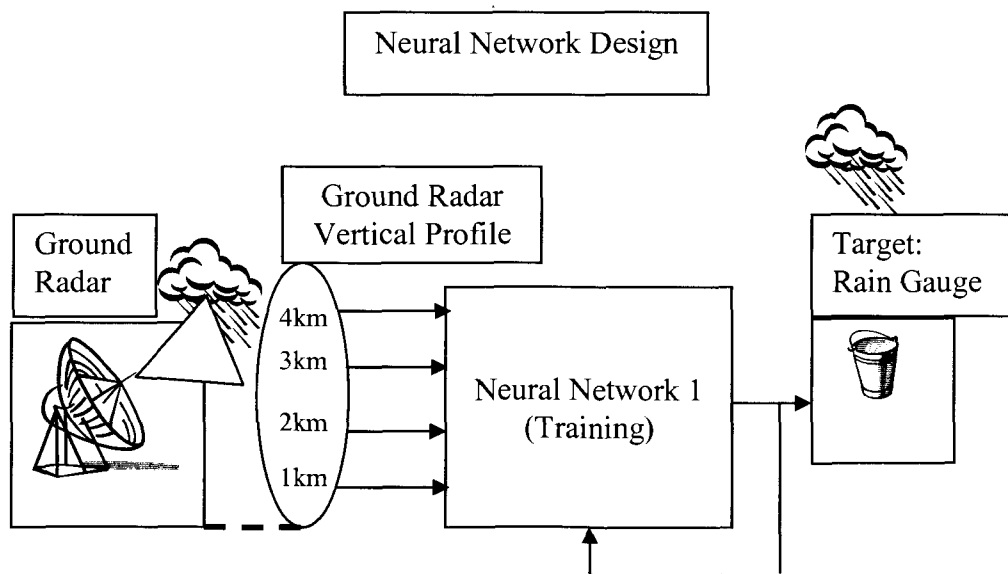


Figure 4.6: Neural Network Training: Input ground radar reflectivity. Target: Rain gauge.

4.3.2 TESTING AND VALIDATING THE NETWORK

At the end of any day, once the network is trained, and then in the following day, when we have new data available, this data is used to estimate rain rate using the neural network that was trained in the previous day. The estimation was validated against the rain gauge measurements of that day. Figure 4.7 shows a representation of the rain rate estimation using the trained neural network.

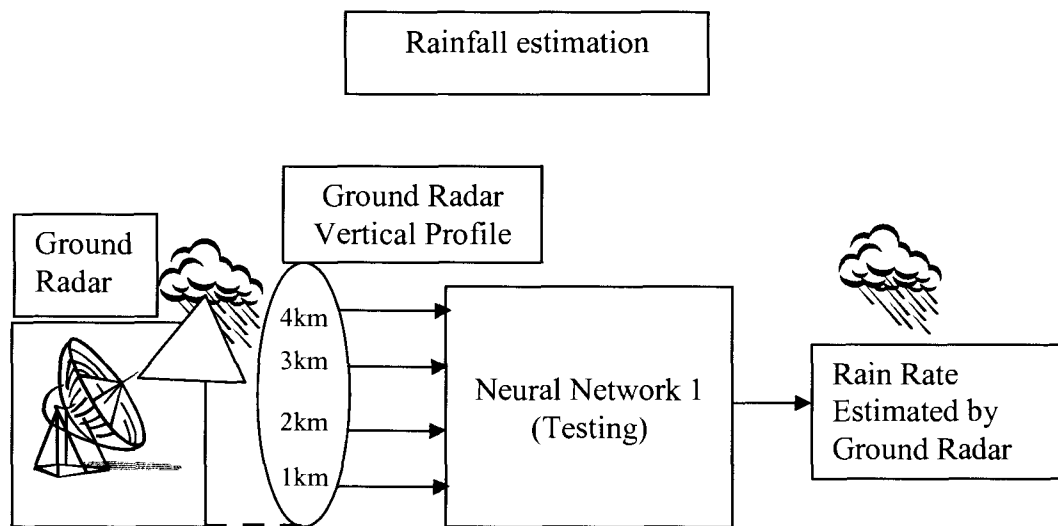


Figure 4.7: Rain rate estimation using trained neural network.

4.3.3 PERFORMANCE EVALUATION

The performance of the network was calculated using the evaluation criteria mentioned in chapter 2 (FracBias, Corr., NSE, and FRMSE). The network performance was also compared with the simple Z-R relation used in NEXRAD radars, and with the Best-Fit statistical technique.

Tables 4.1, 4.2, 4.3, 4.5, 4.6, 4.7, 4.8, 4.9 and 4.10 show hourly rainfall accumulation scores of the adaptive neural network using data from year 2005, 2006, 2007 and 2008 over KMLB KHGX and KWAJ. As shown in the tables, the performance of the neural network approach is much better than the performance of the Z-R relation. It is also shown that the performance of the neural technique is very close or sometimes better than the performance of the Best-Fit method even though the fitting was done “after the fact”. As we see, the Z-R relation has significant bias compared to the rain gauge measurements, while the neural network product has less biases. The same was also shown in Table 4.4 where instantaneous rainfall rate scores are calculated.

The tables also show that the correlation and the FRMSE scores of the neural networks are better than that for the Z-R relation. The neural networks score higher correlation and lower FRMSE while the Z-R scores lower correlation and higher FRMSE which means a lower variation from truth (rain gauge) in the favor of the neural network technique. The proposed technique has good scores compared to the Best-Fit method as well. As we see, the neural network scores are either very close or sometimes better than the Best-Fit scores taking into consideration again that the Best-Fit was done after the fact. Figures 4.8, 4.9, 4.10, 4.11, 4.12, 4.13, 4.14, 4.15, 4.16 and 4.17 show the same conclusions that can be entailed from the tables. The figures show better scatter and standard deviation plots of the neural network performance when compared to the Z-R plots shown at the end of Chapter 2. The figures show a competitive performance when compared to the best fit figures shown in the same chapter.

Table 4.1: Performance evaluation of the NN rain rate estimation , the Z-R estimation, and the Best-Fit estimation against rain gauge. Data from year 2005 over KMLB. (Hourly Rainfall Accumulation).

KMLB 2005	FracBias (%)	Corr.	NSE	FRMSE (%)
NN Est. vs. Rain Gauge	1.6	0.86	0.25	38.6
Z-R Est. vs. Rain Gauge	-32.3	0.82	0.40	54.3
Best Fit Est. vs. Rain Gauge	-22.8	0.87	0.30	44.0

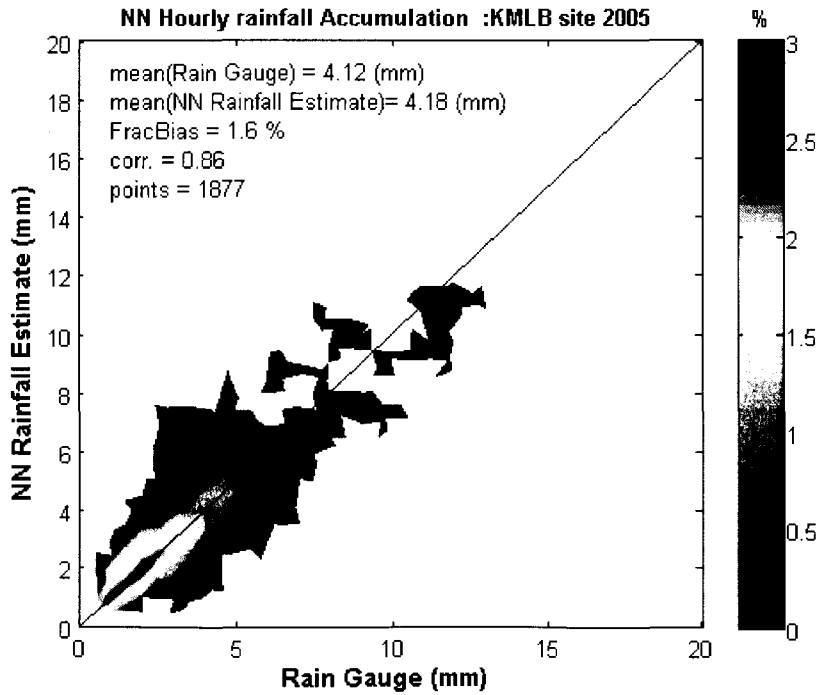


Figure 4.8: Actual rain gauge vs. NN estimate. Data from year 2005 over KMLB. (Hourly Rainfall Accumulation).

Table 4.2: Performance evaluation of the NN rain rate estimation , the Z-R estimation, and the Best-Fit estimation against rain gauge. Data from year 2006 over KMLB. (Hourly Rainfall Accumulation).

KMLB 2006	FracBias (%)	Corr.	NSE	FRMSE (%)
NN Est. vs. Rain Gauge	2.4	0.81	0.30	44.2
Z-R Est. vs. Rain Gauge	-44.9	0.72	0.50	68.8
Best Fit Est. vs. Rain Gauge	-26.5	0.80	0.36	51.5

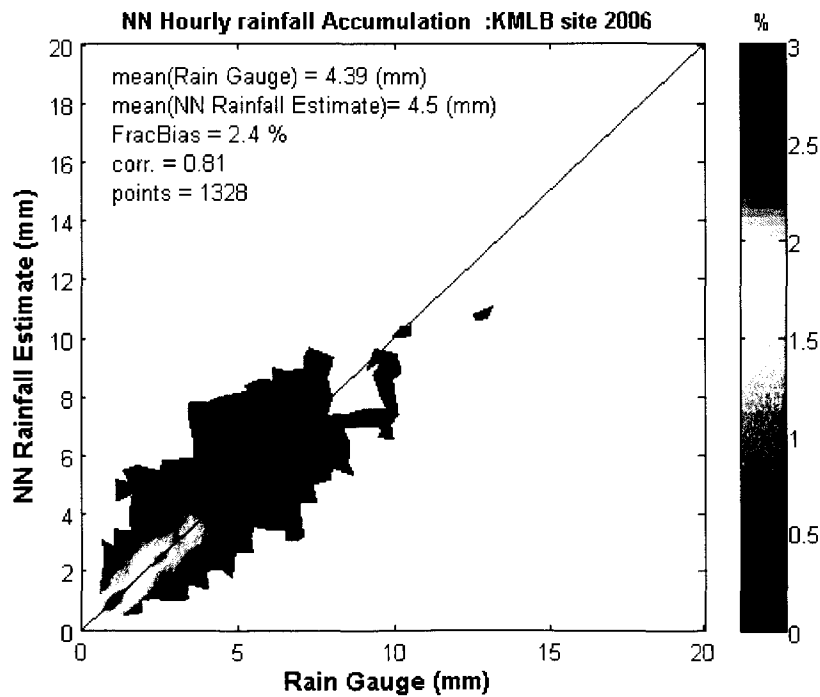


Figure 4.9: Actual rain gauge vs. NN estimate. Data from year 2006 over KMLB. (Hourly Rainfall Accumulation).

Table 4.3: Performance evaluation of the NN rain rate estimation , the Z-R estimation, and the Best-Fit estimation against rain gauge. Data from year 2007 over KMLB. (Hourly Rainfall Accumulation).

KMLB 2007	FracBias (%)	Corr.	NSE	FRMSE (%)
NN Est. vs. Rain Gauge	3.1	0.82	0.31	45.9
Z-R Est. vs. Rain Gauge	-44.0	0.75	0.51	68.4
Best Fit Est. vs. Rain Gauge	-16.6	0.82	0.32	46.8

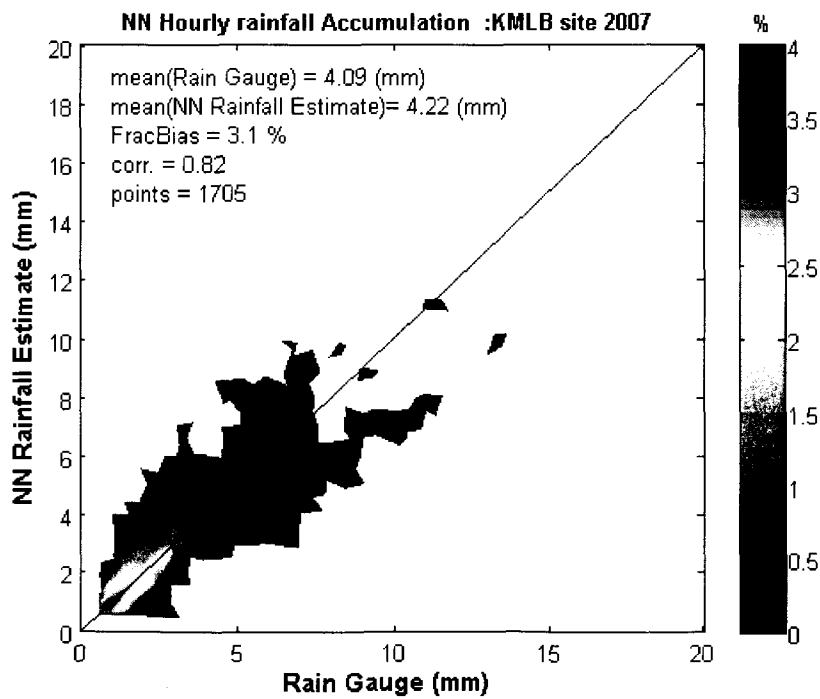


Figure 4.10: Actual rain gauge vs. NN estimate. Data from year 2007 over KMLB. (Hourly Rainfall Accumulation).

Table 4.4: Performance evaluation of the NN rain rate estimation , the Z-R estimation, and the Best-Fit estimation against rain gauge. Data from year 2008 over KMLB. (Instantaneous Rainfall).

KMLB 2008	FracBias (%)	Corr.	NSE	FRMSE (%)
NN Est. vs. Rain Gauge	10.4	0.71	0.51	73.9
Z-R Est. vs. Rain Gauge	-44.8	0.62	0.61	104.6
Best Fit Est. vs. Rain Gauge	-11.8	0.74	0.45	70.5

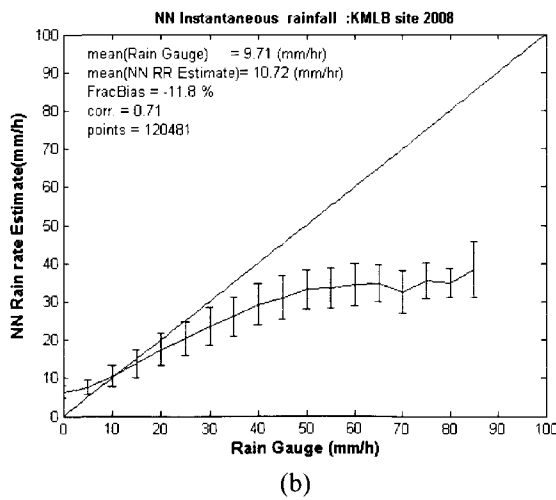
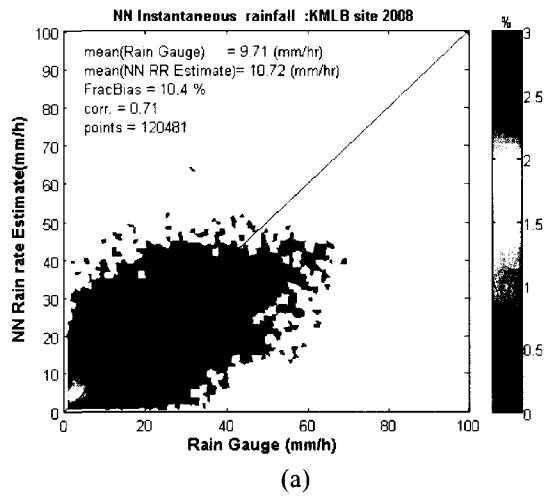
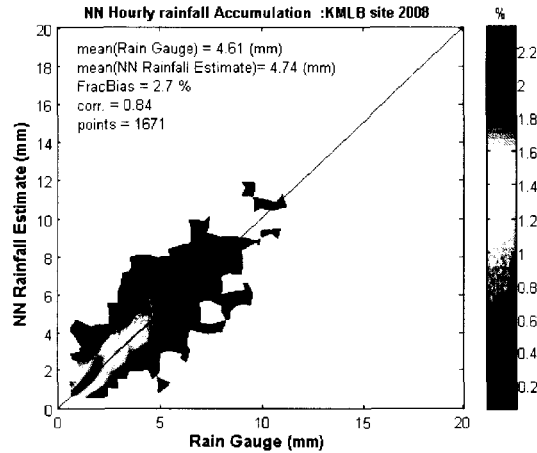


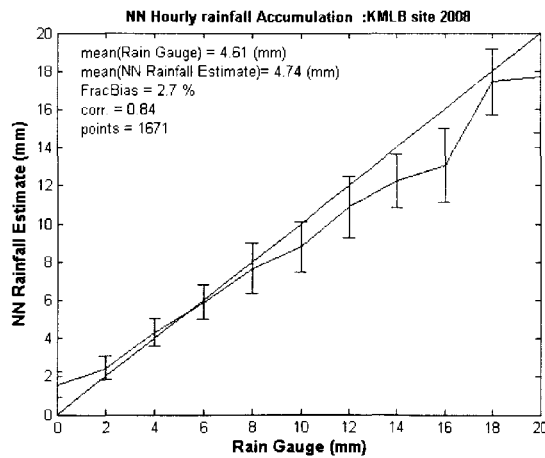
Figure 4.11: Actual rain gauge vs. NN estimate. a) Scatter plot. b) Standard deviation plot. Data from year 2008 over KMLB. (Instantaneous Rainfall).

Table 4.5: Performance evaluation of the NN rain rate estimation , the Z-R estimation, and the Best-Fit estimation against rain gauge. Data from year 2008 over KMLB. (Hourly Rainfall Accumulation).

KMLB 2008	FracBias (%)	Corr.	NSE	FRMSE (%)
NN Est. vs. Rain Gauge	2.7	0.84	0.27	40.9
Z-R Est. vs. Rain Gauge	-44.5	0.65	0.52	74.4
Best Fit Est. vs. Rain Gauge	-19.9	0.83	0.30	45.8



(a)



(b)

Figure 4.12: Actual rain gauge vs. NN estimate. a) Scatter plot. b) Standard deviation plot. Data from year 2008 over KMLB. (Hourly Rainfall Accumulation).

Table 4.6: Performance evaluation of the NN rain rate estimation , the Z-R estimation, and the Best-Fit estimation against rain gauge. Data from year 2005 over KHGX. (Hourly Rainfall Accumulation).

KHGX 2005	FracBias (%)	Corr.	NSE	FRMSE (%)
NN Est. vs. Rain Gauge	0.3	0.79	0.29	40.0
Z-R Est. vs. Rain Gauge	-31.7	0.69	0.50	69.4
Best Fit Est. vs. Rain Gauge	-23.6	0.80	0.34	44.3

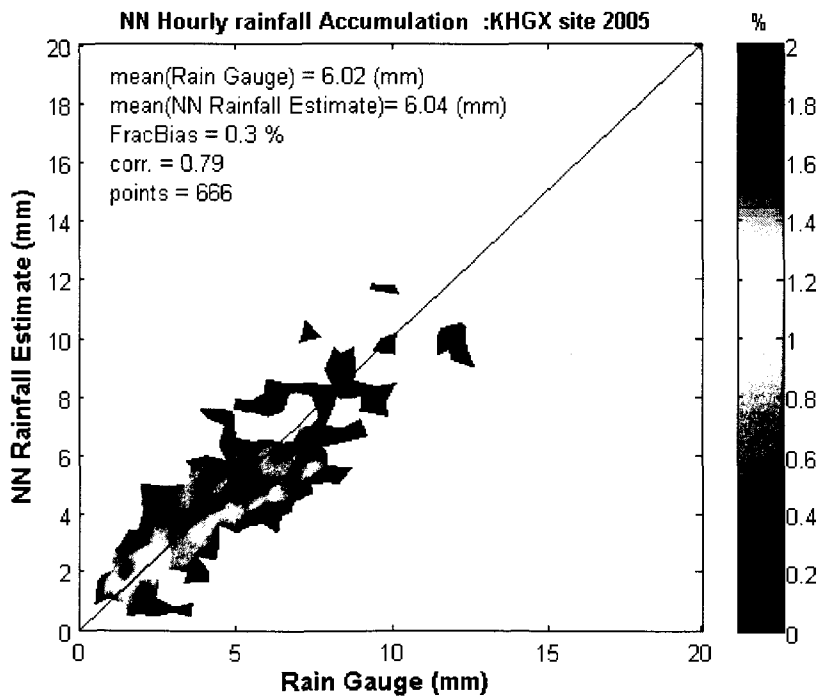


Figure 4.13: Actual rain gauge vs. NN estimate. Data from year 2005 over KHGX. (Hourly Rainfall Accumulation).

Table 4.7: Performance evaluation of the NN rain rate estimation , the Z-R estimation, and the Best-Fit estimation against rain gauge. Data from year 2006 over KHGX. (Hourly Rainfall Accumulation).

KHGX 2006	FracBias (%)	Corr.	NSE	FRMSE (%)
NN Est. vs. Rain Gauge	6.30	0.84	0.24	35.1
Z-R Est. vs. Rain Gauge	-42.0	0.75	0.48	61.5
Best Fit Est. vs. Rain Gauge	-9.7	0.86	0.24	33.3

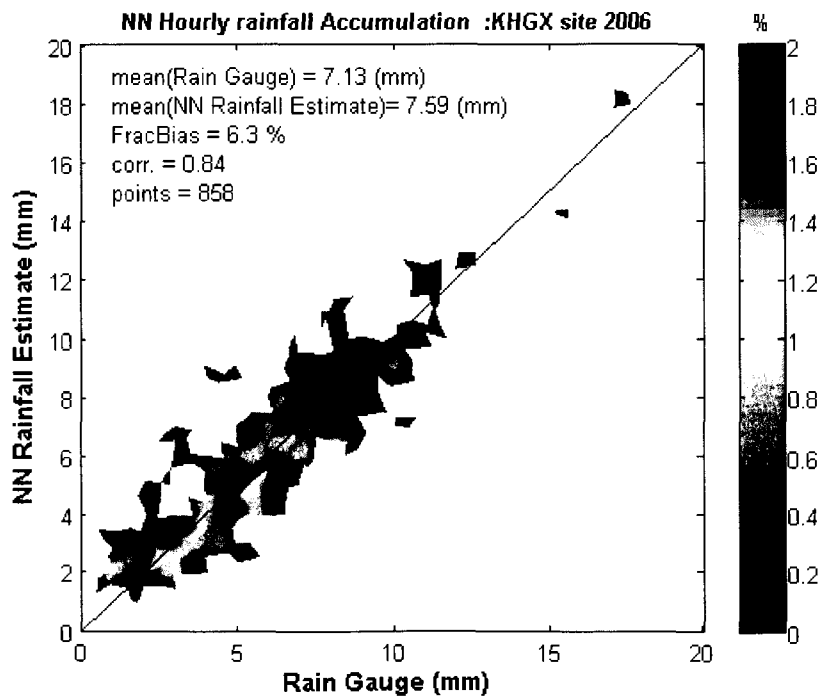
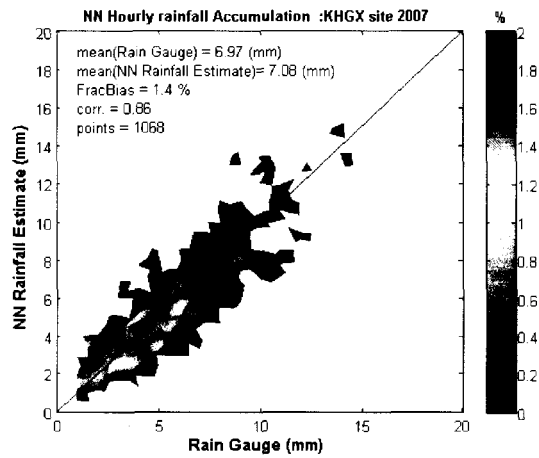


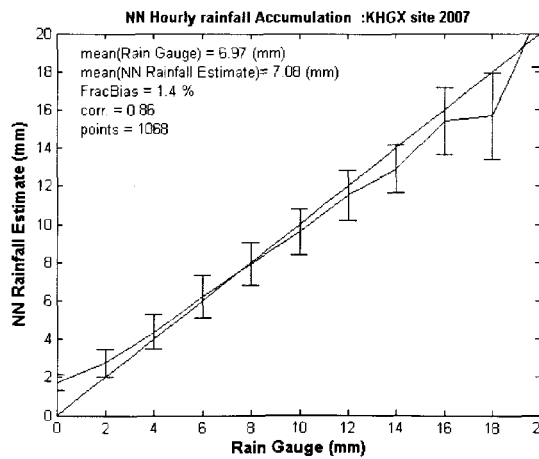
Figure 4.14: Actual rain gauge vs. NN estimate. Data from year 2006 over KHGX. (Hourly Rainfall Accumulation).

Table 4.8: Performance evaluation of the NN rain rate estimation , the Z-R estimation, and the Best-Fit estimation against rain gauge. Data from year 2007 over KHGX. (Hourly Rainfall Accumulation).

KHGX 2007	FracBias (%)	Corr.	NSE	FRMSE (%)
NN Est. vs. Rain Gauge	1.4	0.86	0.23	32.5
Z-R Est. vs. Rain Gauge	-46.9	0.71	0.53	67.1
Best Fit Est. vs. Rain Gauge	-19.8	0.84	0.29	38.4



(a)



(b)

Figure 4.15: Actual rain gauge vs. NN estimate. a) Scatter plot. b) Standard deviation plot. Data from year 2007 over KHGX. (Hourly Rainfall Accumulation).

Table 4.9: Performance evaluation of the NN rain rate estimation , the Z-R estimation, and the Best-Fit estimation against rain gauge. Data from year 2006 over KWAJ. (Hourly Rainfall Accumulation).

KWAJ 2006	FracBias (%)	Corr.	NSE	FRMSE (%)
NN Est. vs. Rain Gauge	-4.0	0.82	0.35	57.4
Z-R Est. vs. Rain Gauge	-53.7	0.80	0.57	85.3
Best Fit Est. vs. Rain Gauge	-12.1	0.80	0.37	61.0

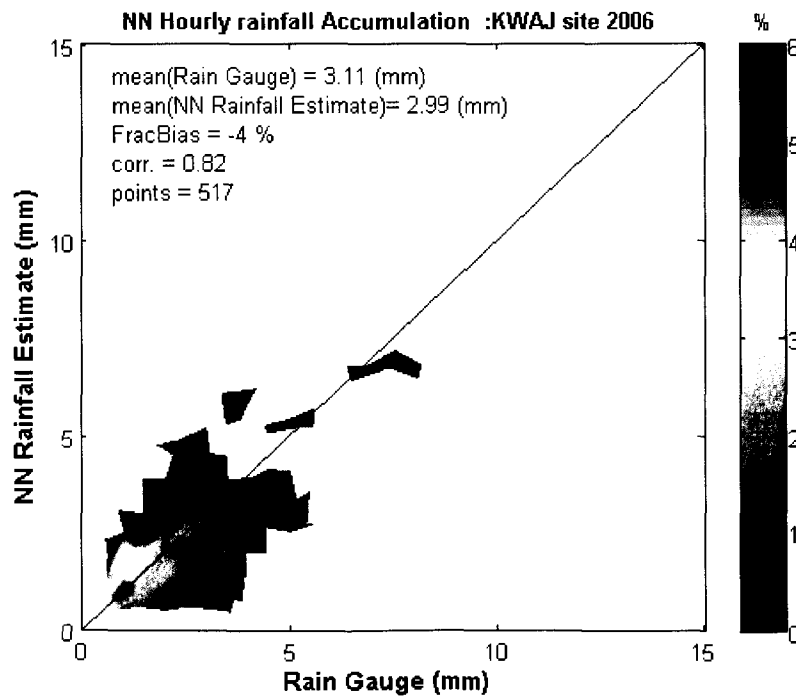
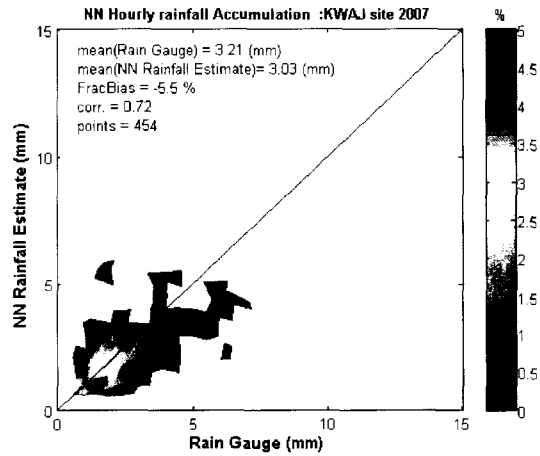


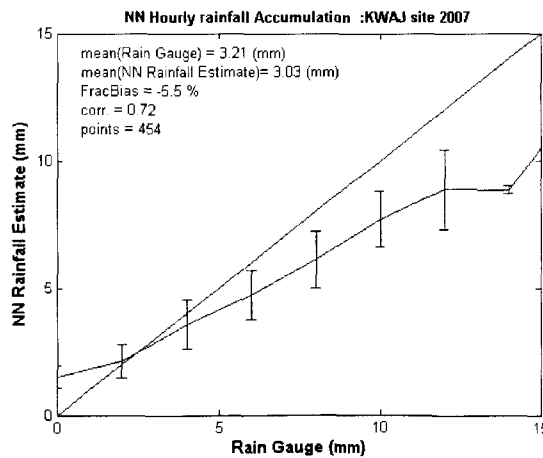
Figure 4.16: Actual rain gauge vs. NN estimate. Data from year 2006 over KWAJ. (Hourly Rainfall Accumulation),

Table 4.10: Performance evaluation of the NN rain rate estimation , the Z-R estimation, and the Best-Fit estimation against rain gauge. Data from year 2007 over KWAJ. (Hourly Rainfall Accumulation).

KWAJ 2007	FracBias (%)	Corr.	NSE	FRMSE (%)
NN Est. vs. Rain Gauge	-5.5	0.72	0.39	58.8
Z-R Est. vs. Rain Gauge	-53.7	0.64	0.60	83.4
Best Fit Est. vs. Rain Gauge	-0.8	0.72	0.40	60.2



(a)



(b)

Figure 4.17: Actual rain gauge vs. NN estimate. a) Scatter plot. b) Standard deviation plot. Data from year 2007 over KWAJ. (Hourly Rainfall Accumulation).

4.3.4 TESTING THE DESIGNED NETWORK WITH ALTERNATIVE SITE RADAR/GAUGE DATA

In order to evaluate the generalization capability of the designed networks, we test KMLB NN using KHGX data. The same training technique described before was done in this scenario; the network was adaptively trained on daily base and the data from any day was tested by the network designed the day before. The same scoring parameters were used as before. Table 4.11 shows the performance evaluation of estimating the rain rate. The table still shows better performance of the neural networks compared to the Z-R relation, which means that this technique can be generalized to include other areas. This idea is yet to be studied for other climatological areas.

Table 4.11: Performance evaluation of KMLB NN testing KHGX data. (Hourly Rainfall Accumulation).

	FracBias (%)	Corr.	NSE	FRMSE (%)
KHGX Est. using KMLB NN: 2005	-23.0	0.83	0.31	41.9
KHGX Est. using KMLB NN: 2006	-24.6	0.83	0.32	42.6
KHGX Est. using KMLB NN: 2007	-24.1	0.82	0.32	41.7

4.3.5 EFFECT OF RADAR MEASUREMENT HEIGHTS ON RAIN RATE ESTIMATION USING NEURAL NETWORKS

In the last two sections, the neural network was designed and tested based on radar measurements taken up to 4km height starting at 1 km with 1km spacing. In this section, we are trying to investigate the effect of the height going from 3 km up to 10 km keeping

the same spacing. In other words, we need to find out whether radar measurements for heights lower or higher than 4km would improve the performance of the network or not?

To answer this question, we first calculated the correlation between rain gauge measurements and the radar reflectivity factor measured at different heights starting at 1km and up to 10 km. We noticed that the correlation starts to decrease after the 4km height, as shown in Table 4.12. This was noticed for most of the radars in most of the years.

Table 4.12: Correlation between rain gauge and radar reflectivity at different heights (1 to 10 km).

KMLB	KMLB	KMLB	KMLB	KHGX	KHGX	KHGX	KWAJ	KWAJ
2005	2006	2007	2008	2005	2006	2007	2006	2007
0.5244	0.5291	0.4932	0.3754	0.4998	0.5135	0.5417	0.2853	0.3377
0.5429	0.5502	0.5049	0.4258	0.4638	0.4949	0.5163	0.3616	0.5518
0.4916	0.5066	0.4588	0.4005	0.4234	0.4417	0.4718	0.1895	0.5473
0.4442	0.4596	0.4210	0.3589	0.3884	0.3885	0.4294	0.1612	0.5232
0.3966	0.4249	0.3893	0.3485	0.3593	0.3492	0.3892	0.2422	0.4588
0.3671	0.3916	0.3660	0.3294	0.3295	0.3163	0.3506	0.2329	0.4440

In continuation to answer the previous question, the neural networks were trained and tested using rain gauges and radar measurements at different heights (3km to 10 km). Tables 4.13, 4.14, 4.15, 4.16, 4.17, 4.18, 4.19, 4.20, and 4.21 show the results of this test over KWAJ, KHGX and KMLB sites. The tables show that when the radar measurements

were taken from 1km and up to 4 km height, the performance was better than that if we take radar measurements up to height lower or higher than 4 km. The red rows in the tables indicate the performance of the networks for radar measurements from 1km and going up to 4 km for most of the radars in most of the years. The red rows in all tables show that measurements up to 4km height were giving the best performance compared to the other heights.

It is worth mentioning that taking radar measurements higher than 4km will reduce the number of good (valid) profiles that can be used to train the network; this is because of low rain rate measurements are mostly related to weak storms, which usually do not have measured reflectivity at higher altitudes. Therefore, considering measurements at higher altitudes would eliminate weak storms from taking part.

Table 4.13: The effect of using radar measurements from different heights on the performance of the NN rain rate estimator. Data from year 2005 over KMLB. (Hourly Rainfall Accumulation)

Height (Km)	FracBias (%)	Corr.	NSE	FRMSE (%)
3	0.6	0.87	0.26	38.0
5	1.8	0.85	0.26	40.3
6	2.0	0.86	0.26	39.4
7	4.9	0.79	0.32	51.3
8	9.1	0.77	0.36	58.4
9	16.3	0.77	0.41	64.5
10	22.0	0.73	0.47	73.3

Table 4.14: The effect of using radar measurements from different heights on the performance of the NN rain rate estimator. Data from year 2006 over KMLB. (Hourly Rainfall Accumulation)

Height (Km)	FracBias (%)	Corr.	NSE	FRMSE (%)
3	2.5	0.81	0.31	46.9
5	1.6	0.80	0.30	44.8
6	2.7	0.80	0.31	46.7
7	3.4	0.77	0.33	50.6
8	9.8	0.73	0.40	58.9
9	15.1	0.68	0.45	68.2
10	20.9	0.64	0.51	73.7

Table 4.15: The effect of using radar measurements from different heights on the performance of the NN rain rate estimator. Data from year 2007 over KMLB. (Hourly Rainfall Accumulation)

Height (Km)	FracBias (%)	Corr.	NSE	FRMSE (%)
3	3.2	0.82	0.31	46.8
5	3.1	0.81	0.31	46.1
6	1.7	0.80	0.32	46.4
7	1.9	0.77	0.33	50.2
8	5.9	0.74	0.35	54.3
9	5.5	0.69	0.39	60.9
10	8.6	0.67	0.42	65.6

Table 4.16: The effect of using radar measurements from different heights on the performance of the NN rain rate estimator. Data from year 2008 over KMLB. (Hourly Rainfall Accumulation)

Height (Km)	FracBias (%)	Corr.	NSE	FRMSE (%)
3	1.2	0.84	0.27	41.4
5	4.3	0.82	0.29	44.2
6	3.9	0.77	0.31	50.3
7	4.6	0.76	0.33	51.8
8	10.7	0.76	0.37	56.9
9	14.9	0.75	0.41	62.2
10	28.0	0.59	0.58	96.3

Table 4.17: The effect of using radar measurements from different heights on the performance of the NN rain rate estimator. Data from year 2005 over KHGX. (Hourly Rainfall Accumulation)

Height (Km)	FracBias (%)	Corr.	NSE	FRMSE (%)
3	0.7	0.77	0.29	41.2
5	-0.9	0.80	0.27	38.9
6	-0.4	0.84	0.26	36.5
7	-0.6	0.80	0.28	40.4
8	2.2	0.81	0.28	40.2
9	2.6	0.82	0.29	39.0
10	6.9	0.73	0.34	49.1

Table 4.18: The effect of using radar measurements from different heights on the performance of the NN rain rate estimator. Data from year 2006 over KHGX. (Hourly Rainfall Accumulation)

Height (Km)	FracBias (%)	Corr.	NSE	FRMSE (%)
3	5.4	0.84	0.25	35.6
5	6.8	0.82	0.25	38.0
6	7.9	0.81	0.27	40.5
7	5.8	0.79	0.29	43.4
8	8.0	0.81	0.31	44.9
9	10.0	0.76	0.34	49.1
10	11.6	0.75	0.35	51.8

Table 4.19: The effect of using radar measurements from different heights on the performance of the NN rain rate estimator. Data from year 2007 over KHGX. (Hourly Rainfall Accumulation)

Height (Km)	FracBias (%)	Corr.	NSE	FRMSE (%)
3	4.4	0.86	0.24	33.7
5	1.7	0.84	0.24	34.7
6	1.1	0.85	0.24	34.7
7	2.2	0.81	0.27	39.7
8	2.1	0.84	0.28	38.5
9	0.8	0.83	0.28	39.0
10	5.8	0.81	0.31	47.7

Table 4.20: The effect of using radar measurements from different heights on the performance of the NN rain rate estimator. Data from year 2006 over KWAJ. (Hourly Rainfall Accumulation)

Height (Km)	FracBias (%)	Corr.	NSE	FRMSE (%)
3	3.2	0.81	0.37	58.7
5	-5.0	0.82	0.37	55.4
6	-6.8	0.73	0.40	61.5
7	-2.0	0.71	0.44	62.7
8	0.5	0.70	0.47	65.9
9	-4.5	0.59	0.53	80.6
10	16.1	0.44	0.75	102.5

Table 4.21: The effect of using radar measurements from different heights on the performance of the NN rain rate estimator. Data from year 2007 over KWAJ. (Hourly Rainfall Accumulation)

Height (Km)	FracBias (%)	Corr.	NSE	FRMSE (%)
3	2.1	0.72	0.41	62.1
5	-5.3	0.63	0.45	69.3
6	-3.6	0.66	0.45	70.8
7	-1.2	0.57	0.51	87.7
8	2.3	0.66	0.49	75.7
9	30.4	0.75	0.64	92.2
10	-19.3	0.69	0.51	88.5

4.4 USING PRINCIPAL COMPONENT ANALYSIS TO IMPROVE THE PERFORMANCE OF THE RBF NN

4.4.1 PRINCIPAL COMPONENT ANALYSIS

In this section, the spatial variability of the radar reflectivity factor Z along 4 CAPPI levels is explored by applying the Principal Component Analysis (PCA) over the

standardized values of $Z_i(i=1,\dots,4)$, where Z_i represents the radar reflectivity factor measured at height i . The standardized values of Z_i are given by

$$\check{Z}_i = (Z_i - E[Z_i]) / \sqrt{\text{Var}[Z_i]} \quad (4.8)$$

where $E[Z_i]$ and $\text{Var}[Z_i]$ denote the sample mean and variance of Z_i . Standardization is necessary due to the different range values Z_i might have. If we define \mathbf{S}_z to be the sample covariance matrix of $\check{\mathbf{Z}}$, with elements $(\mathbf{S}_z)_{ij}$ given by

$$(\mathbf{S}_z)_{ij} = \text{Cov}[\check{Z}_i, \check{Z}_j] = \sum_{s=1}^M (\check{Z}_i)_s (\check{Z}_j)_s / M : (i=1,\dots,4; j=1,\dots,4) \quad (4.9)$$

where M is the number of input patterns, then we need to find the eigenvectors \mathbf{e} and the eigenvalues \mathbf{D} of the covariance matrix as below,

$$\mathbf{e}^{-1} \mathbf{S}_z \mathbf{e} = \mathbf{D} \quad (4.10)$$

After that we calculate the Principal Components PC's that are associate with the eigenvalues using

$$\text{PC}_1 = \mathbf{e}_1^T \check{\mathbf{Z}}, \text{PC}_2 = \mathbf{e}_2^T \check{\mathbf{Z}}, \dots, \text{PC}_4 = \mathbf{e}_4^T \check{\mathbf{Z}}, \quad (4.11)$$

The goal of using the PCA concept in this contest is to reduce the dimensionality of the training data to a level where we still can get good performance. In this section, we are going to train the neural network using the PC's rather than the radar reflectivity factor Z . To get benefit from this concept and to reduce the dimensionality of the training data, we are going to neglect those PC's with small eigenvalues. There are two methods to decide which PC's to neglect. The first one is to sum the eigenvalues from the largest

to the lowest, and when the sum exceeds a certain threshold we stop adding eigenvalues, and we use only those PC's whose eigenvalues were considered in the addition. Another way to find out which PC's to include is to use the Fisher's Maximum Coverage Test (Mielke and Berry, 2007).

4.4.2 PERFORMANCE EVALUATION OF RBF NN USING PCA

The PCA concept was applied to the data from years 2005, 2006, 2007 and 2008 over KMLB, KWAJ and KHGX sites. It was found that two principal components were enough to give good performance or even better than that using four levels of radar reflectivity factor to train the network. Two input configurations were tested in this regard, in each one the performance of the neural network was measured as well as the time it takes the neural network to train, and the number of neurons needed (network size). The goal why we include the training time and the network size is to see the effect of the size of the input data and to see how feasible the network can be in order to be applied in real life.

- **Input Configuration 1:**

This input configuration is the same one used in the previous evaluations. The network was trained using radar measurements at 1, 2, 3 and 4km heights, and rain gauges were the target. The reason we show this input configuration here is to show the training time and the network size at each case in order to find out the improvement brought by PCA technique.

Figure 4.18 shows the configuration of the input where radar reflectivity factor at four different heights was used to train the network. The performance of the neural network using this input configuration is shown in Table 4.22.

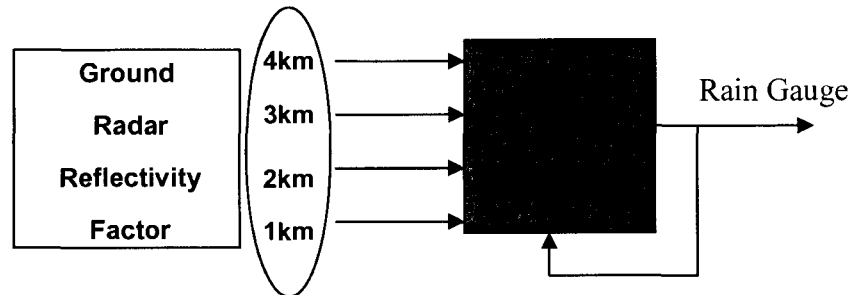


Figure 4.18: Schematic of NN trained with input configuration 1.

Table 4.22: The performance of the RBF NN using radar data as. (Hourly rainfall accumulation).

Site/Year						
KWAJ 2006	-4.0	0.82	0.35	57.4	475	45
KWAJ 2007	-5.5	0.72	0.39	58.8	820	29
KHGX2005	0.3	0.79	0.29	40.0	1010	22
KHGX2006	6.3	0.84	0.24	35.1	1629	34
KHGX2007	1.4	0.86	0.23	32.5	2523	25
KMLB 2005	1.6	0.86	0.25	38.6	2154	39
KMLB 2006	2.4	0.81	0.30	44.2	831	34
KMLB 2007	3.1	0.82	0.31	45.9	1911	62
KMLB 2008	2.7	0.84	0.27	40.9	5328	37

- **Input Configuration 2:**

In this configuration, the network was trained using the PC's calculated from the radar measurements at 1, 2, 3 and 4km heights. Only two principal components were used in the training together with their corresponding rain gauges. The chosen PC's were

those whose eigenvalues accumulation is more than the threshold value chosen. Figure 4.19 shows a schematic of this configuration and Table 4.23 shows the neural networks performance when using this input configuration. As we see in Table 4.23, the performance of the neural networks was improved. The main improvements happened in the training time. The training time was reduced on average by almost 50% of the original training time that was spent using the previous input configuration, in addition, the other performance metrics such as (FracBias, Corr., NSE, and FRMSE) were almost the same in most of the cases. Another improvement of using this configuration is the reduction of the network complexity; the previous network was designed using 4-D input vectors, while this network is designed using 2-D input vectors. As can be seen from the table, the network size got reduced by about 50% in most of the cases. This reduction is very important especially when the network is going to be implemented in real time.

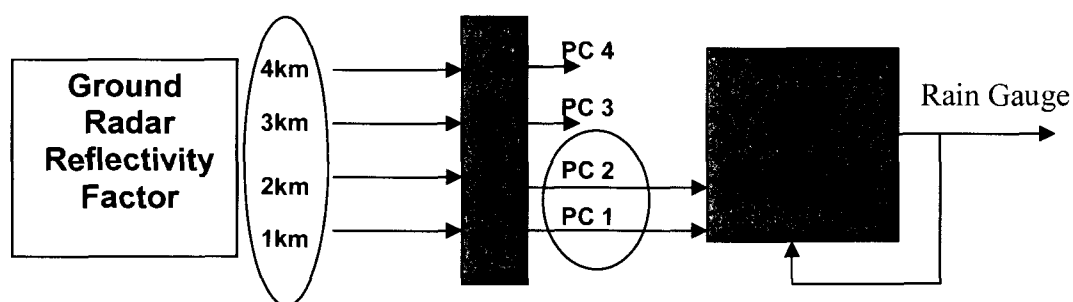


Figure 4.19: Schematic of NN trained with input configuration 2.

Table 4.23: The performance of the RBF NN using 2 PC's as input: Fixed eigen vectors. (Hourly rainfall accumulation) .

Site/Year						
KWAJ 2006	-6.8	0.79	0.38	61.7	283	20
KWAJ 2007	-5.9	0.77	0.36	53.0	439	11
KHGX2005	1.2	0.76	0.30	42.8	641	6
KHGX2006	6.5	0.85	0.24	34.4	997	7
KHGX2007	2.7	0.85	0.24	33.5	1611	18
KMLB 2005	0.7	0.85	0.25	39.6	1324	18
KMLB 2006	0.9	0.82	0.29	43.7	508	15
KMLB 2007	2.6	0.80	0.33	47.9	1124	19
KMLB 2008	1.9	0.83	0.28	42.1	2716	15

The previous results in Tables 4.23 were achieved while the eigen vectors are fixed. The eigen vectors were calculated from the training data set that was used to create the first initial model of the neural network, and were used to calculate the principal components that were used to train and test the network. Another attempt was done where the eigen vectors were recalculated from the updated training data adaptively and used to calculate the principal components that were used to train and test the network. The principal components of the radar reflectivity factor were calculated and used to train and test the network. As shown in Tables 4.24; the performance of the networks was almost the same with sometimes a slight increase in the training time occurred because of the need to recalculate the eigen vectors.

As just shown, the PC's were calculated from radar data taken up to 4 km height. The PC's could be calculated form data up to 10 km height for example, but it is better to

do that from a 4-point radar reflectivity factor (4km height) which would give us the chance to use this method for most kinds of storms weak or strong).

Table 4.24: The performance of the RBF NN using 2 PC's as input: Variable eigen vectors. (Hourly rainfall accumulation) .

Site/Year						
KWAJ 2006	-7.8	0.74	0.39	68.1	297	19
KWAJ 2007	-5.9	0.76	0.36	54.1	439	13
KHGX2005	1.4	0.76	0.31	42.7	632	17
KHGX2006	6.2	0.85	0.24	34.1	1014	17
KHGX2007	2.6	0.85	0.24	34.4	1537	15
KMLB 2005	0.5	0.86	0.25	37.8	1349	16
KMLB 2006	1.3	0.80	0.31	46.3	517	16
KMLB 2007	2.5	0.80	0.32	47.6	1164	20
KMLB 2008	-0.6	0.82	0.28	43.7	2726	21

4.5 USING BAYESIAN NEURAL NETOWK TO IMPROVE RAINFALL ESTIMATION

4.5.1 INTRODUCTION

In the previous sections, RBF neural network was used to estimate rainfall rate. In this section different neural network architecture is used to do the same homework. Bayesian neural network (BN) is going to be used in order to reduce the complexity of the network taking into considerations the performance of the estimation as well as the training time. BN is a modified version of another neural network architecture called Multilayer Perceptrons Neural Network (MLP). MLP neural network was shown and

proved that it can be use to estimate rainfall from radar measurements (Xiao and Chandrasekar, 1997).

4.5.2 MULTILAYER PERCEPTRONS NEURAL NETWORK ARCHITECTURE

MLP neural network is shown in Figure 4.20. It usually consists of input layer, hidden layer and output layer. Training the network is in a supervised manner where there is a target to train against is done with error back-propagation algorithm. The error back-propagation algorithm consists of two passes through the layers of the network. The

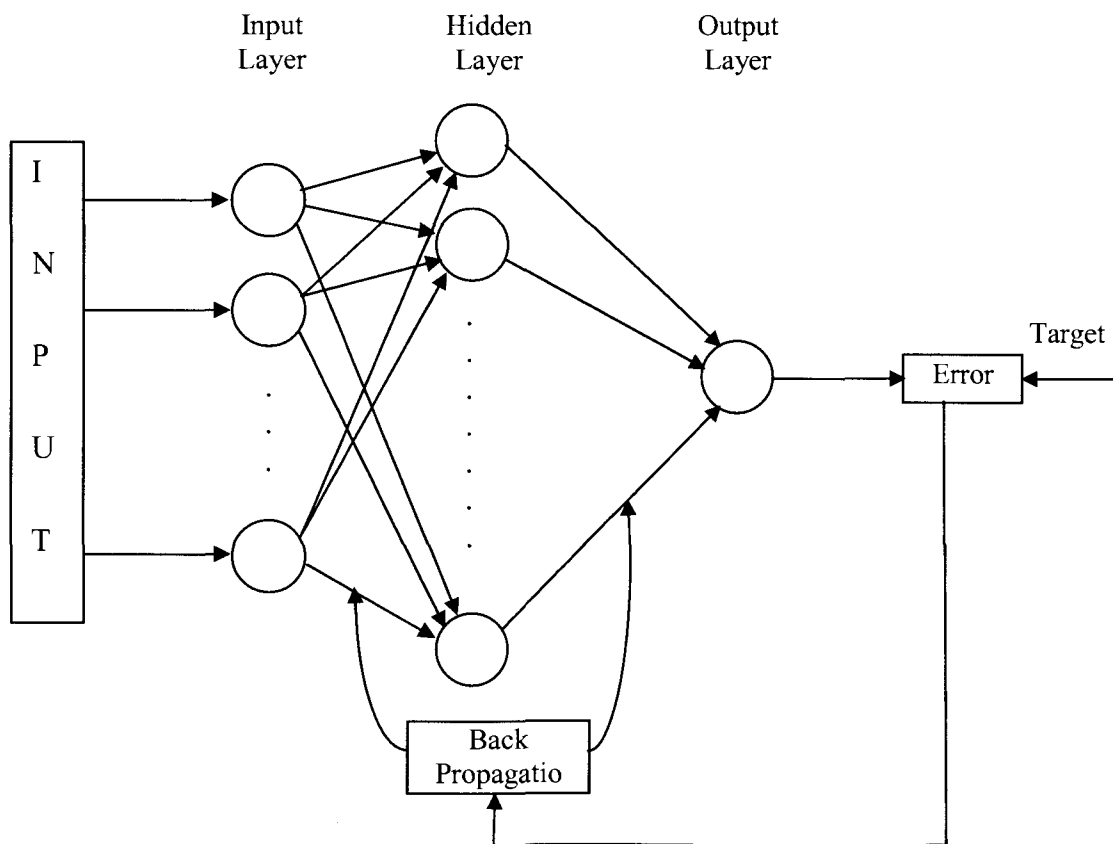


Figure 4.20: Schematic Multilayer Perceptrons Neural Network.

first pass is forward pass, where the training input data is applied to the input neurons of the network and its outputs propagate through the network, layer by layer, until an output is produced by the network. Weights between neurons of layers are initially assigned in random. In the second pass which is called backward pass, the error between the network output and the desired responses (target) is computed and used to adjust the weights. Adjusting the weights is done using the gradient descent algorithm described in (Hayken, 1999). The output layer was modeled by a linear function, while each neuron in the hidden layer is modeled by a nonlinear activation function. In this work, the logistic function expressed by the following equation was used:

$$a = \text{logsig}(n) = \frac{1}{(1 + \exp(-n))} \quad (4.12)$$

4.5.3 BAYESIAN NEURAL NETWORK DEVELOPMENT

Training the MLP network is carried out to minimize an objective function F that can be expressed by

$$F = \sum_{i=1}^N (e_i)^2 \quad (4.13)$$

where e is the error between the network estimate and the desired output (target: t), and N is the number of training patterns. To improve the generalization capability of the network a modification of the objective function is made where the weights are taken into considerations. The objective function C is defined as follows:

$$C = F + \lambda \sum_{i=1}^W (w_i)^2 = F + \lambda Ew \quad (4.14)$$

where λ is a regularization parameter, and W is the number of weights in the network. The goal of including the weights in the cost function C is to ensure smooth response in cases when the network produces large weights. If we assume the weights \mathbf{w} to be random variable, the density function for the weights can be written according to Bayes' rule as:

$$p(\mathbf{w} | t, \lambda) = \frac{p(t | \mathbf{w})p(\mathbf{w} | \lambda)}{p(t | \lambda)} \quad (4.15)$$

If we assume that the noise in the training set data is Gaussian and that the prior distribution for the weights is Gaussian, then the probability densities can be written as:

$$p(t | \mathbf{w}) = \frac{1}{\pi^{N/2}} \exp(-F) \quad (4.16)$$

$$p(\mathbf{w} | \lambda) = \frac{1}{(\pi / \lambda)^{W/2}} \exp(-\lambda E\mathbf{w}) \quad (4.17)$$

Recall Bayes' rule from 4.15 we can write:

$$\begin{aligned} p(\mathbf{w} | t, \lambda) &= \frac{1}{A} \exp(-(F + \lambda E\mathbf{w})) \\ \dots\dots\dots &= \frac{1}{A} \exp(-C) \end{aligned} \quad (4.18)$$

where A is a factor. Then the goal is to minimize the cost function C , or in other words to maximize the posterior function $p(\mathbf{w}|t)$. Further details about this type of neural networks and how to find the regularization parameter λ can be found in (Foresee and Hagan, 1997).

4.5.4 PERFORMANCE OF BAYESIAN NEURAL NETWORK

The network was trained and tested using data from KWAJ, KHGX and KMLB. Training data has a size of four representing radar reflectivity at 1, 2, 3 and 4 km heights. Older training data was pruned every time we have newer data that is close to the older data. The way to do pruning is already described in previous sections in this chapter. The network is trained at the end of the day after pruning is done, and today's network is used to test tomorrow's data. Two architectures of Bayesian neural network are tested; the first architecture has one hidden layer with four neurons in that layer. The second architecture is with two hidden layer where the first layer has four neurons and the second layer has two neurons. The same performance metrics considered before were calculated in these scenarios. Table 4.25 shows the performance of the RBF NN and the BN with one hidden layer in the latter one. Table 4.26 shows the performance of both networks but when two hidden layers were used in the BN.

As we see from Table 4.25, both networks (RBF NN and BN) have almost the same performance; the main point in this table is the number of hidden units and the number of centers. As we see from the table, the BN requires less number of hidden units compared with RBF NN which requires more centers to converge to the answer, but due to the back propagation that is used in training the BN, BN usually needs more training time.

Table 4.26 shows both networks results but for the BN the number of layers was two with four neurons in the first layer and two in the second. The scenario was done in order to check the generalization ability of the network when the size of the network is

Table 4.25: The performance of the RBF NN vs BN. BN has one hidden layer of four neurons. (Hourly rainfall accumulation).

Site/Year						
KWAJ 2006/ RBF	-4.0	0.82	0.35	57.4	475	45
KWAJ 2006/ BN	-4.2	0.81	0.36	58.3	2535	4
KWAJ 2007/ RBF	-5.5	0.72	0.39	58.8	820	29
KWAJ 2007/ BN	-7.1	0.72	0.38	58.7	2004	4
KHGX2005/ RBF	0.3	0.79	0.29	40.0	1010	22
KHGX2005/ BN	0.1	0.79	0.29	39.9	4529	4
KHGX2006/ RBF	6.3	0.84	0.24	35.1	1629	34
KHGX2006/ BN	5.4	0.85	0.24	34.1	5302	4
KHGX2007/ RBF	1.4	0.86	0.23	32.5	2523	25
KHGX2007/ BN	0.9	0.86	0.23	32.0	5102	4
KMLB 2005/ RBF	1.6	0.86	0.25	38.6	2154	39
KMLB 2005/ BN	0.5	0.87	0.25	37.5	3736	4
KMLB 2006/ RBF	2.4	0.81	0.30	44.2	831	34
KMLB 2006/ BN	2.2	0.81	0.30	45.1	4291	4
KMLB 2007/ RBF	3.1	0.82	0.31	45.9	1911	62
KMLB 2007/ BN	1.7	0.82	0.31	45.4	4146	4
KMLB 2008/ RBF	2.7	0.84	0.27	40.9	5328	37
KMLB 2008/ BN	2.4	0.84	0.27	41.5	4277	4

increased by adding one more layer. It was recommended by (Xiao and Chandrasekar, 1997) that adding a second hidden layer would improve the generalization ability of the network if the size of the training data is enough to make the network converge. From the table, we see that the performance of the new BN is almost the same as the previous one, which tells us that both networks (the one-hidden layer BN and the two-hidden layer BN) have almost the same generalization capability. In this case, it is recommended to use the simpler network which is the BN network with one hidden layer and not the one with two hidden layers.

From Table 4.25 and 4.26, a conclusion can be drawn: in the application where simpler network is required and time is not a constraint, the BN is better to use. In the other hand, when time is a constraint and adaptability is important, RBF is better to use because BN is not well suited to be adaptively trained while RBF is.

Table 4.26: The performance of the RBF NN vs BN. BN has two hidden layers, layer one has four neurons and layer two has two neurons. (Hourly rainfall accumulation).

Site/Year						
KWAJ 2006/ RBF	-4.0	0.82	0.35	57.4	475	45
KWAJ 2006/ BN	-5.4	0.82	0.36	57.9	3424	4
KWAJ 2007/ RBF	-5.5	0.72	0.39	58.8	820	29
KWAJ 2007/ BN	-4.8	0.69	0.41	62.5	2975	4
KHGX2005/ RBF	0.3	0.79	0.29	40.0	1010	22
KHGX2005/ BN	0.9	0.79	0.28	39.6	6256	4
KHGX2006/ RBF	6.3	0.84	0.24	35.1	1629	34
KHGX2006/ BN	5.8	0.84	0.24	35.1	7621	4
KHGX2007/ RBF	1.4	0.86	0.23	32.5	2523	25
KHGX2007/ BN	2.5	0.86	0.23	32.4	4418	4
KMLB 2005/ RBF	1.6	0.86	0.25	38.6	2154	39
KMLB 2005/ BN	0.5	0.86	0.25	38.4	5595	4
KMLB 2006/ RBF	2.4	0.81	0.30	44.2	831	34
KMLB 2006/ BN	2.4	0.82	0.29	44.2	4793	4
KMLB 2007/ RBF	3.1	0.82	0.31	45.9	1911	62
KMLB 2007/ BN	2.6	0.82	0.31	45.4	6238	4
KMLB 2008/ RBF	2.7	0.84	0.27	40.9	5328	37
KMLB 2008/ BN	1.3	0.84	0.27	40.8	6499	4

4.6 USING ENSEMBLE AVERAGE NEURAL NETWORKS TECHNIQUE TO IMPROVE RAINFALL ESTIMATION

4.6.1 INTRODUCTION

In this section, a hybrid or an ensemble of neural networks is constructed which is good or better in the MSE sense than any individual neural network in the ensemble if some conditions are valid. The good thing about this approach is that it uses all the built networks without knowing which network would give better estimate for certain input, and without discarding any network in the ensemble. Ensemble neural networks have been employed to improve results in classification and regression applications (Jimenez 1998; Maqsood et al. 2004; and Shen and Kong 2004). The idea can be described by building different neural networks, getting the estimate out of each one and averaging them all. Figure 4.21 shows a schematic of three neural networks forming an ensemble by averaging their individual outputs. One can argue that we could build different networks, and simply take the one which has the best performance. This is inefficient because the best network among these might not be always the best especially for totally new data. We will show how the ensemble neural networks can outperform individual networks.

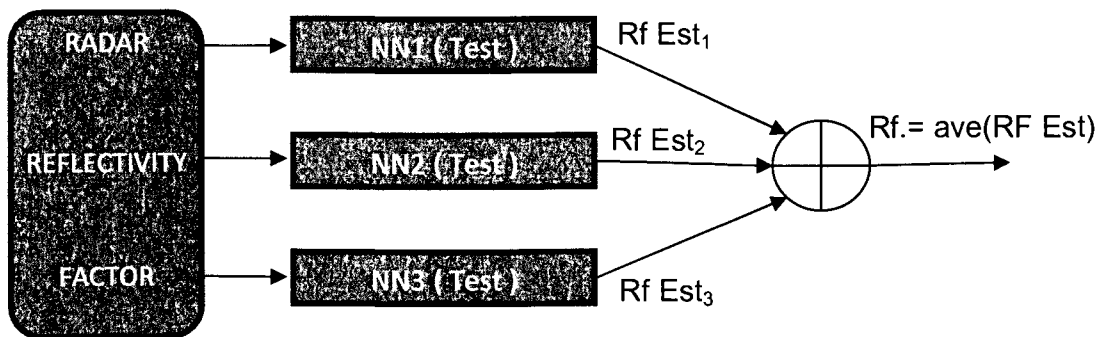


Figure 4.21: Schematic of Ensemble of three Neural Networks.

4.6.2 ENSEMBLE METHOD

To do the ensemble estimator, we will be building a basic ensemble of networks where the output of all estimators is averaged to give a single estimate. To prove this method mathematically, let's assume the function to be estimated to be $f(x)$. What we need is to find the best estimate of $f(x)$ from a group of estimators. We will call the new estimate of $f(x)$ to be $f_{ens}(x)$. If we define $m_i(x) = f(x) - f_i(x)$ to be the error function between the true value $f(x)$ and the estimated value $f_i(x)$ based on estimator i . The mean square error of estimator i can be written as

$$MSE[f_i(x)] = E[m_i^2(x)] \quad (4.19)$$

If the ensemble average estimate $f_{ens}(x)$ can be written as

$$f_{ens}(x) = \frac{1}{N} \sum_{i=1}^N f_i(x) \quad (4.20)$$

then, the mean square error of the ensemble estimate can be calculated as

$$\begin{aligned} MSE[f_{ens}(x)] &= E\left[\left(\frac{1}{N} \sum_{i=1}^N m_i(x)\right)^2\right] \\ &= \frac{1}{N^2} E\left[\sum_{i=1}^N m_i(x)^2\right] + \frac{1}{N^2} E\left[\sum_{i \neq j}^N m_i(x)m_j(x)\right] \end{aligned} \quad (4.21)$$

Now, if we assume that the $m_i(x)$ are mutually independent with zero mean, then

$MSE[f_{ens}(x)]$ can be simplified by

$$MSE[f_{ens}(x)] = \frac{1}{N^2} E\left[\sum_{i=1}^N m_i(x)^2\right] \quad (4.22)$$

If we define the average mean square error \overline{MSE} to be

$$\overline{MSE} = \frac{1}{N} \sum_{i=1}^N E[m_i(x)^2] \quad (4.23)$$

then, $MSE[f_{ens}(x)]$ can be further simplified by

$$MSE[f_{ens}(x)] = \frac{\overline{MSE}}{N} \quad (4.24)$$

This is powerful, by averaging the estimators we can reduce the mean square error by a factor of N , but again this is based on the assumption that the $m_i(x)$ are mutually independent with zero mean.

4.6.3 PERFORMANCE OF THE ENSEMBLE AVERAGE NEURAL NETWORKS

To examine this technique, data from KMLB, KHGX and KWAJ were used to test three networks. The first network is the regular RBF NN used in most of this dissertation. The second and third networks are Bayesian networks with one and two hidden layers, respectively. The first Bayesian network has four neurons in its hidden layer, and the second Bayesian network has four neurons in its first hidden layer, while the second hidden layer has two. The output of all these networks was averaged and compared to the actual output. Results are shown in Tables 4.27, 4.28, 4.29, 4.30, 4.31, 4.32, 4.33, 4.34 and 4.35. In the tables: NN1 is RBF NN, NN2 is BN with single hidden layer and NN2 is BN with two hidden layers. As shown in the tables, the ensemble technique tries to improve the estimate, it gives some improvement but it is not significant because the data is not mutually independent and as clearly shown the mean of the error (bias) of each estimator is not zero. This would make our assumption in equations 4.21 and 4.22 invalid, which means the MSE of the ensemble will not be the average of the MSE of the individual estimators. That is the reason why we have MSE more than what we should get. Good thing about this technique is that even if we do not know which estimator

should be used, which is usually the case; the performance of this technique would be at least better than or equal the performance of the worst.

Table 4.27: The performance of the individual networks vs. the ensemble average estimate. Data from KWAJ 2006. (Hourly rainfall accumulation).

	FracBias (%)	Corr.	NSE	FRMSE (%)
	-4.0	0.82	0.35	57.4
	-4.2	0.81	0.36	58.3
	-5.4	0.82	0.36	57.9
	-4.5	0.82	0.35	56.3

Table 4.28: The performance of the individual networks vs. the ensemble average estimate. Data from KWAJ 2007. (Hourly rainfall accumulation).

	FracBias (%)	Corr.	NSE	FRMSE (%)
	-5.5	0.72	0.39	58.8
	-7.1	0.72	0.38	58.7
	-4.8	0.69	0.41	62.5
	-5.8	0.72	0.38	58.8

Table 4.29: The performance of the individual networks vs. the ensemble average estimate. Data from KHGX 2005. (Hourly rainfall accumulation).

	FracBias (%)	Corr.	NSE	FRMSE (%)
	0.3	0.79	0.29	40.0
	0.1	0.79	0.29	39.9
	0.9	0.79	0.28	39.6
	0.4	0.79	0.28	39.6

Table 4.30: The performance of the individual networks vs. the ensemble average estimate.
Data from KHGX 2006. (Hourly rainfall accumulation).

	FracBias (%)	Corr.	NSE	FRMSE (%)
	6.3	0.84	0.24	35.1
	5.4	0.85	0.24	34.1
	5.8	0.84	0.24	35.1
	5.8	0.85	0.24	34.5

Table 4.31: The performance of the individual networks vs. the ensemble average estimate.
Data from KHGX 2007. (Hourly rainfall accumulation).

	FracBias (%)	Corr.	NSE	FRMSE (%)
	1.4	0.86	0.23	32.5
	0.9	0.86	0.23	32.0
	2.5	0.86	0.23	32.4
	1.6	0.86	0.23	31.9

Table 4.32: The performance of the individual networks vs. the ensemble average estimate.
Data from KMLB 2005. (Hourly rainfall accumulation).

	FracBias (%)	Corr.	NSE	FRMSE (%)
	1.6	0.86	0.25	38.6
	0.5	0.87	0.25	37.5
	0.5	0.86	0.25	38.4
	0.9	0.87	0.25	37.7

Table 4.33: The performance of the individual networks vs. the ensemble average estimate.
Data from KMLB 2006. (Hourly rainfall accumulation).

	FracBias (%)	Corr.	NSE	FRMSE (%)
	2.4	0.81	0.30	44.2
	2.2	0.81	0.30	45.1
	2.4	0.82	0.29	44.2
	2.3	0.82	0.29	43.9

Table 4.34: The performance of the individual networks vs. the ensemble average estimate.
Data from KMLB 2007. (Hourly rainfall accumulation).

	FracBias (%)	Corr.	NSE	FRMSE (%)
	3.1	0.82	0.31	45.9
	1.7	0.82	0.31	45.4
	2.6	0.82	0.31	45.4
	2.4	0.82	0.30	45.1

Table 4.35: The performance of the individual networks vs. the ensemble average estimate.
Data from KMLB 2008. (Hourly rainfall accumulation).

	FracBias (%)	Corr.	NSE	FRMSE (%)
	2.7	0.84	0.27	40.9
	2.4	0.84	0.27	41.5
	1.3	0.84	0.27	40.8
	2.1	0.85	0.27	40.4

4.7 VALIDATION AGAINST TRMM GROUND VALIDATION AT KWAJ SITE

4.7.1 TRMM GROUND VALIDATION

TRMM Ground Validation (GV) system is an important system that is part of TRMM mission. Its function is to support TRMM to improve some of the measuring and estimation techniques (Reflectivity and rain rate). The GV system has 10 ground validation sites around the world as shown in Figure 3.6 in addition to their gauge networks. The main ground validation sites are located at Florida, Texas, Darwin, and Kwajalein. In this section, we are going to validate the rainfall estimated by the neural network designed by KWAJ radar using the radar/gauge products provided by the GV site. Before we go to the validation, let's describe briefly how the GV system estimates

rainfall from the radar measurements and the gauges around. The radar rainfall estimation is done using the power law Z-R relation ($Z=AR^B$; $A=300$, $B=1.4$). The rainfall accumulation of a month is first calculated and then compared to the gauge accumulations. Bulk adjustment is used to calibrate the coefficient A to force agreement between the radar and the gauge data. Then the radar rainfall accumulation of that month is recalculated using the new coefficient A . More information and details about this algorithm can be found at TRMM GV site at [http://trmm-fc.gsfc.nasa.gov/trmm_gv/gv_products/level_2.html] and [http://trmm-fc.gsfc.nasa.gov/trmm_gv/Ground_truth/sites/florida/melb/Mel_results.html].

4.7.2 VALIDATION AGAINST KWAJ RADAR RAINFALL ESTIMATE

The data from KWAJ site in years 2006 and 2007 were tested using the RBF neural network estimator and compared to the actual gauge. Input to the network was the radar reflectivity factor at heights 1, 2, 3, and 4km. The GV rainfall estimate for this data was also compared to the actual gauge. The neural network rainfall estimation was converted to monthly accumulation to match the gauge accumulation provided by the GV site. Data was taken for certain gauges and certain months as shown in [http://trmm-fc.gsfc.nasa.gov/trmm_gv/gv_products/level_2/scatter_plots/kwaj_data/kwaj_2006_v7_diff.txt] and [http://trmm-fc.gsfc.nasa.gov/trmm_gv/gv_products/level_2/scatter_plots/kwaj_data/kwaj_2007_v7_diff.txt].

Tables 4.36 and 4.37 show the performance metrics (Bias, Corr., and NSE) that are used to do the comparison between the neural network estimation and the GV estimation

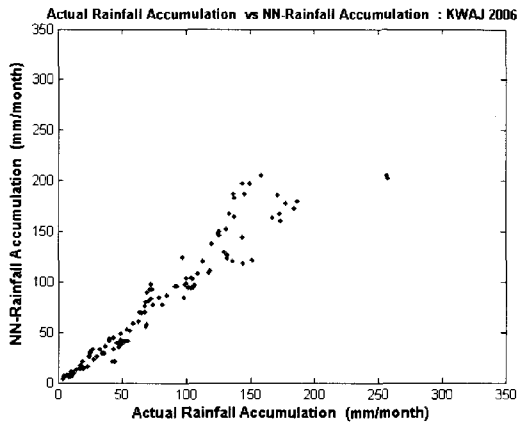
for years 2006 and 2007, respectively. Figures 4.22, and 4.23 show the scatter plot of the same data represented by the metrics shown in the same tables. As can be seen from the tables and the figures; the neural network performance is very close or better than the GV performance when both compared against the rain gauge. The neural network performance has small bias, high correlation and low NSE, which means low variation from the truth. The goal of this section is to validate the output of the neural network to a confident algorithm which is the GV output in this case in order to see how good the neural network estimate in comparison to other estimators. It is worth mentioning that the GV estimate is taken “after the fact”; i.e., the coefficient A in the Z-R relation is recalculated based on any month data (reflectivity and gauges) and then the rainfall accumulation for that month is recalculated using the adjusted Z-R relation, while in the neural network estimation, the rainfall accumulation of any day was calculated based on a model that was built based on data up to the day before.

Table 4.36: The performance of the NN rainfall accumulation and the GV rainfall accumulation Compared with the actual rainfall accumulation at KWAJ site in 2006.

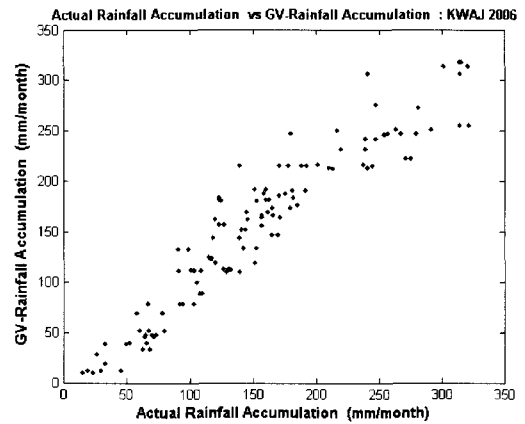
Year: 2006	Bias (mm)	Corr.	NSE
NN vs. Actual RG	1.3985	0.9605	0.1377
ZR vs. Actual RG	0.7018	0.9448	0.1324

Table 4.37: The performance of the NN rainfall accumulation and the GV rainfall accumulation Compared with the actual rainfall accumulation at KWAJ site in 2007.

Year: 2007	Bias (mm)	Corr.	NSE
NN vs. Actual RG	2.9614	0.9728	0.1368
ZR vs. Actual RG	0.2755	0.9208	0.1783

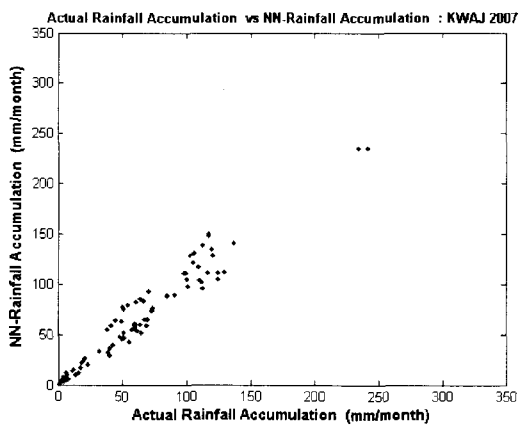


(a)

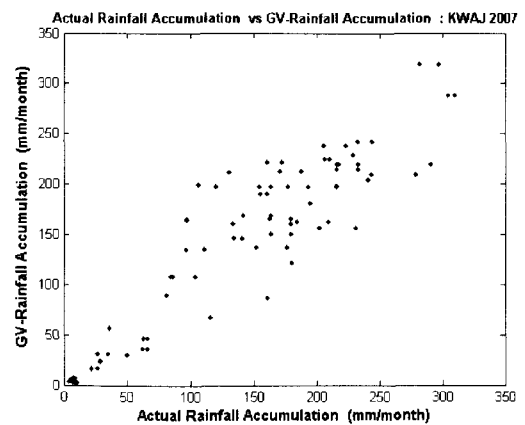


(b)

Figure 4.22: (a) Scatter plot of the NN rainfall accumulation vs. the actual rainfall accumulation. (b) Scatter plot of the GV rainfall accumulation vs. the actual rainfall accumulation. KWAJ site in year 2006.



(a)



(b)

Figure 4.23: (a) Scatter plot of the NN rainfall accumulation vs. the actual rainfall accumulation. (b) Scatter plot of the GV rainfall accumulation vs. the actual rainfall accumulation. KWAJ site in year 2007.

CHAPTER 5

RAIN RATE ESTIMATION USING TRMM-PR MEASUREMENTS BASED ON NEURAL NETWORK

5.1 INTRODUCTION

Tropical Rainfall Measuring Mission (TRMM) Precipitation Radar (PR) is known to be the first observation platform for mapping precipitation over the tropics. It is a unique instrument, capable of providing high-resolution vertical profile of precipitation. TRMM measured rainfall is important in order to study the precipitation distribution all over the globe in the tropics. Ground validation is a critical important component in TRMM system. Fundamental challenges exist in performing TRMM ground validation. The ground sensing systems have quite different characterizations from TRMM in terms of resolution, scale, viewing aspect, and uncertainties in the sensing environments. The horizontal resolution of TRMM PR is about 5km, much coarser compared to rain gauges in the spatial scale. Another challenge is that during a single weather event, available data pairs for comparison (TRMM vertical profile of reflectivity versus rain gauge measurement) are scarce because of TRMM's limited overpasses. It is impractical to deploy a dense gauge network for TRMM PR validation. In this work, we introduce a novel technique to improve the estimation of TRMM-PR rainfall product.

5.2 TWO-STAGE NEURAL NETWORK FOR TRMM-PR RAINFALL ESTIMATION

In this chapter a novel hybrid Neural Network model is presented to train ground radars for rainfall estimation using rain gauge data and subsequently using the trained ground radar neural network rainfall estimate as target to train TRMM PR based Neural network for rainfall estimation. This hybrid neural network model will derive the relation between rain gauges and ground radar measurements, and transfer this relation to adaptive rainfall estimation for TRMM precipitation radar.

In ground radar rainfall estimation, it is easy to obtain large amount of training pairs because ground radar is able to scan over the same location in fine temporal resolution, which is not possible for TRMM. To solve this issue in TRMM, two neural networks will be created and used for global precipitation mapping and ground validation. The first neural network is built based on ground radar data and rain gauges. Then, the matched TRMM-PR profiles with the corresponding ground radar (GR) measurements are used to train the second neural network using rainfall estimated from the first neural network. Figure 5.1 shows a schematic of the general idea for this network.

Radial Basis function (RBF) neural network is capable of learning the complex functional relation from high dimension input space to target space. It is shown and demonstrated in the previous chapter that RBF Neural Network is capable of learning the relation between ground radar measurements and rain gauge data. Therefore, the same network architecture will be used in this chapter to train the second NN.

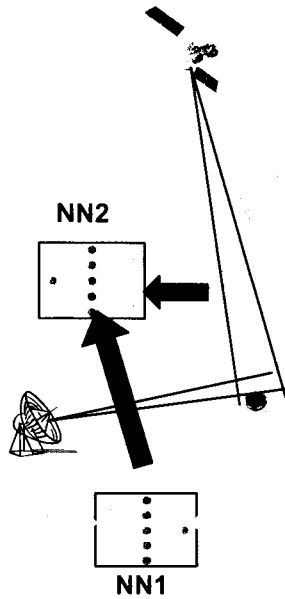


Figure 5.1: Two-stage neural network system for TRMM rainfall estimation.

5.3 DEVELOPMENT OF THE HYBRID NEURAL NETWORK TECHNIQUE FOR TRMM-PR RAINFALL ESTIMATION

The process of building this hybrid neural network rainfall estimator has four main steps: ground validation (GV) neural network design, alignment between TRMM-PR and GV products, TRMM neural network design, and product validation. These steps are described in the coming subsections.

5.3.1 GROUND VALIDATION NEURAL NETWORK DESIGN

In this step we construct a neural network (NN1) to estimate rainfall based on GV radar. This network is trained with the GV radar reflectivity and the corresponding rain gauge data which makes this network to have the advantage of having large population of sample pairs and smaller scale mismatch. This neural network is trained adaptively and

weights are updated in daily base. This network was already described, designed and tested in the previous chapter.

5.3.2 TRMM-PR AND GROUND RADAR DATA ALIGNMENT

The goal of this hybrid neural network model is to derive the relation between rain gauges and ground radar measurements, and transfer this relation to adaptive rainfall estimation for TRMM precipitation radar. The means to do that is to do alignment between the GV radar measurements and TRMM-PR measurements. The alignment process done by (Bolen and Chandrasekar, 2003) is used to align TRMM-PR reflectivity product with the ground radar reflectivity measurements. Resampling the ground-based and spaceborne datasets to a common grid provides a means by which the radar reflectivity factors can be compared at different heights. The final product of aligning the TRMM-PR and GV radar products has a resolution of (4 x 4 x 0.5 km). Figure 5.2 shows the geometry between TRMM-PR and GR-based measurements.

An example of the alignment output is shown in Figure 5.3. Data were taken from KHGX radar in Houston. As we see, there is good matching between these two products. For more statistical results about the alignment procedure, please see Chapter 3. The results presented in Chapter 3 show that radar reflectivity factor derived from the PR data after attenuation correction agrees to within about 1 dB bias for most of the cases. This bias will be automatically compensated for during the training process of the second neural network.

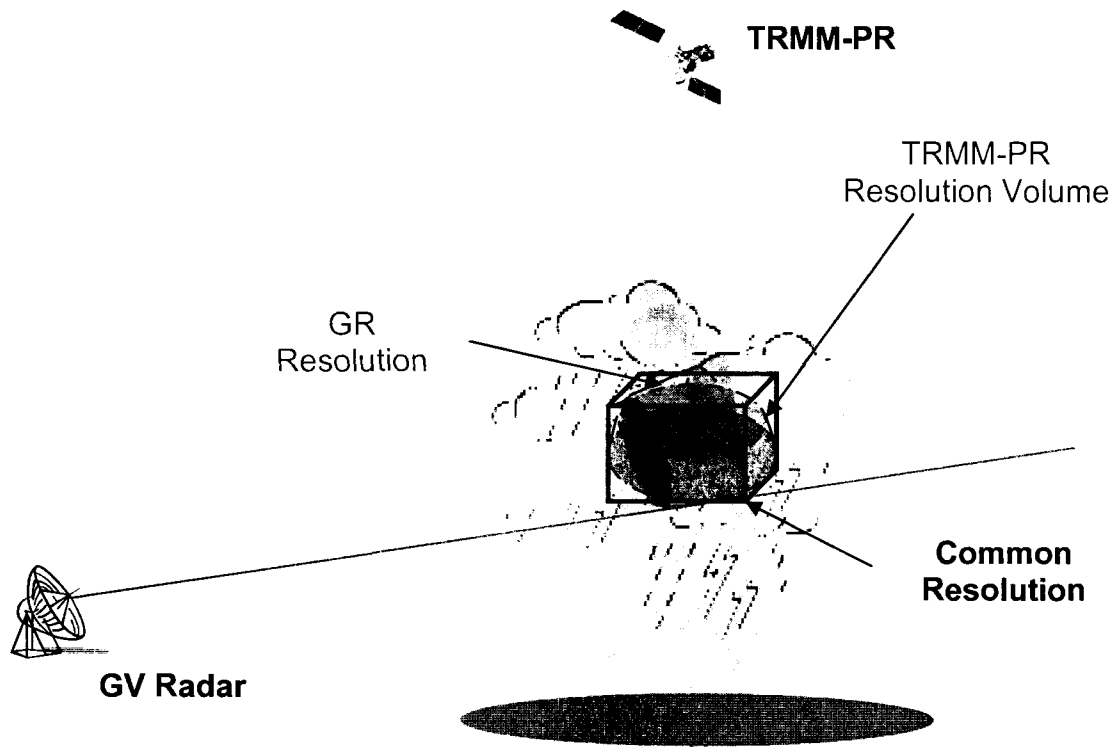


Figure 5.2: Geometry between TRMM-PR and GR-based measurements

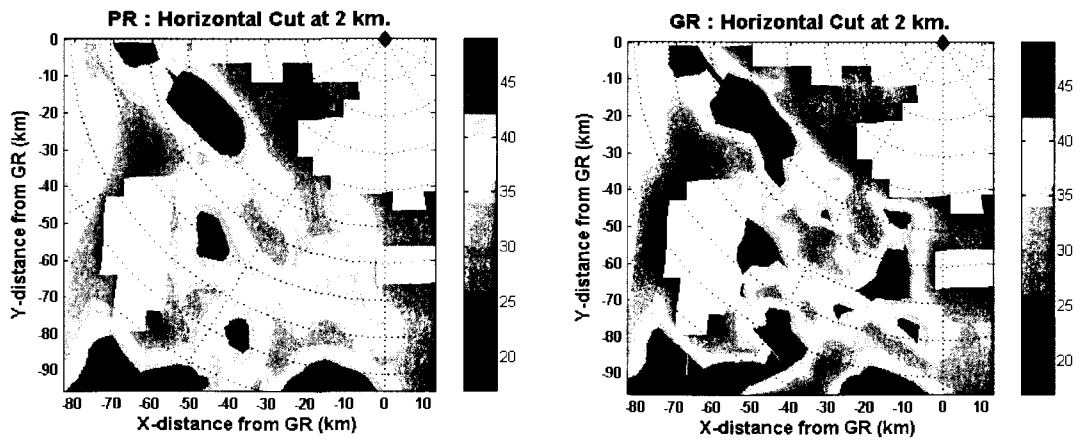


Figure 5.3: An example of aligned snapshot of TRMM PR reflectivity and GR reflectivity. The snapshot was taken in January 28, 2005 at 09:33:00 UTC in Houston TX.

5.3.3 DESIGNING TRMM-PR NEURAL NETWORK

The second neural network is designed using TRMM reflectivity vertical profiles starting at 1km and going up to 4 km with 1km vertical resolution. These profiles were aligned with the GV reflectivity profiles as shown in the previous step. The target of this network is the rainfall estimated by the first neural network with GR data that is aligned to TRMM data which will also be used to train the second network.

Training this neural network was based on the same technique used in the GV neural network. The only difference between them is that the first neural network was trained every day while the second neural network was trained every overpass. Rainfall estimation was done using the model of the previous overpass. The whole process of training TRMM –PR neural network is shown in Figure 5.4.

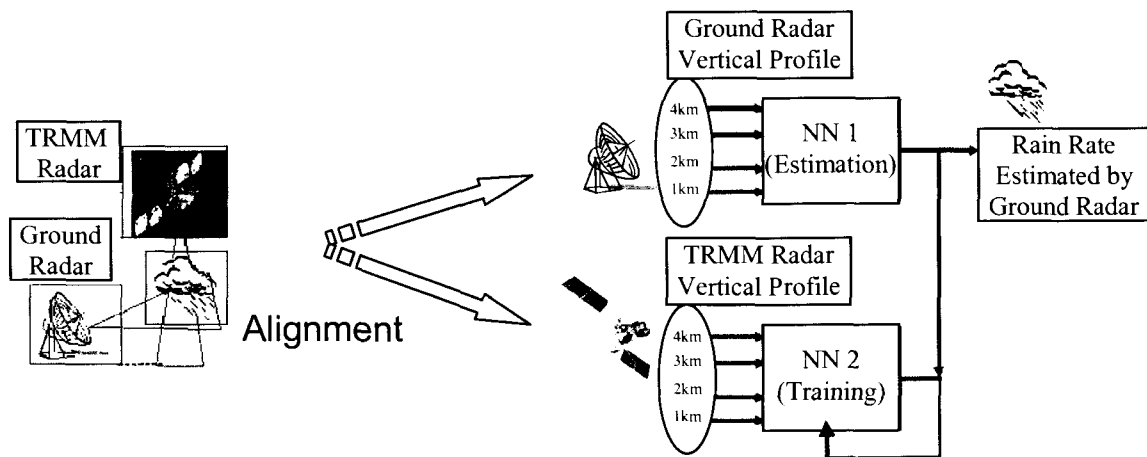


Figure 5.4: Training TRMM-PR neural network using GV neural network rain rate estimate.

5.3.4 PRODUCT VALIDATION

To validate this novel method for global rainfall estimation and mapping, we compare the rain rate estimated by the first network and the second network to the rain gauges. TRMM-PR rain rate product was also compared to the rain gauges in order to do a comparison between TRMM-PR rain rate product and the neural network product. Figure 5.5 demonstrates the two-stage neural network: system testing and evaluation. The same scoring metrics used in the previous chapter were also used to evaluate the performance of each network as well as the performance of TRMM-PR product in this chapter.

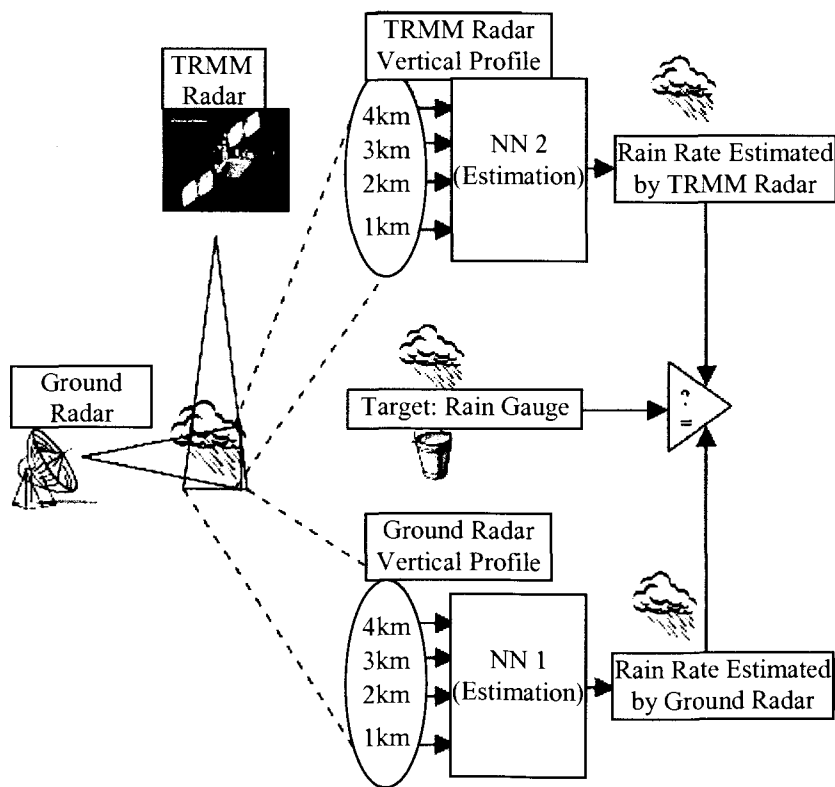


Figure 5.5: Two-stage neural network: system testing and evaluation.

5.3.5 RESULTS AND EVALUATION

Radar data, their TRMM overpasses, and rain gauge observations were used to test this technique during the year 2005, 2006, 2007 and 2008 over Melbourne-Florida, Houston-Texas and Kwajalein-Marshall Islands areas. TRMM-PR rain rate product was used in this evaluation in order to see how much improvements we can get using this neural network method.

For the first neural network, radar data were collected where the lowest height level of the CAPPI scans is 1 km and the highest level is 4 km. Horizontal resolution of the ground radar data was set to be 1km. The spacing between levels is chosen to be 1 km. The gauge data were maintained by the NASA TRMM program. The same gauge networks that were used in the previous chapter were also used in this chapter. Data within 100km was only considered. The radar parameter of interest in this work was radar reflectivity factor Z_h .

TRMM data were collected from overpasses over Melbourne, Houston and Kwajalein sites. TRMM data were aligned to the GV radars data with a final resolution of both products to be 4 x 4 x 0.5 km. Data starting at 1km height and going up to 4 km height with 1 km spacing were used to train the second network. There were around 600 overpasses over each site in each year. On average, there are around 30 overpasses with precipitation. The performance of the rainfall product estimated from TRMM PR neural network is compared against TRMM standard products. A direct gauge comparison study is done to demonstrate the improvement brought in by the neural networks.

Tables 5.1, 5.2, 5.3, 5.4, 5.5, 5.6, 5.7 and 5.8 show the scores of the hybrid neural network scheme using data from year 2005, 2006, 2007 and 2008 over KMLB, KWAJ and KHGX. As shown in the tables, the performance of the neural network approach is better than the performance of TRMM product. As we can see, TRMM product has significant bias compared to the rain gauge measurements, while the neural network product has less bias.

The tables also show that the correlation and the FRMSE scores of the rainfall estimated by the neural networks are better than that for TRMM product. The neural networks score higher correlation with the rain gauges and lower FRMSE while TRMM product scores lower correlation and higher FRMSE which means less variation from truth (rain gauge) in the favor of the neural network technique.

Figures 5.6, 5.7, 5.8, 5.9, 5.10, 5.11, 5.12 and 5.13 show the same conclusions that can be entailed from the tables. The figures show better scatter plots of both neural networks against TRMM standard product; neural networks show lower bias and higher correlation.

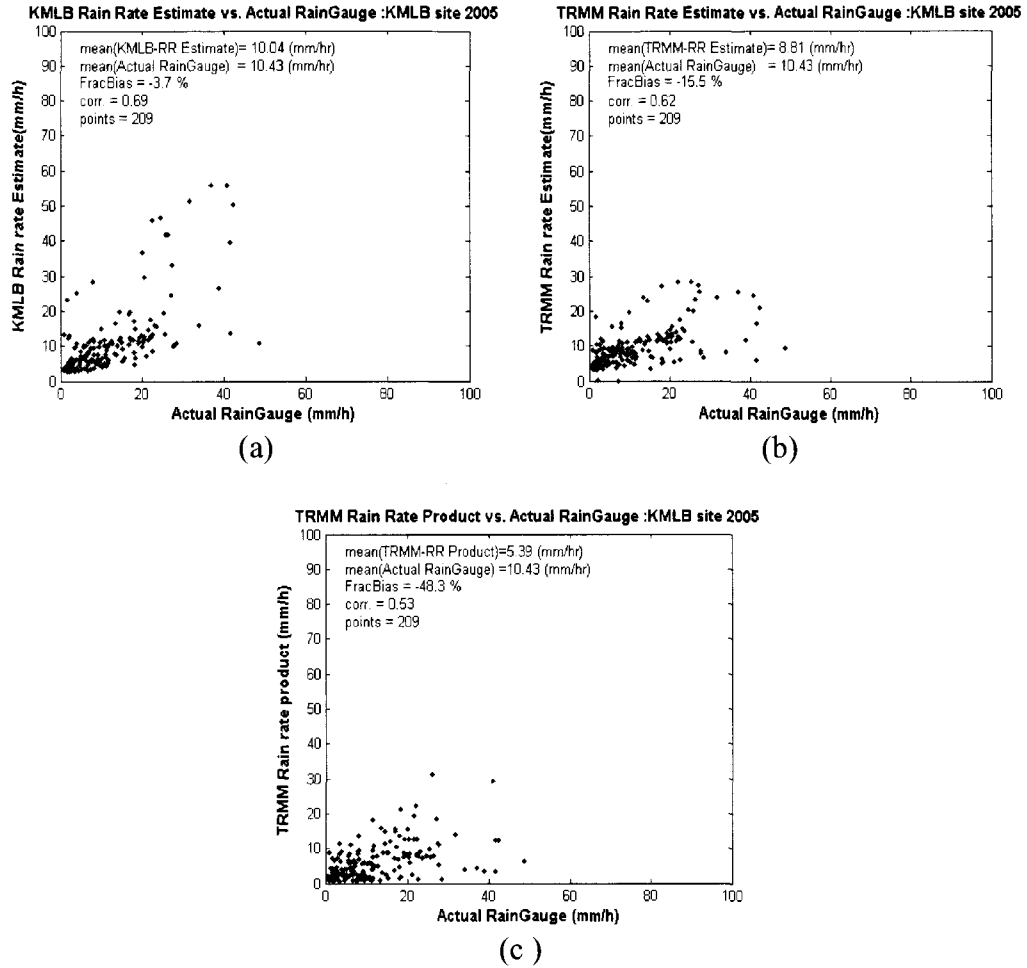


Figure 5.6: Actual rain gauge vs. a) GV radar NN rain rate estimate b) TRMM-PR NN rain rate estimate c) TRMM-PR rain rate product. Data from year 2005 over KMLB. (Instantaneous rainfall).

Table 5.1: Performance evaluation of the GV NN rain rate estimation, TRMM-PR NN rain rate estimate, and TRMM-PR rain rate product. Data from year 2005 over KMLB. (Instantaneous rainfall).

Year 2005	FracBias (%)	Corr.	NSE	FRMSE (%)
KMLB NN Est. vs. Rain Gauge	-3.7	0.69	0.50	73.3
TRMM NN Est. vs. Rain Gauge	-15.5	0.62	0.50	74.6
TRMM Product vs. Rain Gauge	-48.3	0.53	0.58	92.7

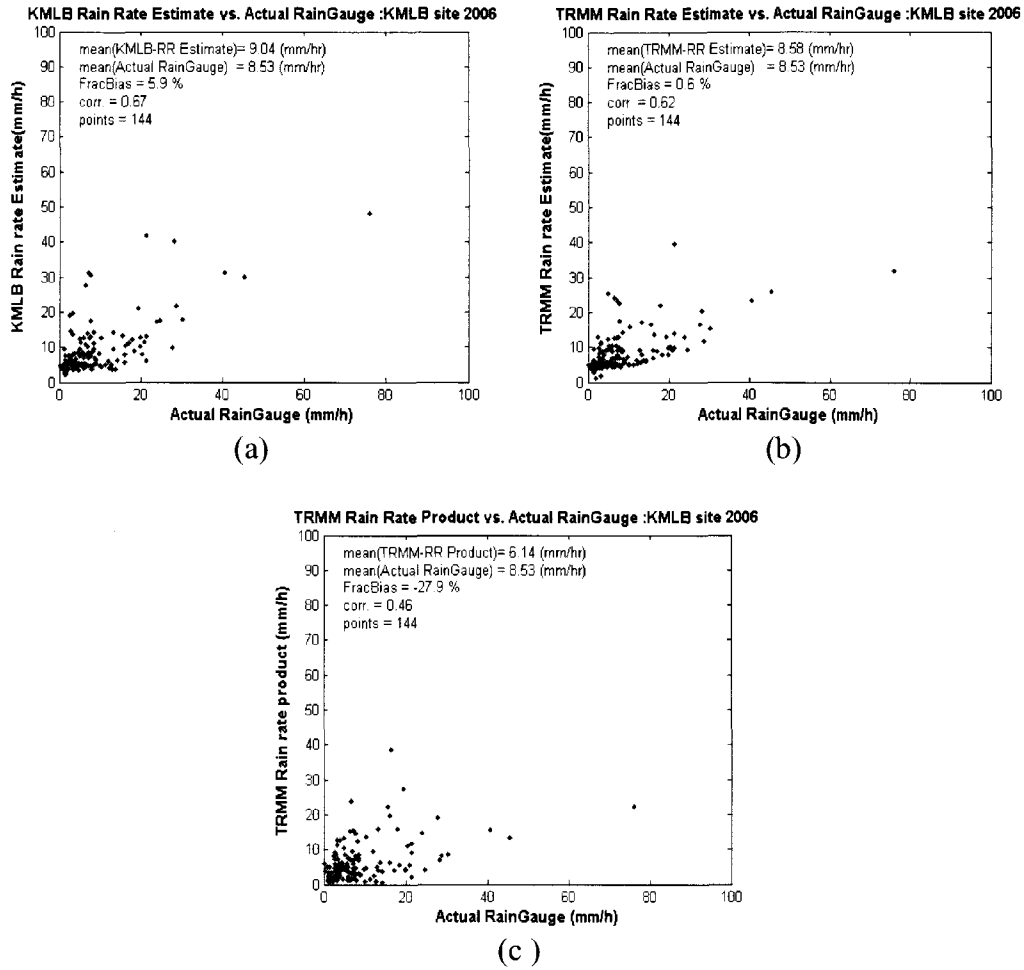


Figure 5.7: Actual rain gauge vs. a) GV radar NN rain rate estimate b) TRMM-PR NN rain rate estimate c) TRMM-PR rain rate product. Data from year 2006 over KMLB. (Instantaneous rainfall).

Table 5.2: Performance evaluation of the GV NN rain rate estimation, TRMM-PR NN rain rate estimate, and TRMM-PR rain rate product. Data from year 2006 over KMLB. (Instantaneous rainfall).

Year 2006	FracBias (%)	Corr.	NSE	FRMSE (%)
KMLB NN Est. vs. Rain Gauge	5.9	0.67	0.59	84.1
TRMM NN Est. vs. Rain Gauge	0.6	0.62	0.60	88.1
TRMM Product vs. Rain Gauge	-27.9	0.46	0.64	105.1

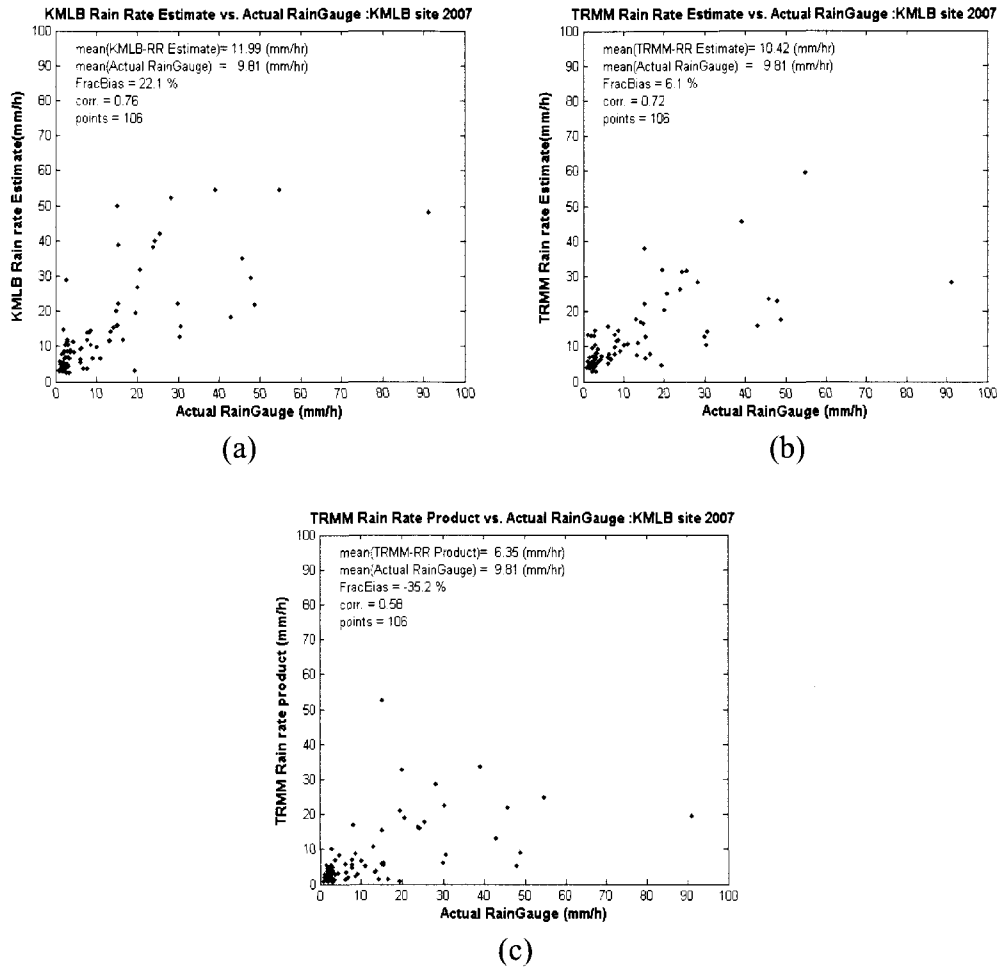


Figure 5.8: Actual rain gauge vs. a) GV radar NN rain rate estimate b) TRMM-PR NN rain rate estimate c) TRMM-PR rain rate product. Data from year 2007 over KMLB. (Instantaneous rainfall).

Table 5.3: Performance evaluation of the GV NN rain rate estimation, TRMM-PR NN rain rate estimate, and TRMM-PR rain rate product. Data from year 2007 over KMLB. (Instantaneous rainfall).

Year 2007	FracBias (%)	Corr.	NSE	FRMSE (%)
KMLB NN Est. vs. Rain Gauge	22.1	0.76	0.61	98.4
TRMM NN Est. vs. Rain Gauge	6.1	0.72	0.57	100.4
TRMM Product vs. Rain Gauge	-35.2	0.58	0.58	123.3

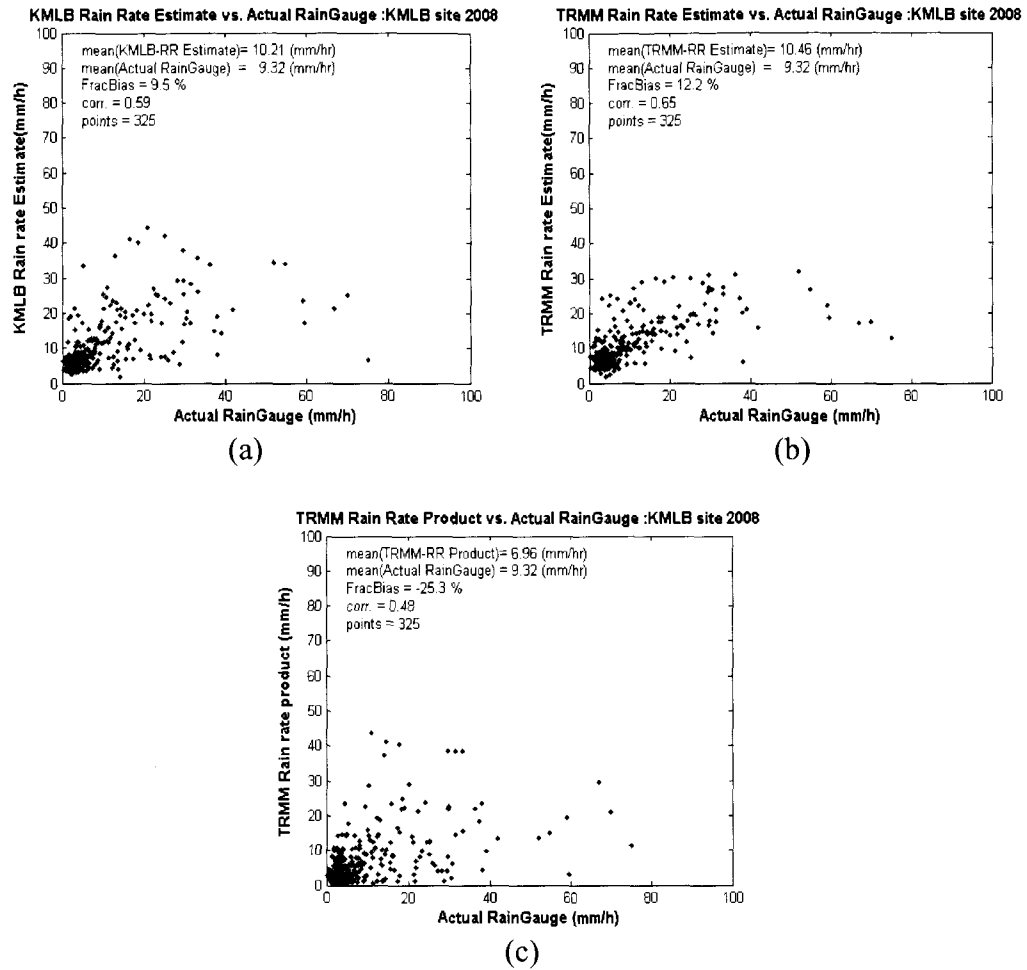


Figure 5.9: Actual rain gauge vs. a) GV radar NN rain rate estimate b) TRMM-PR NN rain rate estimate c) TRMM-PR rain rate product. Data from year 2008 over KMLB. (Instantaneous rainfall).

Table 5.4: Performance evaluation of the GV NN rain rate estimation, TRMM-PR NN rain rate estimate, and TRMM-PR rain rate product. Data from year 2008 over KMLB. (Instantaneous rainfall).

Year 2008	FracBias (%)	Corr.	NSE	FRMSE (%)
KMLB NN Est. vs. Rain Gauge	9.5	0.59	0.60	100.6
TRMM NN Est. vs. Rain Gauge	12.2	0.65	0.58	95.9
TRMM Product vs. Rain Gauge	-25.3	0.48	0.64	114.0

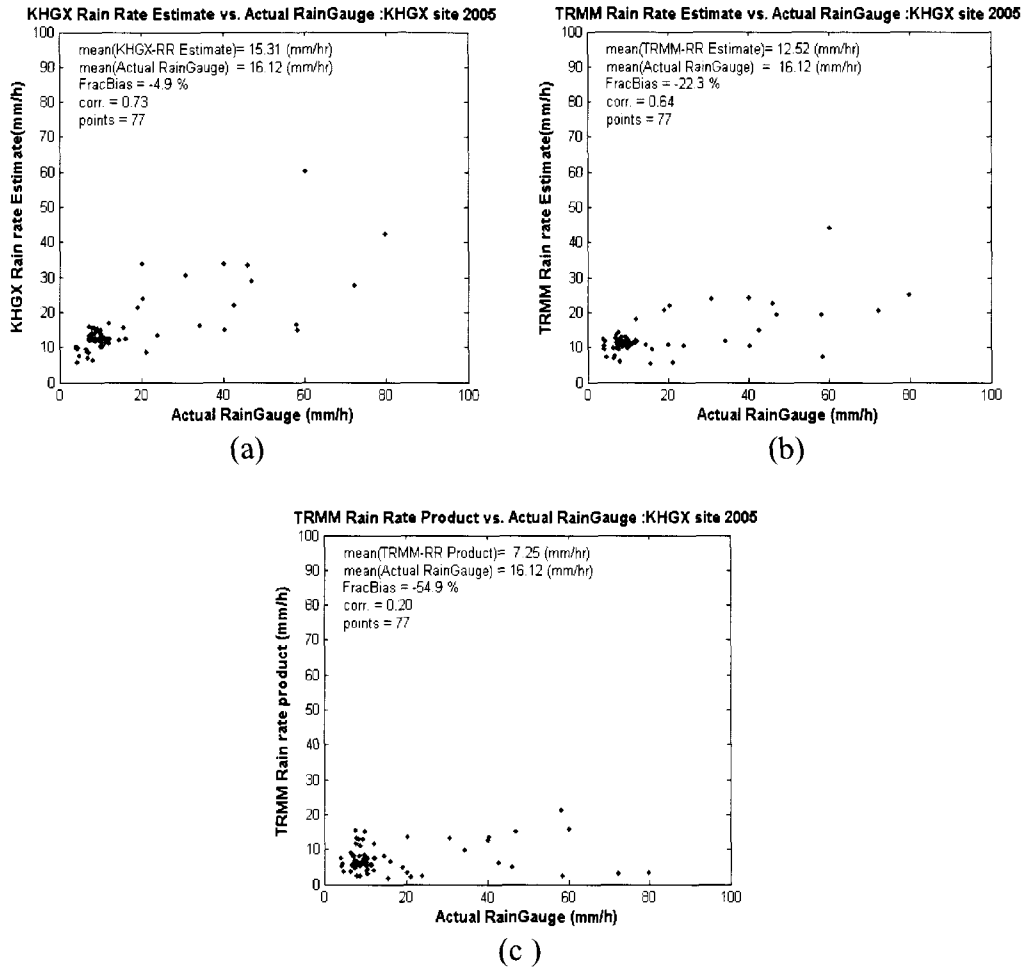


Figure 5.10: Actual rain gauge vs. a) GV radar NN rain rate estimate b) TRMM-PR NN rain rate estimate c) TRMM-PR rain rate product. Data from year 2005 over KHXG. (Instantaneous rainfall).

Table 5.5: Performance evaluation of the GV NN rain rate estimation, TRMM-PR NN rain rate estimate, and TRMM-PR rain rate product. Data from year 2005 over KHXG. (Instantaneous rainfall).

Year 2005	FracBias (%)	Corr.	NSE	FRMSE (%)
KHXG NN Est. vs. Rain Gauge	-4.9	0.73	0.43	72.3
TRMM NN Est. vs. Rain Gauge	-22.3	0.64	0.46	86.6
TRMM Product vs. Rain Gauge	-54.9	0.20	0.62	113.4

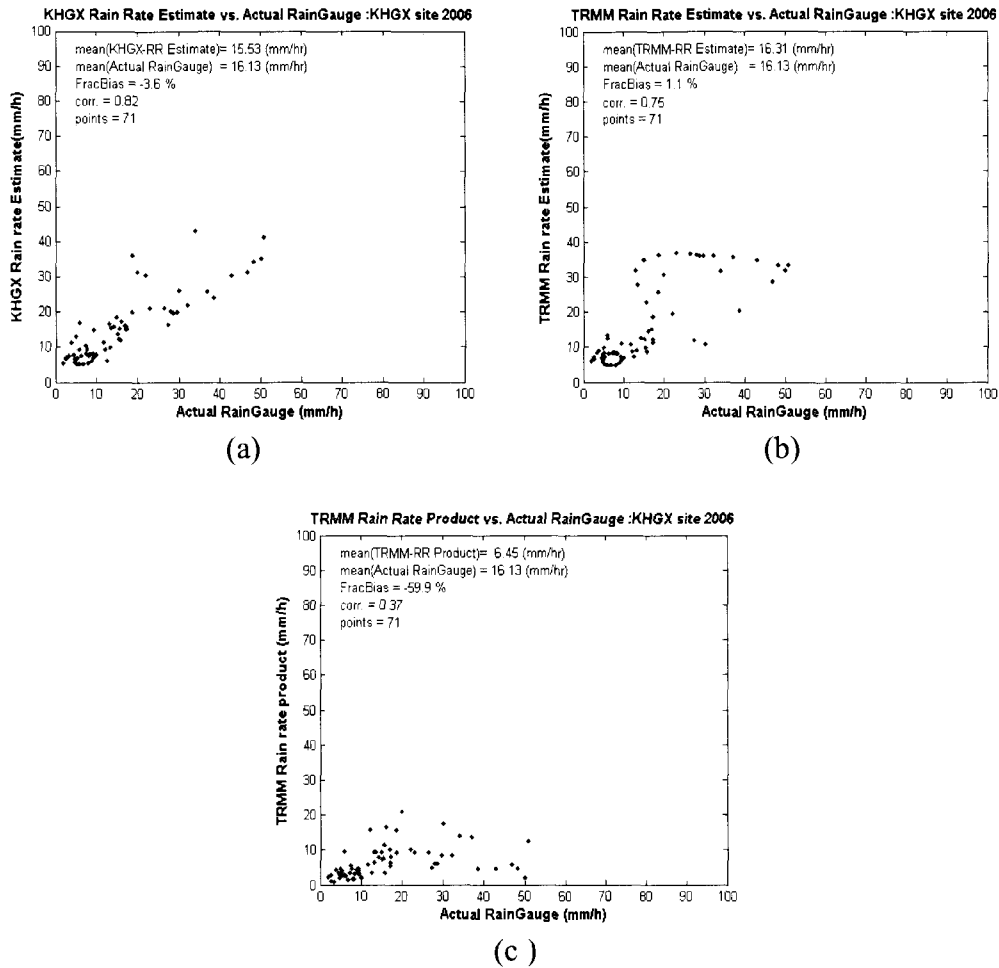


Figure 5.11: Actual rain gauge vs. a) GV radar NN rain rate estimate b) TRMM-PR NN rain rate estimate c) TRMM-PR rain rate product. Data from year 2006 over KHXG. (Instantaneous rainfall).

Table 5.6: Performance evaluation of the GV NN rain rate estimation, TRMM-PR NN rain rate estimate, and TRMM-PR rain rate product. Data from year 2006 over KHXG. (Instantaneous rainfall).

Year 2006	FracBias (%)	Corr.	NSE	FRMSE (%)
KHXG NN Est. vs. Rain Gauge	-3.6	0.82	0.31	43.8
TRMM NN Est. vs. Rain Gauge	1.1	0.75	0.37	51.1
TRMM Product vs. Rain Gauge	-59.9	0.37	0.61	93.0

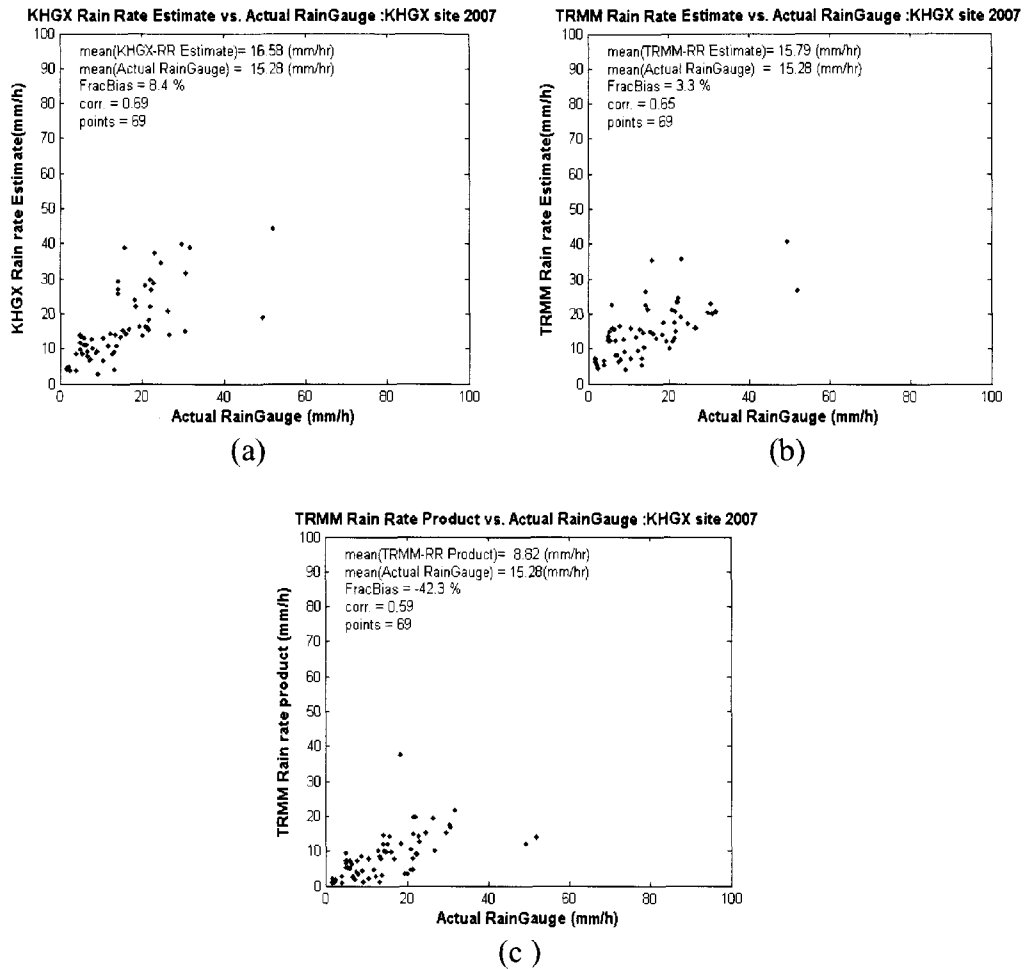


Figure 5.12: Actual rain gauge vs. a) GV radar NN rain rate estimate b) TRMM-PR NN rain rate estimate c) TRMM-PR rain rate product. Data from year 2007 over KHXG. (Instantaneous rainfall).

Table 5.7: Performance evaluation of the GV NN rain rate estimation, TRMM-PR NN rain rate estimate, and TRMM-PR rain rate product. Data from year 2007 over KHXG. (Instantaneous rainfall).

Year 2007	FracBias (%)	Corr.	NSE	FRMSE (%)
KHXG NN Est. vs. Rain Gauge	8.4	0.69	0.39	53.3
TRMM NN Est. vs. Rain Gauge	3.3	0.65	0.41	51.7
TRMM Product vs. Rain Gauge	-42.3	0.59	0.48	68.4

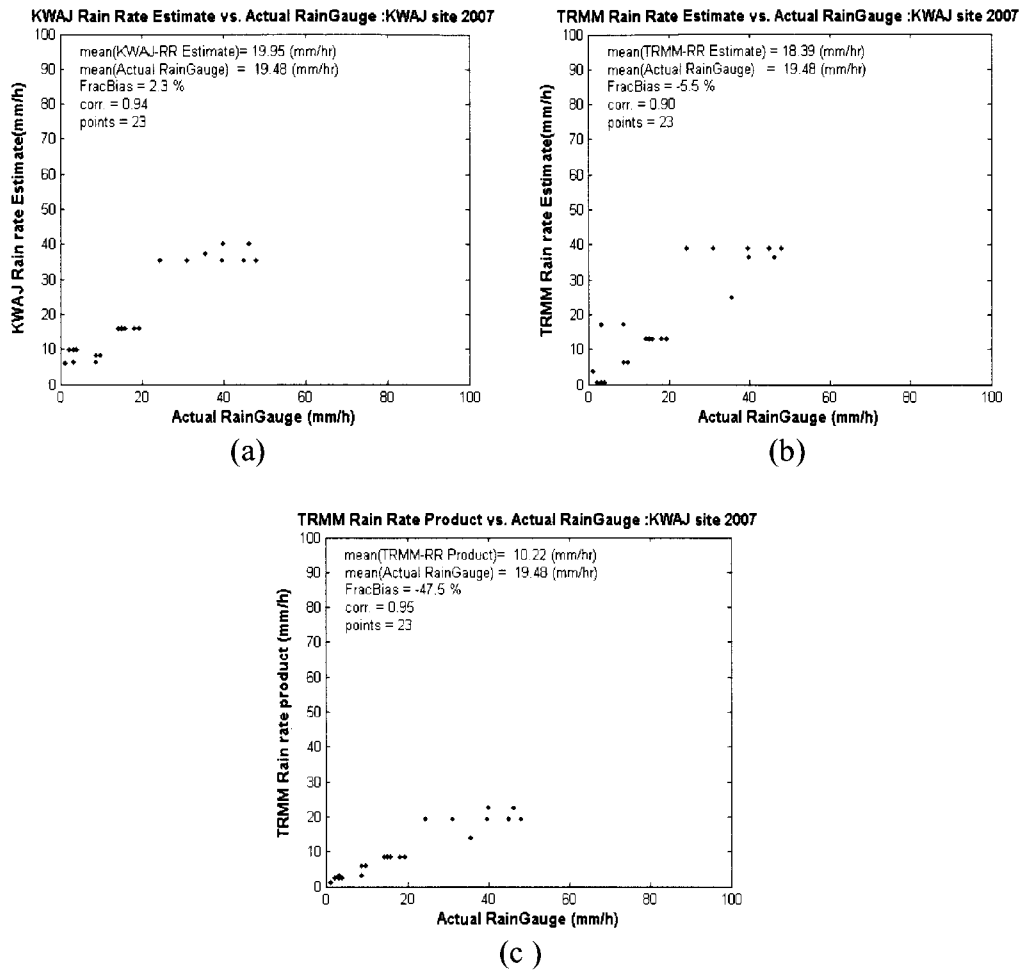


Figure 5.13: Actual rain gauge vs. a) GV radar NN rain rate estimate b) TRMM-PR NN rain rate estimate c) TRMM-PR rain rate product. Data from year 2007 over KWAJ. (Instantaneous rainfall).

Table 5.8: Performance evaluation of the GV NN rain rate estimation, TRMM-PR NN rain rate estimate, and TRMM-PR rain rate product. Data from year 2007 over KWAJ. (Instantaneous rainfall).

Year 2007	FracBias (%)	Corr.	NSE	FRMSE (%)
KWAJ NN Est. vs. Rain Gauge	2.3	0.94	0.21	27.4
TRMM NN Est. vs. Rain Gauge	-5.5	0.90	0.27	34.2
TRMM Product vs. Rain Gauge	-47.5	0.95	0.47	65.8

5.3.6 TESTING EACH NETWORK WITH ALTERNATIVE RADAR/GAUGE DATA

In order to evaluate the generalization capability of the designed neural networks (KMLB NN and KHGX NN); we test each neural network with the other data from the other site. In other words, we test KMLB NN using KHGX data, and we test KHGX NN using KMLB data. The same training technique described before was done in this scenario; the first neural network was adaptively trained on daily base and the data from any day was tested by the network designed in the day before. The second network was adaptively trained every time we have available TRMM overpass over the site, and the data from any overpass was tested by the network designed based on the previous overpass.

The same scoring parameters were used as before. Tables 5.9, 5.10, 5.11, 5.12, 5.13 and 5.14 show the performance evaluation of estimating rain the rate of each site from the network built by data from the other site. The performance of both networks is included in these tables. The tables also show the performance evaluation of TRMM standard product. All these evaluations were done against the rain gauge at that moment. As we see the tables still show better performance of the neural networks compared to TRMM standard product, and also they show that both networks have close performance when both compared with rain gauges, which means that mapping the relation between the ground radar reflectivity factor and the rain gauge was done and passed through the alignment process that was done, and another format of this relation was achieved to relate TRMM reflectivity factor with the rain gauges. A final remark to say here is that

based on the tables, this technique can be generalized to include other areas as we will see later when both networks were tested with other NEXRAD sites.

Table 5.9: Performance evaluation of the GV NN rain rate estimation, TRMM-PR NN rain rate estimate, and TRMM-PR rain rate product. Data from year 2005 over KMLB. Estimation based on KHGX NN. (Instantaneous rainfall).

Year 2005	FracBias (%)	Corr.	NSE	FRMSE (%)
GR NN Est. vs. Rain Gauge	-1.7	0.67	0.52	75.8
TRMM NN Est. vs. Rain Gauge	-13.6	0.55	0.54	79.0
TRMM Product vs. Rain Gauge	-48.2	0.53	0.58	92.7

Table 5.10: Performance evaluation of the GV NN rain rate estimation, TRMM-PR NN rain rate estimate, and TRMM-PR rain rate product. Data from year 2006 over KMLB. Estimation based on KHGX NN. (Instantaneous rainfall).

Year 2006	FracBias (%)	Corr.	NSE	FRMSE (%)
GR NN Est. vs. Rain Gauge	9.3	0.62	0.62	90.5
TRMM NN Est. vs. Rain Gauge	5.1	0.63	0.61	87.1
TRMM Product vs. Rain Gauge	-27.9	0.46	0.64	105.1

Table 5.11: Performance evaluation of the GV NN rain rate estimation, TRMM-PR NN rain rate estimate, and TRMM-PR rain rate product. Data from year 2007 over KMLB. Estimation based on KHGX NN. (Instantaneous rainfall).

Year 2007	FracBias (%)	Corr.	NSE	FRMSE (%)
GR NN Est. vs. Rain Gauge	27.4	0.76	0.64	98.7
TRMM NN Est. vs. Rain Gauge	5.3	0.73	0.60	100.6
TRMM Product vs. Rain Gauge	-35.2	0.58	0.58	123.3

Table 5.12: Performance evaluation of the GV NN rain rate estimation, TRMM-PR NN rain rate estimate, and TRMM-PR rain rate product. Data from year 2005 over KHGX. Estimation based on KMLB NN. (Instantaneous rainfall).

Year 2005	FracBias (%)	Corr.	NSE	FRMSE (%)
GR NN Est. vs. Rain Gauge	-2.4	0.72	0.46	71.7
TRMM NN Est. vs. Rain Gauge	-26.0	0.59	0.45	88.4
TRMM Product vs. Rain Gauge	-54.9	0.20	0.62	113.4

Table 5.13: Performance evaluation of the GV NN rain rate estimation, TRMM-PR NN rain rate estimate, and TRMM-PR rain rate product. Data from year 2006 over KHGX. Estimation based on KMLB NN. (Instantaneous rainfall).

Year 2006	FracBias (%)	Corr.	NSE	FRMSE (%)
GR NN Est. vs. Rain Gauge	-5.8	0.88	0.26	37.0
TRMM NN Est. vs. Rain Gauge	-3.0	0.74	0.36	51.7
TRMM Product vs. Rain Gauge	-59.9	0.37	0.61	93.0

Table 5.14: Performance evaluation of the GV NN rain rate estimation, TRMM-PR NN rain rate estimate, and TRMM-PR rain rate product. Data from year 2007 over KHGX. Estimation based on KMLB NN. (Instantaneous rainfall).

Year 2007	FracBias (%)	Corr.	NSE	FRMSE (%)
GR NN Est. vs. Rain Gauge	9.8	0.68	0.40	52.8
TRMM NN Est. vs. Rain Gauge	3.0	0.65	0.41	51.3
TRMM Product vs. Rain Gauge	-42.3	0.59	0.48	68.4

5.3.7 RAINFALL MAPS GENERATION

Each network in the hybrid network designed before is tested for some instances of TRMM-PR as well as their corresponding ground radar measurements. Figures 5.14, 5.15 and 5.16 show instances seen by KMLB radar and overpassed by TRMM radar. Each instance was tested by the KMLB neural network that was designed in the year the instance was measured. The same goes for Figures 5.17 and 5.18; these figures show instances seen by KHGX radar and overpassed by TRMM radar and tested by the neural network that was designed based on KHGX radar measurements and their TRMM radar overpasses.

The top row of the figures shows two maps of the reflectivity factor from both radars. The second row shows the rainfall maps generated by both neural networks. The third row shows a map of TRMM standard rainfall product. The last row of the figures shows two scatter plots; one is for the output of the neural networks versus each other, and the second shows the output of TRMM NN versus TRMM standard product.

As we see from the figures, the maps generated by the neural networks are showing better representation of the storm compared to TRMM product; TRMM product tends to underestimate the rainfall while the neural network technique captures the storm better. The figures also show through the scatter plots how close the output of both networks to each other, and how TRMM-PR standard product tends to underestimate rain rate compared to the neural networks output.

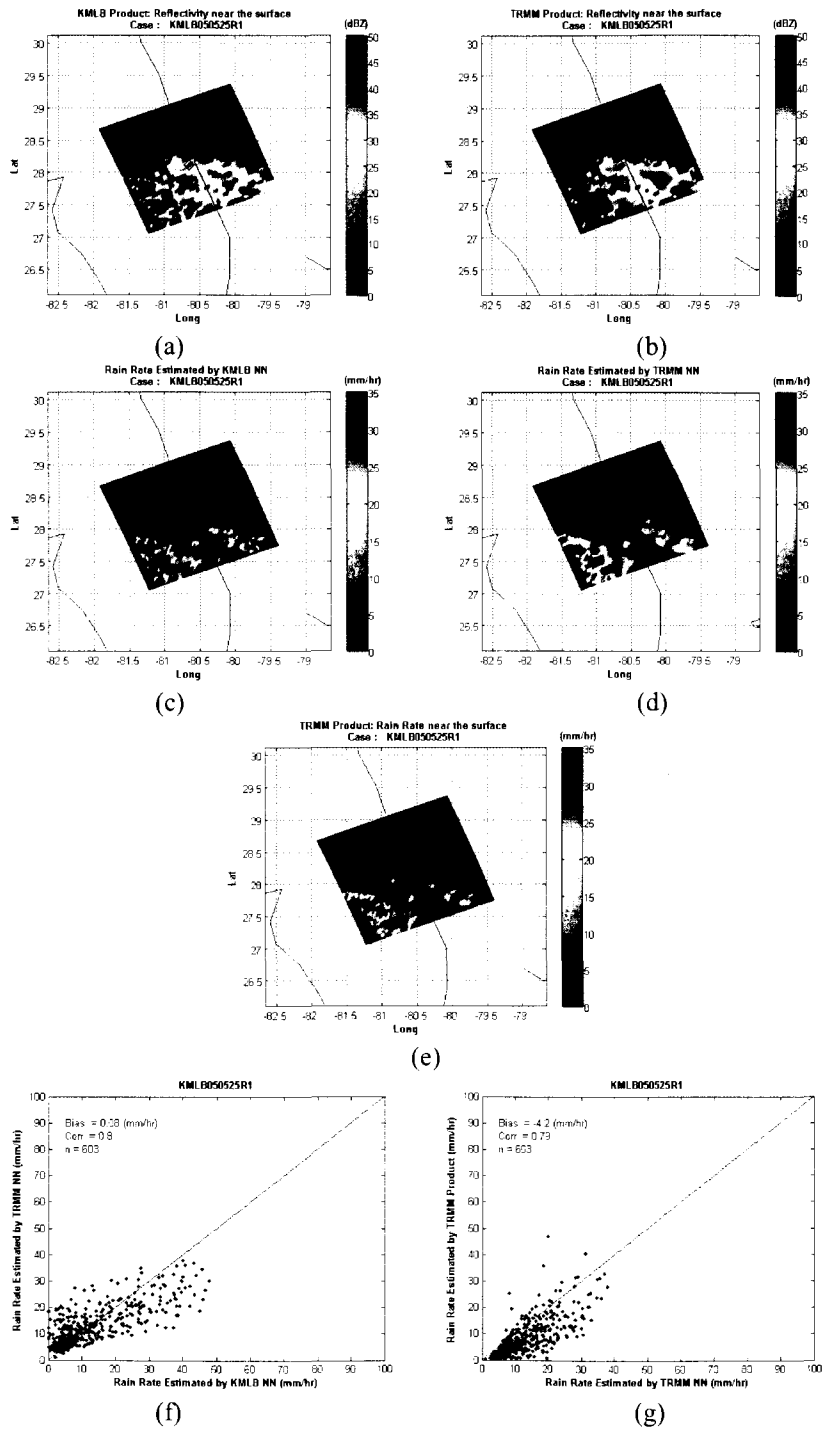


Figure 5.14: (a) KMLB reflectivity (b) TRMM-PR reflectivity (c) KMLB-NN rain rate estimate (d) TRMM-NN rain rate estimate (e) TRMM-PR rain rate product (f) KMLB-NN rain rate estimate vs. TRMM-NN rain rate estimate (g) TRMM-PR rain rate product vs. TRMM-NN rain rate estimate. (Case: KMLB: 05/25/2005).

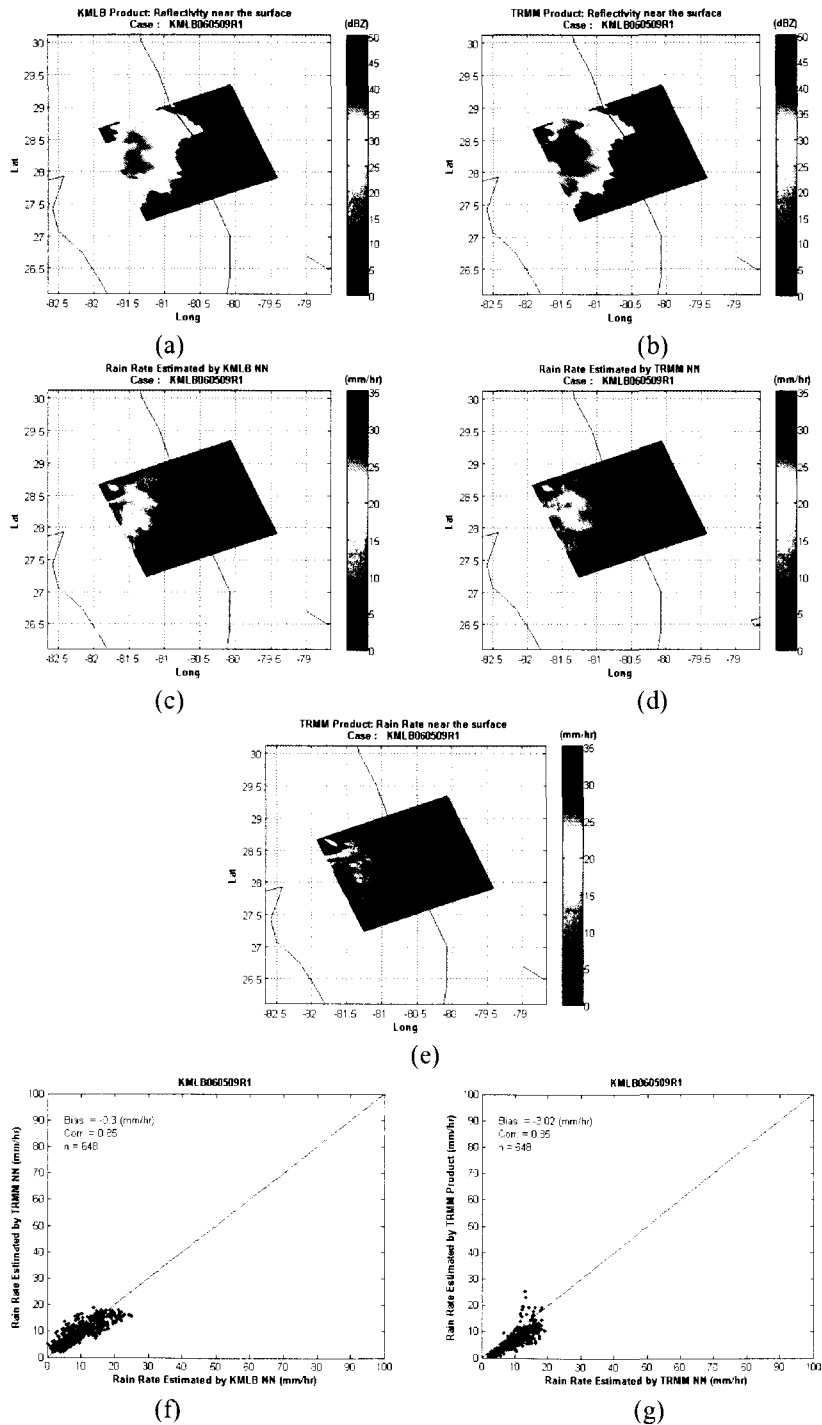


Figure 5.15: (a) KMLB reflectivity (b) TRMM-PR reflectivity (c) KMLB-NN rain rate estimate (d) TRMM-NN rain rate estimate (e) TRMM-PR rain rate product (f) KMLB-NN rain rate estimate vs. TRMM-NN rain rate estimate (g) TRMM-PR rain rate product vs. TRMM-NN rain rate estimate. (Case: KMLB: 05/09/2006).

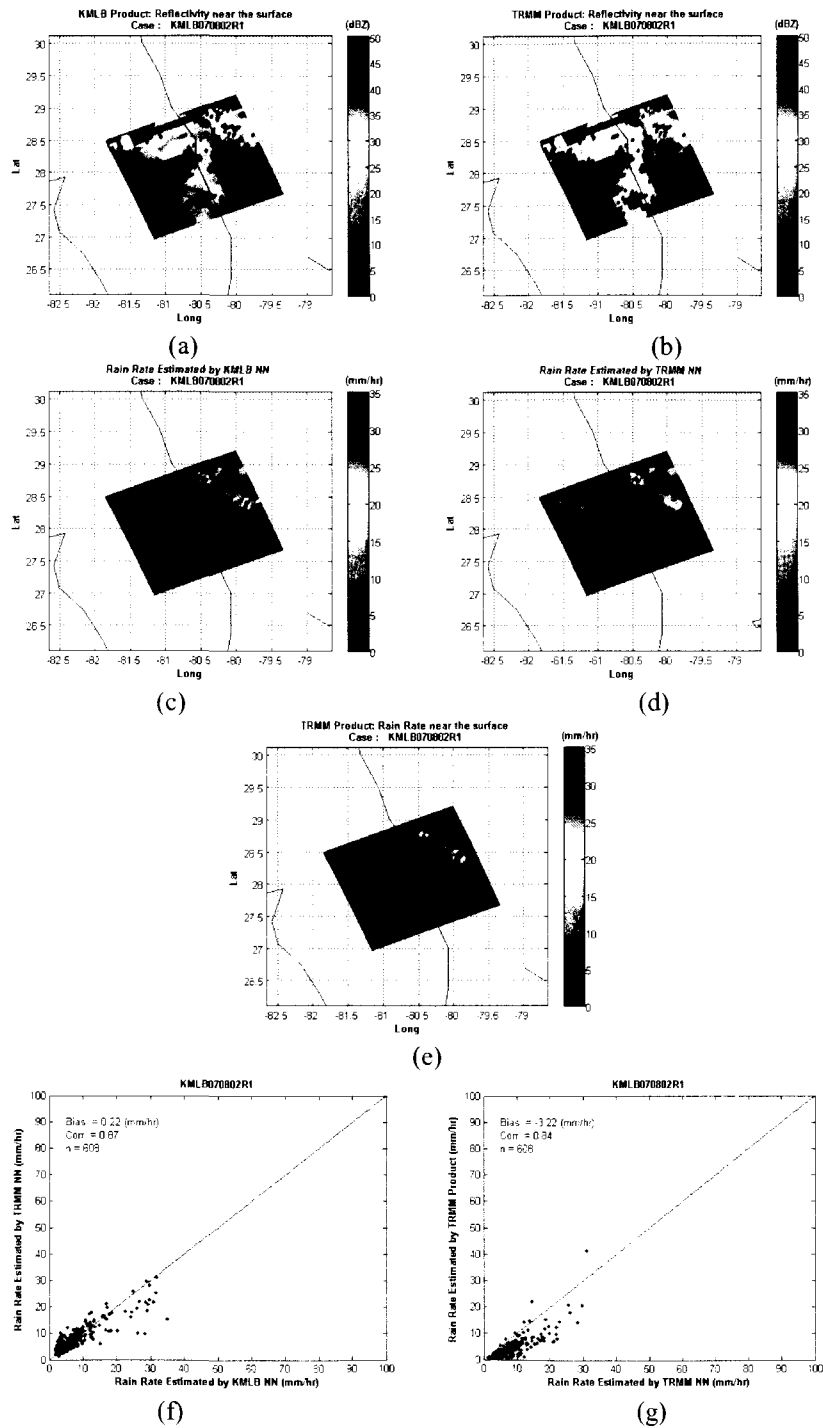


Figure 5.16: (a) KMLB reflectivity (b) TRMM-PR reflectivity (c) KMLB-NN rain rate estimate (d) TRMM-NN rain rate estimate (e) TRMM-PR rain rate product (f) KMLB-NN rain rate estimate vs. TRMM-NN rain rate estimate (g) TRMM-PR rain rate product vs. TRMM-NN rain rate estimate. (Case: KMLB: 08/02/2007).

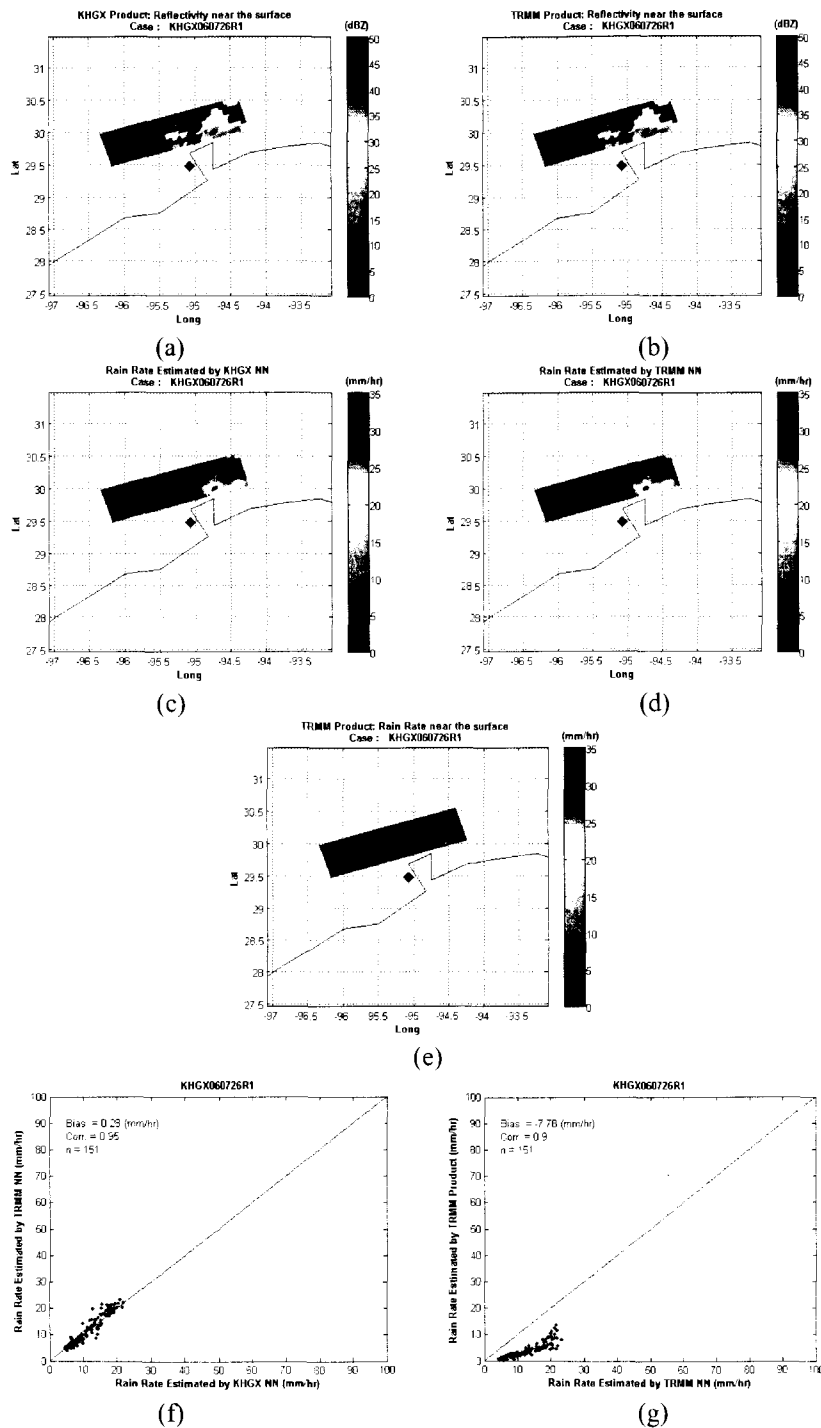


Figure 5.17: (a) KHXG reflectivity (b) TRMM-PR reflectivity (c) KHXG -NN rain rate estimate (d) TRMM-NN rain rate estimate (e) TRMM-PR rain rate product (f) KHXG -NN rain rate estimate vs. TRMM-NN rain rate estimate (g) TRMM-PR rain rate product vs. TRMM-NN rain rate estimate. (Case: KHGX: 07/26/2006).

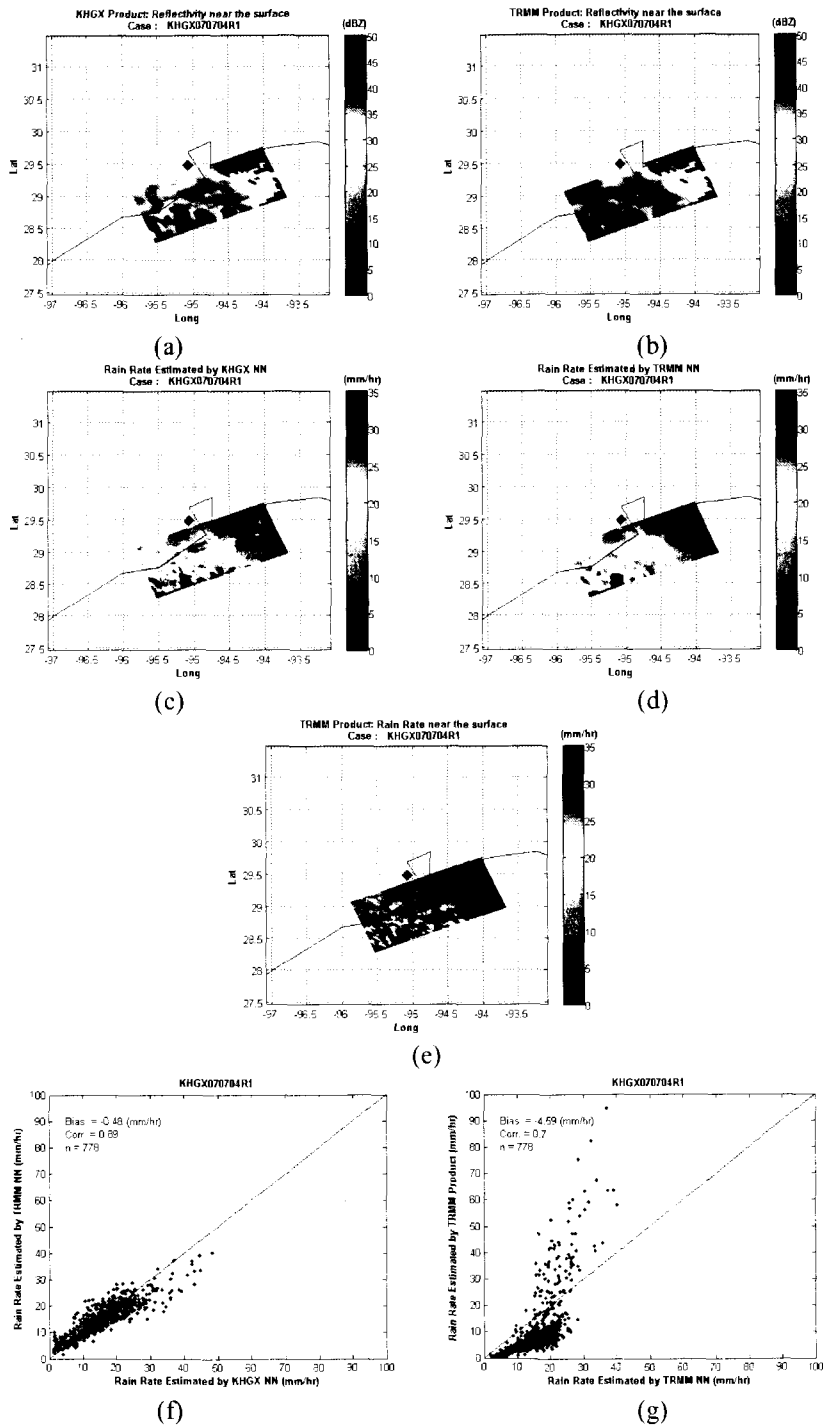


Figure 5.18: (a) KHXG reflectivity (b) TRMM-PR reflectivity (c) KHXG -NN rain rate estimate (d) TRMM-NN rain rate estimate (e) TRMM-PR rain rate product (f) KHXG -NN rain rate estimate vs. TRMM-NN rain rate estimate (g) TRMM-PR rain rate product vs. TRMM-NN rain rate estimate. (Case: KHGX: 07/04/2007).

5.3.8 RAINFALL MAPS GENERATION USING ALTERNATIVE SITE'S NEURAL NETWORK

In this section each site's neural network was used to generate rainfall maps from data generated at the other site. In other words; KMLB NN was used to generate rainfall maps from KHGX data, and KHGX NN was used to generate rainfall maps from KMLB data. The goal of this test is again to check for generalization as well as to see if we get the same conclusions drawn in the previous section.

Again Figures 5.19 and 5.20 show instances seen by KHGX radar and overpassed by TRMM radar. Each instance was tested by the KMLB neural network that was designed in the year the instance was measured. The same goes for Figures 5.21, 5.22, and 5.23; these figures show instances seen by KMLB radar and overpassed by TRMM radar and tested by the neural network that was designed based on KHGX radar measurements and their TRMM radar overpasses.

The figures have the same description used in the previous section; the top row of the figures shows two maps of the reflectivity factor from both radars. The second row shows the rainfall maps generated by both neural networks but in this case the network was designed using the other site's data. The third row shows a map of TRMM standard rainfall product. The last row of the figures shows two scatter plots; one is for the output of both neural networks versus each other, and the second shows the output of TRMM NN versus TRMM standard product.

As we see from the figures, the neural networks were generalized and they were giving good performance when tested with data have never seen before; the performance here is close to the performance achieved in the last section, the maps generated by the

neural networks are showing better representation of the storm compared to TRMM product; TRMM product tends to underestimate the rainfall while the neural network technique captures the storm better. The figures also show through the scatter plots how close the output of both networks to each other, and how TRMM-PR standard product tends to underestimate rain rate when compared to the neural networks output.

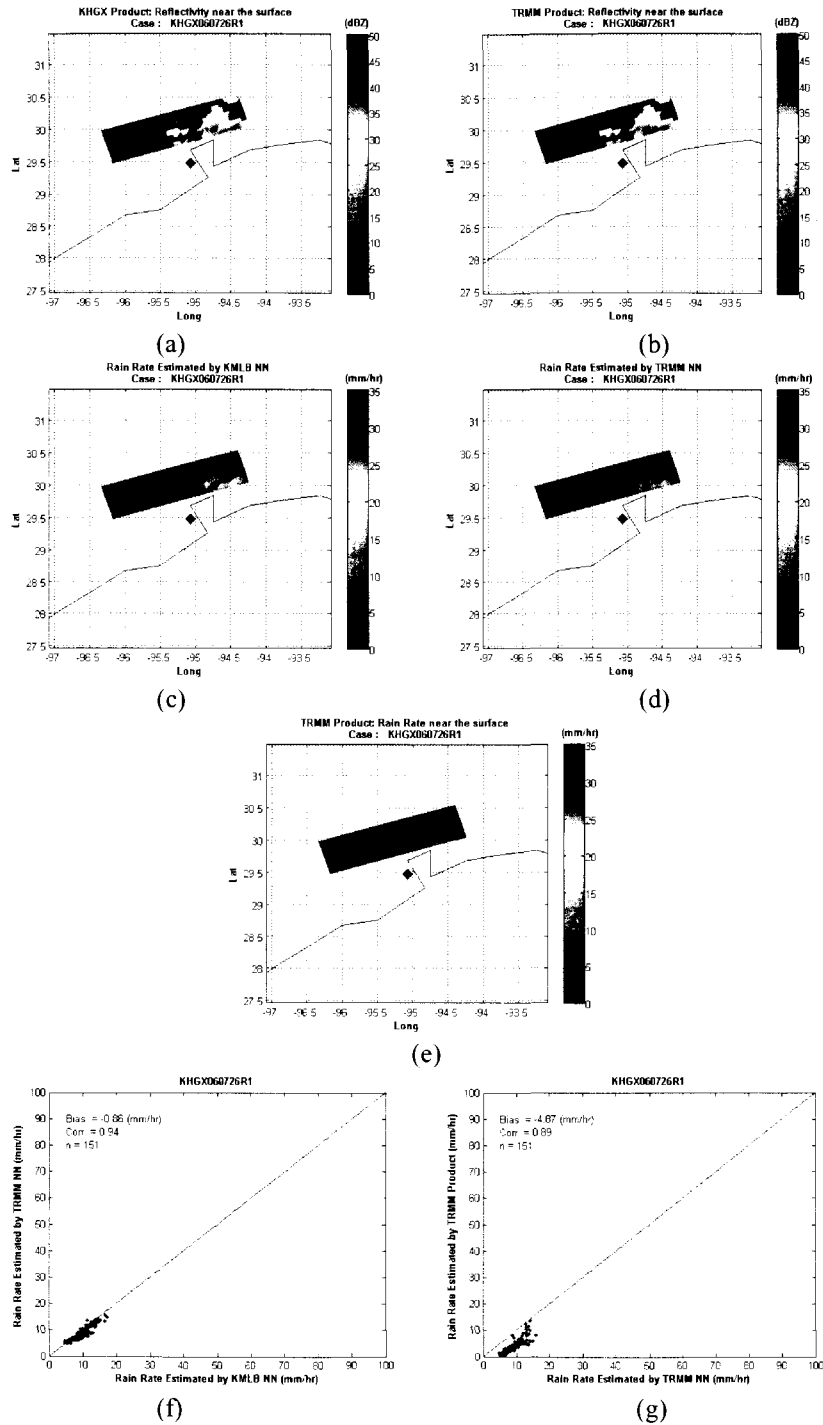


Figure 5.19: (a) KHGX reflectivity (b) TRMM-PR reflectivity (c) KMLB-NN rain rate estimate (d) TRMM-NN rain rate estimate (e) TRMM-PR rain rate product (f) KMLB-NN rain rate estimate vs. TRMM-NN rain rate estimate (g) TRMM-PR rain rate product vs. TRMM-NN rain rate estimate. (Case: KHGX: 07/26/2006).

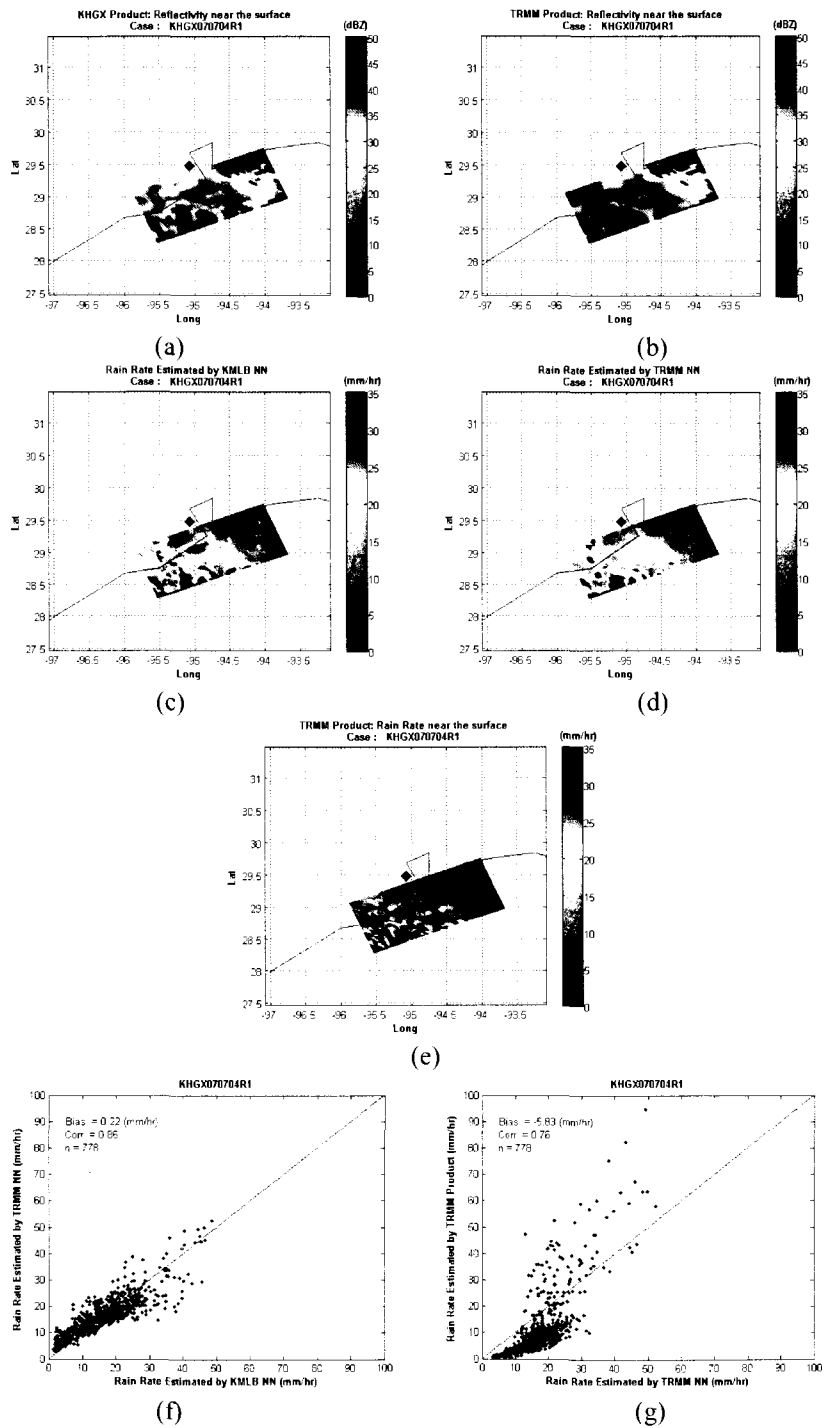


Figure 5.20: (a) KHGX reflectivity (b) TRMM-PR reflectivity (c) KMLB-NN rain rate estimate (d) TRMM-NN rain rate estimate (e) TRMM-PR rain rate product (f) KMLB-NN rain rate estimate vs. TRMM-NN rain rate estimate (g) TRMM-PR rain rate product vs. TRMM-NN rain rate estimate. (Case: KHGX: 07/04/2007).

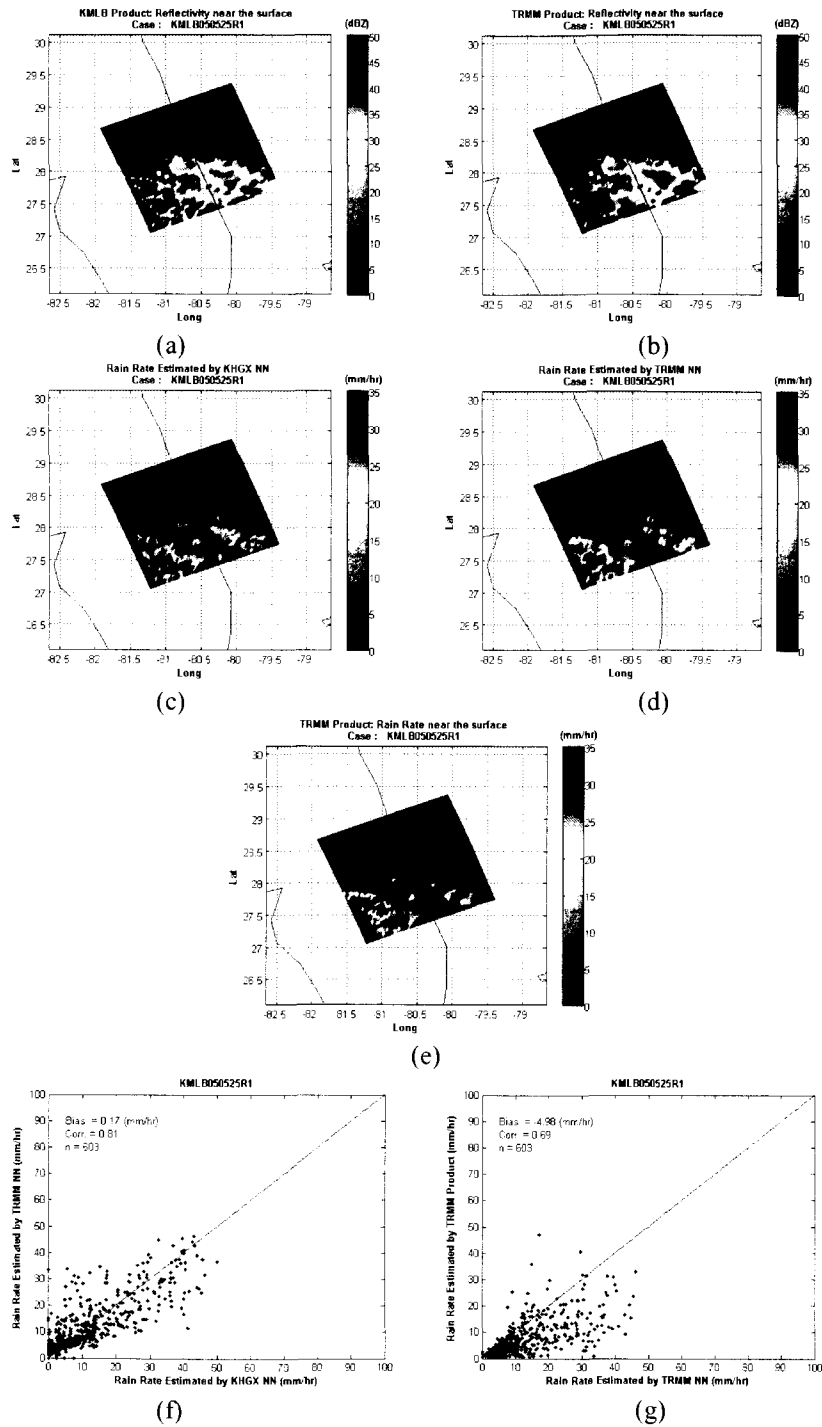


Figure 5.21: (a) KMLB reflectivity (b) TRMM-PR reflectivity (c) KHGX -NN rain rate estimate (d) TRMM-NN rain rate estimate (e) TRMM-PR rain rate product (f) KHGX -NN rain rate estimate vs. TRMM-NN rain rate estimate (g) TRMM-PR rain rate product vs. TRMM-NN rain rate estimate. (Case: KMLB : 05/25/2005).

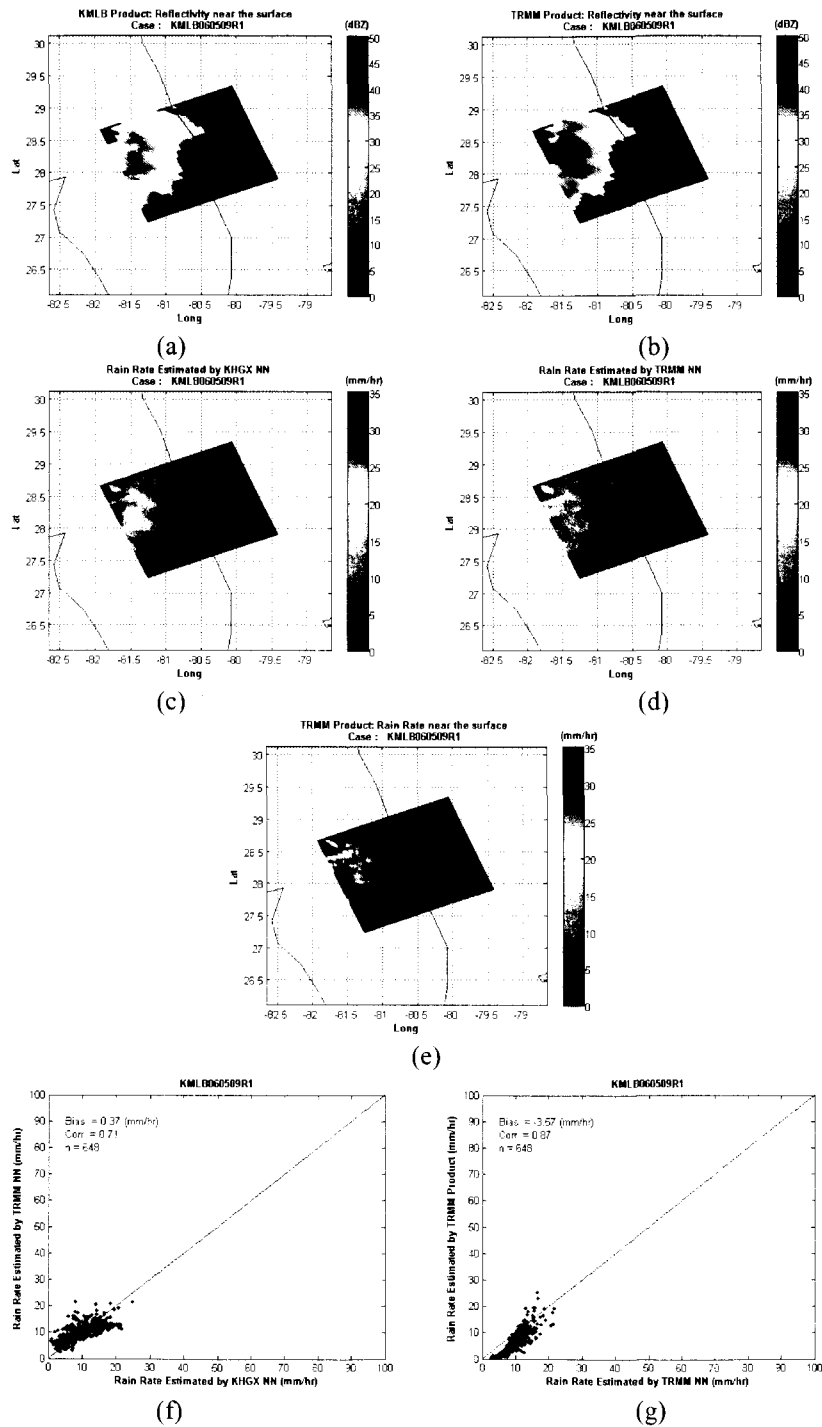


Figure 5.22: (a) KMLB reflectivity (b) TRMM-PR reflectivity (c) KHGX -NN rain rate estimate (d) TRMM-NN rain rate estimate (e) TRMM-PR rain rate product (f) KHGX -NN rain rate estimate vs. TRMM-NN rain rate estimate (g) TRMM-PR rain rate product vs. TRMM-NN rain rate estimate. (Case: KMLB : 05/09/2006).

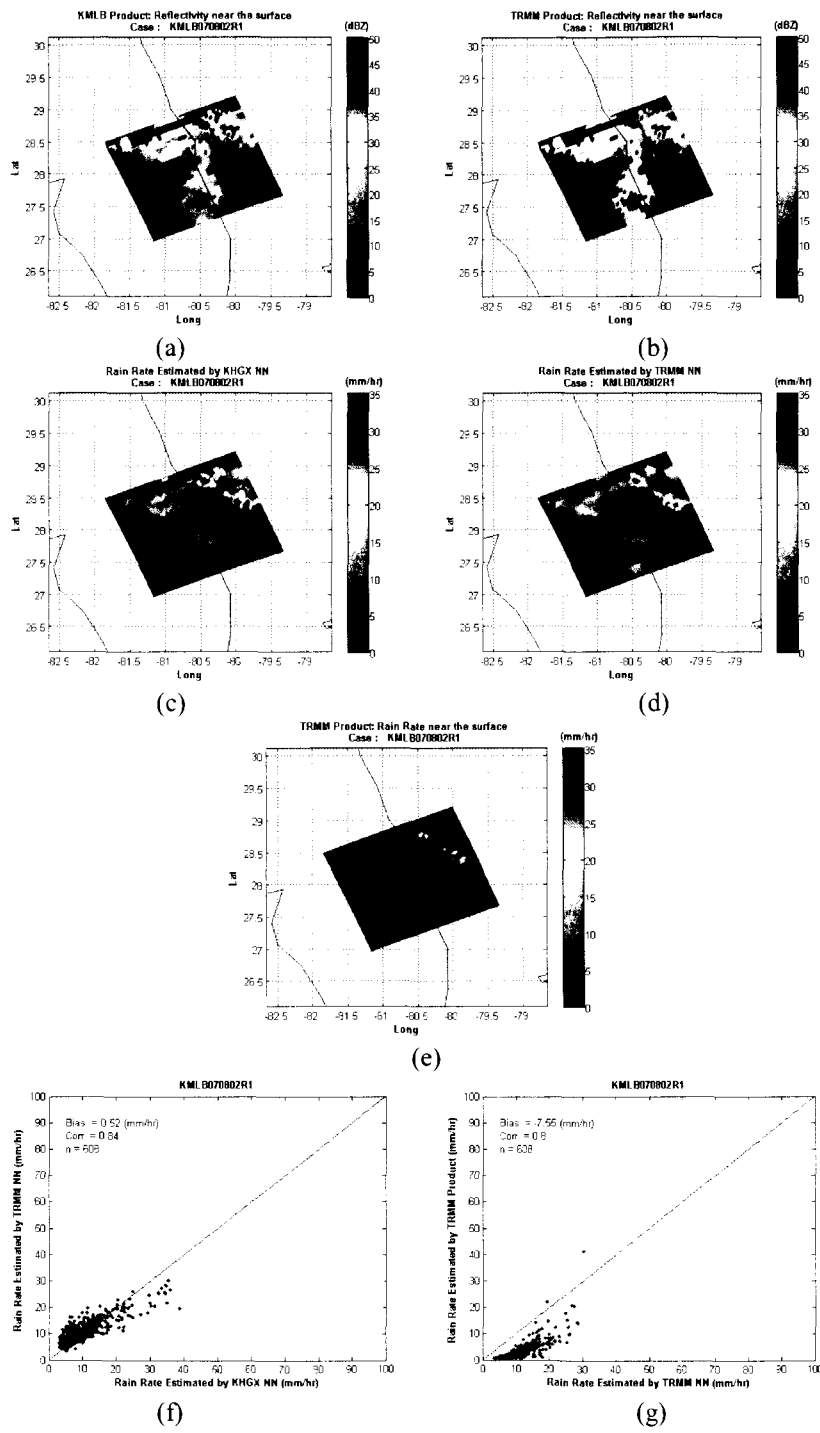


Figure 5.23: (a) KMLB reflectivity (b) TRMM-PR reflectivity (c) KHGX -NN rain rate estimate (d) TRMM-NN rain rate estimate (e) TRMM-PR rain rate product (f) KHGX -NN rain rate estimate vs. TRMM-NN rain rate estimate (g) TRMM-PR rain rate product vs. TRMM-NN rain rate estimate. (Case: KMLB : 08/02/2007).

5.3.9 RAINFALL MAPS GENERATION USING DATA FROM OTHER NEXRAD SITES

In this section we tested the designed neural networks with instances from other NEXRAD radars instances and their TRMM-PR overpasses. Two instances from two NEXRAD radars were tested; the first instance was around KEVX (Eglin AFB, FL) radar (01/27/2007 at 03:59:44UTC) and the second instance was around KSHV (Shreveport, LA) radar (10/27/2006 at 03:12:50UTC). Figure 5.24 shows the location of two three sites circled in green, and it also shows the location of KMLB and KHGX (KHGX) circled in red. Table 5.15 shows the full name of four five sites as well as their corresponding latitudes and longitudes.

Both designed neural networks at each site were used to generate rainfall maps from the two instances mentioned above. The goal of this test is again to check for generalization as well as to see if we can use the designed neural networks to test for other NEXRAD radars. Figures 5.25 and 5.26 show the two instances as well as their TRMM-PR overpassing measurements. Each instance was tested by the KMLB neural network that was designed in the year the instance was measured. The figures have the same description used in the previous section; the top row of the figures shows two maps of the reflectivity factor from both radars. The second row shows the rainfall maps generated by both neural networks designed at KMLB site. The third row shows a map of TRMM standard rainfall product. The last row of the figures shows two scatter plots; one is for the output of both neural networks versus each other, and the second shows the output of TRMM NN versus TRMM standard product. The same figures description goes

for Figures 5.27 and 5.28; these figures show the same instances but testing was based on the neural networks designed at KHGX site.

As can be seen from the figures, the neural networks were generalized and they were giving good performance when tested with data have never seen before, the performance achieved by KMLB NN is close to the performance achieved by KHGX NN. Again the maps generated by the neural networks are showing better representation of the storm compared to TRMM product; TRMM product tends to underestimate the rainfall while the neural network technique captures the storm better. The figures also show through the scatter plots how close the output of both networks (ground radar network and TRMM network) to each other. This would lead us to the conclusion that the network can also be applied to other geographical regions beyond the ground validation sites.

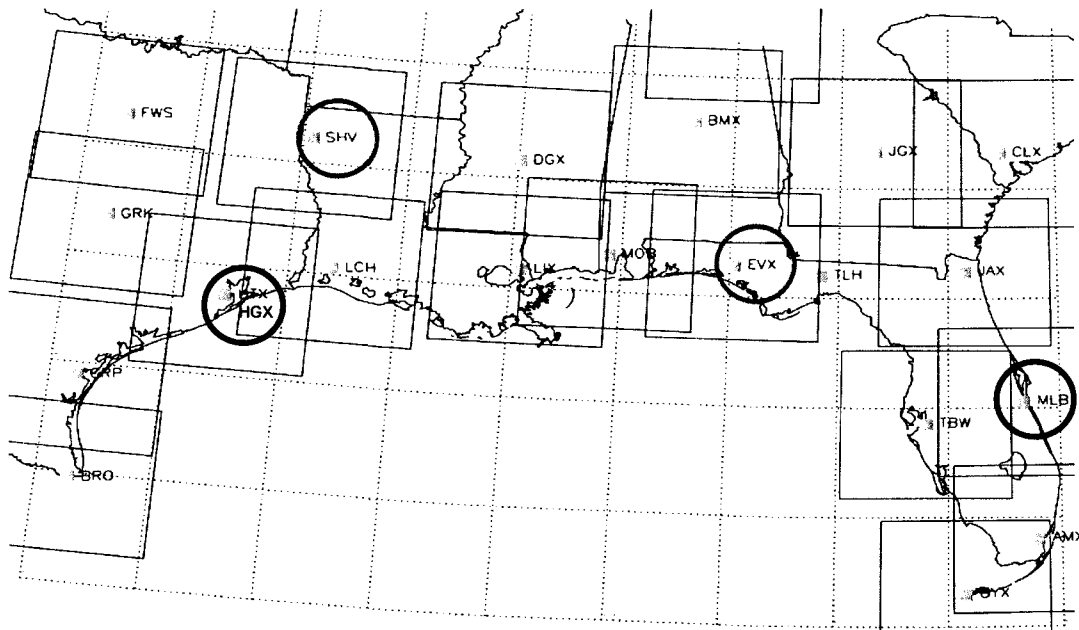


Figure 5.24: Location of NEXRAD radars in the southeastern US. Green-circled used to design the neural networks. Red-circled used for validation.

Table 5.15: NEXRAD sites used in this study

Site Short Name	Site Full Name	Latitude	Longitude
KMLB	Melbourne, FL	28.1133N	80.6542W
KHGX	Houston, TX	29.4719N	95.0792W
KEVX	Eglin AFB, FL	30.5644N	85.9214W
KSHV	Shreveport, LA	32.4508N	93.8414W

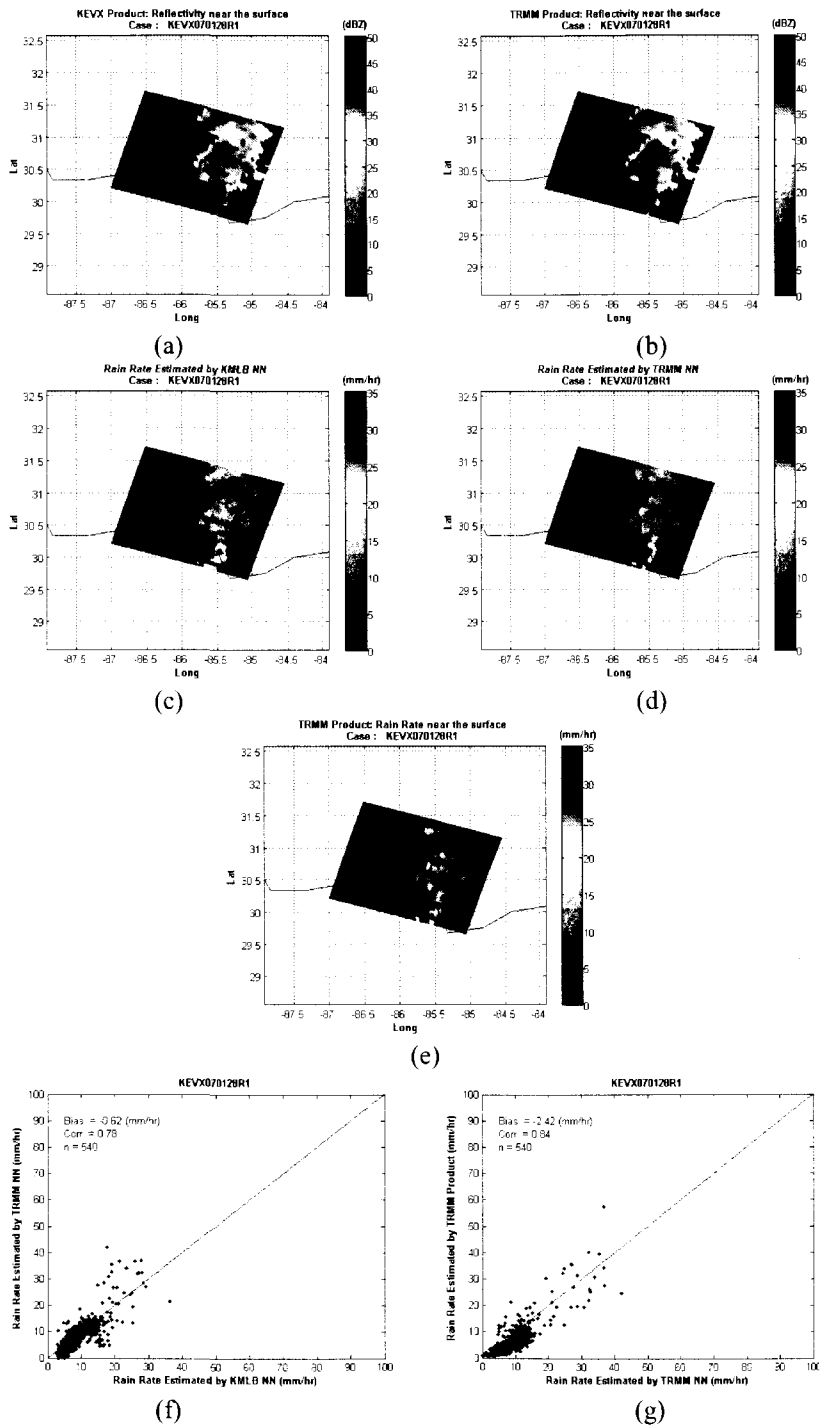


Figure 5.25: (a) KEVX reflectivity (b) TRMM-PR reflectivity (c) KMLB-NN rain rate estimate (d) TRMM-NN rain rate estimate (e) TRMM-PR rain rate product (f) KMLB-NN rain rate estimate vs. TRMM-NN rain rate estimate (g) TRMM-PR rain rate product vs. TRMM-NN rain rate estimate. (Case: KEVX: 01/28/2007).

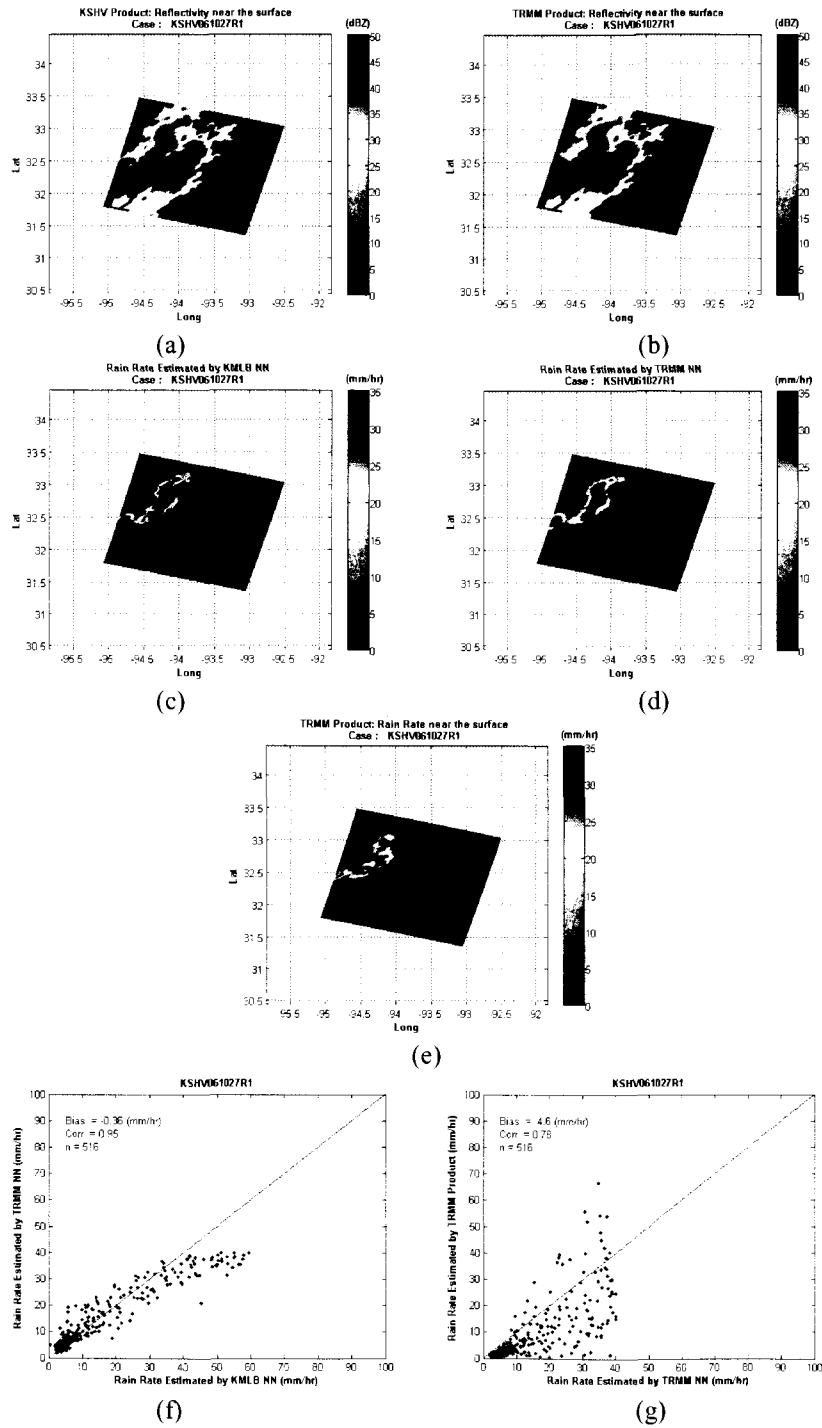


Figure 5.26: (a) KSHV reflectivity (b) TRMM-PR reflectivity (c) KMLB-NN rain rate estimate (d) TRMM-NN rain rate estimate (e) TRMM-PR rain rate product (f) KMLB-NN rain rate estimate vs. TRMM-NN rain rate estimate (g) TRMM-PR rain rate product vs. TRMM-NN rain rate estimate. (Case: KSHV: 10/27/2006).

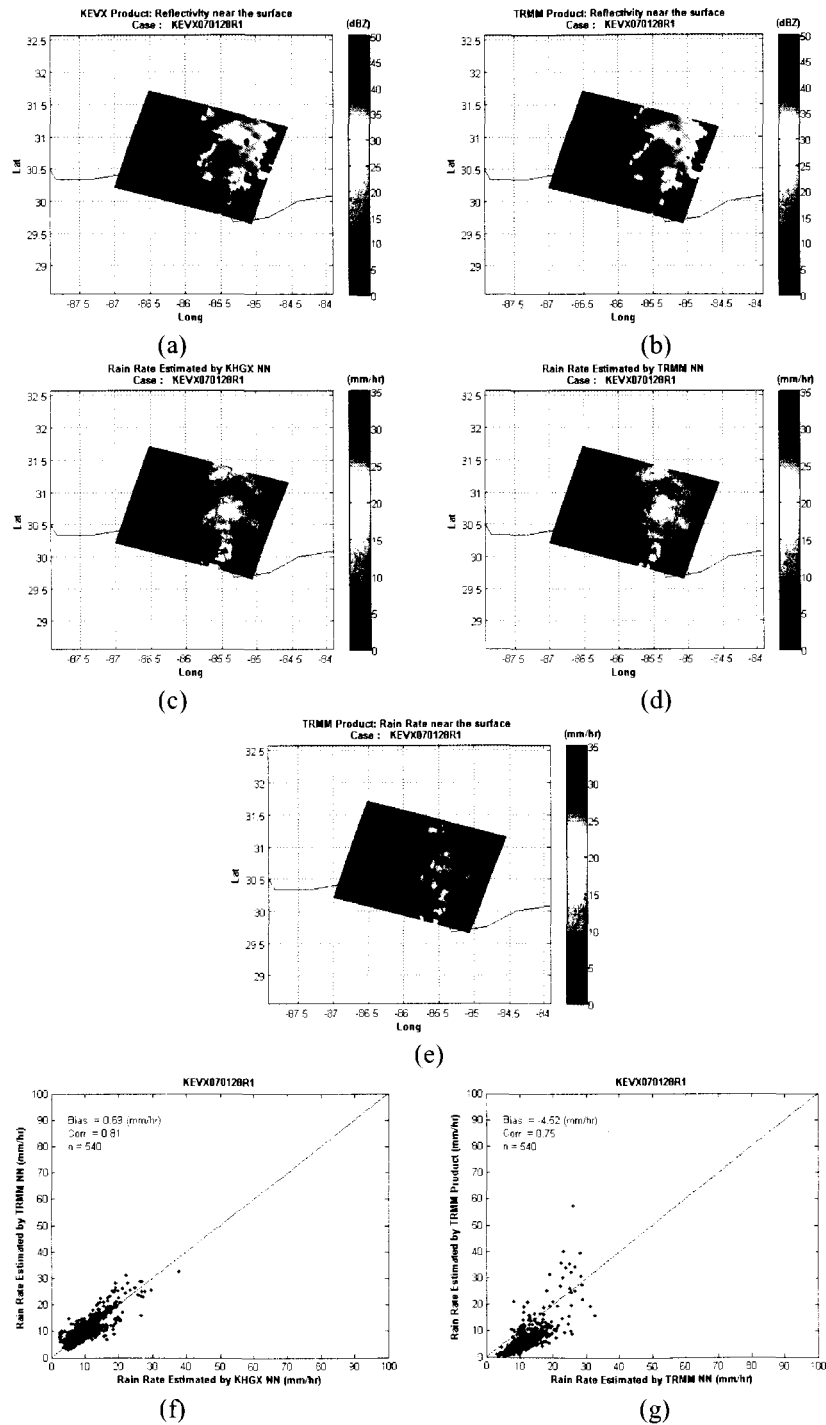


Figure 5.27: (a) KEVX reflectivity (b) TRMM-PR reflectivity (c) KHGX-NN rain rate estimate (d) TRMM-NN rain rate estimate (e) TRMM-PR rain rate product (f) KHGX-NN rain rate estimate vs. TRMM-NN rain rate estimate (g) TRMM-PR rain rate product vs. TRMM-NN rain rate estimate. (Case: KEVX: 01/28/2007).

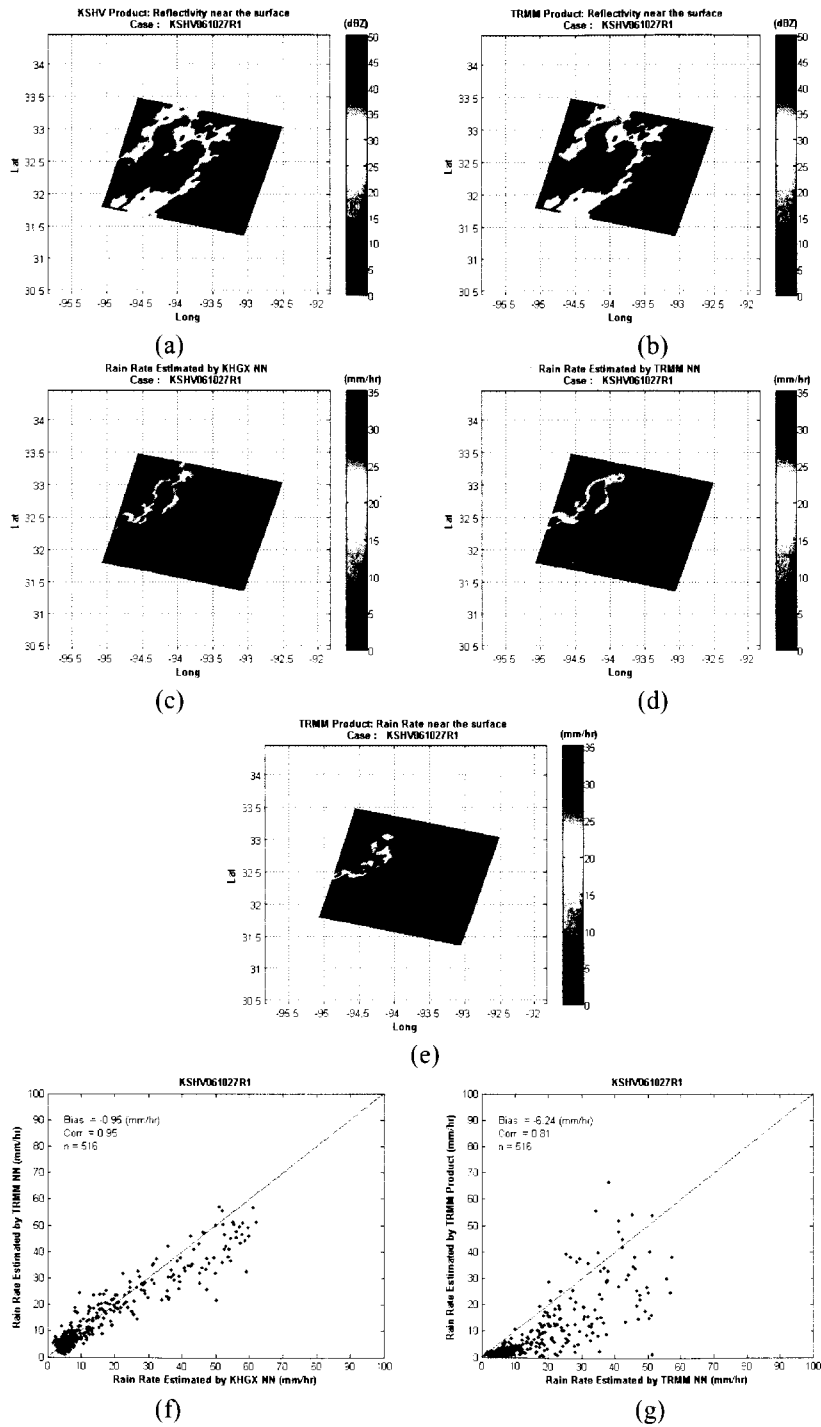


Figure 5.28: (a) KSHV reflectivity (b) TRMM-PR reflectivity (c) KHGX-NN rain rate estimate (d) TRMM-NN rain rate estimate (e) TRMM-PR rain rate product (f) KHGX-NN rain rate estimate vs. TRMM-NN rain rate estimate (g) TRMM-PR rain rate product vs. TRMM-NN rain rate estimate. (Case: KSHV : 10/27/2006).

5.4 GLOBAL RAINFALL MAPS GENERATION

In this section, monthly global rainfall maps are generated using TRMM-NN that was designed at KMLB site in year 2008. The monthly rainfall maps are generated and compared to TRMM-PR monthly rainfall maps. Monthly surface rainfall totals are derived by multiplying the mean rainfall rate by the total number of hours in each month. TRMM-PR rainfall maps are taken from TRMM-3A26 product. TRMM-PR maps are generated based on TRMM-PR 2A25 product. Description of how TRMM-PR rainfall maps are generated can be found at [<http://trmm.gsfc.nasa.gov/3a26.html>]. Resolution of these maps is $5^{\circ} \times 5^{\circ}$ (lat, long).

Figures 5.29, 5.31, 5.33, 5.35, 5.37, 5.39, 5.41, 5.43, 5.45, 5.47, 5.49 and 5.51 show global rainfall maps for each month in year 2008. In these figures, the top left panel is the rainfall accumulation map generated by the neural network at each month. The top right panel is the rainfall accumulation map generated by TRMM-PR 3A26 product. The bottom left panel shows the zonal mean of the rain accumulation generated by both TRMM-PR and NN products. The bottom right panel shows the scatter plot of zonal mean of the rain accumulation generated by both TRMM-PR and NN products. Figure 5.53 shows global rainfall maps for the whole year of 2008. Description of the panels in this figure is the same as in the monthly figures described above.

As can be seen in the figures, the maps generated by the neural network estimator are some times very similar to the maps generated by TRMM-PR product. This can be seen easily in the zonal mean plots and scatter plots in most of the months. This trial of creating global rainfall maps from a neural network designed at a single place (KMLB in

this case) was not meant to compare the two products to see which one is better or to test the closeness of the neural network product to TRMM-PR product. Again, these global maps were generated using a neural network designed based on a local data. The closeness and the behavior that was noticed from the plots indicate that there is a good potential the technique can be used to generate global rainfall maps. To get better results, different neural networks need to be designed from different meteorological areas, and then the globe can be tested so that any area is tested using a neural network that is designed based on data taken from neighboring area. Table 5.16 shows numerical comparison between the neural network maps and TRMM-PR maps. Again, the table shows good potential of using the neural network technique to generate global rainfall maps. As shown in the table, the bias was not significant; the overall NSE of year 2008 was less than 0.08, together with the high correlation shown are good indications of how the two outputs are close to each other.

Table 5.16: NN rainfall accumulation estimate vs. TRMM-PR rainfall accumulation product.

Month of 2008	FracBias (%)	Corr.	NSE	FRMSE (%)
January	-2.6	0.91	0.19	23.6
February	-19.7	0.95	0.22	28.9
March	-2.2	0.97	0.12	14.8
April	-1.1	0.97	0.09	12.4
May	-6.6	0.95	0.13	17.1
June	-10.9	0.96	0.16	20.3
July	-5.4	0.92	0.18	21.3
August	-11.9	0.96	0.17	20.4
September	8.5	0.97	0.11	15.6
October	8.9	0.99	0.09	11.5
November	14.1	0.97	0.14	17.5
December	16.6	0.94	0.17	21.6
Year 2008	-1.0	0.97	0.07	9.2

To get fair comparison between the maps generated by the NN and the maps generated by TRMM-PR product; two areas were selected and compared to each other. Figures 5.30, 5.32, 5.34, 5.36, 5.38, 5.40, 5.42, 5.44, 5.46, 5.48, 5.50 and 5.52 show the rainfall maps for each month in year 2008 but over KMLB and KHGX areas as shown by the squares drawn on the maps. In these figures, the top left panel is the rainfall accumulation map generated by the neural network at each month. The top right panel is the rainfall accumulation map generated by TRMM-PR 3A26 product. The bottom left panel shows the scatter plot of the rain accumulation generated by both TRMM-PR and NN products over KMLB area, while the bottom right panel shows the scatter plot of the rain accumulation generated by both TRMM-PR and NN products over KHGX area. Figure 5.54 shows rainfall maps for the whole year of 2008 over those two areas. Description of the panels in this figure is the same as in the monthly figures.

As can be seen in the figures, the maps generated by the neural network estimator are very similar to the maps generated by TRMM-PR product on average. This can be seen easily in the scatter plots and by comparing the maps generated by both. Tables 5.17 and 5.18 show numerical comparison between the neural network maps and TRMM-PR maps over KMLB and KHGX, respectively. Table 5.17 shows that on average, TRMM-PR product underestimates the neural network product by 83mm with high correlation and small NSE which is less than 0.09. This tells us a better idea about TRMM-PR rainfall estimate; if we believe that the neural network is right, then TRMM-PR rain estimate over KMLB underestimates rain gauge, and this was shown in previous sections of this Chapter. On the other hand, the results over KHGX area show that TRMM-PR rain

estimate overestimates the neural network estimate with slight bias. It is worth mentioning that even if TRMM-PR over KMLB area underestimates the neural network; the bias between these two products is considered to be small (83mm) taking into considerations that the NSE was less than 0.09. This shows us again the potentiality of using the neural networks to build rainfall estimator that can be used to generate local rainfall maps.

Table 5.17: NN rainfall accumulation estimate vs. TRMM-PR rainfall accumulation product. (KMLB area)

Month of 2008	FracBias (%)	Corr.	NSE	FRMSE (%)
January	40.6	0.96	0.40	42.4
February	-11.8	0.99	0.11	17.0
March	1.1	-0.34	0.14	15.4
April	9.9	0.97	0.11	20.6
May	-3.3	0.91	0.18	20.2
June	-14.8	0.58	0.22	26.7
July	2.2	0.84	0.07	9.2
August	4.5	0.99	0.05	6.5
September	7.9	0.97	0.11	14.4
October	15.7	0.99	0.15	15.9
November	22.3	0.99	0.22	25.6
December	17.3	0.90	0.18	25.0
Year 2008	7.2	0.71	0.08	11.2

Table 5.18: NN rainfall accumulation estimate vs. TRMM-PR rainfall accumulation product. (KHGX area)

Month of 2008	FracBias (%)	Corr.	NSE	FRMSE (%)
January	22.9	0.90	0.32	38.2
February	-17.5	0.96	0.17	20.5
March	-6.7	0.98	0.11	18.0
April	-13.7	0.98	0.13	15.5
May	-11.0	0.97	0.11	17.7
June	-13.0	0.99	0.18	25.7
July	-2.4	0.99	0.04	6.9
August	0.7	0.96	0.06	7.4
September	-0.2	0.94	0.19	25.4
October	10.5	0.91	0.11	14.5
November	13.7	0.99	0.16	19.3
December	30.7	0.99	0.30	43.8
Year 2008	-0.6	0.95	0.08	10.4

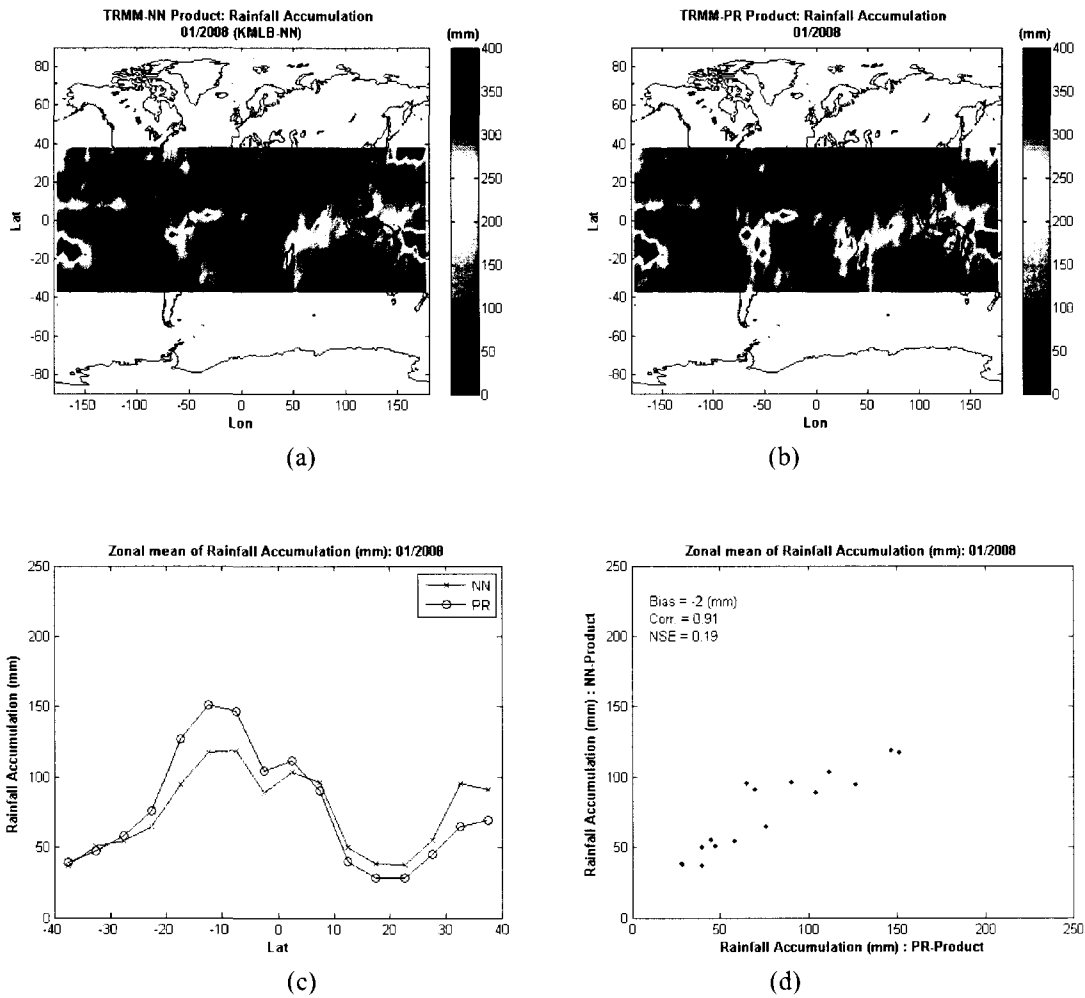


Figure 5.29: (a) Global Rainfall accumulation map generated by the NN (b) Global Rainfall accumulation map generated by TRMM-PR product (c) Zonal mean of the rainfall accumulation. (d) Scatter plot of Zonal mean of the rainfall accumulation. Maps resolution is $5^{\circ} \times 5^{\circ}$ (lat, long), and data from (01/2008).

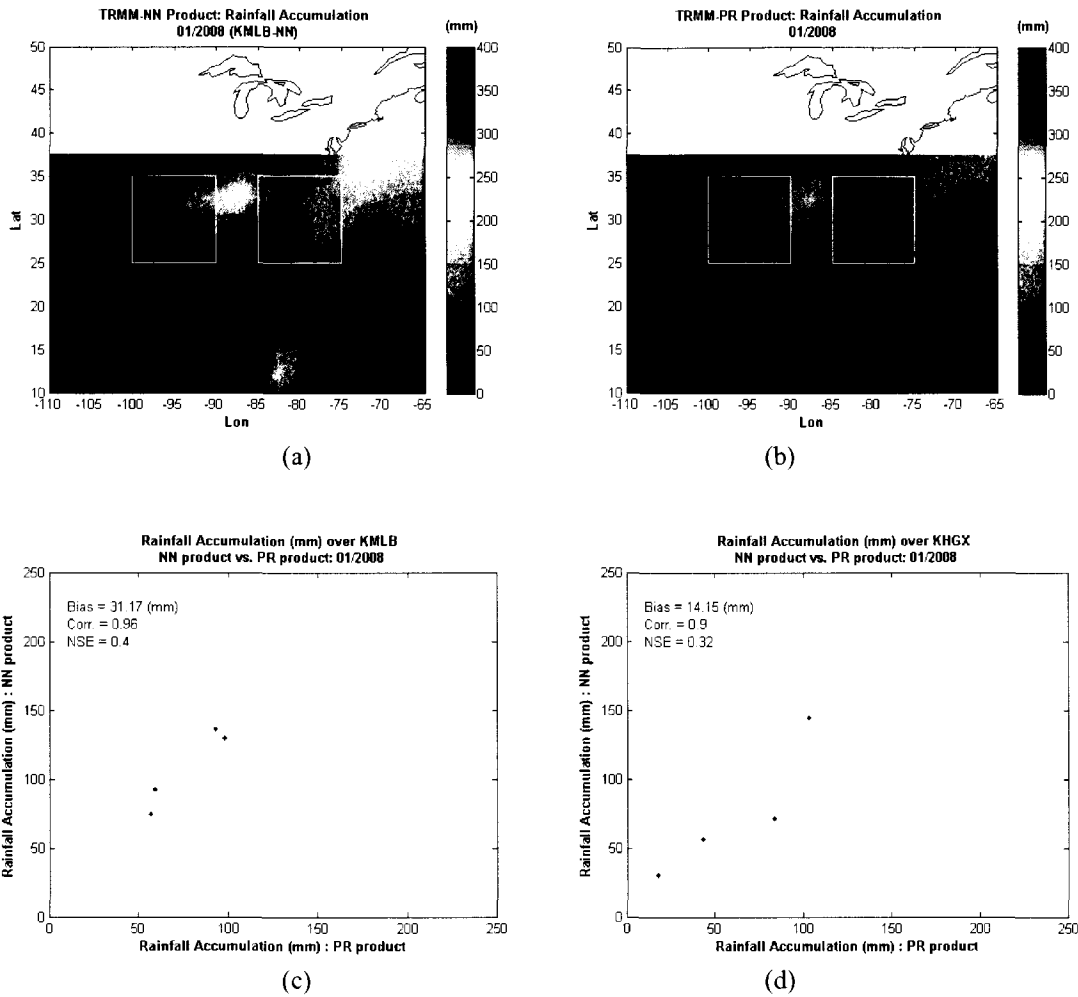


Figure 5.30: (a) Rainfall accumulation map over KMLB and KHGX areas generated by the NN (b) accumulation map over KMLB and KHGX areas generated by TRMM-PR product (c) Scatter plot of NN rainfall accumulation vs. TRMM-PR rainfall accumulation over KMLB area. (d) Scatter plot of NN rainfall accumulation vs. TRMM-PR rainfall accumulation over KHGX area. Maps resolution is $5^{\circ} \times 5^{\circ}$ (lat, long), and data from (01/2008).

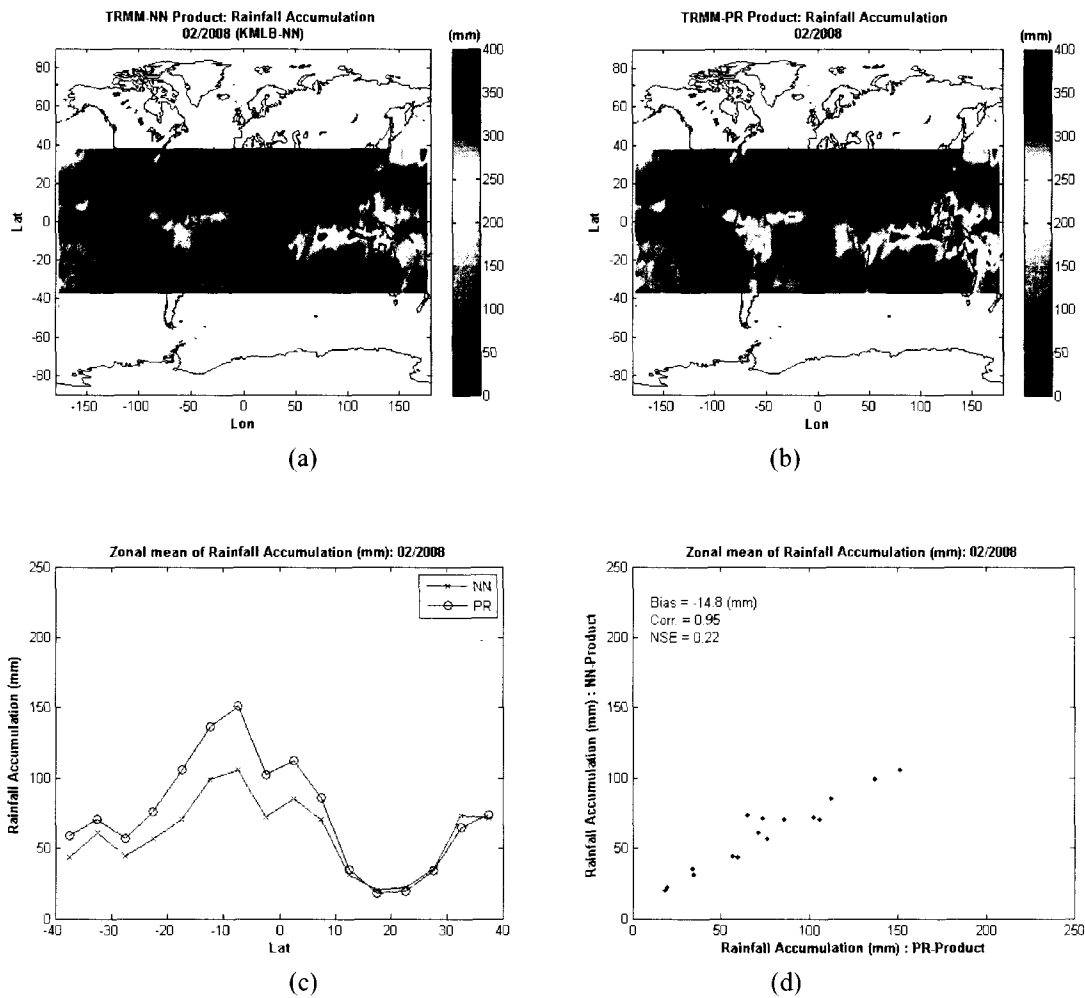


Figure 5.31: (a) Global Rainfall accumulation map generated by the NN (b) Global Rainfall accumulation map generated by TRMM-PR product (c) Zonal mean of the rainfall accumulation. (d) Scatter plot of Zonal mean of the rainfall accumulation. Maps resolution is $5^{\circ} \times 5^{\circ}$ (lat, long), and data from (02/2008).

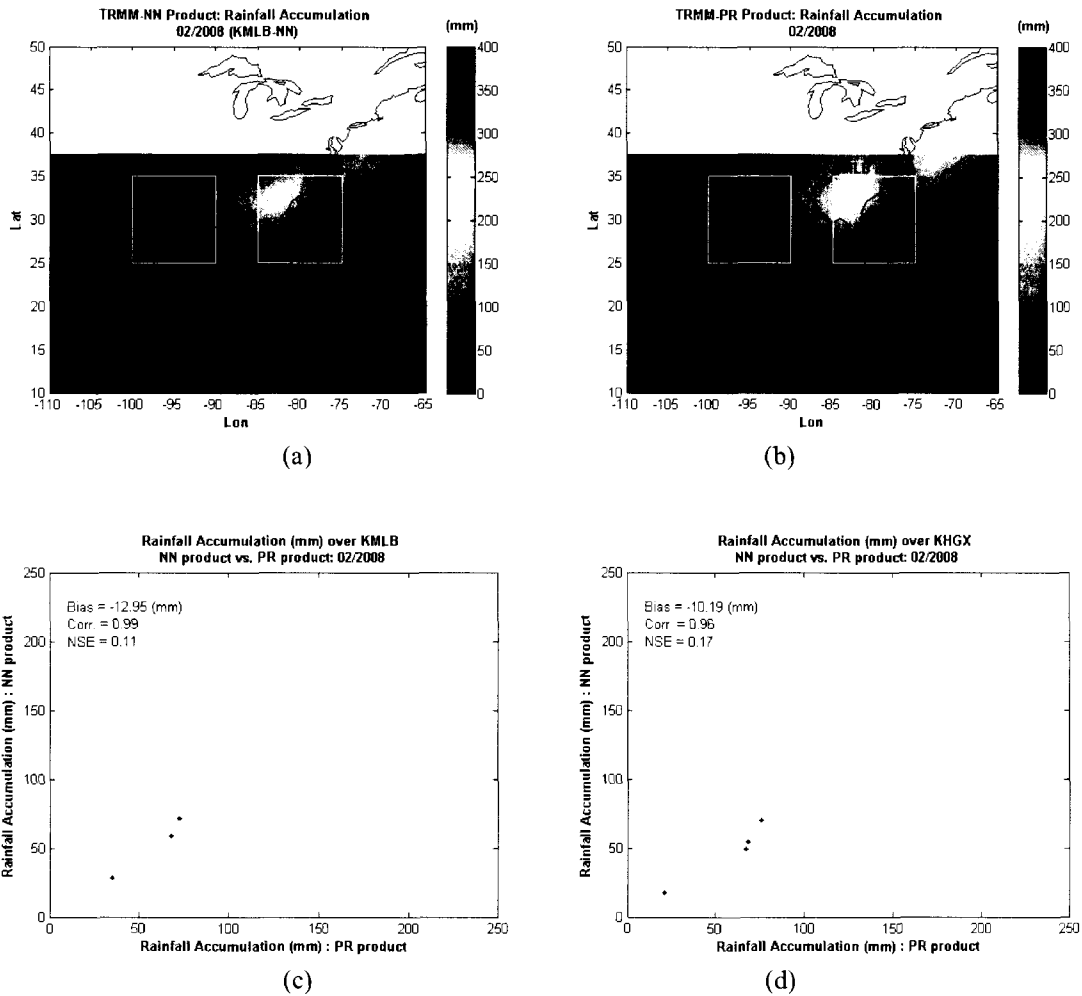


Figure 5.32: (a) Rainfall accumulation map over KMLB and KHGX areas generated by the NN (b) accumulation map over KMLB and KHGX areas generated by TRMM-PR product (c) Scatter plot of NN rainfall accumulation vs. TRMM-PR rainfall accumulation over KMLB area. (d) Scatter plot of NN rainfall accumulation vs. TRMM-PR rainfall accumulation over KHGX area. Maps resolution is $5^{\circ} \times 5^{\circ}$ (lat, long), and data from (02/2008).

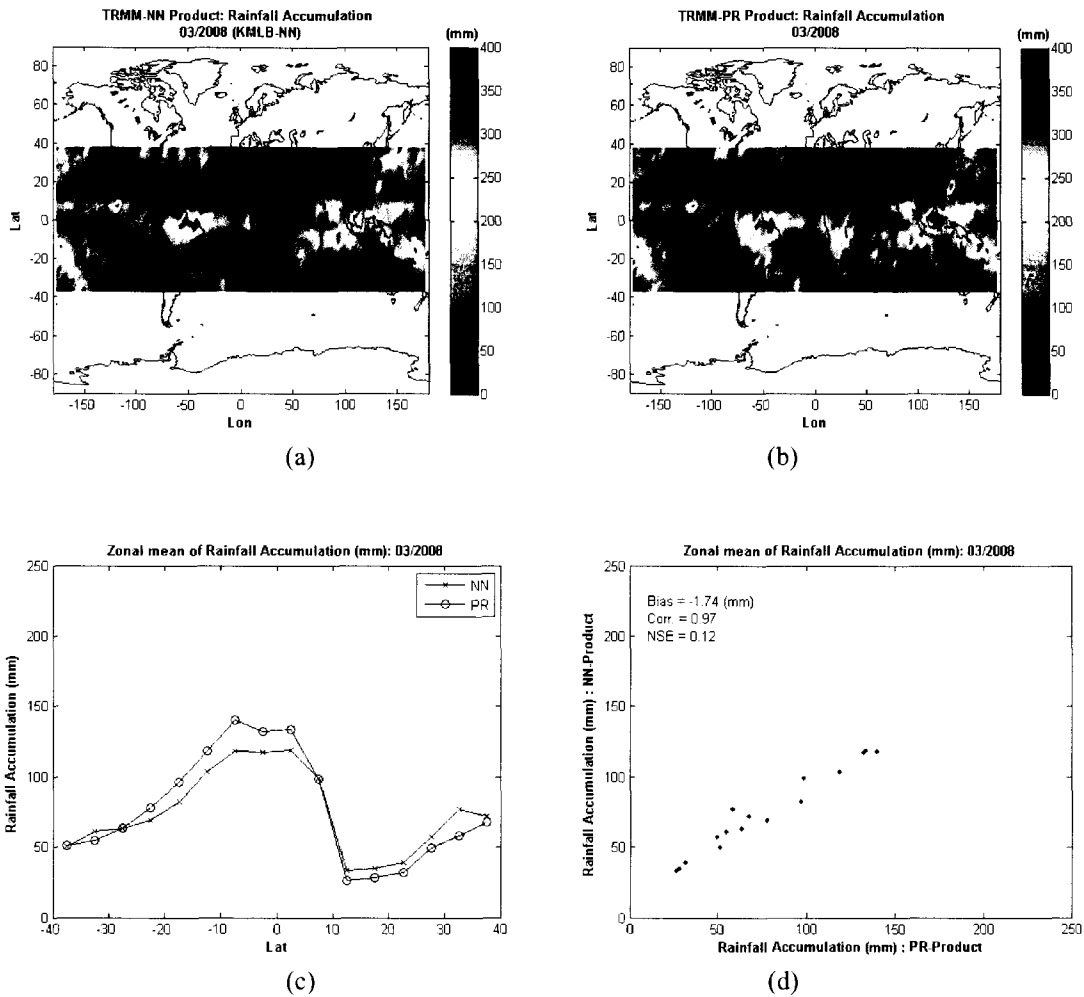


Figure 5.33: (a) Global Rainfall accumulation map generated by the NN (b) Global Rainfall accumulation map generated by TRMM-PR product (c) Zonal mean of the rainfall accumulation. (d) Scatter plot of Zonal mean of the rainfall accumulation. Maps resolution is $5^{\circ} \times 5^{\circ}$ (lat, long), and data from (03/2008).

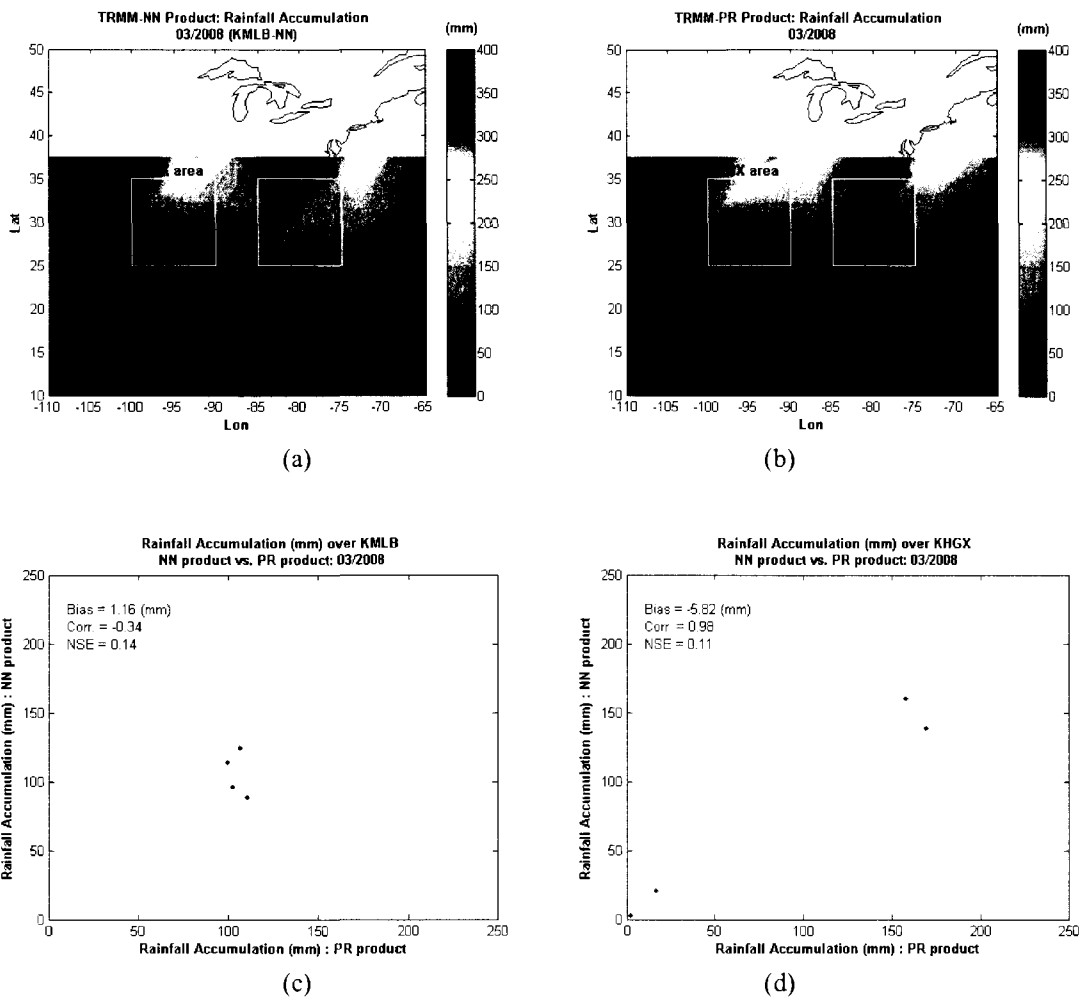


Figure 5.34: (a) Rainfall accumulation map over KMLB and KHGX areas generated by the NN (b) accumulation map over KMLB and KHGX areas generated by TRMM-PR product (c) Scatter plot of NN rainfall accumulation vs. TRMM-PR rainfall accumulation over KMLB area. (d) Scatter plot of NN rainfall accumulation vs. TRMM-PR rainfall accumulation over KHGX area. Maps resolution is $5^{\circ} \times 5^{\circ}$ (lat, long), and data from (03/2008).

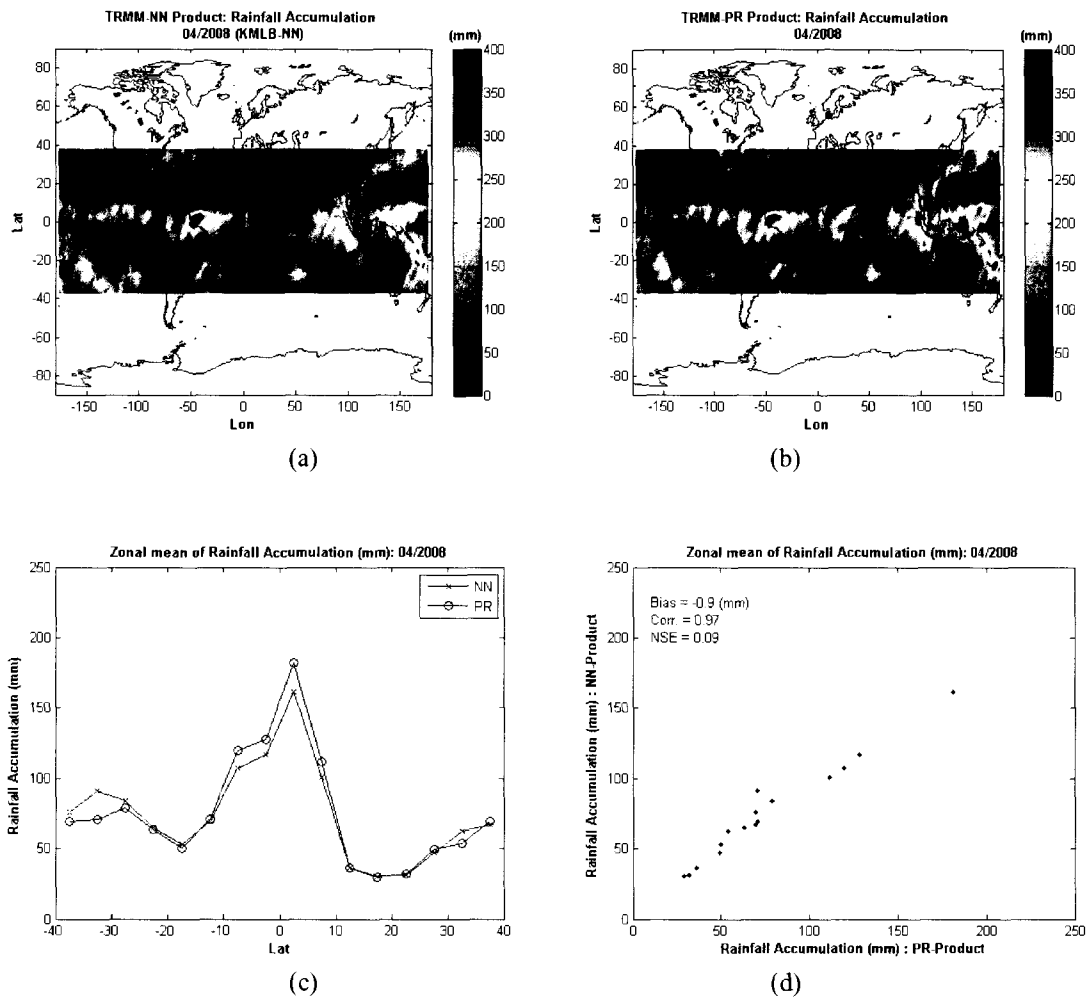


Figure 5.35: (a) Global Rainfall accumulation map generated by the NN (b) Global Rainfall accumulation map generated by TRMM-PR product (c) Zonal mean of the rainfall accumulation. (d) Scatter plot of Zonal mean of the rainfall accumulation. Maps resolution is $5^{\circ} \times 5^{\circ}$ (lat, long), and data from (04/2008).

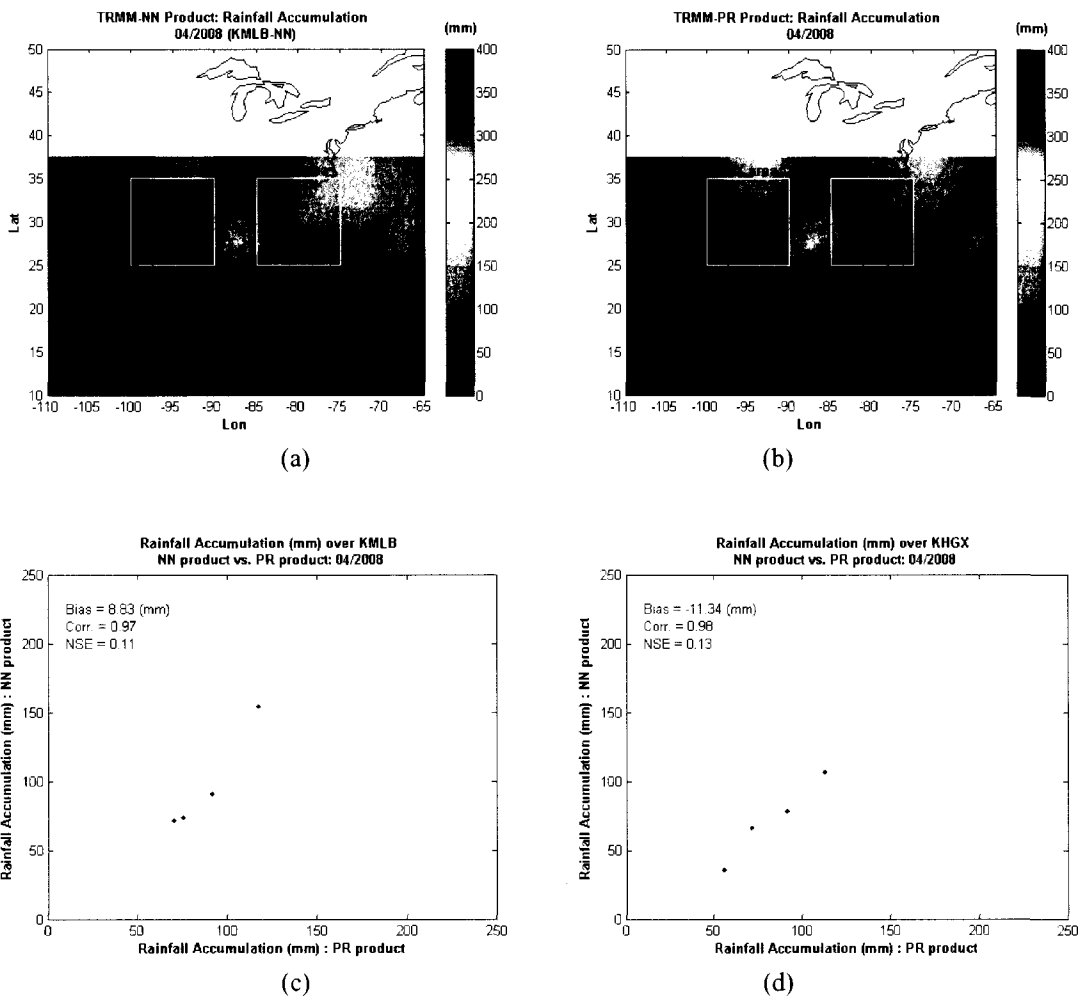


Figure 5.36: (a) Rainfall accumulation map over KMLB and KHGX areas generated by the NN (b) accumulation map over KMLB and KHGX areas generated by TRMM-PR product (c) Scatter plot of NN rainfall accumulation vs. TRMM-PR rainfall accumulation over KMLB area. (d) Scatter plot of NN rainfall accumulation vs. TRMM-PR rainfall accumulation over KHGX area. Maps resolution is $5^{\circ} \times 5^{\circ}$ (lat, long), and data from (04/2008).

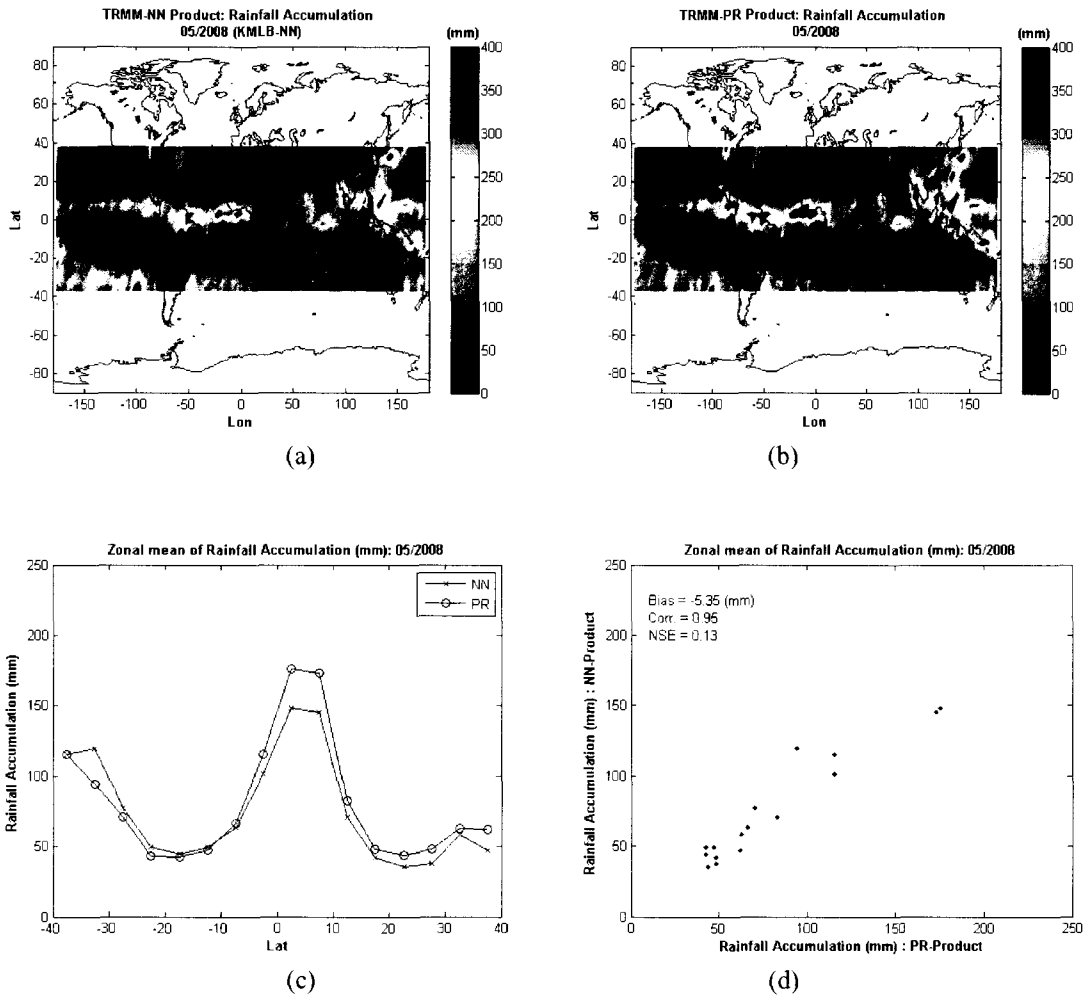


Figure 5.37: (a) Global Rainfall accumulation map generated by the NN (b) Global Rainfall accumulation map generated by TRMM-PR product (c) Zonal mean of the rainfall accumulation. (d) Scatter plot of Zonal mean of the rainfall accumulation. Maps resolution is $5^{\circ} \times 5^{\circ}$ (lat, long), and data from (05/2008).

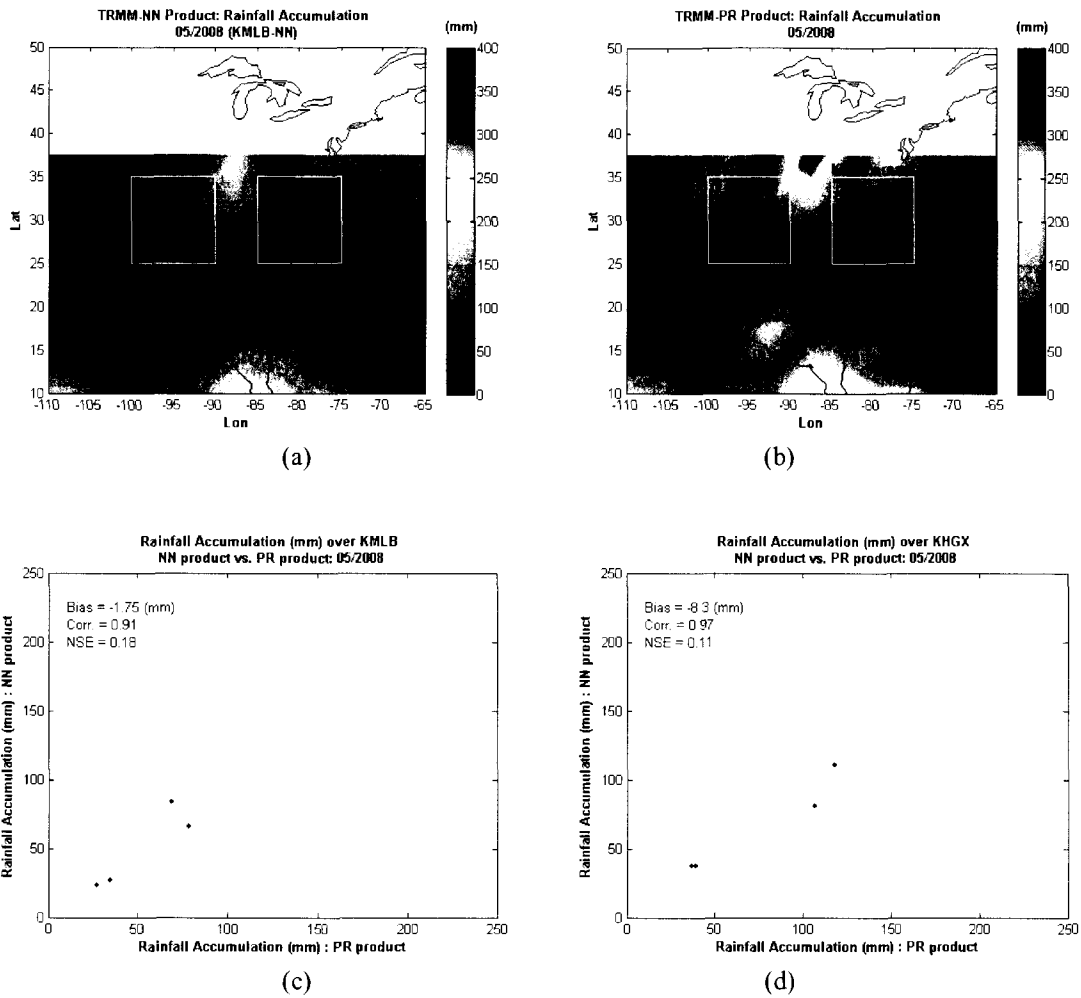


Figure 5.38: (a) Rainfall accumulation map over KMLB and KHGX areas generated by the NN (b) accumulation map over KMLB and KHGX areas generated by TRMM-PR product (c) Scatter plot of NN rainfall accumulation vs. TRMM-PR rainfall accumulation over KMLB area. (d) Scatter plot of NN rainfall accumulation vs. TRMM-PR rainfall accumulation over KHGX area. Maps resolution is $5^{\circ} \times 5^{\circ}$ (lat, long), and data from (05/2008).

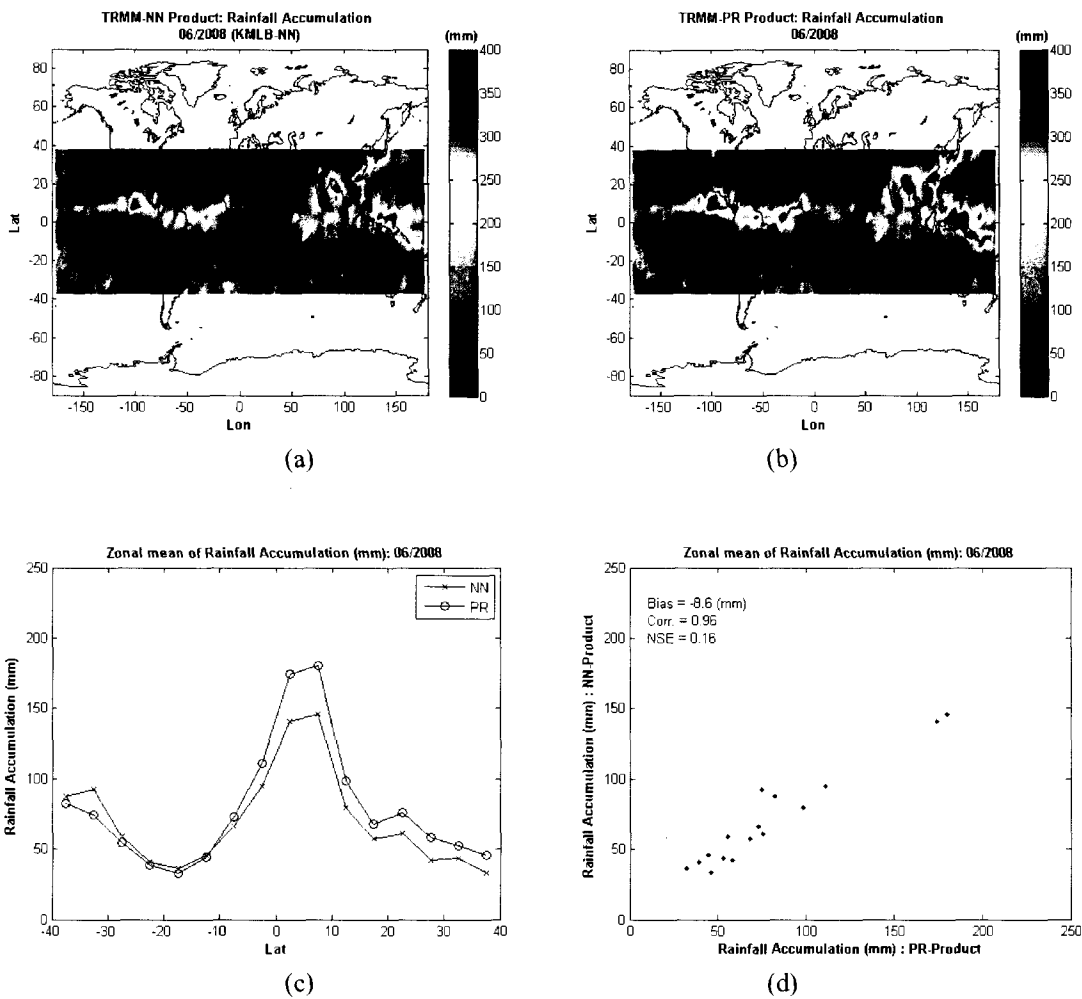


Figure 5.39: (a) Global Rainfall accumulation map generated by the NN (b) Global Rainfall accumulation map generated by TRMM-PR product (c) Zonal mean of the rainfall accumulation. (d) Scatter plot of Zonal mean of the rainfall accumulation. Maps resolution is $5^{\circ} \times 5^{\circ}$ (lat, long), and data from (06/2008).

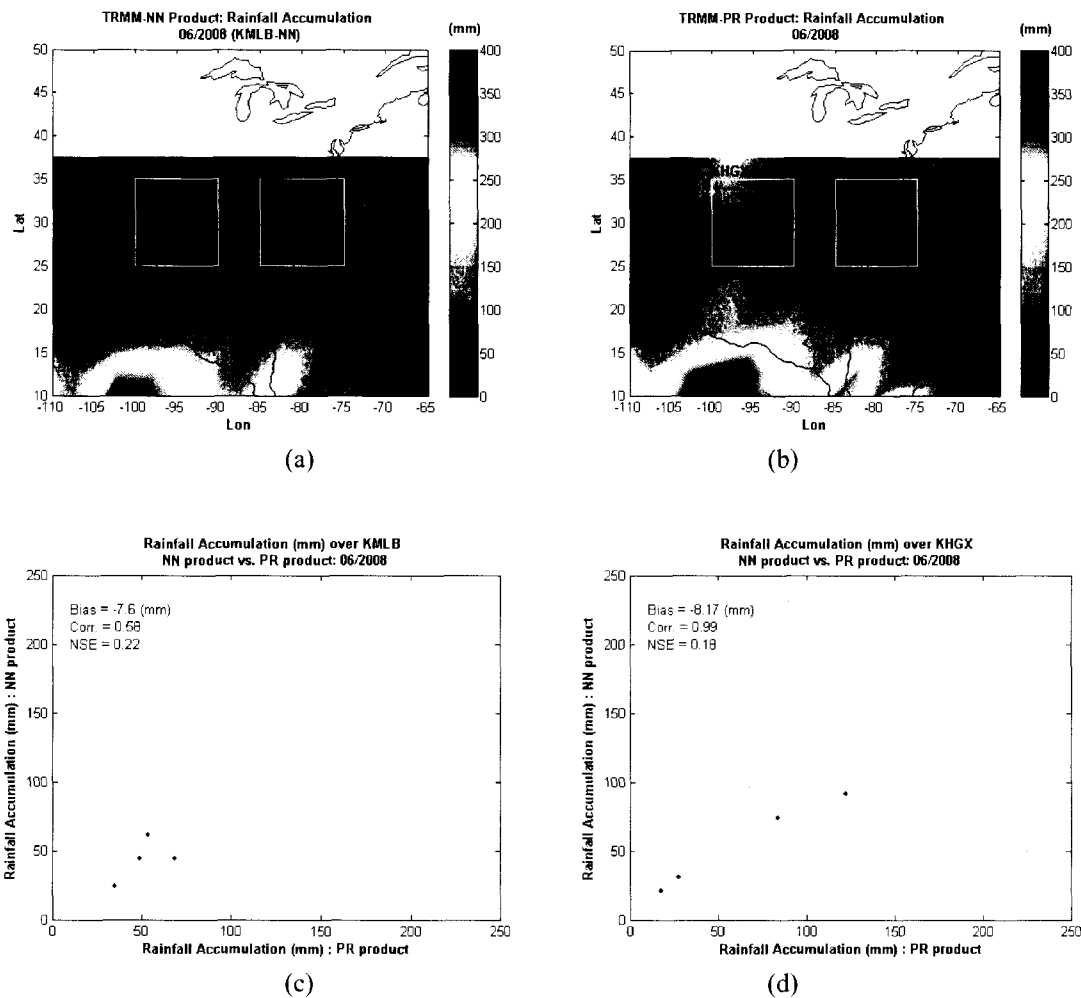


Figure 5.40: (a) Rainfall accumulation map over KMLB and KHGX areas generated by the NN (b) accumulation map over KMLB and KHGX areas generated by TRMM-PR product (c) Scatter plot of NN rainfall accumulation vs. TRMM-PR rainfall accumulation over KMLB area. (d) Scatter plot of NN rainfall accumulation vs. TRMM-PR rainfall accumulation over KHGX area. Maps resolution is $5^{\circ} \times 5^{\circ}$ (lat, long), and data from (06/2008).

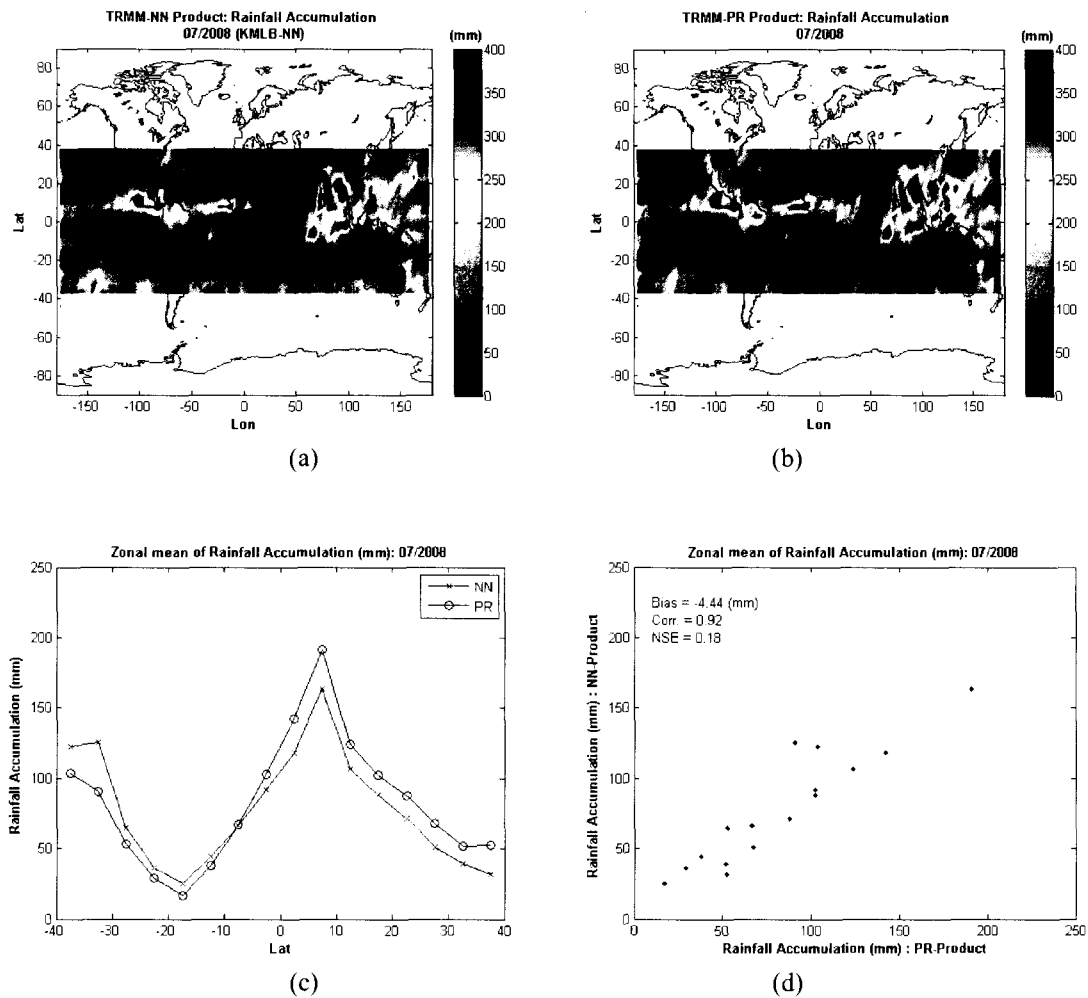


Figure 5.41: (a) Global Rainfall accumulation map generated by the NN (b) Global Rainfall accumulation map generated by TRMM-PR product (c) Zonal mean of the rainfall accumulation. (d) Scatter plot of Zonal mean of the rainfall accumulation. Maps resolution is $5^{\circ} \times 5^{\circ}$ (lat, long), and data from (07/2008).

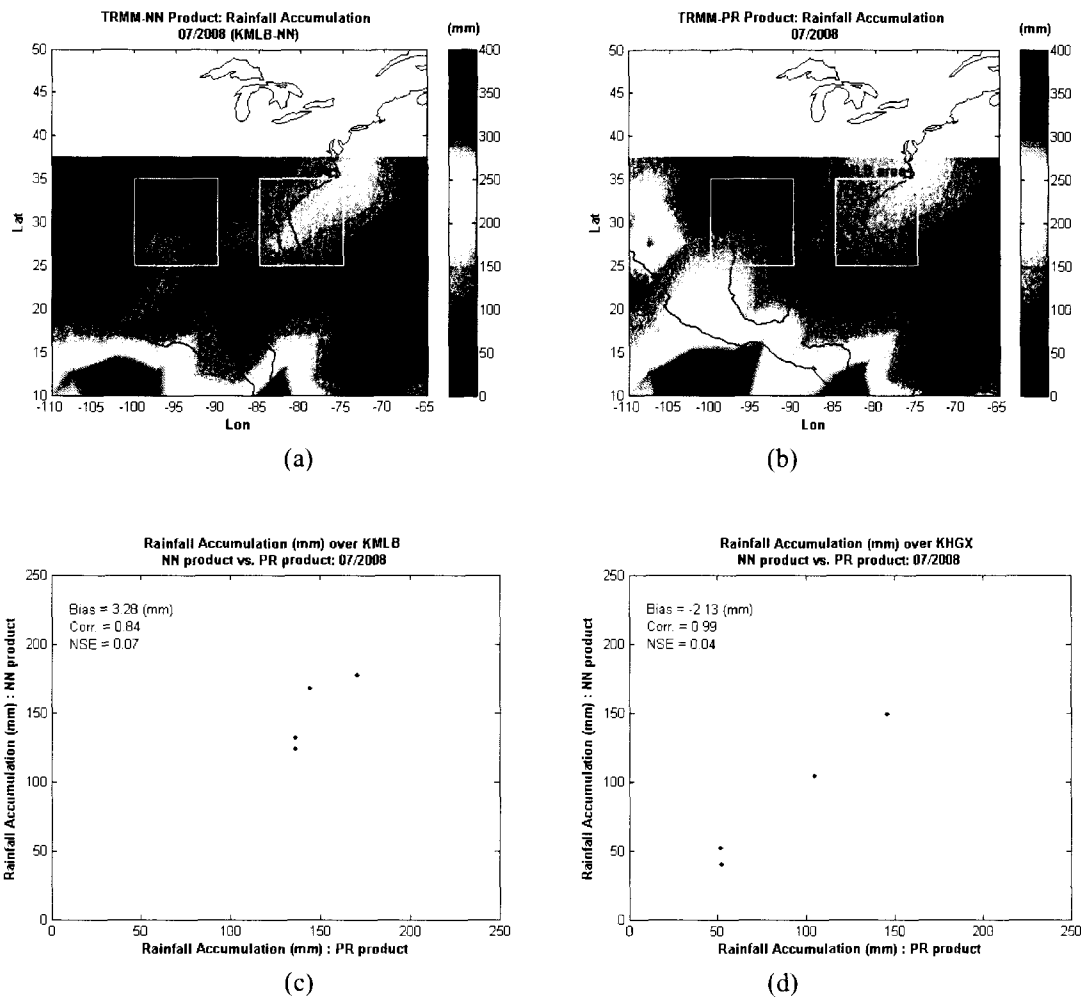


Figure 5.42: (a) Rainfall accumulation map over KMLB and KHGX areas generated by the NN (b) accumulation map over KMLB and KHGX areas generated by TRMM-PR product (c) Scatter plot of NN rainfall accumulation vs. TRMM-PR rainfall accumulation over KMLB area. (d) Scatter plot of NN rainfall accumulation vs. TRMM-PR rainfall accumulation over KHGX area. Maps resolution is $5^{\circ} \times 5^{\circ}$ (lat, long), and data from (07/2008).

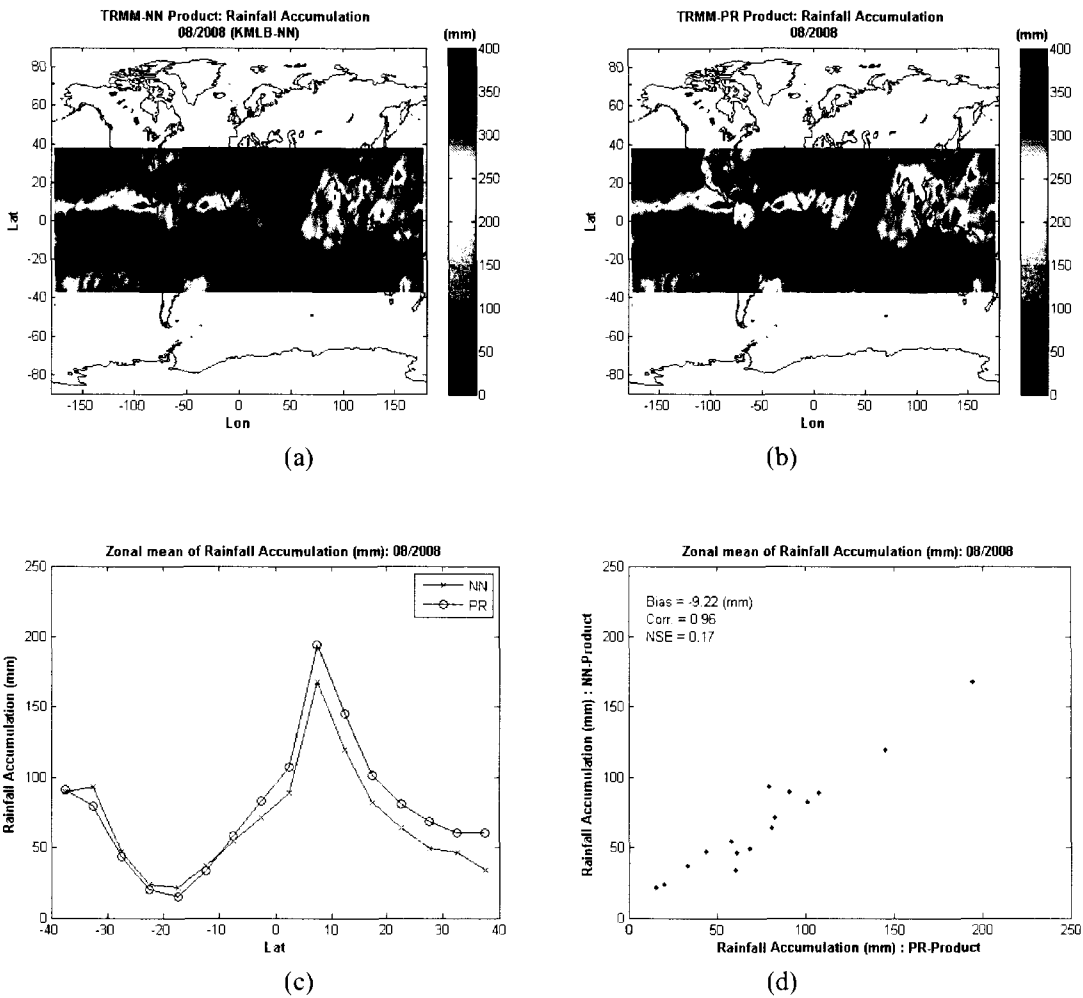


Figure 5.43: (a) Global Rainfall accumulation map generated by the NN (b) Global Rainfall accumulation map generated by TRMM-PR product (c) Zonal mean of the rainfall accumulation. (d) Scatter plot of Zonal mean of the rainfall accumulation. Maps resolution is $5^{\circ} \times 5^{\circ}$ (lat, long), and data from (08/2008).

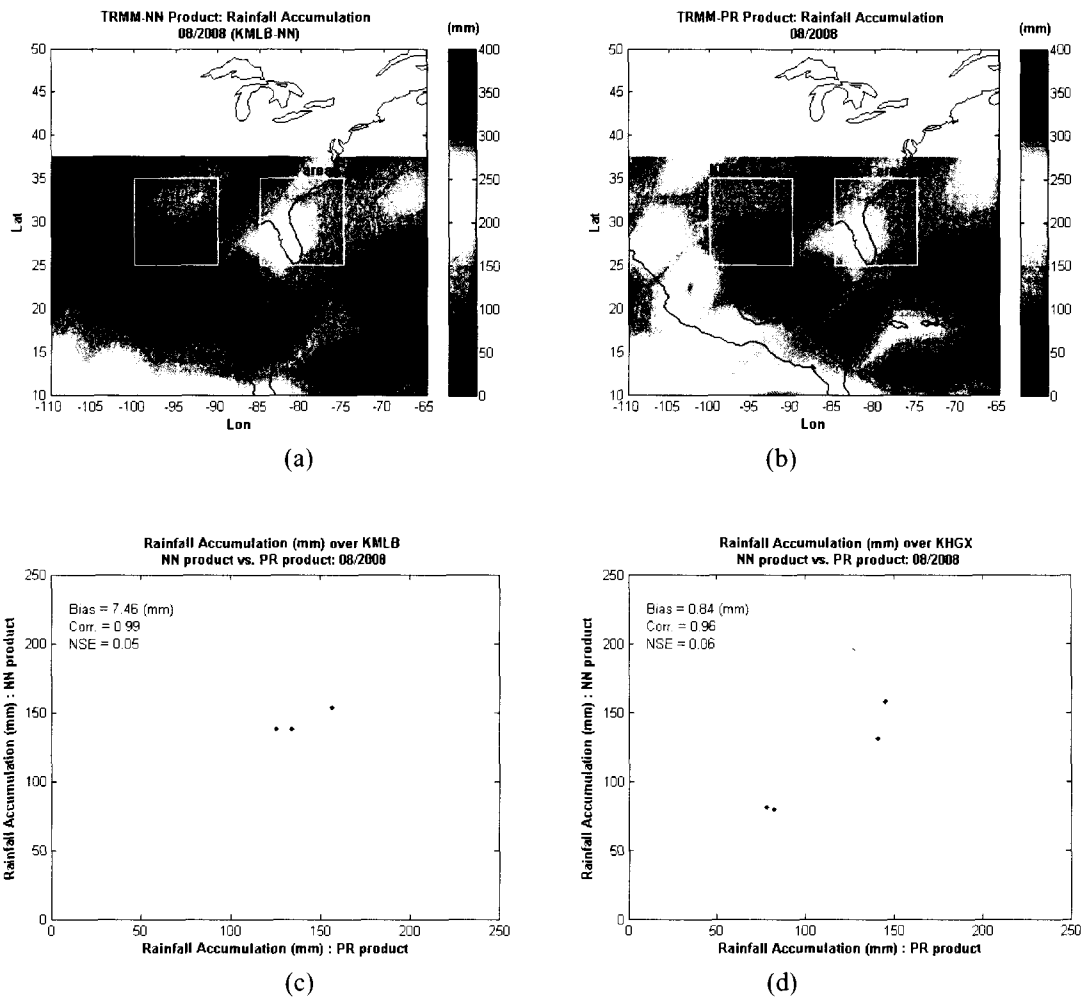


Figure 5.44: (a) Rainfall accumulation map over KMLB and KHGX areas generated by the NN (b) accumulation map over KMLB and KHGX areas generated by TRMM-PR product (c) Scatter plot of NN rainfall accumulation vs. TRMM-PR rainfall accumulation over KMLB area. (d) Scatter plot of NN rainfall accumulation vs. TRMM-PR rainfall accumulation over KHGX area. Maps resolution is $5^{\circ} \times 5^{\circ}$ (lat, long), and data from (08/2008).

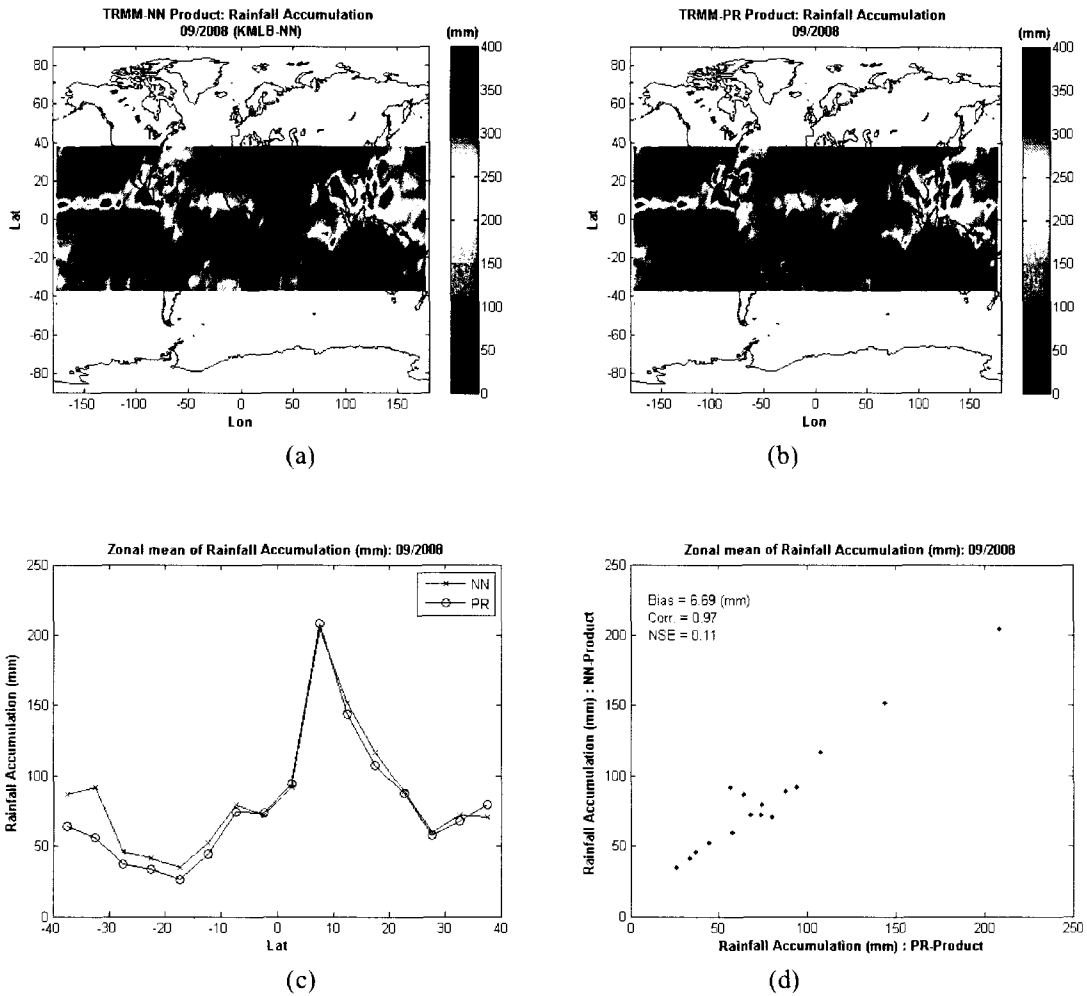


Figure 5.45: (a) Global Rainfall accumulation map generated by the NN (b) Global Rainfall accumulation map generated by TRMM-PR product (c) Zonal mean of the rainfall accumulation. (d) Scatter plot of Zonal mean of the rainfall accumulation. Maps resolution is $5^{\circ} \times 5^{\circ}$ (lat, long), and data from (09/2008).

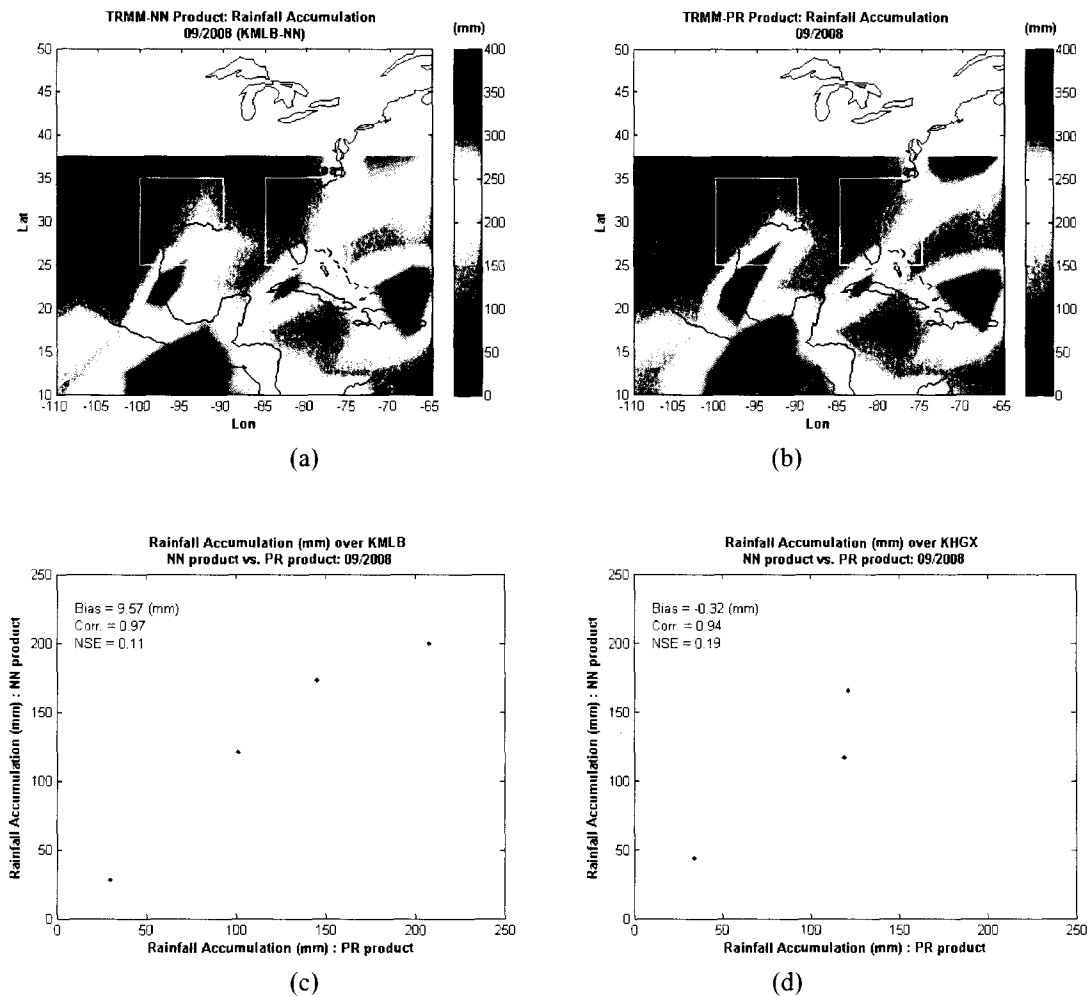


Figure 5.46: (a) Rainfall accumulation map over KMLB and KHGX areas generated by the NN (b) accumulation map over KMLB and KHGX areas generated by TRMM-PR product (c) Scatter plot of NN rainfall accumulation vs. TRMM-PR rainfall accumulation over KMLB area. (d) Scatter plot of NN rainfall accumulation vs. TRMM-PR rainfall accumulation over KHGX area. Maps resolution is 5°x5° (lat, long), and data from (09/2008).

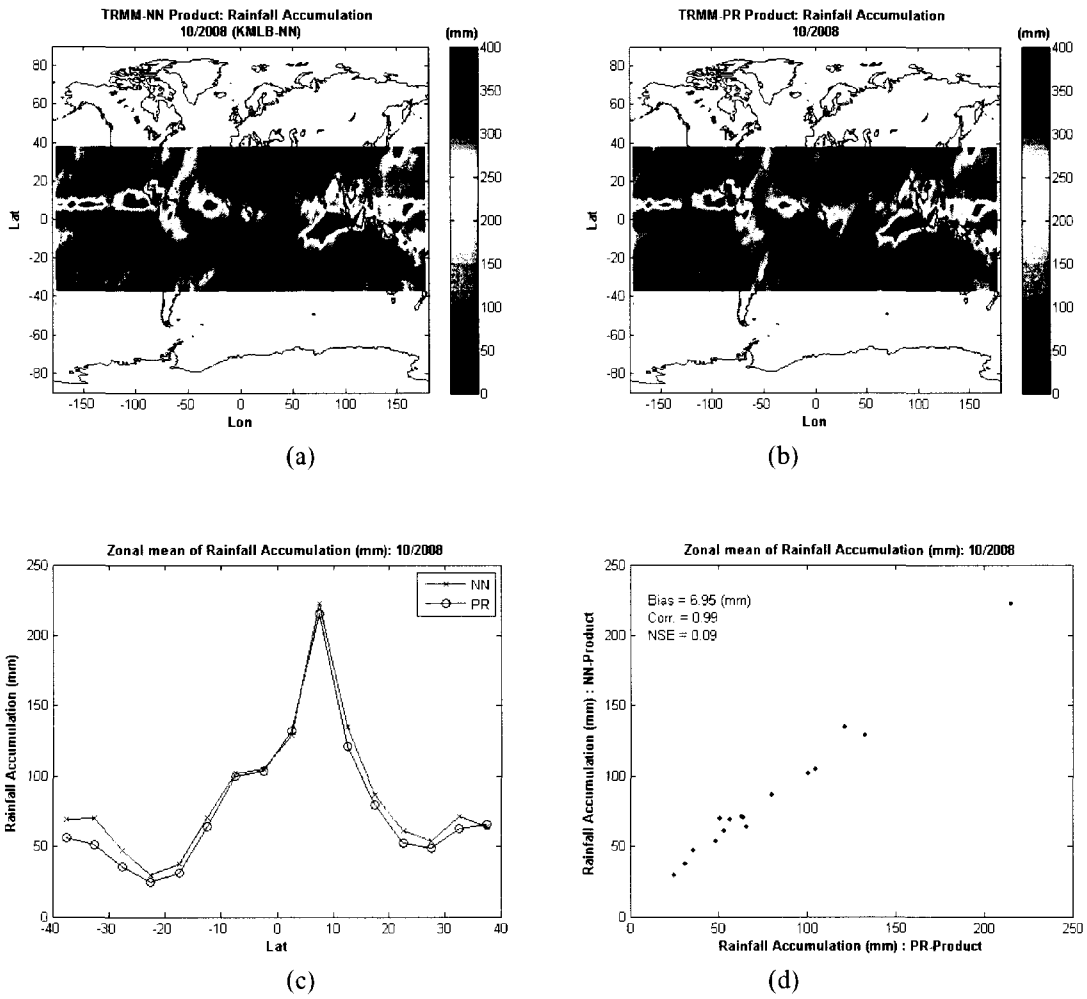


Figure 5.47: (a) Global Rainfall accumulation map generated by the NN (b) Global Rainfall accumulation map generated by TRMM-PR product (c) Zonal mean of the rainfall accumulation. (d) Scatter plot of Zonal mean of the rainfall accumulation. Maps resolution is $5^{\circ} \times 5^{\circ}$ (lat, long), and data from (10/2008).

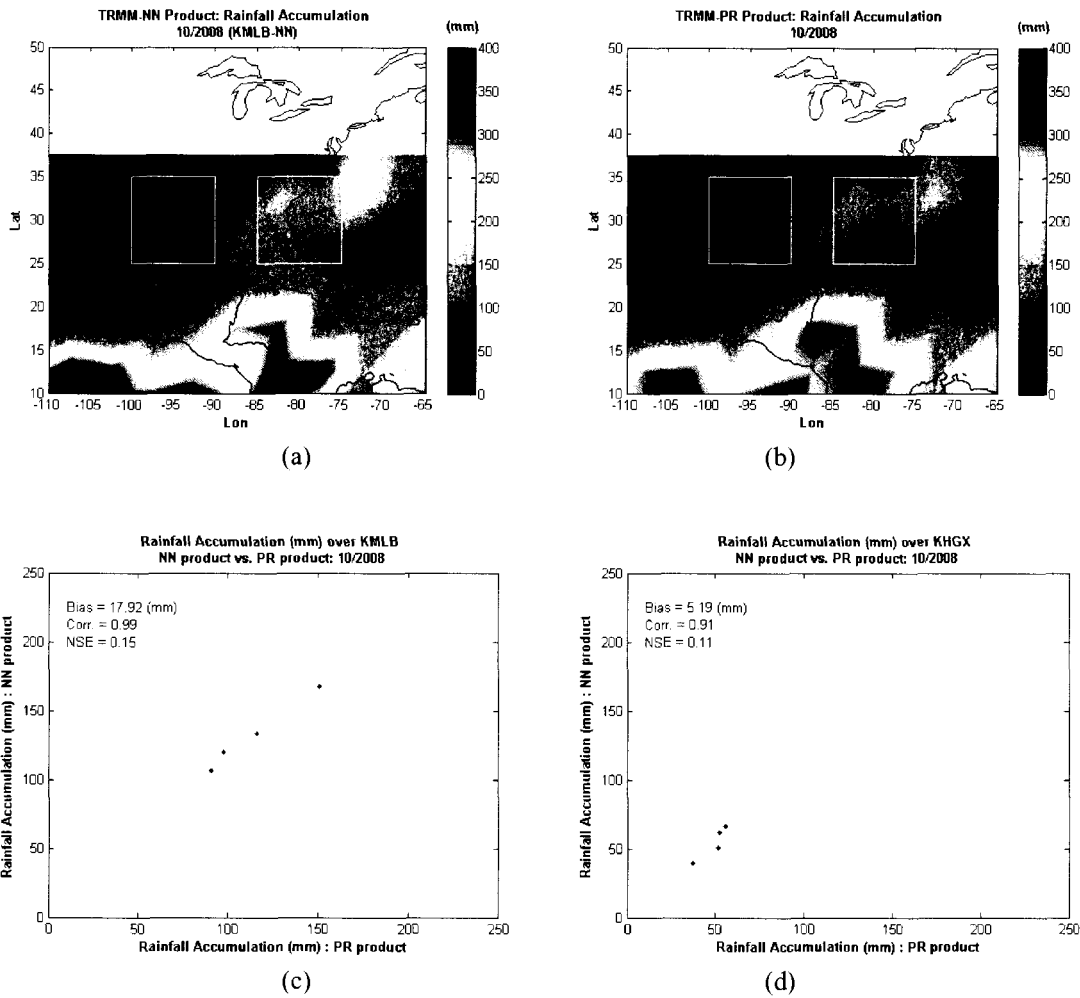


Figure 5.48: (a) Rainfall accumulation map over KMLB and KHGX areas generated by the NN (b) accumulation map over KMLB and KHGX areas generated by TRMM-PR product (c) Scatter plot of NN rainfall accumulation vs. TRMM-PR rainfall accumulation over KMLB area. (d) Scatter plot of NN rainfall accumulation vs. TRMM-PR rainfall accumulation over KHGX area. Maps resolution is $5^{\circ} \times 5^{\circ}$ (lat, long), and data from (10/2008).

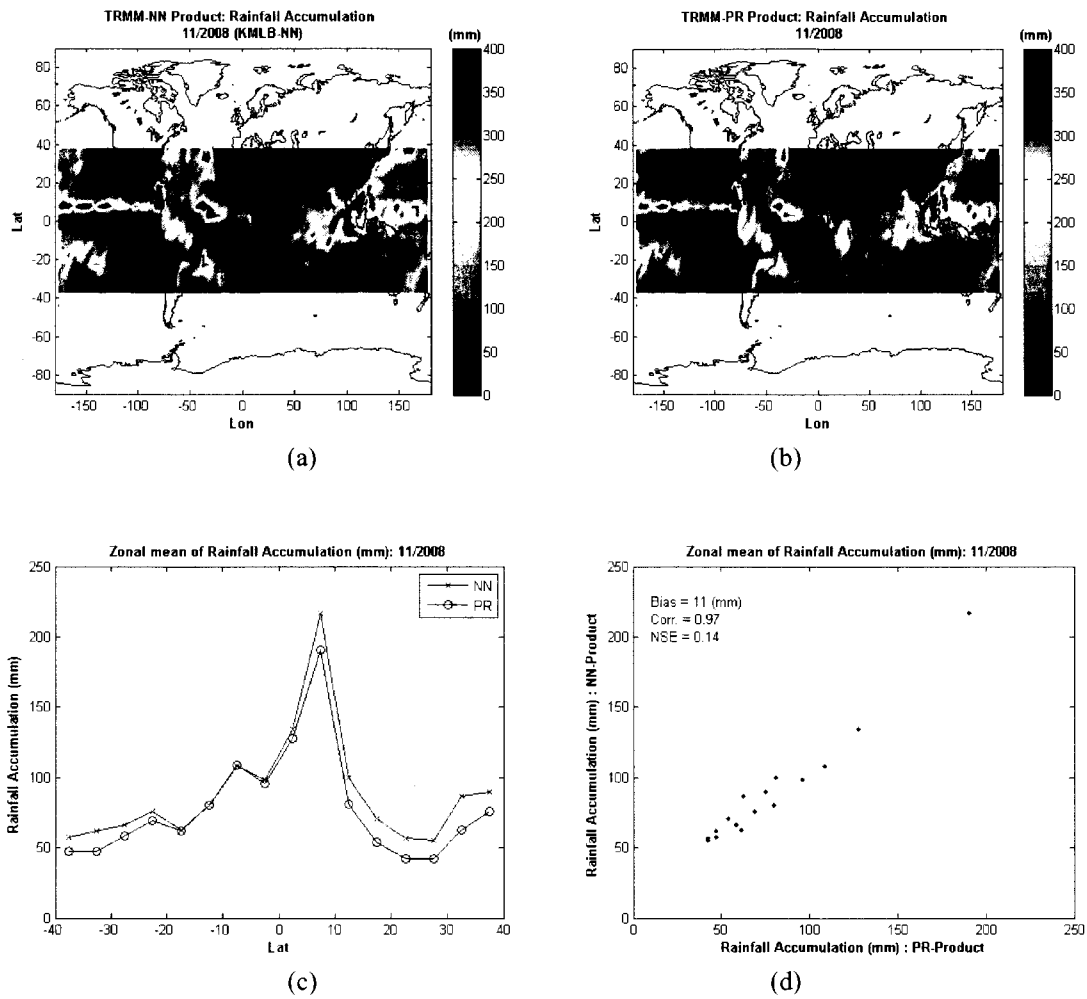


Figure 5.49: (a) Global Rainfall accumulation map generated by the NN (b) Global Rainfall accumulation map generated by TRMM-PR product (c) Zonal mean of the rainfall accumulation. (d) Scatter plot of Zonal mean of the rainfall accumulation. Maps resolution is $5^{\circ} \times 5^{\circ}$ (lat, long), and data from (11/2008).

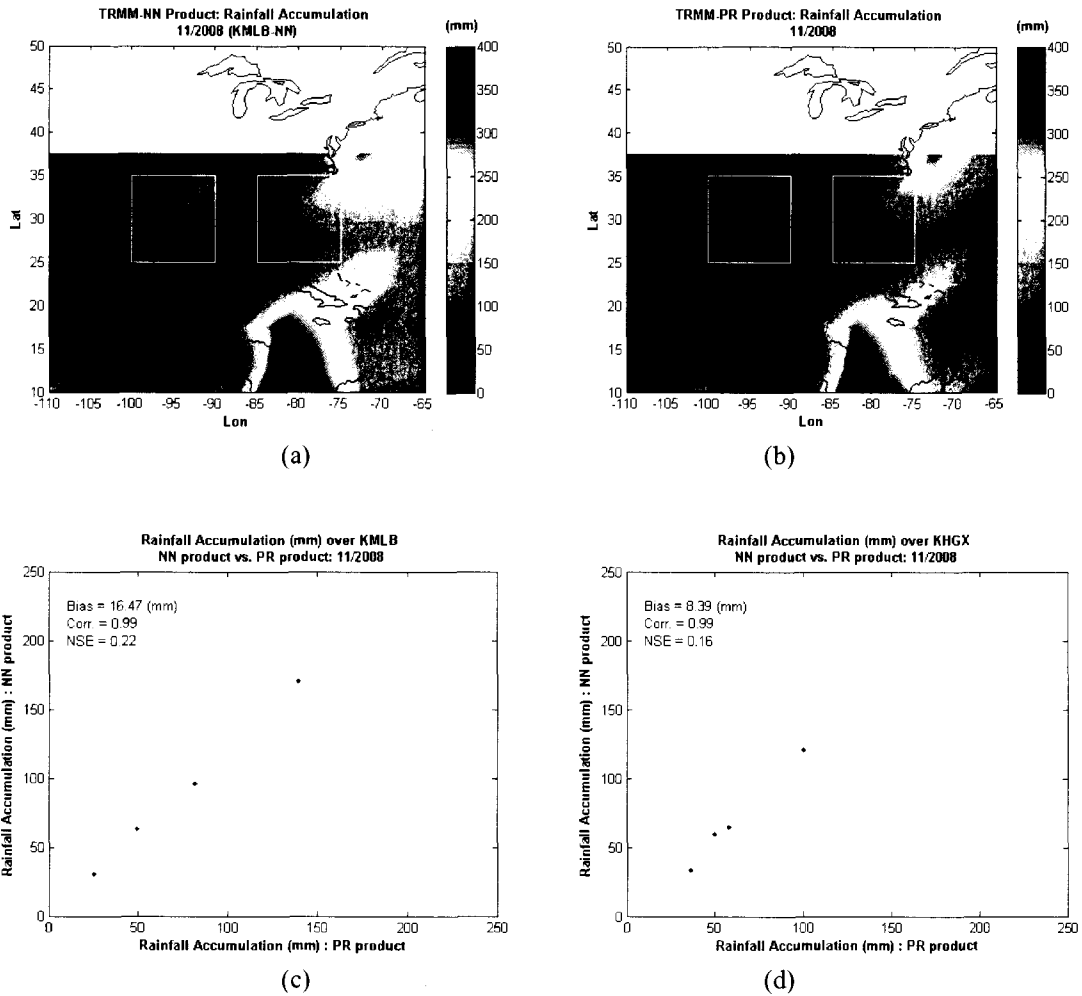


Figure 5.50: (a) Rainfall accumulation map over KMLB and KHGX areas generated by the NN (b) accumulation map over KMLB and KHGX areas generated by TRMM-PR product (c) Scatter plot of NN rainfall accumulation vs. TRMM-PR rainfall accumulation over KMLB area. (d) Scatter plot of NN rainfall accumulation vs. TRMM-PR rainfall accumulation over KHGX area. Maps resolution is $5^{\circ} \times 5^{\circ}$ (lat, long), and data from (11/2008).

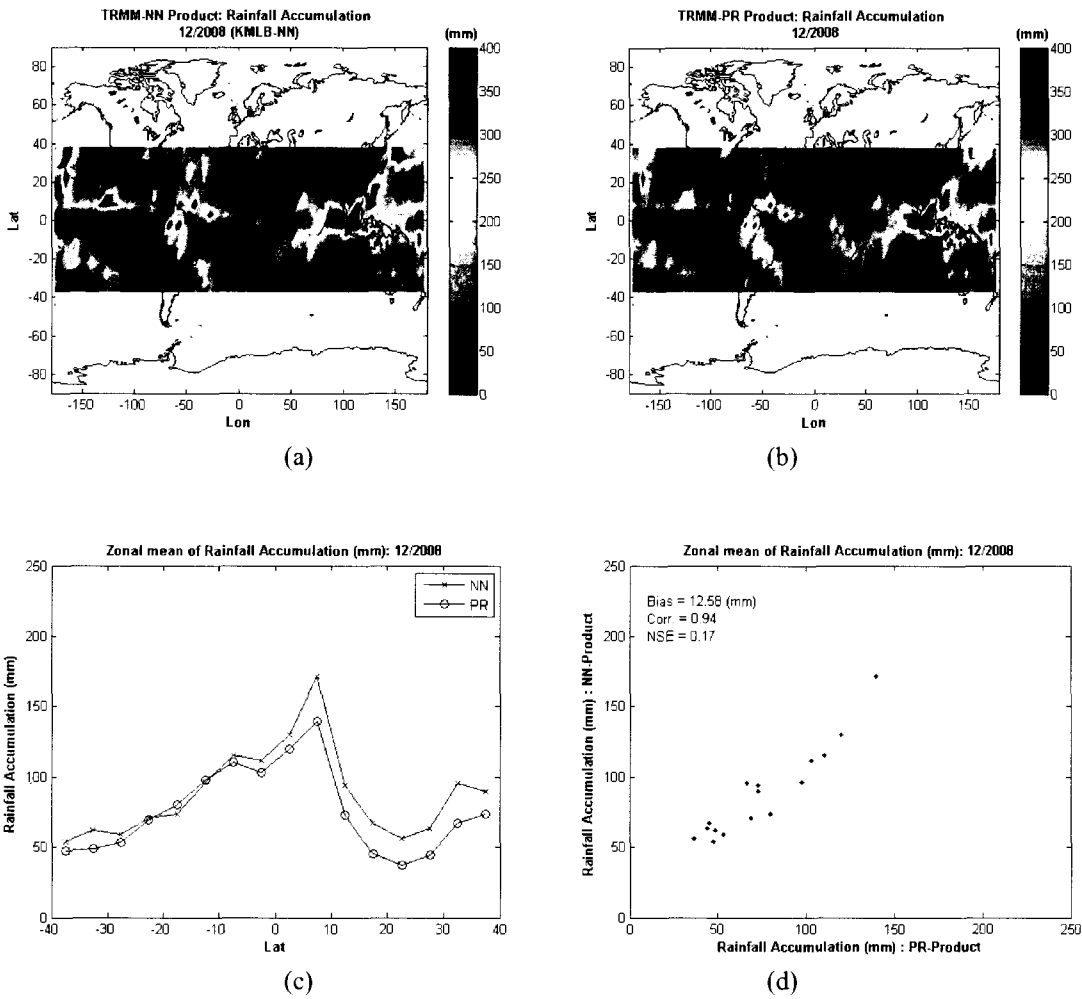


Figure 5.51: (a) Global Rainfall accumulation map generated by the NN (b) Global Rainfall accumulation map generated by TRMM-PR product (c) Zonal mean of the rainfall accumulation. (d) Scatter plot of Zonal mean of the rainfall accumulation. Maps resolution is $5^{\circ} \times 5^{\circ}$ (lat, long), and data from (12/2008).

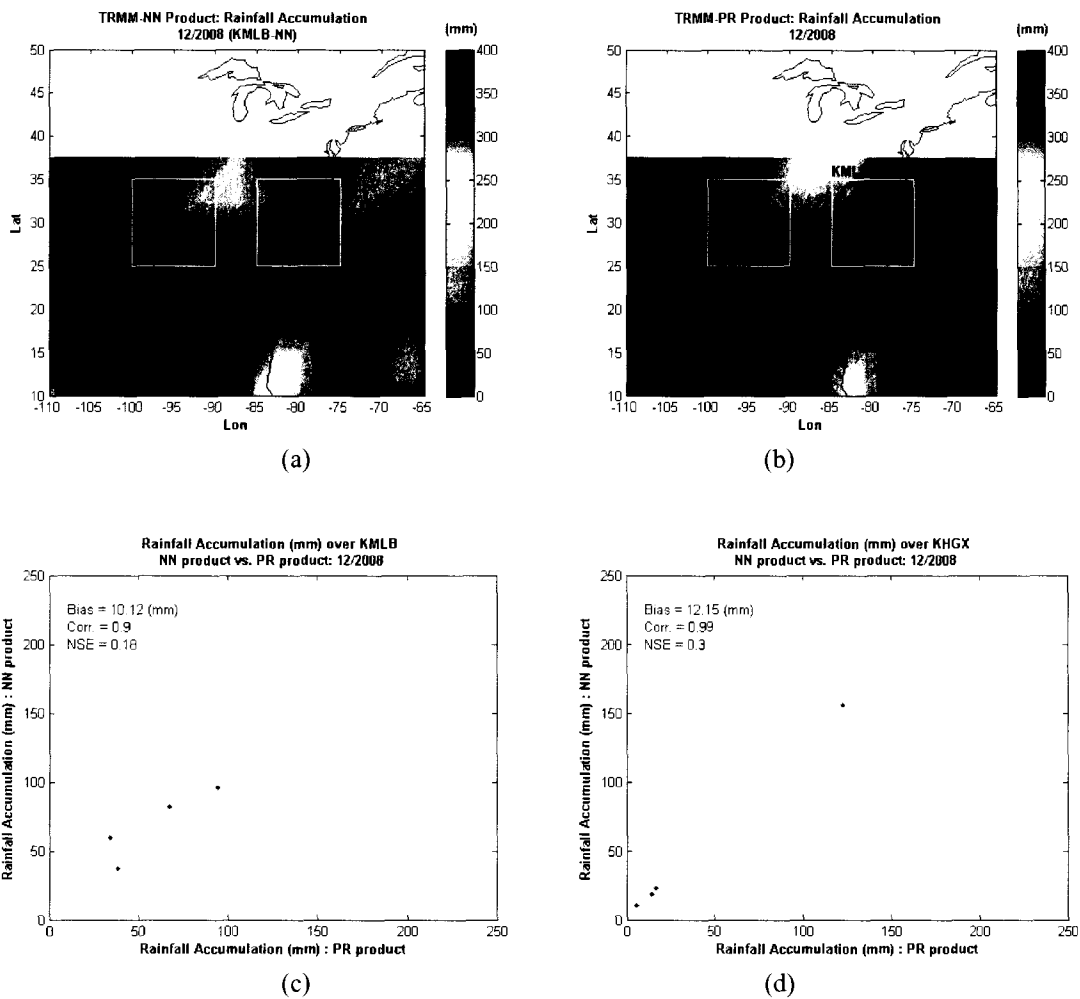


Figure 5.52: (a) Rainfall accumulation map over KMLB and KHGX areas generated by the NN (b) accumulation map over KMLB and KHGX areas generated by TRMM-PR product (c) Scatter plot of NN rainfall accumulation vs. TRMM-PR rainfall accumulation over KMLB area. (d) Scatter plot of NN rainfall accumulation vs. TRMM-PR rainfall accumulation over KHGX area. Maps resolution is $5^{\circ} \times 5^{\circ}$ (lat, long), and data from (12/2008).

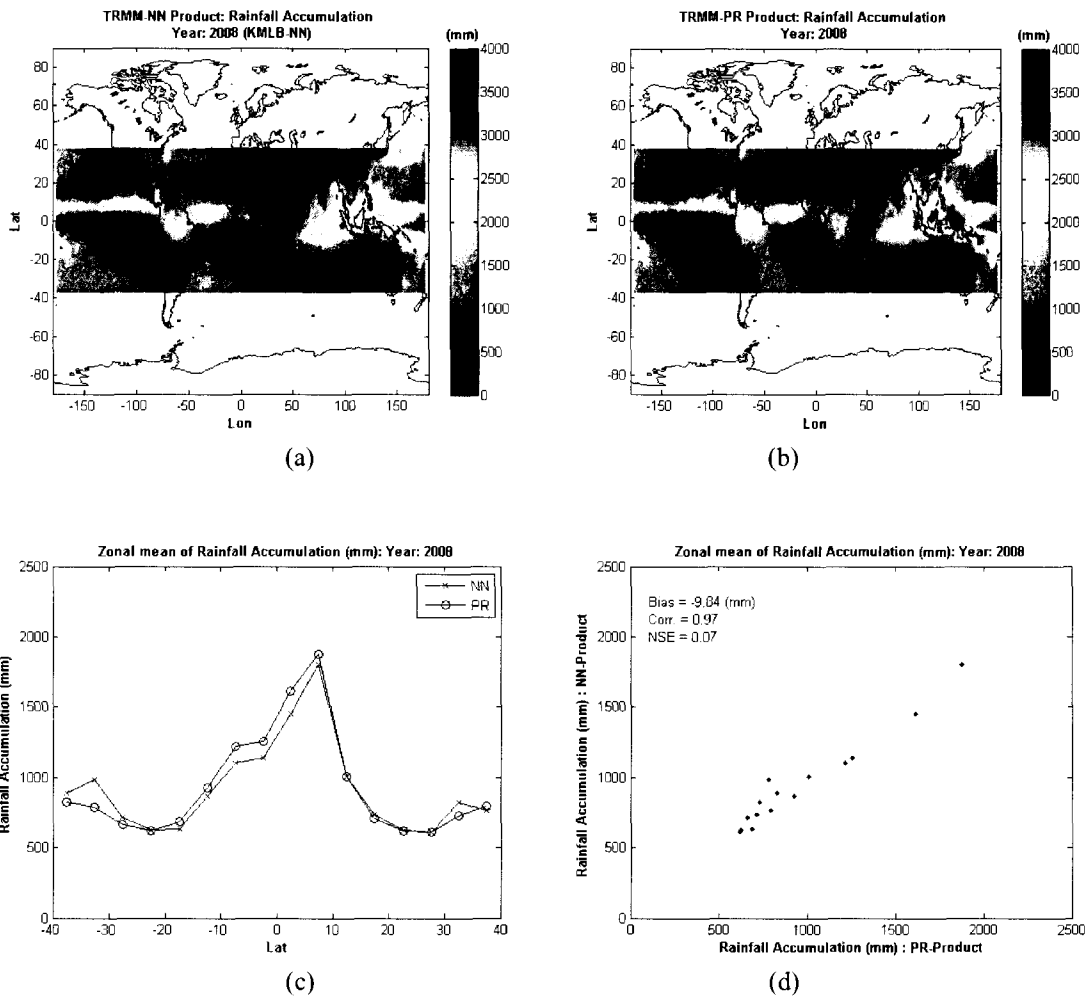


Figure 5.53: (a) Global Rainfall accumulation map generated by the NN (b) Global Rainfall accumulation map generated by TRMM-PR product (c) Zonal mean of the rainfall accumulation. (d) Scatter plot of Zonal mean of the rainfall accumulation. Maps resolution is $5^{\circ} \times 5^{\circ}$ (lat, long), and data from (Year 2008).

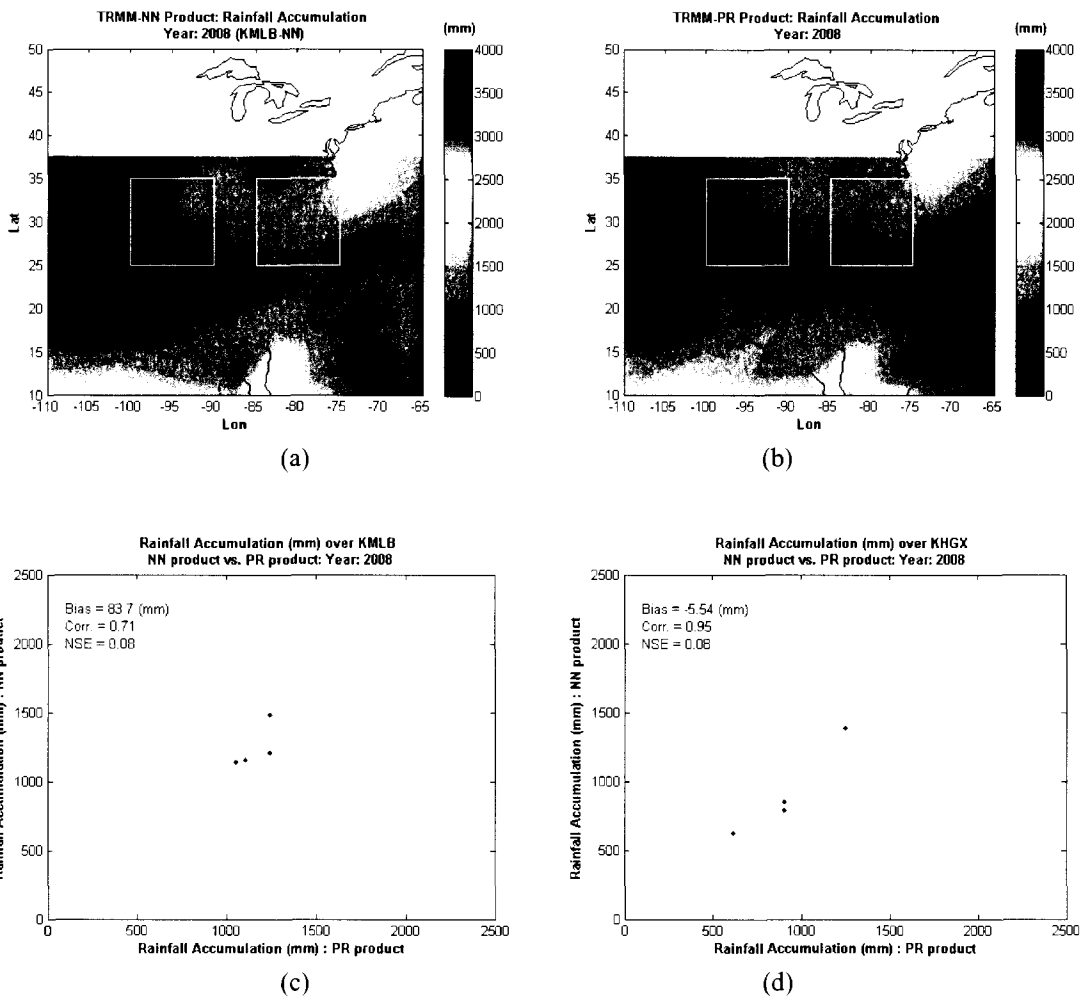


Figure 5.54: (a) Rainfall accumulation map over KMLB and KHGX areas generated by the NN (b) accumulation map over KMLB and KHGX areas generated by TRMM-PR product (c) Scatter plot of NN rainfall accumulation vs. TRMM-PR rainfall accumulation over KMLB area. (d) Scatter plot of NN rainfall accumulation vs. TRMM-PR rainfall accumulation over KHGX area. Maps resolution is $5^{\circ} \times 5^{\circ}$ (lat, long), and data from (Year 2008).

CHAPTER 6

SUMMARY AND FUTURE WORK

6.1 SUMMARY

The main goal of this research is to estimate rain rate from ground radar and spaceborne radar measurements using neural networks. Radial basis function neural network was the main neural network architecture applied to do the estimation.

Two approaches were used to do rainfall estimation. The first approach was based on a neural network that is designed based on rain gauges and ground radar measurements. Three ground radars were used in this regard: KMLB NEXRAD, KWAJ NEXRAD radar and KHGX NEXRAD radar. Five rain gauge networks were taken around these three radars; KMLB radar has three rain gauge networks: KSC, SFL, STJ, KWAJ radar has only one rain gauge network named after the radar (KWAJ), and KHGX radar also has one rain gauge network: HAR.

The second approach was based on a hybrid neural network technique where a two-stage neural network was designed. The first network was based on rain gauges and ground radar measurements. This network was used to map the relation between the ground radar reflectivity factor and the rain gauges as first stage to a second stage of the hybrid network where TRMM-PR measurements aligned with the ground radar measurements that were used in the first stage were used to train another network with

rainfall estimated based on those ground radar measurements by the first network as a target.

The following points summarize the activities that have been completed in this dissertation. This section groups the tasks according to their major goals:

- **Estimating Rainfall from ground radar measurements using neural networks:**
 - A neural network technique was used to estimate rainfall from ground radar measurements. The effect of the radar vertical profile height on rainfall estimation was examined. It was found that measurements up to 4km were giving better performance in most of the cases.
 - The neural network performance was compared with the Z-R relation and with a statistical approach (Best-Fit) against the rain gauge. It was found that the neural network performance was better in most of the cases. The Z-R relation was underestimating the rain rate and was unable to capture the storm variations in most of the cases.
 - The designed neural network was validated using different datasets from different years and different locations. It was found that the network was generalized and was able to estimate rainfall from datasets have never seen and from other locations.
 - The “Principal Component Analysis” (PCA) concept was used as a trial to improve the performance of estimation. Two principal components were used to train the neural network. It was shown that significant improvements were achieved in terms of statistical metrics (FracBias, correlation, NSE, and

FRMSE) and in terms of reducing the training time and the network complexity.

- Bayesian Neural network (BN) was used as another architecture to do rainfall estimation; this network proves its capability in this regard with the advantage of reducing the network complexity significantly at the expense of increasing the training time.
 - Ensemble average neural network technique was used to improve rainfall estimation; the ensemble was based on RBF neural network, and BN neural network. This technique can add a significant improvement to the estimation by reducing the MSE of the ensembled output by a factor up to the number of the networks in the ensemble. This reduction is conditioned by how small the bias of the individual networks is, and how much mutually independent the errors of the individual networks are.
 - Validation the performance of the neural network against TRMM GV estimate at KWAJ site. The network shows competitive performance that can be better than the GV performance.
- **Estimating Rainfall from satellite radar measurements (TRMM-PR) using neural networks:**
 - A novel hybrid neural network was designed to estimate rainfall from TRMM-PR measurements. This hybrid network has two stages, the first one is a neural network designed based on ground radar measurements and rain

gauges. The second network is designed based on TRMM-PR radar measurements and rainfall estimated by the first network.

- It was shown that the performance of this hybrid neural technique is better than the performance of TRMM-PR rain rate standard product when both were compared with rain gauges; TRMM-PR rain rate standard product tends to underestimate the rain gauge.
 - When comparing the performance of the two stages in this hybrid method to each other, it can be shown that both have close performance compared to rain gauge. This indicates that the first neural network maps to the second neural network the relation between the radar reflectivity factor and the rain gauges. The mapping was done through aligning the ground radar measurements with TRMM-PR radar measurements
 - The designed neural network was validated using different datasets from different years and different locations. It was found that the network was generalized and was able to estimate rainfall from datasets that have never seen or even from other locations.
- **Rainfall maps generation using radar/satellite measurements and neural network estimators.**
 - Instantaneous rainfall maps were generated by applying ground radars measurements and TRMM-PR measurements. The ground radars data was applied to the network that was built based on ground radar measurements,

while TRMM-PR data was applied to the network that was built based on TRMM-PR measurements.

- The generated instantaneous rainfall maps from both networks were very similar to each other, and both were giving representation of the storm better than TRMM product.
- To validate the instantaneous rainfall maps generation at each site, similar maps were generated using the neural network that was built based on the other site's data. It was shown that these maps were similar to those maps generated using the same site's neural network and were giving similar performance.
- To do more validation, we applied the designed neural networks at KMLB and KHGX to generate instantaneous rainfall maps by testing other NEXRAD radars data. Two radars were chosen: KEVX (Eglin AFB, FL), and KSHV (Shreveport, LA). It was shown that the designed neural networks are generalized and can be applied to estimate rainfall at other geographical regions beyond the ground validation sites.
- Global monthly rainfall maps were generated and compared to TRMM standard generated rainfall maps, and the hybrid neural network shows the possibility to produce global rainfall maps.

6.2 FUTURE WORK

Several suggested topics to be done after this dissertation. They are mostly about performance improvement and validation, and can be summarized as follows:

- **Performance improvement**

- The performance of the estimation can be improved by building a “Rain/No Rain” detection neural network running simultaneously with the estimation network.
- Including other radar measurements like the path integrated attenuation (PIA).
- The global rainfall accumulation maps can be generated with better performance if we use neural networks designed by data from different meteorological areas, rather than using one regime.
- The hybrid technique can be improved in the next mission (GPM) where measurements from Dual-Precipitation Radar (DPR) will be available.

- **Performance validation**

Different ideas are suggested to do more validation of the designed neural networks:

- Validating this method based on other ground validation radars in other climatological areas.
- Validating this method using the Next Generation Multisensor Quantitative Precipitation Estimates QPE (Q2). The Q2 project is a joint initiative by the National Oceanic and Atmospheric Administration, and the National Severe Storms Laboratory NSSL to improve river forecasts, flood watches and

warnings as well as to enhance various hydrometeorological services for numerous users and customers. At the time of this dissertation, the Q2 data estimates were considered preliminary and not publicly available.

BIBLIOGRAPHY

- Atlas, D. and Ulbrich C. W.: "Path- And Area- Integrated Rainfall Measurement By Microwave Attenuation In The 1-3 Cm Band". *J. Appl. Meteor.*, 16, 1322–1331, 1977.
- Awaka, J., Furuhashi Y., Hoshiyama M., and Nishitsuji A.: "Model Calculations Of Scattering Properties Of Spherical Brightband Particles Made Of Composite Dielectrics". *J. Radio Res. Lab.*, 32, 73–87, 1985.
- Barrett E. and Martin D.: "The Use Of Satellite Data In Rainfall Monitoring". Academic Press, London, 1981.
- Bolen Steven M. and V. Chandrasekar: "Methodology for Aligning and Comparing Spaceborne Radar and Ground-Based Radar Observations". *Journal of Atmospheric and Oceanic Technology*, Vol. 20, No. 5, pp.647–659, 2003.
- Chen S., Grant P. M. and Cowan C. F. N.: "Orthogonal Least Squares Algorithms For Training Multi-Output Radial Basis Function Networks". *IEEE transaction on neural networks*, 2, :302-309, 1991.
- Ebert E. and Le Marshall J.: "An Evaluation Of Infrared Satellite Rainfall Estimation Techniques Over Australia". *Australian Meteorological Magazine*, 1995.
- Foresee Dan, F. and Hagan, M.T.: "Gauss-Newton approximation to Bayesian learning", *Neural Networks International Conference*. 9-12 Jun 1997. Volume: 3, pp: 1930-1935, Houston, TX, USA.
- Gairola R.M., Cecile Mallet, Nicolas Viltard And Emmanuel Moreau: "Estimation Of Rainfall From TRMM-TMI And Precipitation Radar Using Neural Network Approach". *Megha –Tropiques 2nd Scientific Workshop*, 2-6 July 2001, Paris, France.

Haykin Simon: “Neural Networks: A Comprehensive Foundation”, second edition, Prentice_Hall, 1999.

Hollinger J. P., Pierce J. L., And Poe G. A.: “SSM/I Instrument Evaluation,” *IEEE Trans. Geosci. Remote Sensing*, Vol. 28, Pp. 781–790,1990.

http://nasadaacs.eos.nasa.gov/articles/2004/2004_clouds.html

http://trmm-fc.gsfc.nasa.gov/trmm_gv

http://trmm-fc.gsfc.nasa.gov/trmm_gv/gv_products/level_2/scatter_plots/kwaj_data/kwaj_2006_v7_diff.txt

http://trmm-fc.gsfc.nasa.gov/trmm_gv/gv_products/level_2/scatter_plots/kwaj_data/kwaj_2007_v7_diff.txt

http://trmm-fc.gsfc.nasa.gov/trmm_gv/ground_truth/sites/florida/melb/Mel_results.html

http://trmm-fc.gsfc.nasa.gov/trmm_gv/gv_products/level_2.html

http://trmm-fc.gsfc.nasa.gov/trmm_gv/index.html

<http://trmm.gsfc.nasa.gov/3a26.html>

<http://www.desktopdoppler.com/help/nws-nexrad.htm>

<http://www.roc.noaa.gov>

<http://www.roc.noaa.gov/eng/nexradtech.asp>

- Iguchi Toshio, Toshiaki Kozu, Robert Meneghini, Jun Awaka and Kenichi Okamoto. :
 “Rain-Profiling Algorithm for the TRMM Precipitation Radar”. American
 Meteorological Society, Journal of Applied Meteorology Volume 39. 2000.
- Jimenez Daniel: “Dynamically weighted ensemble neural networks for classification.
 Neural Networks Proceedings, 1998. IEEE World Congress on Computational
 Intelligence. Anchorage, AK, USA. 4-8 May 1998 Volume: 1, 753-756.
- Kozu T., Kawanishi T., Kuroiwa H., Kojima M., Oikawa K., Kumagai H., Okamoto K.,
 Okumura M., Nakatuka H., and Nishikawa K.: “Development of Precipitation Radar
 Onboard the Tropical Rainfall Measuring Mission (TRMM) Satellite”. Proceedings of
 the IEEE 2001 Trans. Geoscience and Remote Sensing, 39, 102-116.
- Kozu Toshiaki, Iguchi Toshio, Shimizu Kunio and Kashiwagi Nobuhisa : “Estimation Of
 Raindrop Size Distribution Parameters Using Statistical Relations Between Multi-
 Parameter Rainfall Remote Sensing Data”. International Conference on Radar
 Meteorology, 29th, Montreal, Canada, 12-16 July 1999. pp. 689-692. 1999.
- Kummerow, C., Olson, W. S. And Giglio, L.: “A Simplified Scheme For Obtaining
 Precipitation And Vertical Hydrometeor Profiles From Passive Microwave Sensors”.
 IEEE Trans. Geosci. and Remote Sensing, 34: 1213–1232., 1996.
- Li Wanyu, V. Chandrasekar, Gang Xu :”Investigations in Radar Rainfall Estimation
 Using Neural Networks:..IGARSS, 2003.
- Li Wanyu , V. Chandrasekar: “Rainfall Estimation from Vertical Profiles Of Reflectivity
 Using Neural Networks”. IGARSS 2002.
- Liao, L., and R. Meneghini, 2009: “Validation of TRMM Precipitation Radar through
 Comparison of Its Multiyear Measurements with Ground-Based Radar”. J. Appl.
 Meteor. Climatol., **48**, 804–817.
- Liu Hongping, V. Chandrasekar, and E. Gorgucci: “Detection Of Rain/No Rain
 Condition On The Ground Based On Radar Observations”. IEEE Transactions On
 Geoscience And Remote Sensing, Vol. 39, No. 3, March 2001

- Liu Hongping, V. Chandrasekar, and Gang Xu: "An Adaptive Neural Network Scheme for Radar Rainfall Estimation from WSR- 88D Observations". *Journal of Applied Meteorology*, Vol. 40, 28 February 2001.
- Louis Battan J.: "Radar Observation Of The Atmosphere". University Of Chicago Press, 1973.
- Maqsood Imran, Muhammad Riaz Khan, Ajith Abraham: "An ensemble of neural networks for weather forecasting". *Neural Computing & Application*. 2004, 13: 112–122.
- Mark, J.L. Orr: "Introduction to Radial Basis Function Networks". 1996
- Marshall J. S, and Palmer W. McK.: "The Distribution Of Raindrops With Size". *Journal of Meteorology*, Vol. 5, pp: 165-166, 1948.
- Mielke Paul W., Jr., Kenneth J. Berry: "Permutation Methods, A distance Function Approach", 2nd Edition, 2007.
- Okamoto K., Iguchi T., Takahashi N., Ushio T., Awaka J., Shige S., and Kubota T., 2007: "High precision and high resolution global precipitation map from satellite data", ISAP 2007 Proceedings, pp. 506-509.
- Orlandini Stefano and Isabella Morlini: "Artificial Neural Network Estimation Of Rainfall Intensity From Radar Observations". *Journal of Geophysical Research*, Vol.105, pp.24849-24861. Oct 2000.
- Shen Zhang Quan, Fan Sheng Kong: "Dynamically Weighted Ensemble Neural Networks for Regression Problems". *Proceedings of the Third International Conference on Machine Learning and Cybernetics*, Shanghai 26-29 August 2004.
- Tapiador F. J., Kidd C., Hsu K. L. And Marzano F. : "Neural Networks In Satellite Rainfall Estimation". *Meteorol. Appl.* 11, 83–91,2004.
- Teschl Reinhard, Walter L. Randeu and Franz Teschl: "Improving weather radar estimates of rainfall using feed-forward neural networks": *Neural Networks*,

Computational Intelligence in Earth and Environmental Sciences, Vol. 20, Issue 4, Pages 519- 527. May 2007.

TRMM-PR Manual, Version 6, 2005.

TRMM Manual February 2001.

Tsintikidis Dimitris, Jeffrey L. Haferman, Emmanouil N. Anagnostou, Witold F. Krajewski, And Theodore F. Smith: "A Neural Network Approach To Estimating Rainfall From Spaceborne Microwave Data". IEEE Transactions On Geoscience And Remote Sensing, Vol. 35, No. 5, September 1997.

Viltard Nicolas, Corinne Burlaud, Christian D. Kummerow: "Rain Retrieval From TMI Brightness Temperature Measurements Using A TRMM PR-Based Database". American Meteorological Society, 2006.

Xiao Rongrui, V. Chandrasekar, Liu H. and Gorgucci E.: "Detection of Rain/No Rain Condition on ground From Radar Data Using A Kohonen Neural Network". Geoscience and Remote Sensing Symposium Proceedings, 1998.

Xiao Rongrui, and V. Chandrasekar: "Development Of A Neural Network Based Algorithm For Rainfall Estimation From Radar Observations". IEEE Transaction On Geoscience And Remote Sensing, VOL. 35, NO. 1, JANUARY 1997.

Xiao Rongrui and V. Chandrasekar : "Multiparameter Radar Snowfall Estimation Using Neural Network Techniques". Proceedings IGARSS 1996, Geoscience and Remote Sensing Symposium (1996), pp. 566-568. 1996.

Zafar B., Mubarak K., V. Chandrasekar: "Evaluation of Precipitation Type Determination from TRMM Observation". Proc. IEEE Conf. on Geoscience and Remote Sensing, 2003, 3175-3177.